1-1-2011

Reliability Assessment, Performance Prediction and Life-Cycle Management of Fatigue Sensitive Structures Based on Field Test Data

Kihyon Kwon
Lehigh University

Follow this and additional works at: http://preserve.lehigh.edu/etd

RELIABILITY ASSESSMENT, PERFORMANCE PREDICTION

AND LIFE-CYCLE MANAGEMENT OF FATIGUE SENSITIVE

STRUCTURES BASED ON FIELD TEST DATA

by

Kihyon Kwon

Presented to the Graduate and Research Committee

of Lehigh University

in Candidacy for the Degree of

Doctor of Philosophy

in

Structural Engineering

Lehigh University

May 2011

Approved and recommended for acceptance as a dissertation in partial fulfillment of the requirement for the degree of Doctor of Philosophy.

_____

Date

_____

Dr. Dan M. Frangopol, Dissertation Advisor

Professor of Civil and Environmental Engineering

Lehigh University

_____

Accepted Date

Committee Members:

_____

Dr. John L. Wilson, Committee Chair

Professor of Civil and Environmental Engineering

Lehigh University

_____

Dr. Stephen P. Pessiki, Committee Member

Professor of Civil and Environmental Engineering

Lehigh University

_____

Dr. Ben T. Yen, Committee Member

Professor Emeritus of Civil and Environmental

Engineering, Lehigh University

_____

Dr. Kurt Maute, External Committee Member

Associate Professor of Aerospace Engineering Sciences

University of Colorado at Boulder

ii

ACKNOWLEDGMENTS

TABLE OF CONTENTS

LIST OF TABLES

LIST OF FIGURES

ABSTRACT

In the analysis of structural deterioration processes of steel bridges, fatigue is one of the primary safety concerns. Therefore, fatigue performance assessment and life-cycle prediction have to be used throughout the anticipated service life of fatigue sensitive structures for mitigating fatigue damage and preventing sudden fatigue failure. The preservation of long-term satisfactory structural performance by using optimal maintenance-management interventions under uncertainty is more effectively achieved by the integration of structural health monitoring (SHM) data in the prediction models.

The main goal of this study is to develop efficient probabilistic approaches for the reliability assessment, performance prediction, and life-cycle management of fatigue sensitive bridge and ship structures by incorporating SHM data. In order to achieve this goal, SHM data for existing structures are used in investigating the current practices and methodologies associated with performance assessment and life-cycle maintenance-management of fatigue sensitive structures.

In order to quantify the performance of bridge or ship structures, the time-dependent reliability assessment and lifetime performance prediction for fatigue are investigated. A novel approach for reliability assessment, performance prediction and life-cycle management of fatigue sensitive structures by integrating the SHM data is proposed. Integrating probabilistic lifetime sea loads obtained from model test data into fatigue performance assessment of high-speed ship structures is also proposed. An approach for the reliability-based bridge maintenance interventions by incorporating

1

both crack growth and probability of detection models is developed. Methods for the optimization of life-cycle maintenance of structural systems sensitive to fatigue by considering reliability-based performance measures are developed as well. Finally, an approach for the system-based reliability assessment and prediction of ship structures is presented.

The suitability and applicability of the proposed probability-based approach are illustrated on bridge and ship structures including existing highway bridges, a joint high-speed sealift ship, an aluminum crew boat, and a single hull girder ship. These applications demonstrate that damage identification and remedies for fatigue sensitive structures under uncertainty are more rationally performed by integrating SHM data into the time-dependent reliability assessment, performance prediction, and life-cycle management interventions.

CHAPTER 1

INTRODUCTION

1.1 OVERVIEW

In many metallic structures fatigue is one of the most common failure mechanisms (Pachurin 2008). Therefore, in the design and assessment phases of such structures fatigue has been one of the primary safety concerns. In the United States, numerous fatigue tests were conducted in the 1960s and 1970s in order to establish stress range-fatigue life (*S-N*) relationships for various categories of fatigue details in an effort to guide fatigue design (Fisher et al. 1998). The resulting *S-N* relationships using a logarithmic scale have provided the basis of the current AASHTO Specifications (AASHTO 2008) and have been used in design as well as assessment. However, in fatigue life assessment, considerable differences between true and estimated fatigue lives often exist because of various uncertainties (Fisher et al. 1998 and Maddox 2003). In addition, due to the uncertainty associated with fatigue loading, a reliable fatigue life prediction is not always possible. Consequently, the development of a robust probabilistic approach is essential for reliable fatigue life assessment and performance prediction considering various uncertainties associated with fatigue resistance and load effect. Furthermore, the development of probability-based performance measures will provide the necessary framework to plan and apply optimal life-cycle management interventions on fatigue sensitive structures.

Structural reliability analysis has been well developed and widely applied in many fields. Reliability theory is concerned with determining the probabilistic

3

measure of safe performance that may be regarded as a complementary function of the probability of failure (Thoft-Christensen & Baker 1982 and Ang & Tang 1984). As a performance measure of structural details of bridge and ship structures susceptible to fatigue, the reliability assessment and lifetime performance prediction can be investigated considering both fatigue resistance (capacity) and load effect (demand) under uncertainties associated with environmental and mechanical stressors, errors in design, fabrication and/or construction, and unexpected traffic and wave conditions. Currently, the *S-N* approach for all identified detail categories has been widely accepted to assess fatigue resistance of aging metallic structures including steel bridges, steel and aluminum ships, in conjunction with the well-known Miner's rule (Miner 1945). On the other hand, more accurate and reliable load effects can be predicted from field test data including long-term monitoring and model test programs. Nevertheless, due to the restrictions associated with the continuous collection of loading history as well as the deterministic *S-N* approach, efforts have to be made for improving the fatigue reliability evaluation models through the accurate treatments of the important random parameters.

In 1982, the ASCE Committee on Fatigue and Fracture Reliability (1982) proposed the use of probabilistic distributions for fatigue reliability analysis. The useful application of several probability density functions (PDFs) for lifetime predictions was reported by Chung (2004), Pourzeynali and Datta (2005), and Liu et al. (2010a), among others. The prediction models can be effectively developed based on the *S-N* values and SHM data. In this context, two important parameters (fatigue detail coefficient in terms of fatigue resistance and equivalent stress range in terms of fatigue

loading) have to be treated under uncertainty in fatigue reliability assessment. Fatigue life estimation below the constant amplitude fatigue threshold (CAFT) of steel bridges can be based on a bi-linear *S-N* approach (Crudele & Yen 2006). This is due to the fact that in some cases the current AASHTO *S-N* procedure has been found to provide a negative remaining life, implying that the estimation is overly conservative with respect to real fatigue life (Connor et al. 2005 and Yen et al. 2009). To avoid unnecessary retrofit or repair actions, a more realistic estimation of fatigue life is essential based on a bi-linear *S-N* relationship with different slopes above and below the CAFT.

In case of fatigue life estimation of steel ship structures, although the *S-N* relationships have been well documented with the statistical information (BS 5400, 1980), understanding the effect of sea loading associated with sea states, ship speeds, and relative wave headings is still a challenge. For a more reliable estimation of the long-term structural performance, potential lifetime load effects including low frequency wave-induced and high frequency slam-induced whipping loadings can be predicted from available field test data by using a probabilistic approach.

In recent years, modern concepts of structural evaluation using SHM programs under uncertainty have been developed (Frangopol & Estes 1997, Frangopol & Messervey 2007, Frangopol & Liu 2007). The development of SHM systems including data acquisition, collection, interpretation and integration algorithms is beneficial to make more accurate structural diagnosis of deteriorating structures as well as prognosis of future performance for maintenance decisions. However, efficient applications of SHM for assessing time-dependent structural reliability are still in their

infancy (Frangopol et al. 2008). Clearly, integration of SHM data into structural performance assessment as well as life-cycle management is desirable for the improved preservation of long-term satisfactory structural performance and optimal maintenance-management of fatigue sensitive structures.

Reliability-based structural management associated with inspection, monitoring, repair/retrofit and maintenance interventions has become an efficient approach to allocate limited financial resources to balance lifetime structural reliability and life-cycle cost using single-objective or multi-objective optimization (Estes & Frangopol 1999, Frangopol & Maute 2003, Kong & Frangopol 2005, and Liu et al. 2010b). Reliability-based life-cycle management can assist decision-makers in making rational decisions on maintenance strategies in order to keep structures serviceable and safe with limited maintenance funds (Frangopol et al. 1997, Thoft-Christensen 1998, and Frangopol 2002). Although numerous optimization methods are available, finding optimal life-cycle management strategies for fatigue sensitive structures is a field of great interest.

1.2 OBJECTIVES

The following are the main objectives of this study:

1. Investigate the applicability of current practices and field test data for fatigue life estimation under uncertainty.

2. Develop approaches for integration of field test data in reliability assessment and performance prediction of fatigue sensitive structures.

3. Develop approaches for integration of the time-dependent fatigue reliability

assessment in a life-cycle maintenance-management.

4. Develop approaches for reliability-based life-cycle optimal management strategies associated with steel and aluminum structures.

1.3 SUMMARY OF PROPOSED APPROACH

In this study, a series of analyses are carried out to examine the fatigue reliability and lifetime performance prediction under uncertainty, and to find optimal life-cycle management strategies of fatigue sensitive structures in a rational way. In order to perform these analyses, three main research tasks are identified: (a) fatigue reliability assessment, (b) lifetime performance prediction, and (c) life-cycle structural management. In each task, the established linear and/or bi-linear S-N approaches based on current specifications are used for assessing fatigue resistance, while available field test data are utilized for estimating fatigue loading.

As a performance measure of metallic structures, fatigue reliability assessment is investigated by formulating the lifetime performance functions based on structural reliability concepts and pertinent probabilistic treatments of important parameters under uncertainty. Available statistical data from the linear (i.e., single slope only) and bi-linear (i.e., double slope) S-N approaches are investigated. In absence of the data, their randomness is investigated by using current fatigue criteria. Fatigue reliability assessment is then performed by incorporating field test data obtained from SHM or scaled model test. The reliability computations are conducted in an efficient way by using reliability software linked to specifically developed computer programs.

7

The time-dependent structural performance is predicted by developing lifetime prediction models. The established stress-range bin histogram data using rain-flow or peak counting method are truncated and used to find appropriate PDFs for lifetime prediction of stress ranges using fitting methods. Moreover, the integration of SHM data and/or FE stress outputs in performance prediction is investigated for updating the time-dependent performance measures. In particular, lifetime performance prediction associated with ultimate strength of fatigue sensitive ship structures subjected to vertical bending is investigated at the system level due to the presence of multiple potential failure modes. The estimation of the time-dependent ultimate strength is based on an empirical formula, where still water and wave-induced bending moments are estimated using the International Association of Classification Societies (IACS) recommendation (2006) and a simplified direct method, respectively.

An approach for the reliability-based bridge inspection/repair interventions by incorporating the crack growth model (CGM) and probability of detection model (PDM) is developed considering three important time-dependent factors: structural performance level, crack growth rate, and crack detection probability. The CGM offers useful information regarding crack propagation with respect to the number of cycles, while the fatigue reliability model (FRM) estimates reliability of structural components with respect to the number of cycles. The PDM is integrated with the FRM and CGM. The application of this combined approach improves the life-cycle bridge management interventions so that proper inspection and repair actions are undertaken.

Methods for the optimization of life-cycle structural maintenance based on the

time-dependent performance measures are developed. For retrofitting distortion-induced fatigue cracking in steel bridges, an approach to finding the optimal cut-off size of the connection details is presented. Two conflicting objectives are formulated: minimization of the cut-off area and maximization of the fatigue reliability of the connection details. The concept of the cut-off size adjustment factor is introduced. This factor is used to model the nonlinear relationship with respect to the cut-off size. To find the lifetime optimum inspection/repair interventions of aluminum ship structures, a method considering three competing objectives, which are fatigue reliability, fatigue damage and life-cycle cost, is developed. The fatigue reliability analysis based on the bi-linear S-N approach and sea loading data is performed for the lifetime performance assessment and prediction, while the life-cycle cost analyses as well as the single- and multi-objective optimization problems are formulated and solved. The genetic algorithm is used in order to solve the multi-objective optimal maintenance planning formulation.

1.4 OUTLINE OF DISSERTATION

The dissertation is divided into eight chapters.

Chapter 1 serves as introduction.

Chapter 2 provides the relevant background information associated with this study and reviews the approaches and methodologies that have been conducted in the field of structural reliability research. The background information pertaining to reliability theory and methods, and reliability-based lifetime structural maintenance interventions is provided. A system-based reliability approach is also provided.

Included in this chapter are reviews of reliability assessment and performance prediction of fatigue sensitive structures, and probabilistic distributions for structural resistance and load effects.

Chapter 3 develops the time-dependent structural reliability evaluation in order to reliably assess and predict lifetime fatigue performance of steel bridge structures under various uncertainties. Time-dependent fatigue reliability assessment and prediction based on the linear *S-N* approach and SHM is investigated. Estimation of fatigue life below the CAFT of steel bridges is also investigated by using a probabilistic method based on the bi-linear *S-N* approach.

Chapter 4 describes the time-dependent reliability assessment of ship structures that is mainly focused on the prediction of lifetime fatigue performance of steel-based and aluminum-based structures, by using a probabilistic approach considering various uncertainties associated with sea environmental and ship operating conditions as well as considering errors in design, fabrication, or construction. The time-dependent fatigue reliability assessment and prediction of high-speed steel ship structures are investigated based on probabilistic lifetime sea loads. Fatigue life estimation of aluminum ship structures is addressed, by incorporating the bi-linear *S-N* approach and SHM into the time-dependent fatigue reliability assessment.

Chapter 5 develops the reliability-based life-cycle structural management strategies for steel bridges. Efficient bridge fatigue assessment and management are addressed by using a combined approach based on prediction models. Bridge retrofit design optimization to find the optimal retrofitting solutions in the floor-beam

connection details is presented by applying both single-objective and bi-objective optimization processes.

Chapter 6 develops the reliability-based life-cycle management of ship structures for fatigue. Life-cycle cost analysis as well as optimization problems considering both single- and multi-objective approaches are described. Applicable lifetime maintenance strategies are investigated for planning inspection and repair interventions of aluminum ships.

Chapter 7 addresses the system-based reliability approach for the potential failure modes in order to estimate and predict lifetime system performance of steel ship structures. Lifetime structural deterioration models are developed at the system level by formulating time-dependent random functions associated with corrosion and fatigue cracking.

Chapter 8 provides the summary, the conclusions drawn from the study, and the recommendations for future work.

CHAPTER 2

BACKGROUND

2.1 INTRODUCTION

This chapter provides the relevant background information associated with this study and reviews the approaches and methodologies that have been conducted in the field of structural reliability research.

The background information pertaining to reliability theory and approach, and reliability-based life-cycle structural management is provided in Section 2.2. Included in this section are reviews of reliability assessment and prediction of deteriorating structures at structural component and system levels, and reliability-based life-cycle management including structural inspections and repairs. The relevant approaches and methods for the reliability assessment of fatigue sensitive structures are described in Section 2.3. The associated conclusions are remarked in Section 2.4.

2.2 RELIABILITY AND LIFE-CYCLE MANAGEMENT

2.2.1 Introduction

A considerable amount of research associated with structural reliability and optimization has been carried out in the civil infrastructure and the marine areas. Nevertheless, the development of the methodology and application relevant to reliability assessment and reliability-based life-cycle management is still in its infancy.

As a performance measure of deteriorating structures, reliability is the analysis of failures, their causes and consequences. Structural reliability evaluation is to assess

12

current condition/safety levels and to predict time-dependent structural performance of deteriorating structures. Such reliability can be possibly extended to lifetime structural performance measures at component levels as well as system levels. Reliability-based life-cycle structural management is to provide the best possible solutions associated with inspection, repair/retrofit, and/or SHM. In this context, the fundamental concept and background related to structural performance assessment and life-cycle management are presented in this section.

2.2.2   Structural Reliability Analysis

Typically, bridge and ship structures have experienced potential deteriorating processes during the entire service life. Therefore, their structural performance should be steadily assessed and predicted. For this purpose, structural reliability approach, which has been applied in many fields, can be used.

In many engineering fields, the concept and methodology for the structural reliability analysis have been well developed and accepted based on potential deterioration mechanisms of structural systems which are classified in various categories including fatigue cracking, corrosion, material yielding, excessive deformation, excessive shear and/or bending moment failure, and buckling failure. For the identified failure mechanisms, reliability assessment and performance prediction of structures are extremely important tasks in order to not only evaluate time-dependent structural performance but also schedule the appropriate management strategies to deteriorating structural systems (e.g., bridge and ship structures). It may become more rational when field test data from SHM are relevantly integrated into

structural reliability assessment and performance prediction of a structure. Eventually, the assessment and prediction of the structure will be used as a decision-making for scheduling life-cycle structural maintenance and management interventions.

Reliability theory is concerned with determining the probabilistic measure of safe performance that may be regarded as a complementary function of the probability of failure (Thoft-Christensen & Baker 1982 and Ang & Tang 1984). Under consideration of resistance and load uncertainties in the analysis, it is necessary to establish a limit-state function between failed and safe states with the well-defined random variables, and it is then possible to perform structural reliability analysis by using applicable computation techniques.

In general, the reliability of a structural component or system is related to the probability of safety for a particular limit state. The general state function can be expressed as:

$$g(X) = g(X_1, \ X_2, \ ...., \ X_n)$$
(2-1)

where $g(X)$ is a response model and X is a random variable vector composed of X_1, X_2, ..., and X_n.

Simply, a limit-state function is comprised of both terms of the capacity and demand representing structural resistance, R, and load effect, S, respectively, and is represented as:

$$g(R, S) = R - S = 0$$
(2-2)

According to governing deterioration processes, it is noted that the defined parameters R and S have to be expressed in terms of other random variables (e.g., $g(\sigma_y, E, \varepsilon) = \sigma_y - E\varepsilon$ for yield strength capacity).

Based on the limit-state function, $g(X)$, the failure and complementary (safe) probabilities of a structural member, P_f and P_S, can be defined, respectively, as (see also Figure 2-1):

$$P_f = P[g(X) \le 0] = \int_\Omega f_X(x) \cdot dX \tag{2-3}$$

$$P_S = P[g(X) > 0] = 1 - P_f \tag{2-4}$$

where X is a vector of random variables with joint probability density function (PDF), $f_X(x)$, and Ω is the failure domain which can be defined for a component reliability problem by:

$$\Omega \equiv \{g(X) \le 0\} \tag{2-5}$$

The reliability index β that is related to the probability of failure is defined as:

$$\beta = \Phi^{-1}(1 - P_f) = -\Phi^{-1}(P_f) \tag{2-6}$$

where $\Phi^{-1}(\cdot)$ denotes the inverse standard normal cumulative distribution function (CDF).

When R and S are considered as statistically independent normally distributed random variables with mean values, μ_R and μ_S, respectively, and standard deviations, σ_R and σ_S, respectively, the mean value and standard deviation of the function, $g(R, S)$ can be derived as:

15

$$\mu_g = \mu_R - \mu_S \qquad (2\text{-}7)$$

$$\sigma_g = \sqrt{\sigma_R^2 + \sigma_S^2} \qquad (2\text{-}8)$$

Then, the probability of failure is

$$P_f = \Phi(-\beta) = \Phi\left(-\frac{\mu_g}{\sigma_g}\right) = \Phi\left(\frac{\mu_S - \mu_R}{\sqrt{\sigma_S^2 + \sigma_R^2}}\right) \qquad (2\text{-}9)$$

A safety margin concept of $g(R, S)$ and the reliability index, β, are illustrated by the PDFs models in Figure 2-2. It can be seen that the reliability index, β, corresponds to the distance from the origin to the mean of the safety margin, μ_g. Thus, the most generalized definition of reliability is the second-moment reliability index, β, which derives from this simple two-dimensional case, and is related to the failure probability (see Eq. 2-9).

In practice, such a two-variable simplification of the limit state may not be possible for many structural reliability problems (e.g., bridge system, ship and offshore structure, nuclear power plant, and so on). Moreover, the joint probability function for the random variables in the limit-state function may not be described precisely due to limited data. Even if the basic variables are mutually independent and all marginal density functions are known, it is often impractical to perform the numerical integration of the multidimensional integral over the failure domain. Therefore, efficient techniques under general conditions can be used to evaluate structural reliability, including first-order method (FORM), second-order method (SORM), Monte Carlo Simulation (MCS), and so on. Among others, the FORM in

many reliability researches has been extensively employed as the most common numerical technique since it provides good approximate solutions for most cases.

2.2.3 System Reliability Analysis

Reliability analysis for structural systems can be taken into consideration as extension and combination of individual reliability evaluation for structural components and/or failure modes because most elements or failure modes within a structure are actually performing as parts of a complex structural system. Quantifying and characterizing the performance and safety of structural systems have been of an increased interest in the area of system reliability (Hendawi & Frangopol 1994 and Estes & Frangopol 1999). In this context, the classical theory of series and parallel system reliability has been well developed for the analysis of complex structural systems. The literature introduces formulations for the reliability of these systems, including the possibility of correlated element strengths (Thoft-Christensen & Baker 1982 and Thoft-Christensen & Murotsu 1986). For a series system, the system limit state is taken by definition corresponding to the first member failure (or weakest link). In the case of the parallel system, the system limit state is defined as failure of all members. In all cases, the system reliabilities can be expressed in terms of the component reliabilities. Since computing system reliability is related to general system reliability, the focus can be on tools and techniques for system reliability modeling and analysis. Furthermore, it is necessary that a combination model of series and parallel systems is developed for applications to more complex systems and that a reliability assessment for component and/or system levels takes into account time-

17

dependent effects such as degrading member resistances with applications of time functions.

For system reliability problems, the failure domain Ω defined in Eq. 2-3 is obtained by:

$$\Omega \equiv \left\{ \bigcup_{k=1}^{n} \bigcap_{i \in C_k} g_i(X) \leq 0 \right\} \tag{2-10}$$

where C_k and n refer to the k-th cut set and the number of cut sets, respectively, where each cut set is defined as an intersection of component failure events.

When each cut set has only one component (see Figure 2-5(a)), the system is referred to as a series system. Its corresponding failure domain and system failure probability P_{fsys} are defined as (Rashedi & Moses 1988):

$$\Omega \equiv \left\{ (g_1 \leq 0) \cup (g_2 \leq 0) \cdots \cup (g_k \leq 0) \cdots \cup (g_n \leq 0) \right\} \tag{2-11a}$$

$$P_{fsys} = P_f(g_1 \leq 0 \ \text{ or } \ g_2 \leq 0 \ \text{ or } \cdots g_k \leq 0 \ \text{ or } \cdots g_n \leq 0) \tag{2-11b}$$

Otherwise, it is referred to as a parallel system where each cut set is connected in parallel as shown in Figure 2-5(b). Its corresponding failure domain and P_{fsys} are

$$\Omega \equiv \left\{ (g_1 \leq 0) \cap (g_2 \leq 0) \cdots \cap (g_k \leq 0) \cdots \cap (g_n \leq 0) \right\} \tag{2-12a}$$

$$P_{fsys} = P_f(g_1 \leq 0 \ \text{ and } \ g_2 \leq 0 \ \text{ and } \cdots g_k \leq 0 \ \text{ and } \cdots g_n \leq 0) \tag{2-12b}$$

As an example of more complex systems, a series-parallel model is shown in Figure 2-5(c). Its corresponding failure domain and P_{fsys} are

$$\Omega \equiv \left[\left\{ (g_1 \leq 0) \cap (g_3 \leq 0) \right\} \cup \left\{ (g_1 \leq 0) \right\} \cup \left\{ (g_1 \leq 0) \cap (g_2 \leq 0) \cap (g_3 \leq 0) \right\} \right] \tag{2-13a}$$

$$P_{fsys} = \left[\{(g_1 \leq 0)\,\text{and}\,(g_3 \leq 0)\}\,\text{or}\,\{(g_1 \leq 0)\}\,\text{or}\,\{(g_1 \leq 0)\,\text{and}\,(g_2 \leq 0)\,\text{and}\,(g_3 \leq 0)\}\right]$$

(2-13b)

As a quantitative way to express structural performance at system levels, the system reliability β_{sys} is estimated by using the computed system failure probability. The defined P_{fsys} can be directly converted to compute β_{sys} as

$$\beta_{sys} = -\Phi^{-1}(P_{fsys})$$

(2-14)

To quantify lifetime performance of deteriorating structures at component or system levels, the reliability approach will be useful if it is performed including: well-defined limit-state function, well-treated deterministic parameters and random variables, well-documented current practices for failure modes, and well-collected (reliable) load effect from SHM. Reliability softwares CalREL (Liu et al. 1989) and RELSYS (Estes & Frangopol 1998) assist the computation of structural reliability.

2.2.4   Reliability-Based Structural Management

Over the past decades, the theories of probability, statistics and reliability have provided the bases for modern structural design codes and specifications. Due to various uncertainties, these probabilistic-based and reliability-based approaches have been acceptably employed to gain more predictable levels of safety and more risk-consistent structures, while utilizing the most recent statistical information on material strengths as well as structural and environmental loads. In recent years, this concept has been spread from design steps into management steps in order to preserve a structural system safely during its entire service life. As a result, a reliability-based

structural management planning has become an efficient approach for allocating limited financial resources to balance lifetime reliability of structural systems and life-cycle cost in an optimal manner (Estes & Frangopol 1999, Faber 2000, Frangopol et al. 2001, Frangopol & Maute 2003, Kong & Frangopol 2005, and Liu et al. 2010b).

Kong et al (2000) proposed two efficient maintenance strategies (i.e., preventive and essential maintenance) based on the performance (reliability) profile with a predefined target level. As shown in Figure 2-3(a), preventive maintenance (e.g., repainting, minor repairs) reduces the rate of deterioration with often improvement of the reliability. On the other hand, essential maintenance (e.g., major repairs, strengthening, replacements) is normally undertaken whenever the reliability hits the predefined target value (see Figure 2-3(b)). Thus, reliability-based maintenance interventions can be effectively adopted for lifetime extension as quantifying performance levels under uncertainties.

In addition, the reliability-based structural management planning can assist decision-makers in making rational decisions on maintenance strategies in order to keep structures serviceable and safe with limited maintenance funds (Frangopol et al. 1997a, Thoft-Christensen 1998, and Frangopol 2002). According to Frangopol and Neves (2003), different maintenance strategies of condition, safety, and cost can be taken into consideration as performance indicators over time to predict the performance of deteriorating structures. Two schematic figures are presented. Figure 2-4(a) and (b) show the effects of maintenance actions associated with safety (performance) index under safety- and time-based maintenances, respectively. The applications of respective maintenance actions lead to the several effects (i) increase in

condition and/or safety immediately, (ii) pause in deterioration of condition and/or safety, and (iii) reduction of the deterioration rates of condition and/or safety. These three representative maintenance strategies can be based on finding optimal solutions regarding life-cycle cost (minimization), condition index (minimization), and safety index (maximization) in a multiple-objective optimization problem (Liu and Frangopol 2005a and 2005b).

Furthermore, life-cycle cost associated with various management scenarios can be more effectively saved if the reliability-based management approach for a decision-making is developed based on the applicable integration of SHM into optimal management planning through the time-dependent deterioration processes.

2.2.4.1 Life-Cycle Cost Analysis

Time-dependent reliability assessment based on SHM data is useful for estimating current and future performance of deteriorating structural members. Based on the performance assessment over time, life-cycle optimization problems can be established to plan optimal management strategies with applicable objective functions. By means of structural reliability assessment before repair, it may be determined that proper repair actions have to be undertaken to improve the deteriorated structural performance. Life-cycle optimization technique may be useful to determine the optimal repair option in a cost-effective manner. Structural performance after repair will be reassessed with the updating of reliability and with Bayesian analysis if load effects are time-dependent. An approach to assess and manage lifetime structural performance can be developed, and especially the integration of SHM into structural

maintenance and management can be used as a beneficial technique to perform reliability assessment and to preserve respective structural performance safely up to the anticipated service life with optimal life-cycle management interventions.

In a cost-effective manner, life-cycle cost analysis (LCA) can be carried out to find optimal maintenance interventions. Different inspection and repair strategies are associated with different expected total life-cycle costs. In general, a successful life-cycle management planning is achieved by the minimization of the expected life-cycle cost. For prescribed damage thresholds (e.g., corrosion, cracking), applicable inspection and repair actions can be scheduled and taken to improve structural performance. In addition, regular and irregular time intervals for inspections and repairs can be used in LCA approach.

In the design or assessment processes, LCA is implemented for the decision making process. LCA is usually formulated considering inspection, repair and expected failure cost using the discount rate of money r. These costs can then be employed in the expected total life-cycle cost, C_{ET}, which is used as an objective function for the optimization problem. Each cost function is calculated as (Estes & Frangopol 2005 and Frangopol et al. 1997b):

$$C_{ET} = C_{INS} + C_{REP} + C_F \qquad (2\text{-}15)$$

$$C_{INS} = \sum_{i=1}^{k} \frac{C_{ins}}{(1+r)^{t_i}} \qquad (2\text{-}16)$$

$$C_{REP} = \sum_{j=1}^{n} \frac{C_{rep}}{(1+r)^{t_j}} \qquad (2\text{-}17)$$

$$C_F = C_f \cdot \max[P_f(t)] \tag{2-18}$$

where C_{INS} and C_{REP} = discounted inspection and repair costs, respectively; C_f and C_F = failure and expected failure costs, respectively; k and n = number of inspections and repairs, respectively; C_{ins} and C_{rep} = undiscounted inspection and repair costs, respectively; t_i and t_j = application time of inspection and repair interventions i and j, respectively; max $[P_f(t)]$ = maximum probability of failure during the intended service life; and r = discount rate of money that is about 2 to 3% as an appropriate discount rate considering the difference between the rate of return on a risk-free investment and the inflation rate (Estes & Frangopol 2005).

2.2.4.2   Optimization

Structural optimization is a process applied in design and assessment cycles which are aimed at finding the best possible solution. Through the structural lifespan, ultimate and/or serviceability limit states have to be investigated according to the code and/or performance requirements. In order to find practical optimal solutions, optimization can be incorporated with structural reliability.

Traditionally, structural optimization theory is associated with deterministic design philosophy. Thus, the general formulation of a structural optimization problem is defined as follows (Kirsch 1993):

Find the design variable vector:

$$\mathbf{X} = (X_1, X_2, ..., X_n)^t \tag{2-19}$$

23

Objective function: $\quad$ *minimize* $\ F = F(\boldsymbol{X})$ $\qquad\qquad$ (2-20)

Subjected to the side constraints:

$$X_i^L \leq X_i \leq X_i^U \qquad \text{for i} = 1, 2, \ldots, \text{n} \qquad\qquad (2\text{-}21)$$

Subjected to the performance constraints:

$$X_i^L \leq X_i \leq X_i^U \qquad \text{for i} = 1, 2, \ldots, \text{n} \qquad\qquad (2\text{-}22)$$

When formulating reliability-based structural optimization problems, the associated design variables can be defined at various levels depending on their nature. These levels may include the following groups (Frangopol 1985, Frangopol & Moses 1994, Thoft-Christensen 1991, and Kirsch 1993): sizing design variables, shape design variables associated with structural configuration, geometric conditions, material design variables according to the type of mechanical and/or physical properties, topological design variables (e.g., the number of spans in a bridge), and structural system types (e.g., truss, framed structures).

More importantly, the life-cycle cost optimization can be established by using single- and multi-objective approaches based on the defined cost functions in Eqs. 2-15 through 2-18. In general, the minimization of the objective function C_{ET} can be used in the single-objective optimization, while the expected maintenance cost C_{MT}, reliability index β, and other interesting criteria (e.g., condition, damage index) can be used as objectives in the multi-objective optimization. In both optimization problems, inspection and repair times for life-cycle management interventions can be defined as possible design variables.

The general forms of formulating the single- and multi-objective optimization problems are

Find the design variables: inspection and repair times, t_i and t_j

(i) for the single-objective optimization

$$\min C_{ET}(t) = \sum_{i=1}^{k} \frac{C_{ins}}{(1+r)^{t_i}} + \sum_{j=1}^{n} \frac{C_{rep}}{(1+r)^{t_j}} + C_f \cdot \max[P_f(t)] \qquad (2\text{-}23)$$

(ii) for the multi-objective optimization

$$\min C_{MT}(t) = \sum_{i=1}^{k} \frac{C_{ins}}{(1+r)^{t_i}} + \sum_{j=1}^{n} \frac{C_{rep}}{(1+r)^{t_j}} \qquad (2\text{-}24)$$

$$\max \; \{\min \; \beta(t)\} \;, \text{or} \; \min \; \{\max \; P_f(t)\} \qquad (2\text{-}25)$$

$$\min \; \{\max \; D(t)\} \;, \text{and/or} \; \min \; \{\max \; C(t)\} \qquad (2\text{-}26)$$

(iii) satisfying the inspection and repair time constraints

$$t_{i-1} < \; t_i < \; t_{life} \; \text{and} \; t_{j-1} < \; t_j < \; t_{life} \qquad (2\text{-}27)$$

and the reliability constraint

$$\min \; \beta(t) > \beta_{t\arg et} \;, \text{or} \; \max \; P_f(t) < P_{f,t\arg et} \qquad (2\text{-}28)$$

where C_{MT} = expected maintenance cost; $D(t)$, $C(t)$ = time-dependent damage and condition index, respectively; $t_i = i$-th inspection time ($i = 1, 2, \ldots, k$), and $t_j = j$-th repair time ($j = 1, 2, \ldots, n$); and β_{target}, $P_{f,target}$ = target reliability and probability of failure index, respectively.

25

The solution of the single-objective optimization can be easily found by *fmincon* optimization function of Matlab (MathWorks 2009) using the sequential quadratic programming method. A unique solution is provided by the single-objective optimization for the decision maker. Due to the budgetary restriction for the single choice, when the decision maker has to choose another (non-optimal) solution, a multi-objective optimization approach can be used alternatively. This is useful because multiple optimal solutions can be provided to the decision maker. In many practical optimization applications, the multi-objective optimization approach has been utilized in order to provide multiple choices (Arora 2004). The defined multi objectives are achieved simultaneously under the predefined constraints. The genetic algorithm (GA) non-dominated sorting method, NSGA-II (Deb et al. 2002) can be effectively used in order to solve the multi-objective optimal maintenance planning formulation.

2.3   RELIABILITY ASSESSMENT OF FATIGUE SENSITIVE STRUCTURES

2.3.1   Fatigue Life Estimation

This section addresses reliability approaches for fatigue life estimation of bridge and ship structures susceptible to fatigue. In particular, these approaches are focused on conducting fatigue reliability assessment and performance prediction over time rather than the applicability of design-based approach. For assessing fatigue resistance and for estimating fatigue loading, the relevant and reliable approaches and methods are herein presented including the *S-N* approach and Miner's rule, fracture mechanics approach, and SHM. Appropriate PDFs used in developing lifetime prediction models under uncertainty are also presented.

2.3.1.1   S-N Approach and Miner's Rule

The *S-N* (i.e., stress-life) approach based on the Miner's rule (Miner 1945) has been widely used and adopted as a useful method for fatigue life evaluation of bridge and ship structures. Fatigue strength of a structural detail is characterized in the relationship between stress range (nominal applied stresses) and cycles to failure for classified detail categories. Typically, the characterized *S-N* relationship is established based on the scatter from numerous test data. Assuming that scatter is measured by the standard deviation in fatigue life, there is an observed increase in it when stress amplitude is decreased. An *S-N* curve derived from a mean *S-N* curve that is shifted two standard deviations lower is commonly used for design purposes and associated with a 2.3% probability of failure assuming the life logarithms to be normally distributed (Fisher et al. 1998 and Maddox 2003). For assessment purposes, a mean *S-N* curve has to be used to realize the true life. It should be kept in mind that the mean value of applied stress associated with a single stress cycle can have a significant influence on the *S-N* curve. However, in this research which is limited to welded details studied extensively by Fisher et al. (1970), the conclusions of the NCHRP Report 102 (Fischer et al. 1970) were adopted as: (a) stress range was the dominant stress variable for all welded details and beams tested, and (b) other stress variables such as minimum stress, mean stress, and maximum stress (although sometimes statistically significant) were not significant for design purposes. Nevertheless, the effect of the random mean stress on the *S-N* relationship can be further investigated.

The *S-N* curves are represented as sloping straight lines in logarithmic scale. The basic *S-N* equation of fatigue strength is

$$R = \left(\frac{A}{N}\right)^{1/m} \tag{2-29}$$

where R = nominal fatigue resistance (stress range), A = fatigue detail coefficient which can be treated as a random variable in a probabilistic approach if uncertainty in fatigue strength is considered, N = number of stress cycles, and m = material constant representing the slope of the S-N curves that can be assumed as m = 3.0 for steel bridges, while the value of m for ship structures varies in the defined categories. A typical set of S-N curves, as that shown in Figure 2-6(a) and (b), can be established based on the AASHTO Specifications (2008) for steel bridges and the BS 5400 (1980) for steel ships, respectively.

Typically, fatigue damage is defined to be cumulative and irreversible. The Palmgren-Miner rule is used to account for this damage accumulation. The linear damage rule proposed by Palmgren in 1924 was further investigated by Miner in 1945 (Fisher et al. 1998). It simply assumes that damage fraction at any particular stress range level is a linear function of the corresponding number of cycles. For a structural detail, the total damage can be expressed as the sum of damage occurrences that have taken place at individual stress range levels (i.e., Miner's rule). The equation known as Miner's rule is

$$D = \Sigma \frac{n_i}{N_i} \tag{2-30}$$

where n_i = number of cycles at stress range level i, and N_i = number of cycles to failure at stress range level i. Theoretically, the fatigue damage ratio, D, is equal to 1.0

at failure, while practically it may be less than 1.0 due to various uncertainties (Fisher et al. 1998 and Ayyub et al. 2002b).

2.3.1.2　Fracture Mechanics Approach

Fatigue is the initiation and propagation of microscopic cracks into macro cracks by the repeated application of stresses (Fisher et al. 1998). For existing steel bridges, examination of fatigue cracking must be an essential consideration because of repeated loading such as traffic. The majority of fatigue life may fully rely on propagation of the initiated cracks under uncertainties including loading history of environmental and mechanical stressors, human errors in fabrication, and unexpected traffic increases. To examine the growth of cracks in details, a fracture mechanics approach can be employed. This approach is based on the linear elastic fracture mechanics (LEFM), assuming that the material is isotropic and linear elastic under small displacements.

Based on the LEFM, crack growth model (CGM) can be developed for evaluating fatigue life associated with crack propagation (i.e., cumulative number of cycles versus crack sizes). Fatigue crack growth curves are commonly generated by using an empirical equation, namely, the Paris equation proposed by Paris & Erdogan (1963) as:

$$\frac{da}{dN} = C \cdot (\Delta K)^B \tag{2-31}$$

where a = crack size, N = number of cycles, and ΔK = stress intensity factor range while C and B are the fatigue coefficient and the fatigue exponent, respectively. The

29

estimation of ΔK is especially complex in common use of welded structures. It can be expressed in terms of crack size as (Barsom & Rolfe 1996):

$$\Delta K(a) = G(a) \cdot \Delta \sigma \cdot \sqrt{\pi \cdot a} \qquad \text{(2-32)}$$

where $\Delta K(a)$ = generalized stress intensity factor range, $G(a)$ = a non-dimensional function of the geometry including various factors (i.e., finite width factor, non-uniform stresses factor, free surface effect factor, and crack shape factor), and $\Delta \sigma$ = stress range. Values for these factors, which are associated with the flaw types caused in critical structural members, can be obtained in the literature (Tada et al. 1973 and Fisher 1984).

By substituting Eq. 2-32 into Eq. 2-31, the equation for estimating the cumulative number of cycles, $N(a)$, is (Fisher 1984):

$$N(a) = \int_{a_i}^{a_f} \frac{da}{C \cdot \left(G(a) \cdot \Delta \sigma \cdot \sqrt{\pi \cdot a} \right)^B} \qquad \text{(2-33)}$$

where a_i = initial crack size and a_f = final (critical) crack size.

The final crack size, a_f, depends on the parameters, C, $\Delta \sigma$, and a_i, which can be treated as random variables in a reliability method. Under these conditions, numerous crack growth curves can be generated by simulation and an appropriate crack growth curve can be identified based on available field test data from SHM and/or non-destructive evaluation (NDE).

For fatigue reliability assessment and management, the CGM representing the cumulative number of cycles and crack sizes can be effectively used to provide cracking information at any given time. In particular, a fracture-based reliability

approach is useful to assess and predict the time-dependent fatigue reliability for fatigue details which are not clearly classified in the *S-N* categories or experience crack growth.

2.3.1.3 Structural Health Monitoring

In bridge and ship structures, various approaches for obtaining reliable information on fatigue loading (e.g, stress range, moment range, crack size) have been developed. Applicable approaches include structural health monitoring (SHM), scaled model test, NDE, simulation, and/or finite element (FE) modeling. Among these methods, SHM is an important issue that is associated increasingly with its integration in the assessment of current performance, time-dependent prediction of deterioration process, and lifetime management planning of structural systems.

Recently, modern probability-based concepts for SHM programs have been developed (Frangopol & Estes 1997, Frangopol & Messervey 2007, and Frangopol & Liu 2007). The development of SHM system is beneficial to make more accurate structural diagnosis as well as prognosis of future performance for maintenance decisions. Based on monitored data at field, reliability application for structural performance assessment has been proposed in many areas (Paik & Frieze 2001, Frangopol et al. 2008, and Liu et al. 2010a). Furthermore, reliability-based system management is essential to be developed with the integration of SHM into optimal management plan as efforts to save effectively life-cycle cost and to reduce uncertainties occurred inevitably during time-variant structural deterioration processes.

In fatigue life assessment of fatigue sensitive structures, monitoring data obtained from SHM provide essential information on load effects caused by traffic or ship operation. A long-term monitoring system will automatically record and store data obtained in installed strain gages whenever any loading events happen during the entire service life. The system may need to be fully automatic, to require little operator intervention, and to be remotely accessible via modem or other wireless communication links (Chong *et al*. 2003). Monitoring programs are mainly performed at potential critical regions where can be identify by FE analysis or previous experiences. By using the rain-flow cycle counting method (Downing & Socie, 1982), stress-range bin histogram data are produced from the collected stress (strain) history. This is widely accepted and used as a useful loading data for fatigue life evaluation.

In general, there are two types of tests to investigate live load effects: controlled and uncontrolled tests. The effects of vehicle speed and position on the bridge deck are captured in the controlled live load tests. On the other hand, the overall influence of real traffic is investigated from the uncontrolled live load testing. Stress-range bin histogram data are usually collected during the uncontrolled monitoring (i.e., SHM). Equivalent stress range, S_{re}, and average daily number of stress cycles, N_{avg}, associated with average daily truck traffic (ADTT) are computed based on the created stress-range bin histogram from the long-term monitoring program. If SHM data for steel bridges is not available, fatigue truck analysis based on the AASHTO fatigue truck model can be alternatively adopted by using influence line analysis to estimate approximately lifetime load effects (i.e., PDF of equivalent stress range). The computed moment ranges can be used to approximately calculate S_{re}.

Typically, fatigue details in bridge and ship structures are subjected to variable amplitude stress ranges rather than constant amplitude fatigue when they are exposed to fatigue loading. For useful estimation of fatigue life, variable amplitude stress ranges can be converted into an equivalent constant amplitude stress range by using Miner's rule (Miner 1945). The estimated S_{re} assists equivalent estimation of fatigue damage with respect to that estimated from variable amplitude stress ranges (Fisher et al. 1998). S_{re} can be computed directly from the stress-range bin histogram and Miner's rule (Miner 1945 and Fisher et al. 1998). The equation is

$$S_{re} = \left[\sum \frac{n_i}{N_{total}} \cdot S_{ri}^m \right]^{\frac{1}{m}} \qquad (2\text{-}34)$$

where n_i = number of observations in the predefined stress-range bin, S_{ri}, N_{total} = total number of observations during the monitoring period T_{shm}, and m = slope of the S-N curve (material constant).

In general, T_{shm} is important in the estimations of S_{re} and N_{avg} from the field monitoring data of steel bridges. The longer the monitoring period T_{shm} is, the more reliable the computations of S_{re} and N_{avg} are. Although the computed S_{re} and N_{avg} from the continuous monitoring data during about two to four weeks may converge or stabilize (Connor & Fisher 2006), it should be emphasized that the achieved stabilities in the estimated S_{re} and N_{avg} within T_{shm} depend primarily on the improved capacity of a continuous SHM to capture the actual loading conditions only. In other words, the actual variability of the loading conditions may be almost completely observed within a continuous period of about two to four weeks. On the other hand, much slower

33

processes of increasing S_{re} due to corrosion deteriorations are commonly undetectable within such a relative short monitoring period. Consequently, it will be essential to perform fatigue reliability assessment with the field monitoring data several times during the entire service life, where T_{shm} may be used to determine the maximum allowable time intervals. The SHM should be continuously performed within the maximum allowable time intervals or occurrences of any physical damage and/or significant change of the loading conditions. Ultimately, further studies on the time-dependent S_{re} and N_{avg} with the availability of a large number of long-term monitoring data may greatly improve lifetime fatigue life evaluation.

2.3.2   Probability Density Function

In fatigue reliability analysis, it is important to use the appropriate probability density functions (PDFs) considering uncertainties associated with fatigue resistance, R, and load effect, S. As mentioned previously, SHM for fatigue reliability assessment and prediction can provide efficient information on fatigue loading, especially for the estimation of equivalent stress range and the cumulative number of stress cycles. Due to the uncertainties, a probabilistic approach for fatigue life evaluation can be applied by using proper PDFs for reliable estimation of lifetime stress ranges as well as time-dependent fatigue resistance.

Based on extensive test results of welded steel bridge details performed by Keating and Fisher (1986), the mean value and standard deviation of the fatigue detail coefficient, A, on a log basis, are calculated. These statistical values can be used in a probabilistic approach when A is treated as random in fatigue reliability evaluation.

The Miner's critical damage accumulation index, Δ, is usually assumed as Lognormal (Wirsching 1984).

The PDF associated with the stress range, S, is commonly assumed as: (a) Lognormal, (b) Weibull, (c) Gamma, or (d) Rayleigh. Three-parameter PDFs including stress range cut-off threshold, s_c, as well as two-parameter PDFs with $s_c = 0$ can be derived. The PDFs of these distributions are

(a) Lognormal distribution

$$f_S(s) = \frac{1}{(s - s_c) \cdot \zeta \cdot \sqrt{2 \cdot \pi}} \cdot \exp\left[-\frac{1}{2} \cdot \left(\frac{\ln(s - s_c) - \lambda}{\zeta} \right)^2 \right] \quad \text{for } s > s_c \qquad (2\text{-}35)$$

where λ = location parameter, ζ = scale parameter, and s_c = cut-off threshold

$$E(S) = \exp(\lambda + 0.5 \cdot \varsigma^2) + s_c, \text{ and } \text{Var}(S) = [E(S) - s_c]^2 \cdot [\exp(\varsigma^2) - 1] \quad (2\text{-}36)$$

(b) Weibull distribution

$$f_S(s) = \frac{\beta}{\alpha} \cdot \left(\frac{s - s_c}{\alpha} \right)^{\beta - 1} \cdot \exp\left[-\left(\frac{s - s_c}{\alpha} \right)^\beta \right] \quad \text{for } s > s_c \qquad (2\text{-}37)$$

where α = scale parameter, β = shape parameter, and $\alpha > 0, \beta > 0$

$$E(S) = \alpha \cdot \Gamma\left(\frac{1}{\beta} + 1 \right) + s_c, \text{ and } \text{Var}(S) = \alpha^2 \cdot \left[\Gamma\left(\frac{2}{\beta} + 1 \right) - \left[\Gamma\left(\frac{1}{\beta} + 1 \right) \right]^2 \right]$$

$$(2\text{-}38)$$

(c) Gamma distribution

$$f_S(s) = \frac{\lambda \cdot [\lambda \cdot (s - s_c)]^{k-1}}{\Gamma(k)} \cdot \exp[-\lambda \cdot (s - s_c)] \quad \text{for } s > s_c \qquad (2\text{-}39)$$

35

where λ = rate parameter, k = shape parameter, and $\lambda > 0$, $k > 0$

$$E(S) = \frac{k}{\lambda} + s_c, \text{ and } \operatorname{Var}(S) = \frac{k}{\lambda^2} \tag{2-40}$$

(d) Rayleigh distribution

$$f_S(s) = \left(\frac{s - s_c}{S_{ro}^2}\right) \cdot \exp\left[-\frac{1}{2}\left(\frac{s - s_c}{S_{ro}}\right)^2\right] \quad \text{for } s > s_c \tag{2-41}$$

where S_{ro} = mode

$$E(S) = \sqrt{\frac{\pi}{2}} \cdot S_{ro} + s_c, \text{ and } \operatorname{Var}(S) = \left(2 - \frac{\pi}{2}\right) \cdot S_{ro}^2 \tag{2-42}$$

The defined $E(S)$ and $\operatorname{Var}(S)$ denote the mean values and dispersions of S, respectively. The parameters of each PDF can easily be calculated by using the relationship between the method of moments and the mean and variance from the stress range data. For each distribution, the equivalent stress range, S_{re}, can be derived using the qth moment of the stress range as follows:

$$E(S^q) = \int_0^\infty s^q \cdot f_S(s) \cdot ds \tag{2-43}$$

$$S_{re} = \left[\int_0^\infty s^q \cdot f_S(s) \cdot ds\right]^{\frac{1}{q}} = [E(S^q)]^{\frac{1}{q}} \tag{2-44}$$

Typically, fatigue sensitive structures are subjected to variable amplitude stress ranges (as indicated in stress range bin histograms) rather than constant amplitude fatigue. For estimation of fatigue life, variable amplitude stress ranges can be converted into an equivalent constant amplitude stress range by using Miner's rule.

The equivalent stress range assists equivalent estimation of fatigue damage with respect to that estimated from variable amplitude stress ranges (Fisher et al. 1998).

2.3.3 Fatigue Reliability Assessment

In civil engineering practice, examination of fatigue cracking must be a consideration for bridges, towers, off-shore platforms, and even naval ship structures under repeated loading (e.g., traffic, wind, wave, and so on). In other words, assessment for fatigue is necessary to be performed continuously with the well-defined fatigue limit state. The stress-range bin histogram data for load effects are collected by rain-flow counting method from SHM data at structural details, while the AASHTO *S-N* curves and the Miner's rule (1945) provide necessary information for fatigue resistance. Measurement error in SHM and traffic increase rate per year may be included as factors in the assessment of the fatigue reliability index (Frangopol et al. 2008 and Liu et al. 2010a).

A basic form of the limit-state function for fatigue reliability assessment is defined when including a measurement error factor, *e*, as:

$$g(X) = \Delta - e \cdot D \tag{2-45}$$

where $D = \sum n_i / N_i = (N / A) \cdot (S_{re})^m$.

In Eq. 2-45, Δ is Miner's critical damage accumulation index in terms of resistance and is assumed as lognormal with mean value of 1.0 and coefficient of variation (COV) of 0.3 for metallic materials, and D is Miner's damage accumulation index in terms of loading. The fatigue detail coefficient, *A*, associated with the defined

37

category can be treated as a random variable in fatigue reliability assessment (Liu et al, 2010a). By using Eq. 2-44, equivalent stress range, S_{re}, is calculated from the stress-range bin histogram and assumed PDF.

Under consideration of uncertainties, assumptions of the probabilistic distributions associated with fatigue loading S as well as resistance R offer an efficient opportunity not only to predict stress ranges during fatigue lifetime but also to estimate fatigue reliability. As an example, the conducted reliability assessment and performance prediction of fatigue sensitive structures are presented in Figure 2-7 (Liu et al. 2010a).

Further detailed procedures and practical applications for reliability assessment and performance prediction of fatigue sensitive structures by integrating field test data are described in the following chapters.

2.4 CONCLUDING REMARKS

In this chapter, the relevant approaches and methods pertaining to structural reliability analysis and reliability-based life-cycle management have been reviewed. This provides useful background information and guidance for applying probabilistic-based approaches to reliability assessment, performance prediction, and life-cycle management of fatigue sensitive structures and for incorporating field test data. Detailed procedures and applications for fatigue reliability assessment and performance prediction of bridge and ship structures by integrating field test data are described in Chapters 3 and 4, respectively. Chapters 5 and 6 deal with reliability-

based life-cycle management of bridge and ship structures, respectively. An approach

for system-based reliability assessment and prediction is presented in Chapter 7.
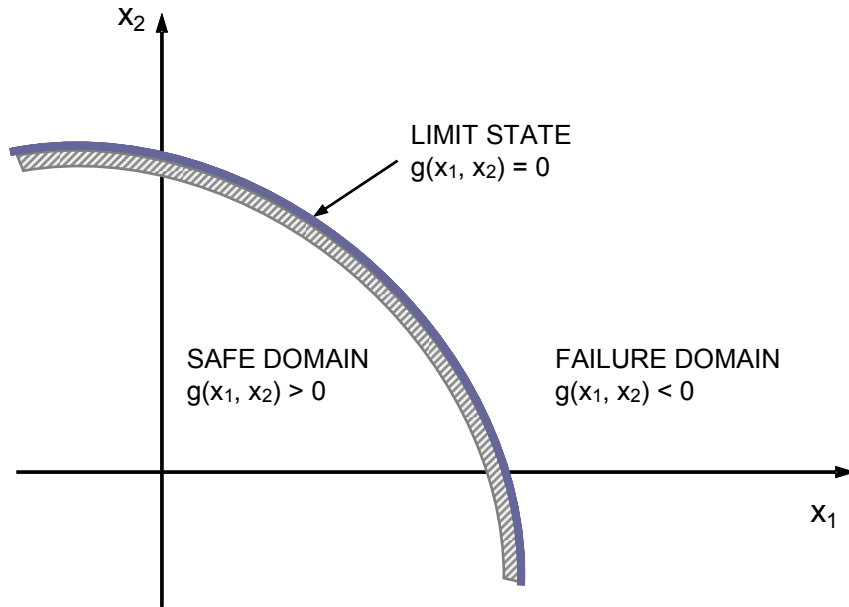
Figure 2-1   Schematic for three state functions: safe, failure and limit.
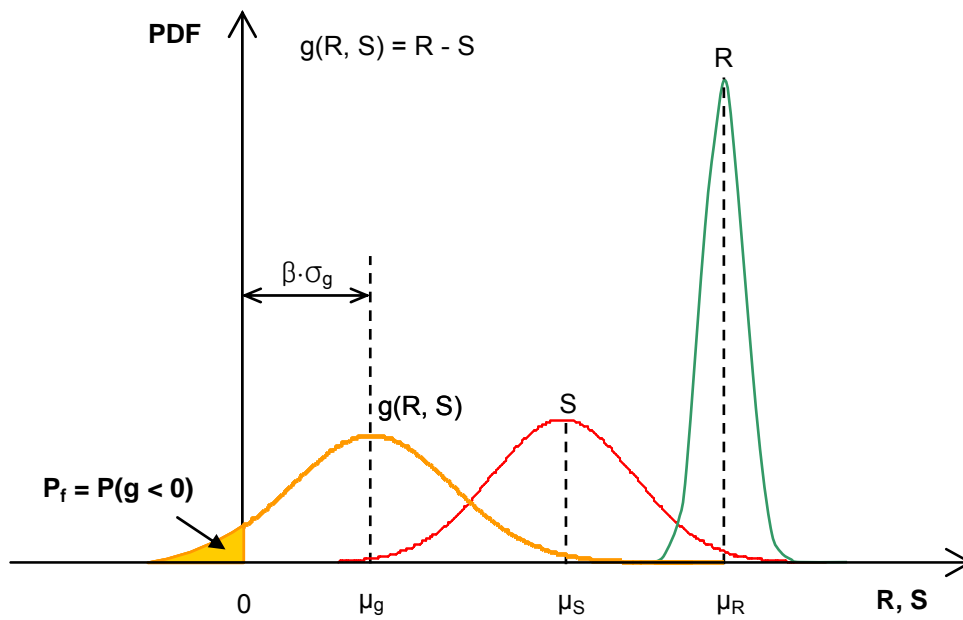
Figure 2-2   Safety margin concept with PDFs.
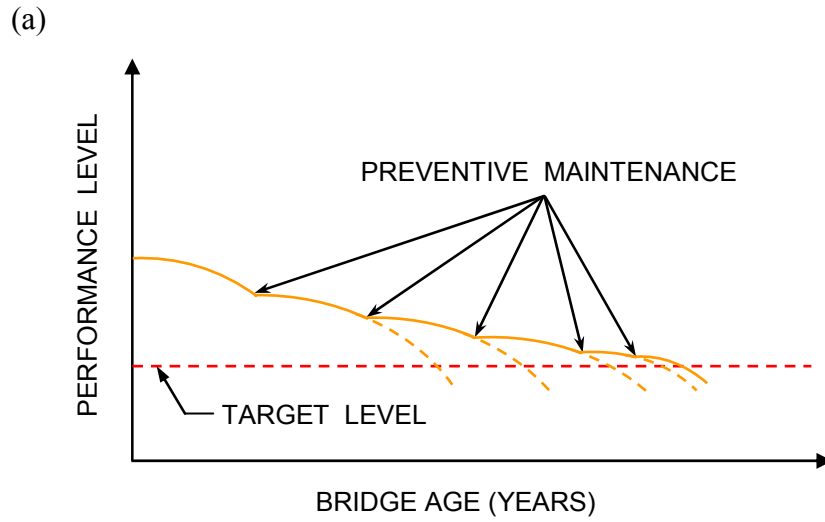
(a) preventive maintenance only
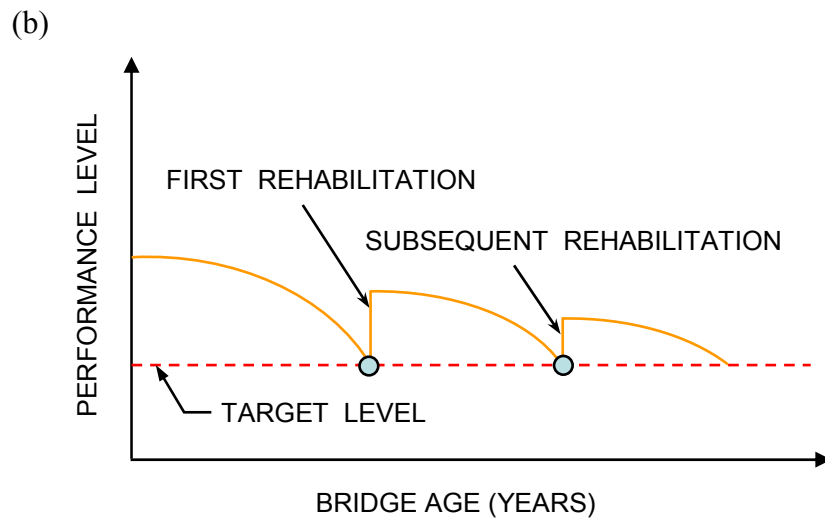
(b) essential maintenance only

Figure 2-3 Schematic lifetime performance profiles by subsequent maintenance
interventions (adapted from Kong et al. 2000).
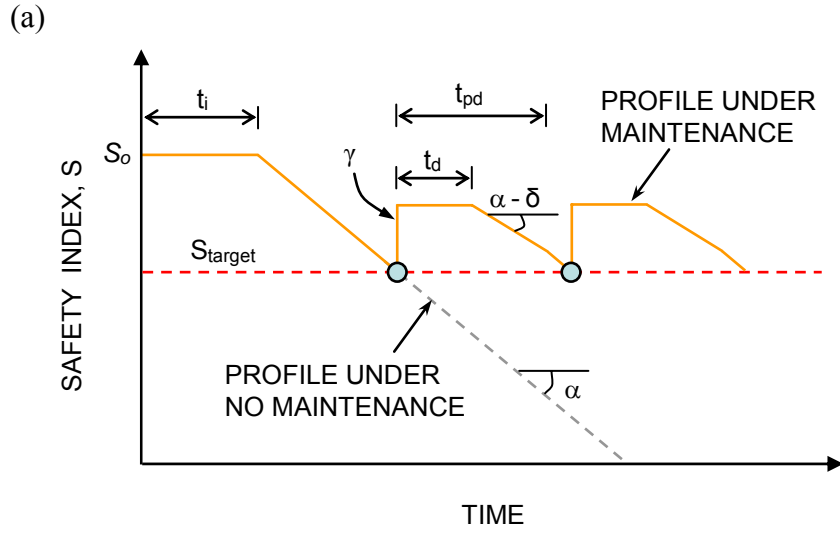
(a) safety index under safety-based maintenance
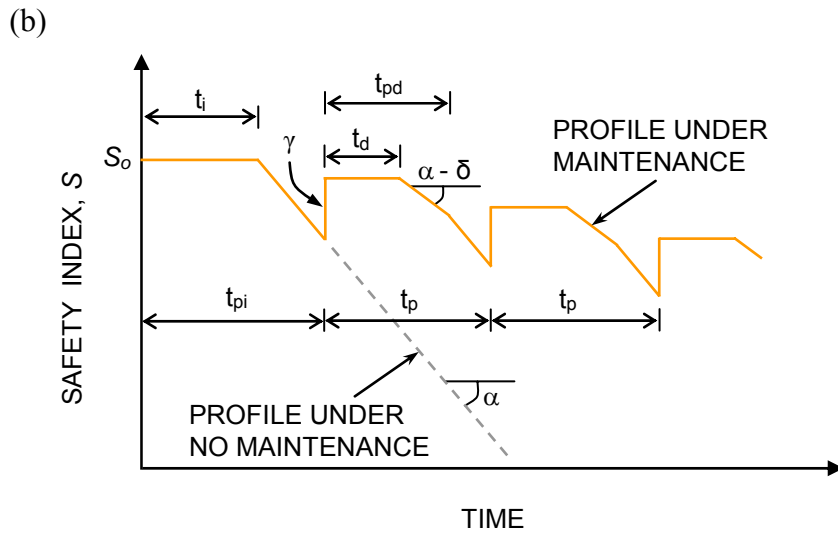
(b) safety index under time-based maintenance

Figure 2-4   Schematic lifetime performance profiles
(adapted from Frangopol & Neves 2003).

(a)
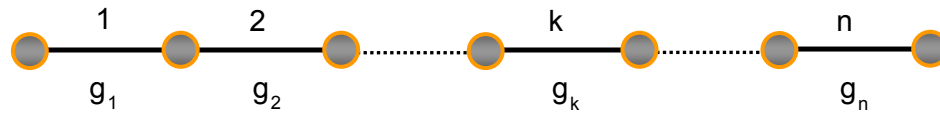
(a) series system model

(b)
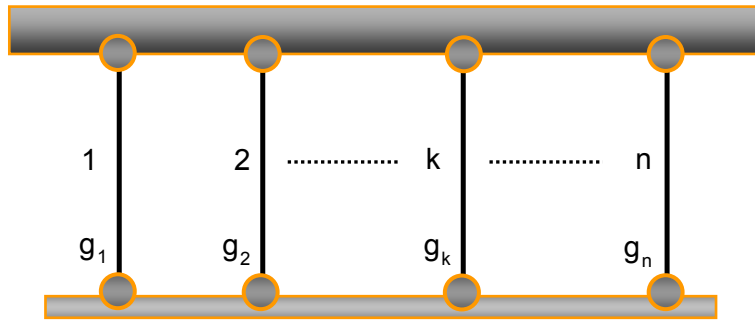
(b) parallel system model

(c)
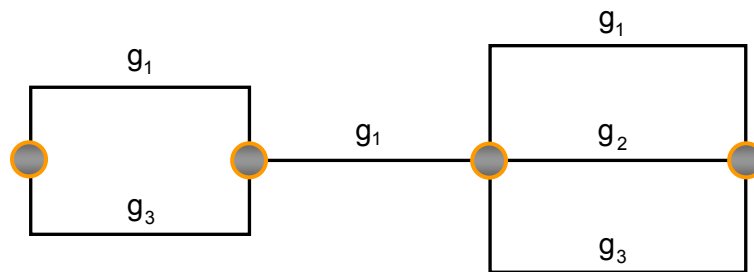
(c) series-parallel system model

Figure 2-5   Structural system models.

(a)

(a) AASHTO (2008)

(b)

(b) BS 5400 (1980)
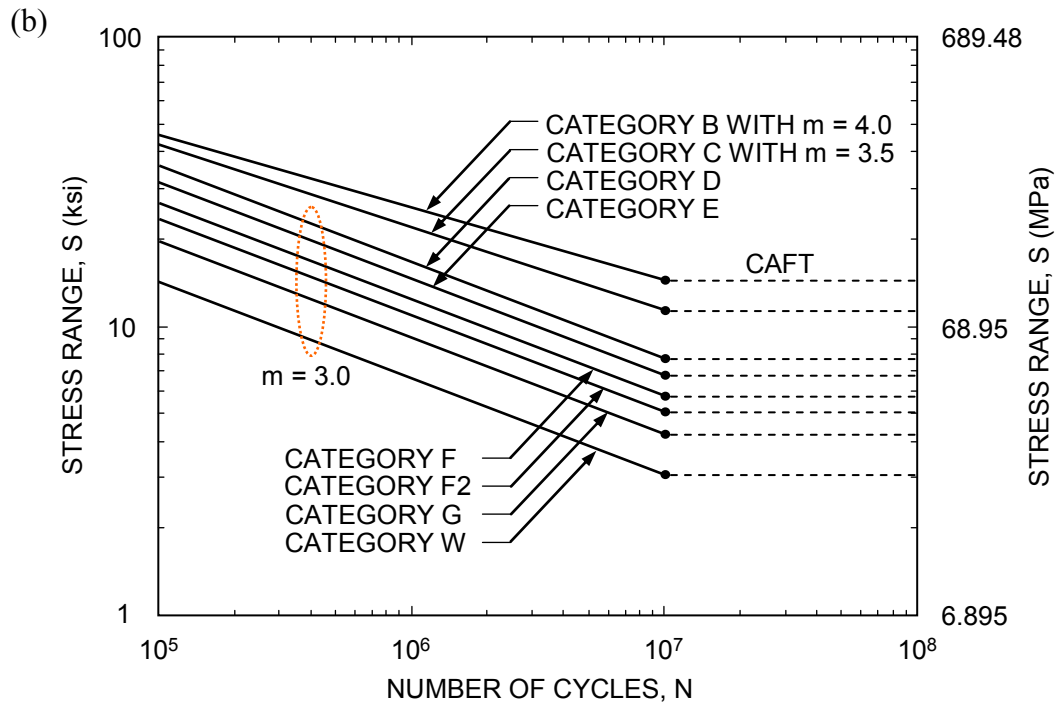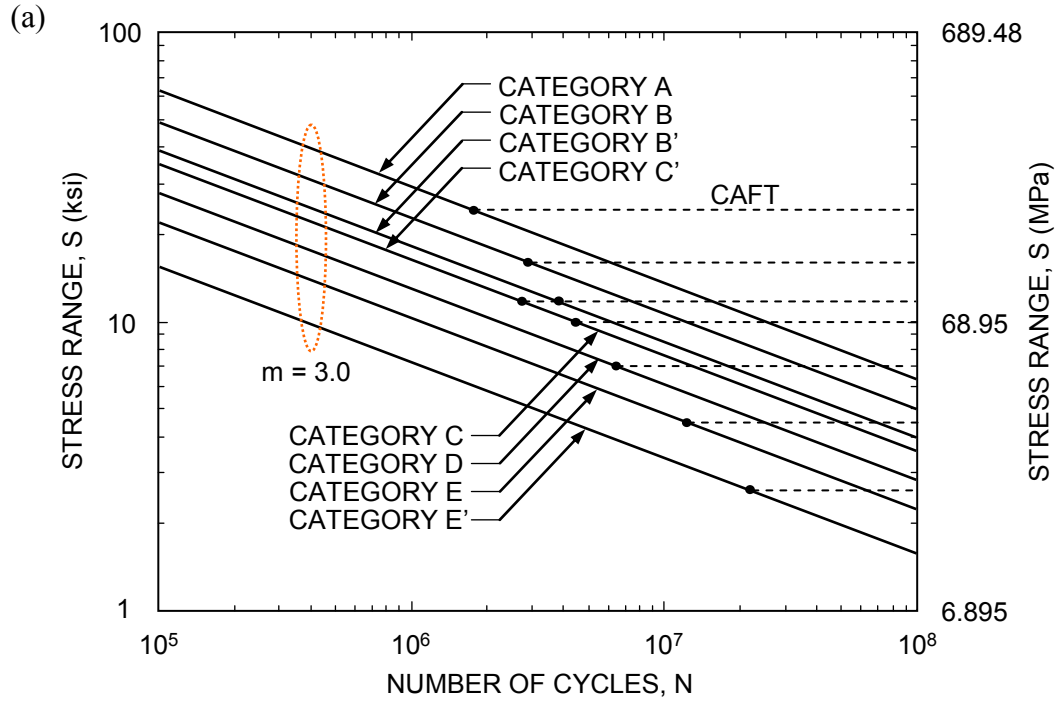
Figure 2-6   The S-N curves.

44
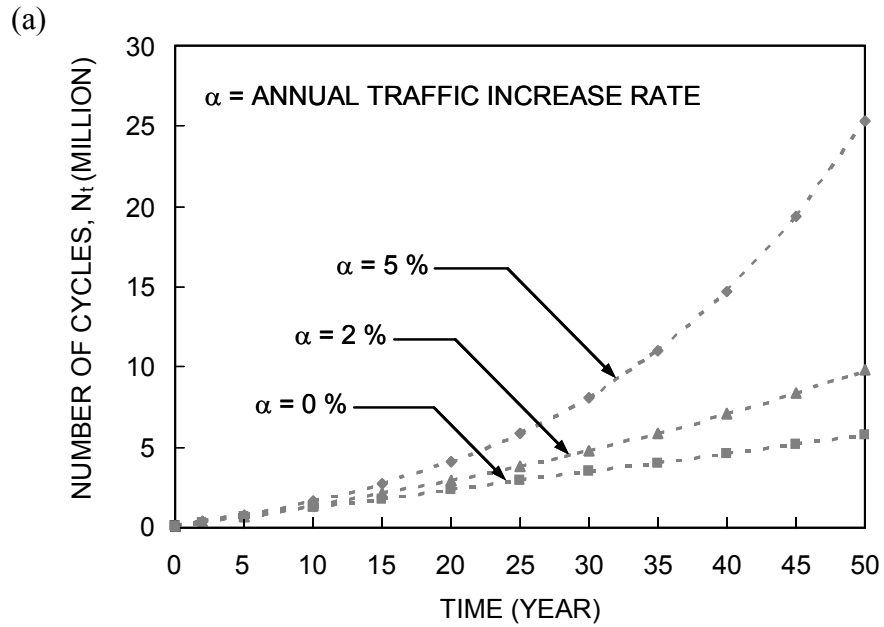
(a) predicted total number of cycles
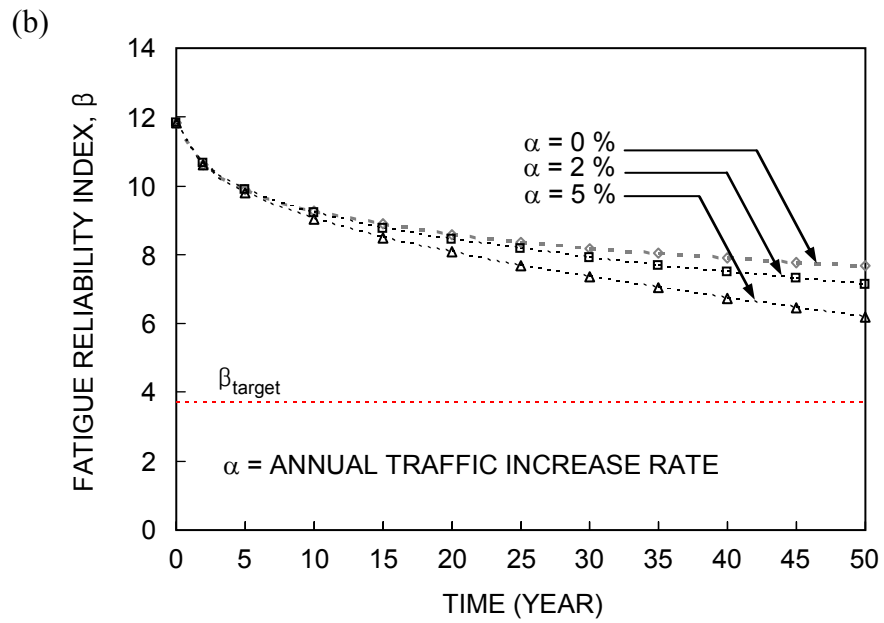
(b) time-dependent reliability index

Figure 2-7   Fatigue reliability assessment and prediction (Liu et al. 2010a).

CHAPTER 3

TIME-DEPENDENT STRUCTURAL RELIABILITY

OF STEEL BRIDGES

3.1   INTRODUCTION

This chapter describes the time-dependent structural reliability evaluation in aiming to reliably assess and predict lifetime fatigue performance of steel bridge structures under various uncertainties associated with environmental and mechanical stressors, errors in design, fabrication and/or construction, and unexpected load effects by traffic.

For fatigue failure mode of existing steel bridges, the linear and bi-linear *S-N* approaches are employed to estimate fatigue resistance, while loading data from structural health monitoring (SHM) are used to estimate load effect. In addition, reliability assessment by integrating a fracture mechanics approach, which identifies the time-dependent fatigue cracks, is addressed. Under uncertainties, an approach using probabilistic distributions associated with stress ranges is presented to effectively predict equivalent stress ranges for bridge fatigue reliability assessment. The fatigue detail coefficient, *A*, and the equivalent stress range, S_{re}, are both treated as random variables in the proposed fatigue reliability approach. These approaches are illustrated on existing steel bridges which are expected to experience finite or infinite fatigue life.

Section 3.2 deals with the time-dependent fatigue reliability assessment and prediction based on the linear *S-N* approach and SHM. Section 3.3 describes

estimation of fatigue life below the constant amplitude fatigue threshold (CAFT) of steel bridges by using a probabilistic approach based on the bi-linear *S-N*, with the integration of SHM data into the time-dependent fatigue reliability assessment. In Section 3.4, the associated summaries and conclusions are presented.

3.2 BRIDGE FATIGUE RELIABILITY ASSESSMENT AND PREDICTION BASED ON THE LINEAR S-N APPROACH AND SHM

3.2.1 Introduction

The initiated fatigue cracks in steel bridges have inevitably propagated due to the increase of service years. While this failure process happens, steel bridge performance may be seriously affected due to excessive and unpredictable crack growth. Therefore, lifetime structural performance for fatigue should be steadily assessed and predicted. For this purpose, a fatigue reliability method based on both the linear *S-N* approach and SHM is proposed.

To date, structural reliability analysis in many engineering fields has been well developed and widely applied. Basically, reliability theory is concerned with determining the probabilistic measure of safe performance. For estimating fatigue reliability, both resistance (capacity) and load effect (demand) have to be evaluated as primary. Typically, bridge fatigue resistance and load demand are evaluated by using the linear *S-N* curves provided in the AASHTO Specifications (2002) and stress-range bin histogram data from a long-term SHM program, respectively. In general, if the AASHTO Category of the structural detail is correctly classified, the necessary information on fatigue resistance of structural members can be easily obtained from

47

the AASHTO Specifications. However, finding the reliable loading history may be impossible without field monitoring data.

Modern concepts for bridge maintenance and monitoring programs under uncertainty have been developed (Frangopol & Estes 1997, Frangopol & Messervey 2007, and Frangopol & Liu 2007). Several researchers have studied the effective design of monitoring systems to produce more reliable results. The measured data from the monitoring systems can be used for fatigue reliability assessment (Frangopol et al. 2008 and Liu et al. 2010). In this context, the application of several probability density functions (PDFs) based on field monitoring data can be effectively considered in prediction models.

In 1982, the ASCE Committee on Fatigue and Fracture Reliability (1982) discussed possible use of probabilistic distributions for fatigue analysis. The application of several PDFs for estimating equivalent stress range was reported by Chung (2004). Weibull, Beta, and Lognormal distributions for loading were used to estimate equivalent stress range. Pourzeynali and Datta (2005) applied Weibull and Lognormal distributions to perform fatigue reliability analysis of suspension bridges. Thus, various PDFs of load effects can be applied in fatigue reliability assessment. However, since fatigue reliability may be significantly affected by the type of PDF of stress range, goodness-of-fit tests have to be conducted to find the best fit.

In fatigue reliability assessment based on the linear S-N approach and SHM, there are two important parameters to consider (i) fatigue detail coefficient, A, in terms of resistance and (ii) equivalent stress range, S_{re}, in terms of loading, respectively. Fatigue detail coefficient, A, is provided as deterministic based on the AASHTO

48

Specifications (2002). Equivalent stress range, S_{re}, is also considered as deterministic. However, these two parameters may need to be taken into account as random variables for more reliable fatigue performance assessment under uncertainties associated with both terms. Accordingly, A and S_{re} are herein treated as random variables.

Indeed, it is extremely important to define the threshold that directly affects calculation of equivalent stress range. This is because fatigue life can be often overestimated or underestimated by the computed equivalent stress ranges according to the predefined cut-off stress ranges. According to Connor and Fisher (2006), the applicable cut-off stress ranges are predefined. It provides the possibility to estimate the mean value and standard deviation of equivalent stress range, S_{re}.

Based on all necessary information from the AASHTO Specifications (2002) and SHM, fatigue reliability analysis of structural members is conducted by using the reliability software CalREL (Liu et al. 1989) and/or RELSYS (Estes & Frangopol 1998). As illustrations, structural details of two existing bridges, the Neville Island Bridge and the Birmingham Bridge, which are both located in Pittsburgh, Pennsylvania, are investigated for fatigue reliability assessment. The Neville Island Bridge is representative for finite fatigue life, whereas the Birmingham Bridge is representative for infinite fatigue life. The field monitoring data for both bridges are provided by the National Engineering Research Center, ATLSS, at Lehigh University (Connor et al. 2004 and 2005).

3.2.2 Limit-State Function for Fatigue

The AASHTO approach to fatigue reliability assessment is based on the *S-N* curves in the AASHTO Specifications (2002) and the Miner's rule (Miner 1945). The corresponding limit-state equations for fatigue details in consideration can be simply expressed as (Raju et al. 1990)

$$g(X) = N_c - N_t = 0 \tag{3-1}$$

where N_c = total number of stress cycles to fatigue failure under variable stress range and N_t = accumulated number of stress cycles applied to the fatigue details during the period from the start of fatigue damages to the time t under consideration. N_c dependent on variable amplitude stress range, S, can be expressed as (Liu et al. 2010)

$$N_c = \frac{A \cdot \Delta}{E(S^q)} \tag{3-2}$$

where A = fatigue detail coefficient which can be treated as a random variable; q = material constant which can be assigned as the constant of 3.0 representing the slope of the *S-N* curve (i.e., $q = m = 3.0$ as defined in Chapter 2); $E(S^q)$ = mean value of S^q indicating the qth moment of S with probability density function (PDF) $f_S(s)$; and Δ = Miner's critical damage accumulation index in terms of resistance which is assumed as lognormal with the mean value of 1.0 and its coefficient of variation (COV) of 0.3 for metallic materials (Wirsching 1984), which is related to the Miner's damage accumulation index, D, (Miner, 1945)

$$D = \sum_{i=1}^{k} \frac{n_i}{N_{ci}} = \frac{N_c}{A} \cdot E(S^q) = \frac{N_c}{A} \cdot \int_0^{\infty} [S^q \cdot f_S(s)] \, ds \tag{3-3}$$

where k = maximum number of stress range levels S_i (i = 1, 2, ..., k) under consideration; n_i = number of cycles under constant stress range level S_i; and N_{ci} = total number of cycles to fatigue failure under constant stress range level S_i.

Similarly, when the accumulated number of stress cycles N_t is represented by the time-dependent PDF g_N (n, t), N_t can be calculated for the entire period of time T. A typical S–N curve is extended for a detail expected to have finite fatigue life (i.e., linear in logarithmic form with the same slope), whereas it stays constant in the constant amplitude fatigue threshold (CAFT) for theoretically infinite fatigue life. After reaching the specified number of cycles, $N_S = A/CAFT^q$, at the specified time, T_S, the S-N curve can continue to decrease (i.e., finite life) or remain constant (i.e., infinite life). Accordingly, N_t can be expressed as

$$N_t = \int_0^{T_S} \int_0^{\infty} [n \cdot g_N(n,t)] \ dn \cdot dt + \int_{T_S}^{T} \int_0^{\infty} [n \cdot g_N(n,t)] \ dn \cdot dt \qquad (3\text{-}4)$$

It is noted that the second term of Eq. 3-4 can be ignored in the calculation of N_t for infinite life (i.e., $N_t = N_S$ when $t > T_S$). Using Eq. 3-4, the limit-state equation 3-1 can be rewritten as

$$g(\boldsymbol{X}) = \frac{A \cdot \Delta}{\int_0^{\infty} [S^q \cdot f_S(s)] \ ds}$$

$$-\left[\int_0^{T_S} \int_0^{\infty} [n \cdot g_N(n,t)] \ dn \cdot dt + \int_{T_S}^{T} \int_0^{\infty} [n \cdot g_N(n,t)] \ dn \cdot dt \right] = 0 \qquad (3\text{-}5)$$

As previously described in Chapter 2, for useful estimation of fatigue life, equivalent stress range, S_{re}, can be acceptably used as the constant amplitude fatigue loading rather than the variable amplitude stress ranges. Consequently, the defined limit-state equation 3-5 is defined in more general form based on the AASHTO Specifications (2008) and Miner's rule (Miner 1945) as follows:

$$g(X) = \Delta - D = \Delta - \left(\frac{N_t}{A}\right) \cdot S_{re}^q = 0 \tag{3-6}$$

3.2.3 Integration of SHM Data into Fatigue Reliability Assessment

Structural health monitoring (SHM) can provide actual information on fatigue loading, that is, $f_S(s)$ and $g_N(n, t)$, especially S_{re}. The PDF $f_S(s)$ can be obtained from the stress-range bin histogram collected by using the rain-flow cycle counting method or other approaches (Downing & Socie 1982 and Clarke et al. 2000) during the monitoring period. Based on the established stress-range bin histogram, S_{re} is computed considering the cubic root of the mean cube of all stress ranges (i.e., $q = 3.0$ or $m = 3.0$), that is

$$S_{re} = \left[\sum \frac{n_j}{N_{total}} \cdot S_{rj}^3\right]^{\frac{1}{3}} \cong \left[\int_0^\infty [S^3 \cdot f_S(s)]\ ds\right]^{\frac{1}{3}} \tag{3-7}$$

It is noted that the histogram data generated from the field monitoring contain typically a large number of low magnitude stress cycles due to light vehicles, low winds or other secondary vibrations, and/or even electrostatic or electromagnetic noises if the strain gage signals are not filtered (Zhou 2006). These low magnitude

stress cycles make no contributions to cumulative fatigue damages, but, when included in the computation of S_{re} in Eq. 3-7, yield its smaller value. As a result, the actual fatigue resistance in a detail may be overestimated from the associated S-N curve. Therefore, S_{re} should be computed only considering higher stress ranges than a predefined stress range cut-off threshold.

From a large number of laboratory experiments under constant amplitude cyclic loading, the CAFT is established for each category classified in the AASHTO Specifications as presented in Table 3-1. Typically, no fatigue cracks appear if the applied stress cycles have the constant amplitude smaller than the corresponding CAFT. For the variable amplitude stress cycles monitored, the upper limit of a cut-off stress range is typically as high as about 25% to 33% CAFT (Connor et al. 2004 and 2005). When the number of cycles corresponding to lower stress ranges is considered, it has been demonstrated that the cumulative fatigue damage by the calculated equivalent stress range becomes asymptotic to the applicable S-N curve (Fisher et al. 1993). Therefore, the lower limit of a stress range cut-off level can be assigned. Sensitivity studies on the predefined thresholds will be conducted in this study by using applicable stress range cut-off thresholds.

For effectively assessing lifetime fatigue performance of steel bridges, it is necessary to integrate a long-term SHM program into the fatigue reliability evaluation (Liu et al. 2010a and Kwon & Frangopol 2008 and 2009). SHM in respective fatigue details can easily provide the histograms of the collected daily number of stress cycles associated with the daily number of passages of the heavy vehicle traffic during the monitoring period T_{shm}. The PDF $g_N(n)$, which is used to fit the histogram of the

collected daily number of stress cycles, represents $g_N(n, t)$ within T_{shm}. The time adjustment factor $\xi(t)$ reflecting T_{shm} and the annual traffic increase rate, α, is considered in $g_N(n, t)$. Thus, Eq. 3-4 can be rewritten as

$$N_t = \int_0^{T_S} \left[\int_0^{\infty} (n \cdot g_N(n)) \, dn \right] \cdot \xi(t) \, dt + \int_{T_S}^{T} \left[\int_0^{\infty} (n \cdot g_N(n)) \, dn \right] \cdot \xi(t) \, dt$$

$$= N_{avg} \cdot \left[\int_0^{T_S} \xi(t) \, dt + \int_{T_S}^{T} \xi(t) \, dt \right] \tag{3-8}$$

where N_{avg} = average daily number of stress cycles which is the mean value of the collected daily number of stress cycles from SHM within T_{shm}. $\xi(t)$ quantifying the variability of during the entire period T is expressed as

$$\xi(t) = 365 \cdot (1 + \alpha)^t \tag{3-9}$$

Therefore, the limit-state equation in Eq. 3-6 can be rewritten as

$$g(X) = \Delta - 365 \cdot N_{avg} \cdot \left[\int_0^{T_S} (1 + \alpha)^t \, dt + \int_{T_S}^{T} (1 + \alpha)^t \, dt \right] \cdot \left(\frac{e \cdot S_{re}^q}{A} \right) = 0 \tag{3-10}$$

where e = measurement error factor in SHM which may be considered as a lognormal distributed random variable with $E(e) = 1.0$ and $COV(e) = 3\%$ (Frangopol et al. 2008). If SHM data is not available, N_{avg} can be approximately estimated based on the well documented data associated with average daily truck traffic (ADTT) and corresponding number of stress cycles (e.g., AASHTO Specifications 2008).

3.2.4   Fatigue Reliability Analysis

Bridge fatigue life can be predicted more reliably if fatigue reliability

evaluation is conducted based on both the AASHTO *S-N* curve for fatigue resistance and SHM data for fatigue loading considering uncertainties. As addressed in Chapter 2, the reliability of a structural component or system is related to the probability of not violating a particular limit state. Based on the limit-state function defined in Eq. 3-10, the fatigue reliability index, β, that is related to the probability of failure, P_f, is estimated. The statistical information on the assumed PDFs for fatigue resistance $R = \Delta \times A$ and load effect $S = N_t \times e \times S_{re}^q$ is directly used in the fatigue reliability analysis. Assuming that Δ, A, e, and S_{re} are lognormal random variables (see, Eqs. 3-6 and 3-10), the equivalent performance function adopted is expressed as

$$g(\boldsymbol{X}) = \ln(R/S) = \ln R - \ln(S) = \ln(\Delta \times A) - \ln(N_t \times e \times S_{re}^q)$$

$$= \ln \Delta + \ln A - (\ln N_t + \ln e + q \cdot \ln S_{re}) \tag{3-11}$$

Therefore, the fatigue reliability index, β, can be explicitly obtained by

$$\beta = \frac{\lambda_\Delta + \lambda_A - (\ln N_t + \lambda_e + q \cdot \lambda_{S_{re}})}{\sqrt{\zeta_\Delta{}^2 + \zeta_A{}^2 + \zeta_e{}^2 + (q \cdot \zeta_{S_{re}})^2}} \tag{3-12}$$

The parameters, λ_y and ζ_y denote the mean value and standard deviation of $\ln y$ (i.e., $y = \Delta$, A, e, or S_{re}), respectively. Detailed information associated with deterministic parameters and random variables is summarized in Table 3-2. It is noted that, in this research, all reliability analyses for estimation of the time-dependent fatigue reliability index are performed using the reliability software CalREL (Liu et al. 1989) or RELSYS (Estes & Frangopol 1998) that takes into account various PDFs associated with the defined random variables.

The procedure for the fatigue reliability evaluation is summarized as follows:

Step 1: *Investigating the S-N values of the fatigue details*

The AASHTO Specifications (2008) provide relevant information including the AASHTO category, CAFT, and *A*, in terms of fatigue resistance *R*. For common steel members, the mean value and coefficient of variation of the Miner's critical damage accumulation index *Δ* (see Eq. 3-10) are assumed to be 1.0 and 0.3, respectively (Wirsching 1984).

Step 2: *Establishing the stress-range bin histogram from the collected SHM data*

At the installed sensor locations, the stress-range bin histograms from SHM data are established by using the rain-flow counting method. In a SHM program, the rain-flow analysis algorithm can be programmed to ignore any stress ranges less than 3.45 MPa (0.5 ksi) since small stress cycles do not contribute to the overall fatigue damage.

Step 3: *Determining the stress range cut-off thresholds*

Due to loading uncertainty, it is essential to determine in a rational way a predefined cut-off stress range level in order to estimate S_{re} from the stress-range bin histogram data. A probabilistic approach is used to assess the mean value and standard deviation of the calculated equivalent stress ranges from predefined stress range cut-off thresholds.

For all welded steel details, the upper limit of a cut-off stress range is typically about 25% to 33% CAFT (Connor et al. 2004 and 2005). The lower limit can be determined from the relationship between the equivalent stress range and the cumulative number of cycles calculated in all stress range cut-off levels (Fisher et al.

1993). Applicable stress range cut-off thresholds are considered in ranges from 3.45 MPa (0.5 ksi) as a minimum to 33% CAFT as a maximum.

A structural component may be driven into fatigue if the maximum stress range exceeds the corresponding CAFT. In other words, the detail may experience finite fatigue life. For this case, frequency (i.e., ratio of the number of cycles exceeding the CAFT to the total cumulative number of cycles) exceeding the CAFT has to be investigated before determining the stress range cut-off thresholds. In a conservative manner, frequency limit, which is considered to be damage-causing, can be set as 0.01 % (Connor et al. 2006). If the calculated frequency at a detail does not exceed this limit, then it is reasonable to conclude that fatigue cracking will not be expected during its lifetime (i.e., fatigue life can be assumed as infinite).

Furthermore, if equivalent stress range corresponding to the 25% CAFT cut-off level exceeds one-half of the CAFT, a detail is expected to experience finite fatigue life. When the calculated S_{re} is larger than 50% CAFT, the AASHTO *S-N* curve has to be extended to assess finite fatigue life. Conversely, fatigue life is theoretically defined as infinite if equivalent stress range is less than 50% CAFT or if the maximum stress range experienced by a detail is less than the CAFT (i.e., frequency = 0.00 %).

Step 4: *Estimating the mean value and standard deviation of S_{re} by PDFs*

Several stress ranges can be predefined as cut-off stress ranges (see Step 3). Based on the truncated stress-range bin histograms, the assumed PDFs (i.e., Lognormal, Weibull, or Gamma) are fitted to the histograms truncated by the predefined cut-off stress ranges. S_{re} is computed by using the assumed PDFs in each cut-off stress range, and then its mean value and standard deviation are calculated.

Step 5: *Determining the average-daily and annual-cumulative number of cycles*

Based on the truncated stress-range bin histograms, the mean value of S_{re} is calculated, and the corresponding total number of cycles is estimated. The total number of cycles is divided by the total monitoring time to estimate the average daily number of cycles, N_{avg} that can be alternatively estimated considering the number of stress cycles per truck passage from the average daily truck traffic, *ADTT*. In the following, the annual cumulative number of cycles, $N_t(t)$, is estimated by using N_{avg} and α (traffic increase rate per year).

Step 6: *Performing fatigue reliability evaluation*

For a given year, the reliability index for fatigue is estimated by using Eq. 3-12 for the lognormal distribution with all necessary information from steps 1 to 5. For the other assumed PDFs (e.g., Weibull, Gamma), the reliability software RELSYS (Estes & Frangopol 1998) can be used to compute fatigue reliability index, β.

3.2.5   Application Example I – Neville Island Bridge

As the first illustration, fatigue reliability assessment of an existing bridge, the Neville Island Bridge located in Pittsburgh, Pennsylvania, is performed by using the PDFs based on the monitoring data. The real monitoring data are provided from field testing performed by the ATLSS Engineering Research Center at Lehigh University.

The Neville Island Bridge carries interstate I-79 over the Ohio River. The main span is a 228.6 m (750 ft) tied arch opened in 1976. During periodic inspections of the bridge, cracks were found at the welded connection between the top flange and transverse connection plates. According to Connor et al. (2005), the cause for cracks

located at the welded connection was the result of floor-beam flexibility and the incompatibility between the floor-beam and the deck slab. In 2004, a complete fatigue and fracture evaluation of the bridge was performed to address the problem identified during periodic inspections with long-term monitoring programs. Four portions of the bridge were selected for field instrumentation (i.e., ramp J, tied-arch, spans 25 and 26, and ramp A) in the monitoring programs. In this study, the monitoring data collected at the channels CH-9 and CH-17 of span 25, as shown in Figure 3-1(a) and (b), respectively, are used to estimate fatigue life by using the proposed fatigue reliability approach. The long-term monitoring of span 25 was conducted from March to April, 2004 for a total of almost 29 days (i.e, T_{shm} = 29). The complete description of the bridge and further details can be found in Connor et al. (2005).

3.2.5.1   Details of Structural Members and SHM Data: Steps 1 and 2

Details of fatigue resistance and monitoring data, which are associated with the two channels CH-9 and CH-17, are used to illustrate the probabilistic fatigue reliability assessment process. Based on the AASHTO Specifications (2002), the AASHTO parameters (i.e., AASHTO Category, CAFT, and A) are investigated at both channels and indicated in Table 3-1. The channel CH-9 installed on the transverse stiffeners at the toe of the stiffener-to-flange weld can be classified as Category C by the AASHTO, whereas the channel CH-17 mounted on the web of the floor-beam at the top flange cope can be classified as Category E. The corresponding CAFTs of the channels CH-9 and CH-17 are 68.9 MPa (10.0 ksi) and 31.0 MPa (4.5 ksi), respectively.

The stress-range bin histogram for the details CH-9 and CH-17 collected by the rain-flow counting method are shown in Figure 3-2(a) and (b), respectively. The maximum stress ranges, 110.3 MPa (CH-9) and 51.7 MPa (CH-17) at both channels exceeds the defined CAFT and also the frequency exceeds the limit of 0.01 % regardless of the predefined stress range cut-off thresholds. Therefore, the fatigue lives of the channels CH-9 and CH-17 are expected as finite (Connor et al. 2005 and Kwon & Frangopol 2010a).

3.2.5.2   Estimation of Equivalent Stress Range by the PDFs: Steps 3 and 4

For efficient fatigue reliability assessment of the selected channels, the collected stress-range bin histogram data at both channels are appropriately truncated. As noted previously, the applicable stress range cut-off thresholds can range between 3.45 MPa (0.5 ksi) as a minimum and 33% CAFT as a maximum. According to the predefined thresholds (i.e., 6.89 MPa to 20.68 MPa) of the channel CH-9 and assuming COV(S_{re}) = 0.2, the fatigue reliability analysis is performed to investigate the effect of stress range cut-off thresholds on fatigue reliability (see Eq. 3-12). Figure 3-3 shows that the fatigue reliability index, β, becomes more critical due to relatively increased cumulative number of cycles at the lower cut-off stress range level under consideration.

Based on the truncated stress-range bin histograms, the PDFs using two- and three-parameter are generated to investigate the effect of shifted distributions considering the stress range cut-off threshold, s_c, on equivalent stress range (see Figure 3-4 and Figure 3-5); in case of two-parameter lognormal PDF, λ and ζ are the

parameters considered. As shown in Table 3-3, the computed equivalent stress ranges in both cases are almost similar regardless of the assumed PDFs. Accordingly, the PDFs considering two-parameter with $s_c = 0$ are used in this study to estimate S_{re} in the fatigue reliability assessment.

Based on the histograms established from the SHM period (i.e., $T_{shm} = 29$ days), the relationship between S_{re} and N_t is plotted in Figure 3-6(a) and (b) with the *S*-*N* curve corresponding to the Categories *C* and *E*, respectively. For the predefined stress range cut-off thresholds, equivalent stress ranges are calculated by using Eq. 3-7. The mean value and standard deviation of the calculated equivalent stress ranges are 31.96 MPa (4.64 ksi) and 4.86 MPa (0.71 ksi) at the channel CH-9, respectively, while those at the channel CH-17 are 13.96 MPa (2.02 ksi) and 4.08 MPa (0.59 ksi), respectively. It is noted that, as a constant cut-off threshold, Connor et al. (2005) selected 17.24 MPa (2.5 ksi) at CH-9 and 6.89 MPa (1.0 ksi) at CH-17. The corresponding equivalent stress ranges by using Eq. 3-7 are 34.92 MPa (5.07 ksi) and 14.94 MPa (2.17 ksi), respectively.

According to the selected stress range cut-off thresholds, the PDFs (i.e., Lognormal, Weibull, and Gamma) fitted on the respective truncated stress-range bin histograms are plotted in Figure 3-7(a), (b), and (c) for the assumed PDFs at the channel CH-9. The notation, CUTi ($i = 1, 2, …, p$), indicates that the stress ranges below i-th among the applicable predefined thresholds are cut off. Each stress range cut-off level is used to calculate its corresponding S_{re} (see Eq. 3-7). The computed mean value, $E(S_{re})$, and standard deviation, $\sigma(S_{re})$, of S_{re} are presented in Table 3-4.

3.2.5.3 Estimation of N_{avg} and $N_t(t)$: Step 5

By using the estimated N_{avg} from the SHM data, the annual cumulative number of cycles, $N_t(t)$, is predicted for the time-dependent fatigue reliability assessment. Through the previous steps, the various PDFs considering uncertainty of load effects were developed in the truncated stress-range bin histograms, and the mean value of the equivalent stress range, $E(S_{re})$, was calculated. The total number of cycles corresponding to the $E(S_{re})$ can be easily estimated from the relationship between the equivalent stress range and the number of cycles accumulated during T_{shm}.

N_{avg} is estimated by the PDFs considered at each channel, as presented in Table 3-4. N_{avg} is herein treated as deterministic with traffic increase rate per year (i.e., $\alpha =$ 0%, 3%). By applying N_{avg} and α, the annual cumulative number of cycles, $N_t(t)$, is easily calculated. It should be noted that since any retrofit options at the channels were not conducted until the long-term monitoring period in 2004, the annual number of cycles has been accumulated from the bridge opening.

3.2.5.4 Fatigue Reliability Analysis: Step 6

All necessary information for the probabilistic fatigue reliability analysis is obtained from steps 1 through 5, and the fatigue reliability analysis is conducted using the reliability software RELSYS (Estes & Frangopol 1998). The effect of the PDF of S_{re} on fatigue reliability is investigated. For this purpose, the fatigue reliability evaluation is performed when S_{re} is assumed Lognormal, Weibull, or Gamma.

As shown in Figure 3-8(a) and (b), the fatigue reliability indices estimated by Weibull and lognormal distributions represent upper and lower bounds, respectively.

A goodness-of-fit test by using the Anderson and Darling (1952) method assigning more weight to the tail of a candidate distribution, was conducted to find a best fit of the PDF. The upper tail not the median of the distribution can be of interest in fatigue areas since design values for fatigue life are determined by the upper tail of the defect size distribution (Tiryakioğlu 2008). Therefore, it can be appropriate for a fatigue limit state. As shown in Figure 3-9, lognormal PDF was the best fit of the stress range data obtained from the SHM. Consequently, bridge fatigue life may be predicted by using lognormal PDFs in both terms.

Accordingly, the fatigue reliability analyses are herein performed by using lognomal PDFs in terms of fatigue resistance and load effect. Based on survival probability of 95% (AASHTO 2002), a target reliability index of 1.65 is assumed implying a failure probability of approximately 0.05. It is noted that a target reliability level may be determined according to the importance levels of respective structural details. As shown in Figure 3-10(a) and (b), the fatigue reliabilities were evaluated at the channels CH-9 and CH-17, and their remaining lifetime was estimated based on the predefined target reliability index of 1.65. The estimated remaining lifetime is then compared to that calculated from the AASHTO basic equation ($N_{rem} = A / S_{re}^3$). Based on this equation, the calculated remaining life at the channels CH-9 and CH-17 is 4 and 29 years, respectively, from the monitoring time, 2004. However, the detail CH-17 in 2004 had already cracks (Connor et al. 2005). Therefore, it is expected that actual fatigue life of the channel CH-17 was completed earlier than the monitoring time. For the channel CH-9, the remaining life after the monitoring is estimated as 2 years, while the remaining life of the channel CH-17 is estimated as -6 years.

Therefore, bridge assessment and prediction using the proposed fatigue reliability approach that is based on the linear *S-N* approach and SHM can be carried out effectively by means of quantifying the time-dependent fatigue damage, when both the fatigue detail coefficient, *A*, and equivalent stress range, S_{re}, were taken into account as random variables.

3.2.6   Application Example II – Birmingham Bridge

As the second illustration, fatigue reliability assessment of an existing bridge, the Birmingham Bridge located in Pittsburgh, Pennsylvania, is performed by using the PDFs based on the monitoring data. The real monitoring data are also provided from field testing performed by the ATLSS Engineering Research Center at Lehigh University.

The Birmingham Bridge carries SR2085 over the Monongahela River. The main span of the structure is a 189.0 m (620 ft) tied arch designed in 1973 and opened in 1976. Multi-girder approach spans flank each side of the tied arch. The floor-beams are spaced at 9.45 m (31 ft) and are 2.84 m (111 in.) deep. In 2002, fatigue cracks have been found in nearly all of the transverse floor-beams at the connection to the tie girders. According to Connor & Fisher (2002), the cracking was the result of relative longitudinal displacement that occurred between the floor system and the tie girder. It was retrofitted to soften the connection by removing a portion of the floor-beam flange and web near the tie girder to prevent stresses within the web gap from concentrating (Connor & Fisher 2002 and Connor et al. 2004). As an inspection of the retrofitted regions, the cut-off region with instrumentation plan was monitored from October to

December, 2003. The long-term monitoring data were collected for a total of almost 40 days. The complete description of the bridge and further details after retrofit can be found in Connor & Fisher (2002) and Connor et al. (2004).

A total of 32 uniaxial strain gages were installed symmetrically on retrofit cut-off regions both upstream and downstream of the bridge. The collected monitoring data at two channels CH-7 and CH-11 (see Figure 3-11) are used to illustrate the fatigue reliability assessment for infinite fatigue life. The AASHTO Specifications (2002) offer necessary information regarding the AASHTO Category, CAFT, and fatigue detail coefficient, A, of CH-7 and CH-11 (see Table 3-1). According to Connor et al. (2004), the channel CH-7 was classified in Category A because the radius of the cut-off has been saw cut and ground smooth, whereas the channel CH-11 was classified as Category B considering the worst case near of the high-strength bolted slip-critical connection. The CAFTs corresponding to the defined Categories A and B are 165 MPa (24 ksi) and 110 MPa (16 ksi), respectively.

The stress-range bin histogram collected at both channels are shown in Figure 3-12(a) and (b). Since the maximum stress range of 68.9 MPa (10.0 ksi) at both channels does not exceed the defined CAFT, the frequency regardless of the stress range cut-off levels is 0.00 %. Accordingly, fatigue life of the details, CH-7 and CH-11 is theoretically expected as infinite. The truncated stress-range bin histograms are reestablished according to the stress range cut-off levels. The PDFs with two- and three-parameter are generated from the truncated stress-range bin histograms, as shown in Figure 3-13 and Figure 3-14. Since the computed equivalent stress ranges in both cases are almost similar regardless of the assumed PDFs (see Table 3-5), the

PDFs considering two-parameter (i.e., $s_c = 0$) are used to estimate S_{re} in the fatigue reliability assessment, as that case of the Neville Island Bridge. Based on the computed equivalent stress ranges in both cases, the two-parameter PDFs are used to evaluate fatigue reliability.

Contrary to the Neville Island Bridge, the AASHTO S-N curve may not be extended below CAFT since fatigue life at both channels is expected as infinite. The stress range cut-off thresholds of the channel CH-7 are set in the range of 6.89 MPa (1.0 ksi) through 27.58 MPa (4.0 ksi), while those of the channel CH-11 are from 3.45 MPa (0.5 ksi) to 13.79 MPa (2 ksi). The relationship between equivalent stress range and total number of cycles, N_t, is plotted on the S-N curve (see Figure 3-15(a) and (b)). The calculated mean value and standard deviation of S_{re} are 25.02 MPa (3.63 ksi) and 6.50 MPa (0.94 ksi) at channel CH-7, respectively, and 16.66 MPa (2.42 ksi) and 5.24 MPa (0.76 ksi) at channel CH-11, respectively. It is noted that the constant cut-off levels at the channels CH-7 and CH-11 were 17.24 MPa (2.5 ksi) and 6.89 MPa (1.0 ksi), respectively, and the corresponding equivalent stress ranges were 25.68 MPa (3.73 ksi) and 15.15 MPa (2.20 ksi), respectively (Connor et al. 2004). The PDFs are fitted on the respective truncated stress-range bin histograms, and the equivalent stress ranges are calculated by using the equations associated with the assumed PDFs. Thus, the computed $E(S_{re})$, $\sigma(S_{re})$, and N_{avg} of the equivalent stress ranges are presented in Table 3-6. The annual traffic increase rate, α, considered (i.e., $\alpha = 0\%$, 3%, and 5%) is used to predict the annual cumulative number of cycles at the channels CH-7 and CH-11. In predicting fatigue life of a retrofitted bridge, it should be noted that the annual cumulative number of cycles may be counted from the retrofitted year of the bridge if

very low stress distributions are developed around structural details up to the retrofit time. In this study, the cumulative number of cycles before retrofit is ignored in the details, CH-7 and CH-11 (Connor et al. 2004 and Liu et al. 2010a).

Fatigue reliability evaluation in the details CH-7 and CH-11 is computed with all necessary information obtained from steps 1 to 5. As described previously, fatigue life of the details is expected as infinite. However, fatigue life of the details after retrofit may be affected if an annual traffic increase is considered since the monitoring time (i.e., 2003). For this reason, the traffic increase rate per year, α, is reflected in the fatigue reliability evaluation of the bridge, and two limits of fatigue reliability index are taken into account as upper and lower bounds to estimate remaining lifetime. The upper reliability index, β_U, is associated with the number of cycles corresponding to the CAFT, $N_{CAFT} = A / CAFT^3$, while the lower reliability index, β_L, is associated with the number of cycles corresponding to S_{re} (i.e., $N_{Sre} = A / S_{re}^3$).

For CH-7 and CH-11, fatigue reliability analyses were performed. As shown in Figure 3-16(a) and (b), as α increases, the fatigue reliability indices are reduced. The upper reliability indices, β_U, of the channels CH-7 and CH-11 are 7.61 and 7.18, respectively. They can be theoretically regarded as the lowest reliability level of these details associated with the assigned traffic increase rate. Thus, the details experience infinite fatigue life. On the other hand, the lower reliability indices, β_L, of 1.77 (CH-7) and 1.81 (CH-11) can be considered to estimate remaining lifetime if the *S-N* curve is assumed to be extended up to the mean values of the equivalent stress ranges. Assuming the annual traffic increase rate 3% and 5%, the remaining lifetime of the detail CH-7 is estimated at about 182 years and 120 years, respectively, while that of

the detail, CH-11 is estimated at 143 years and 97 years, respectively. However, remaining lifetime for $\alpha = 0\%$ indicates infinite fatigue life in the details, CH-7 and CH-11. Thus, the time-dependent fatigue reliability approach can be effectively used for fatigue performance assessment and lifetime prediction of the bridge.

3.2.7 Summary

In this section, a reliability approach for fatigue performance assessment and lifetime prediction of steel bridges based on the *S-N* approach and SHM data was presented. Current AASHTO *S-N* curve associated with the category identified at a detail was used to estimate structural capacity in the fatigue reliability evaluation, whereas field monitoring data were used to estimate equivalent stress range in terms of load demand. Under uncertainties associated with loading history, several PDFs (i.e., Lognormal, Weibull, or Gamma) were used to estimate the mean value and standard deviation of the equivalent stress range considering typical fatigue criteria. The stress-range bin histogram data collected on two existing bridges, the Neville Island Bridge and the Birmingham Bridge, were used to illustrate the proposed approach.

3.3 BRIDGE FATIGUE RELIABILITY ASSESSMENT AND PREDICTION BASED ON THE BI-LINEAR S-N APPROACH AND SHM

In this section, estimation of fatigue life below the CAFT of steel bridges by using a probabilistic approach based on the bi-linear *S-N* procedure is presented.

3.3.1 Introduction

In many steel bridges fatigue cracking is one of the primary safety concerns. In the United States, current AASHTO linear *S-N* approach (2008) using a single slope, $m = 3$ (i.e., $q = 3$), for all identified detail categories has been widely accepted to estimate fatigue life of aging steel bridges. In this approach, an equivalent stress range from a variable amplitude live-load stress range histogram is used for fatigue life estimation (Yen et al. 1990 and AASHTO 2008). However, when the maximum stress range experienced by a detail exceeds the CAFT (i.e., finite fatigue life), fatigue damage is very often over predicted using the current procedure (Yen et al. 2009). This is because the linear *S-N* lines on a logarithmic scale are conservatively extended below the CAFT. For this reason, a relevant extension of the AASHTO *S-N* lines has to be considered for the improvement of the current procedure. A similar application is found in the Eurocode 3 (2005) for which the *S-N* curves have a change in slope (i.e., $m_1 = 3$, $m_2 = 5$) below the CAFT at five-million cycles regardless of the category. However, due to a big difference between the Eurocode and AASHTO in the way that the CAFT is defined and used (Dexter et al. 1997), the extension of the *S-N* lines in the AASHTO can be still made in a different way. For this purpose, a bi-linear *S-N* approach, addressed in Crudele & Yen (2006), is applied for a more realistic estimation of fatigue life of steel bridges by using a probabilistic approach considering loading uncertainty. The proposed approach uses a first slope $m_1 = 3$ with a second slope $m_2 = 4$ below the CAFT, based on their analytical derivations from four different types of variable amplitude stress-range histograms (distributions). In their study, a recorded stress-range histogram was scaled to produce over twenty different values of

maximum and equivalent stress ranges in each type, implying that a broad range of histories are covered.

In recent years, it was shown that the current linear S-N procedure may provide a negative remaining life, implying that the estimation is overly conservative with respect to real fatigue life (Connor et al. 2005 and Yen et al. 2009). For useful estimation of fatigue life, several approaches have been applied to assess the time-dependent structural performance for fatigue under uncertainty (Frangopol et al. 2008, Liu et al. 2010a, and Kwon & Frangopol 2010a). However, these approaches are based on the linear S-N procedure considering only a single slope, $m = 3$, above and below the CAFT. Therefore, bridge maintenance cost can often increase due to unnecessary retrofits or repairs. Crudele & Yen (2006) showed analytically that the hypothetically extended S-N lines for variable stress cycles below the CAFT have a larger slope than that of the lines above the fatigue threshold. Therefore, a bi-linear S-N represented by two different slopes above and below the CAFT can be more rationally adopted for estimating the remaining fatigue life in structural steel details under fatigue.

As described in previous section, the application of several PDFs can be effectively considered for prediction of fatigue life. The well-fitted PDFs associated with stress ranges assist the probabilistic prediction of equivalent stress range under loading uncertainty. In this context, a goodness-of-fit test is conducted to find the best fit. In this study, three PDFs for fatigue reliability assessment using the bi-linear S-N approach are considered as follows: Lognormal, Weibull, and Rayleigh.

Based on all the necessary information from the AASHTO Specifications (2008) and field monitoring data, fatigue life estimation considering the bi-linear S-N

70

approach is conducted by using the reliability software RELSYS (Estes & Frangopol 1998). As an illustration, four different fatigue details of the Neville Island Bridge, which is located in Pittsburgh, Pennsylvania, are investigated. The field monitoring data for the bridge are provided by the Engineering Research Center ATLSS at Lehigh University (Connor et al. 2005).

3.3.2   Effect of the CAFT on Fatigue Life

Current direct extension of the *S-N* line below the CAFT can make the estimation of fatigue life conservative. For more realistic prediction of the remaining fatigue life, the concept of decreasing fatigue threshold (i.e., CAFT) can be employed (Crudele & Yen 2006). The AASHTO Specifications (2008) for all *S-N* categories provide the CAFTs as fatigue thresholds associated with welded structural details. The definition of the CAFT can be associated with the fatigue crack growth threshold. Typically, the fatigue crack growth is estimated by using Paris equation (Paris & Erdogan 1963) as

$$\frac{da}{dN} = C \cdot (\Delta K)^B \qquad (3\text{-}13)$$

where a = crack size, N = number of cycles, ΔK = stress intensity factor range, and C and B are the fatigue coefficient and the fatigue exponent (i.e., $B = 3.0$ for structural steels), respectively. The estimation of ΔK is especially complex in common use of welded structures. It can be expressed in terms of crack size as (Barsom & Rolfe, 1996):

$$\Delta K(a) = G \cdot \Delta \sigma \cdot \sqrt{\pi \cdot a} \qquad (3\text{-}14)$$

where $\Delta K(a)$ = generalized stress intensity factor range, $\Delta\sigma$ = stress range, and G = a non-dimensional function of the geometry including various factors which indicate finite width factor, non-uniform stresses factor, free surface effect factor, and crack shape factor.

For the case of no fatigue crack growth expected (at very low crack growth rates), stress intensity threshold, ΔK_{th}, associated with a hypothetical control value of crack size, a_i, can be derived from Eq. 3-14 by using the CAFT (Crudele & Yen 2006) as follows:

$$\Delta K_{th}(a) = G \cdot CAFT \cdot \sqrt{\pi \cdot a_i} \qquad (3\text{-}15a)$$

$$CAFT = \frac{\Delta K_{th}}{G \cdot \sqrt{\pi \cdot a_i}} \qquad (3\text{-}15b)$$

As the crack size increases with a constant value of ΔK_{th}, the CAFT will decrease as indicated in Eq. 3-15(b). Crudele & Yen (2006) concluded that this can allow subsequent, slightly lower magnitude stress range cycles in a spectrum in order to contribute to the crack growth, implying that the *S-N* has a different slope below the CAFT. In this context, the analytical approach using the concept of decreasing the CAFT was addressed. The procedure is summarized in the flowchart of Figure 3-17.

3.3.3   The Bi-Linear S-N Approach

Four different AASHTO *S-N* categories (i.e., B, C, D, E) were employed in the study performed by Crudele & Yen (2006) using the histogram from recorded live load stresses of a naval structural component. They showed that the computed fatigue lives above the CAFT agree well with those associated with the AASHTO *S-N* curves

for all fatigue categories, but those below the CAFT have to be extended. As a result, the average value of slope of the S-N lines below the CAFT was suggested to be 4. In this research, this value recommended by Crudele & Yen (2006) is used to establish the bi-linear S-N lines for all AASHTO categories (see Figure 3-18). Accordingly, the AASHTO basic equation $R = (A / N)^{1/m}$ is specified as:

$$R_1 = \left(\frac{A_1}{N} \right)^{1/m_1} \quad \text{for } N \leq N_s \tag{3-16a}$$

$$R_2 = \left(\frac{A_2}{N} \right)^{1/m_2} \quad \text{for } N > N_s \tag{3-16b}$$

where $N_s = A / CAFT^m$; $A_1 = A$ and $A_2 = (CAFT^{m_2-m_1}) \cdot A_1$, in which A_1 and A_2 are the fatigue detail coefficients above and below the CAFT, respectively; and $m = m_1 = 3.0$ and $m_2 = 4.0$. The associated bi-linear S-N values are provided in Table 3-7.

As mentioned previously, typical bridge structures are subjected to variable amplitude stress ranges. For useful estimation of fatigue life, these stress ranges are converted into an equivalent constant amplitude stress range by using Miner's rule (Miner 1945). When considering a single slope only (i.e., $m = 3.0$), the linear equivalent stress range can be computed from the stress-range bin histogram based on the current AASHTO S-N approach and Miner' rule as

$$S_{re} = \left[\sum \frac{n_i \cdot S_i^m}{\sum n_i} \right]^{\frac{1}{m}} \tag{3-17}$$

where n_i = number of cycles in the predefined stress-range bin S_i and $\sum n_i$ = total number of cycles to failure (i.e., $\sum n_i = N_{total}$ as defined previously).

73

On the other hand, when considering the *S-N* represented by two different slopes (i.e., $m_1 = 3$, $m_2 = 4$), the following equation can be alternatively used to calculate the bi-linear equivalent stress range, S_{re}^* (Kosteas 1999 and Kwon & Frangopol 2010c).

$$S_{re}^* = \left[\frac{\sum(n_i^o \cdot S_i^{m_1}) + (CAFT^{m_1-m_2}) \cdot \sum(n_j^o \cdot S_j^{m_2})}{\sum n_i^o + \sum n_j^o} \right]^{\frac{1}{m_1}}$$

(3-18)

where n_i^o = number of cycles in the stress-range bin S_i greater than CAFT; n_j^o = number of cycles in the stress-range bin S_j less than CAFT; and $\sum n_i^o + \sum n_j^o$ = total number of cycles to failure. Accordingly, the fatigue life can be deterministically calculated using the bi-linear *S-N* as

$$N^* = \frac{A \cdot CAFT^{m_2-m_1}}{(S_{re}^*)^{m_2}} \quad \text{for } S_{re}^* < CAFT$$

(3-19)

Based on the stress-range bin histogram, the average daily number of cycles, N_{avg}, is estimated. The computed N_{avg} is used to predict bridge service time, *t*, in years as

$$t = \frac{N^*}{365 \cdot N_{avg}}$$

(3-20)

3.3.4 Fatigue Reliability Assessment

A probabilistic approach for realistic fatigue life estimation is herein presented. This approach is developed based on both a fracture mechanics model evaluating the

time-dependent crack growth and a bi-linear *S-N* estimating the bi-linear equivalent stress range. The AASHTO Specifications (2008), monitoring data, and material properties are used to obtain all necessary information.

3.3.4.1 Limit-State Functions Above and Below the CAFT

Based on fracture mechanics with the assumption that G is a constant and $B \neq 2.0$, the performance function associated with crack propagation can be defined by using Eqs. 3-13 and 3-14, as follows

$$g(t) = a_f - a(t)$$

$$= a_f - [a_i^{1-B/2} + (1 - \frac{B}{2}) \cdot C \cdot \Delta\sigma^B \cdot G^B \cdot \pi^{B/2} \cdot N_t(t)]^{2/(2-B)} \tag{3-21}$$

where a_f = final (critical) crack size and a_i = initial crack size which can be estimated by using Eq. 3-15 for the classified *S-N* categories. Typically, fatigue life depends more on a_i than a_f (Fisher et al. 1998). Accordingly, uncertainty associated with the initial crack size can be considered important in fatigue reliability assessment.

By adopting the bi-linear *S-N* approach to estimate the bi-linear equivalent stress range, S_{re}^*, Eq. 3-21 is rewritten as

$$g(t) = \frac{2}{\pi^{3/2}} (\frac{1}{\sqrt{a_i}} - \frac{1}{\sqrt{a_f}}) - C \cdot (S_{re}^*)^3 \cdot (365 \cdot N_{avg} \cdot t) \tag{3-22}$$

In Eq. 3-22, it is assumed that the fatigue exponent of the crack growth rate is 3.0 and the geometric factor is 1.0 (i.e., $B = 3.0$, $G = 1.0$).

Alternatively, fatigue reliability analysis can be conducted considering the bi-linear *S-N* approach only. Based on this approach and Miner's rule (Miner 1945), the associated performance functions are

$$g_1(t) = \Delta - D = \Delta - \left(\frac{N_t(t)}{A} \right) \cdot (S_{re}^*)^{m_1} \quad \text{for } N_t(\text{t}) \leq N_s = A / CAFT^{m_1} \quad (3\text{-}23\text{a})$$

$$g_2(t) = \Delta - \left(\frac{N_t(t)}{(CAFT^{m_2-m_1}) \cdot A} \right) \cdot (S_{re}^*)^{m_2} \quad \text{for } N_t(\text{t}) > N_s \quad (3\text{-}23\text{b})$$

where m_1, m_2 = material constants (i.e., m_1 = 3.0 and m_2 = 4.0 for all *S-N* categories); and A = fatigue detail coefficient which is considered as a random variable (Kwon & Frangopol 2010a).

3.3.4.2 Estimation of Deterministic Parameters and Random Variables

In fatigue reliability analysis, the five parameters (i.e., a_i, a_f, C, S_{re}^*, N_{avg}) defined in the performance function (see Eq. 3-22) can be treated as deterministic or random. The appropriate PDFs for random variables have to be defined due to uncertainties associated with fatigue resistance and load effect. The statistical information on the assumed PDFs is directly used in the reliability analysis. In this study, three parameters a_i, a_f, and C associated with fatigue crack growth are assumed lognormal. The associated probabilistic information is presented in Table 3-8. It is noted that the mean values of a_i vary in the identified *S-N* categories for a given ΔK_{th} = 2.75 MPa $\sqrt{m}$ (Barsom & Rolfe 1999). Three PDFs associated with the stress range, *S*, are herein considered: Lognormal, Weibull, and Rayleigh. The PDFs of these distributions are, respectively:

$$f_S(s) = \frac{1}{s \cdot \zeta \cdot \sqrt{2 \cdot \pi}} \cdot \exp\left[-\frac{1}{2} \cdot \left(\frac{\ln(s) - \lambda}{\zeta} \right)^2 \right] \tag{3-24a}$$

$$f_S(s) = \frac{\beta}{\alpha} \cdot \left(\frac{s}{\alpha} \right)^{\beta-1} \cdot \exp\left[-\left(\frac{s}{\alpha} \right)^{\beta} \right] \tag{3-24b}$$

$$f_S(s) = \left(\frac{s}{S_{ro}^2} \right) \cdot \exp\left[-\frac{1}{2} \left(\frac{s}{S_{ro}} \right)^2 \right] \tag{3-24c}$$

where $s > 0$; λ = mean value of $\ln s$ (location parameter), ζ = standard deviation of $\ln s$ (scale parameter); α = scale parameter, β = shape parameter; $\alpha > 0$, $\beta > 0$; and S_{ro} = mode.

The parameters of each PDF can easily be calculated by using the relationship between the method of moments and the mean and variance from the stress-range bin histogram data (Kwon & Frangopol 2010a). For the linear S-N, the equivalent stress range for each distribution can be derived using the qth moment of the stress range as (see also Eq. 3-7)

$$S_{re} = \left[\int_0^\infty s^q \cdot f_S(s) \cdot ds \right]^{\frac{1}{q}} = \left[\mathrm{E}(S^q) \right]^{\frac{1}{q}} \tag{3-25a}$$

In a similar way, the equivalent stress range for the bi-linear S-N (see Eq. 3-18) is obtained by

$$S_{re}^* = \left[\int_0^{CAFT} (CAFT^{m_1-m_2}) \cdot s^{m_2} \cdot f_S(s) \cdot ds + \int_{CAFT}^\infty s^{m_1} \cdot f_S(s) \cdot ds \right]^{\frac{1}{m_1}} \tag{3-25b}$$

In fatigue reliability evaluation, S_{re}^* that is calculated by using Eq. 3-25(b) is treated as Lognormal, Weibull, or Rayleigh with COV(S_{re}^*) = 0.1, while the other random variables (i.e., a_i, a_f, and C) are assumed as lognormal (see Table 3-8).

3.3.4.3 Fatigue Reliability Analysis

In this study, fatigue reliability analysis based on the established performance function (see Eq. 3-22) is conducted by using the reliability software RELSYS (Estes & Frangopol 1998).

The procedure for the fatigue reliability evaluation is summarized as follows:

Step 1: *Choosing the reliability approach*

Fatigue reliability evaluation can be conducted based on a bi-linear *S-N* approach and/or a fracture mechanics approach. A reliability approach can include initiation and propagation of fatigue cracking. A fracture mechanics reliability assessment may be preferred to the AASHTO *S-N* approach which does not explicitly address existing crack sizes.

Step 2: *Collecting the detail information on structural members*

The AASHTO Specifications (2008) are useful for gaining relevant information including the AASHTO category, CAFT, and *A*. Material properties associated with cracking initiation and propagation (e.g., a_i, a_f , G, ΔK_{th}) are investigated. If ΔK_{th} and CAFT are assigned, the mean value of a_i can be easily estimated for all *S-N* categories (see Eq. 3-15).

Step 3: *Establishing the stress-range bin histogram from long-term monitoring*

The stress-range bin histogram from field monitoring is established using rain-flow counting method (Downing & Socie 1982). Since small cycles do not contribute to the overall fatigue damage, the rain-flow analysis algorithm can be programmed to ignore any stress ranges less than 3.45 MPa (0.5 ksi). Therefore, a stress-range bin histogram is established in the range from its minimum stress range of 3.45 MPa to its maximum stress range together with a bin size of 3.45 MPa.

Step 4: *Predicting the bi-linear equivalent stress range and the average daily number of cycles*

The established stress-range bin histogram can be truncated according to the predefined stress range cut-off threshold in order to estimate an applicable equivalent stress range for fatigue life estimation. A typical limit of a cut-off threshold is about 25% CAFT for all welded steel details that are expected to experience finite fatigue life (Connor & Fisher 2006 and Kwon & Frangopol 2010a). It is noted that predefining the fatigue threshold for infinite fatigue life (i.e., when maximum stress range is less than the CAFT) is not significant relatively. Based on the truncated stress-range bin histogram, the bi-linear equivalent stress range, S_{re}^{*}, is calculated and also the corresponding average daily number of cycles, N_{avg}, is estimated.

Step 5: *Performing the fatigue reliability analysis*

Based on the well-defined performance function (see Eq. 3-22 or 3-23), the time-dependent fatigue reliability evaluation can be performed for the assumed PDFs in terms of fatigue resistance and load effect (e.g., Lognormal, Weibull, Rayleigh) with all necessary information from steps 1 to 4.

3.3.5   Application Example

The individual fatigue lives of four components of the Neville Island Bridge addressed in the application example of Section 3.2.5 are estimated using the proposed reliability approach based on the bi-linear *S-N* in a fracture mechanics model. The SHM data from field testing performed by the ATLSS Engineering Research Center at Lehigh University are used. The complete description of the bridge and further details can be found in Connor et al. (2005).

3.3.5.1   Fatigue Details and SHM data

In 2004, four portions, where consist of ramp J and H, tied-arch, spans 25 and 26, and ramp A in the Neville Island Bridge opened in 1976, were selected for field instrumentation in long-term monitoring programs. The SHM programs were performed for a complete fatigue and fracture evaluation of the bridge. In this study, the SHM data collected at four different channels CH-37 at ramp H and CH-21, CH-16 and CH-18 at span 25 (see Figure 3-19), which are classified as the AASHTO *S-N* categories *A*, *B*, *C* and *E*, respectively, are used as load effects associated with the fatigue categories. As indicated previously, the long-term monitoring period of ramp H and span 25 was about 29 days.

Details of fatigue resistance and SHM data from the selected channels (i.e., CH-37, CH-21, CH-16, and CH-18) are used to estimate fatigue life below the CAFT (as expected to experience finite fatigue life) by the proposed reliability method based on the bi-linear *S-N*. For the classified AASHTO categories (AASHTO 2008), the associated *S-N* parameters (i.e., CAFT, *m*, *A*) are obtained at four channels, as

80

indicated in Table 3-7 (see also Figure 3-18). The channel CH-37 classified as category *A* with CAFT = 165 MPa (24 ksi) was installed on the outside of the girder web adjacent to the transverse knee-brace. At span 25, the channel CH-21 mounted to the diaphragm is classified as category *B* because of the bolted connections without transverse stiffeners (see Figure 3-19(b)). Its corresponding CAFT is 110 MPa (16 ksi). For both channels CH-16 and CH-18, the classified categories are *C* and *E*, respectively, while the CAFTs are 69 MPa (10 ksi) and 31 MPa (4.5 ksi), respectively. Details of sensor locations are shown in Figure 3-19(c).

The stress-range bin histograms for the fatigue details CH-37, CH-21, CH-16 and CH-18 are established by rain-flow counting method, as shown in Figure 3-20(a) to Figure 3-23(a), respectively. At channels CH-16 and CH-18 the maximum stress ranges are 110.3 MPa (16 ksi) and 82.7 MPa (12 ksi), respectively. Since these two values exceed the defined CAFTs, their associated fatigue lives are expected to be finite. On the other hand, the channels CH-37 and CH-21 are theoretically expected to experience infinite fatigue life because their maximum stress ranges are less than CAFTs, as indicated Figure 3-20(a) and Figure 3-21(a). For illustrative purpose, their stress-range bin histogram data are herein scaled up in order to allow the details to experience finite fatigue lives in consideration.

In addition, the average daily number of cycles, N_{avg}, is estimated from the histograms. N_{avg} is calculated by the total number of cycles and the monitoring time period of 29 days. The estimated N_{avg} at the channels CH-37, CH-21, CH-16 and CH-18 is 278, 3290, 3304, and 48434 cycles per day, respectively. By using the estimated N_{avg}, the annual cumulative number of cycles, $N_t(t)$, is predicted for the time-

dependent fatigue reliability assessment. N_{avg} is herein treated as deterministic without considering any traffic increase. It is noted that since no retrofit was conducted from 1976 to 2004 at the channels, the annual cumulative number of cycles has been accumulated from the bridge opening.

3.3.5.2 Estimation of the Bi-Linear Equivalent Stress Range

The collected stress-range bin histogram data are appropriately truncated and scaled up if necessary. As mentioned previously, the applicable stress range cut-off thresholds are 25% CAFT. Based on the truncated stress-range bin histograms, the three PDFs (i.e., Lognormal, Weibull, and Rayleigh) which are commonly employed in fatigue fields, are generated to predict lifetime stress ranges under uncertainty. As shown in Figure 3-20(a) to Figure 3-23(a), the parameters associated with each PDF are estimated by using the relationship between the method of moments and the mean and variance from the stress-range bin histogram data (see Eq. 3-24). These PDFs are used to estimate the linear and bi-linear equivalent stress ranges by applying both the current S-N approach (i.e., m =3 only) and the proposed bi-linear S-N approach (i.e., $m_1 = 3.0$ and $m_2 = 4.0$), respectively.

A goodness-of-fit test is conducted to find the best fit among the defined PDFs, by using the Anderson and Darling (1952) method. The results are shown in Figure 3-20(b) through Figure 3-23(b). As the best fit of the stress range data obtained from the SHM, lognormal PDF is considered at the channels CH-37 and CH-16 classified as categories A and C, respectively, whereas Weibull PDF is well fitted at CH-21 and CH-18 classified as categories B and E, respectively. These best fits can be considered

to compute the linear and bi-linear equivalent stress ranges as load effects for fatigue damage. Nevertheless, three PDFs are applied in this study because a best fit PDF from the truncated histogram may be affected according to the predefined cut-off stress range levels. Therefore, the application of three PDFs would be still useful for more conservative estimation of fatigue life when employing the bi-linear *S-N* approach.

For the assumed PDFs, the equivalent stress ranges for both the linear and bi-linear *S-N* approaches are computed by using Eqs. 3-25(a) and (b). The computed values are presented in Table 3-9. As shown in Table 3-9, the bi-linear equivalent stress range, S_{re}^{*}, at all channels is less than the linear equivalent stress range, S_{re}. Therefore, it is expected that fatigue life may become larger by adopting the bi-linear *S-N* approach. For the details CH-16 and CH-18, the relationship between the linear and bi-linear equivalent stress ranges with respect to the total number of cycles, N_t, is plotted in Figure 3-24(a) and (b) with the *S-N* corresponding to the categories *C* and *E*, respectively.

3.3.5.3 Fatigue Life Estimation Using the Bi-Linear S-N Approach

All necessary information for the fatigue life estimation is obtained from the bi-linear *S-N*, fracture mechanics, and SHM. For the identified fatigue details, the time-dependent fatigue reliability analyses are conducted to predict fatigue life using the reliability software RELSYS (Estes & Frangopol 1998). The effect of the linear and bi-linear equivalent stress ranges on fatigue life is investigated. The computed S_{re}

and S_{re}^* for the assumed three distributions (i.e., Lognormal, Weibull, or Rayleigh) are used for fatigue reliability assessment.

Based on the established performance function (see Eq. 3-22), deterministic parameters and random variables are defined as presented in Table 3-8. For a given ΔK_{th}, different initial crack sizes can be identified according to the classified *S-N* categories in respective fatigue details (see Eq. 3-15). As the CAFT is low, a_i relatively increases. As indicated in Table 3-8, the estimated initial crack sizes for all *S-N* categories are taken into account as the mean values with COV(a_i) = 0.5 (Zhang & Mahadevan 2001), while the mean value of final crack size is considered as 12.7 mm (0.5 in) in all fatigue details (Crudele & Yen 2006) with COV(a_f) = 0.1. The mean value of the crack growth parameter, E(*C*), is 2.50E-13 MPa $\sqrt{m}$ (4.13E-10 ksi $\sqrt{in}$) and its COV(*C*) is 0.54 (Righiniotis 2004). These three parameters (i.e., a_i, a_f, and *C*) are treated as lognormal, while other parameters *G* and *B* are treated as deterministic.

Figure 3-25(a) through Figure 3-28(a) show the results of the crack growth model for the identified *S-N* categories *A*, *B*, *C*, and *E*, by using only the mean values of crack growth parameters. It is observed that the fatigue life in all *S-N* categories is extended by applying the bi-linear equivalent stress range regardless of the assumed type of PDFs. At CH-18, CH-21, and CH-37, the use of lognormal PDF improved largely the fatigue life, whereas Rayleigh PDF at all channels resulted in the most critical fatigue life. For the well-fitted distributions (see Figure 3-20(b) to Figure 3-23(b)), the associated fatigue lives are investigated when reaching the final crack size. In the details CH-37 and CH-21, the fatigue lives increased about 23 and 18 years, respectively, as compared to those by the current procedure. Similarly, the

fatigue lives in the details CH-16 and CH-18 increased about 9 and 7 years, respectively. Connor et al. (2005) stated that although the calculated remaining life of CH-16 is -10 years in 2004, this detail has not cracked. This indicates that the current procedure for the life calculation can provide too conservative fatigue lives. Of course, other possible explanations may be made for the result. For example, the under-estimated remaining life may result from the direct extrapolation of the annual number of cycles estimated from monitoring. However, this is not the case because integration of available monitoring data into fatigue life estimation has been widely accepted. Therefore, fatigue lives in all respective structural details may be estimated by applying the bi-linear equivalent stress range in consideration of two *S-N* slopes for the improvement of the current procedure.

In the following, the time-dependent fatigue reliability analysis is conducted using two different equivalent stress ranges (i.e., S_{re} and S_{re}^{*}) computed from the assumed distributions (i.e., Lognormal, Weibull, and Rayleigh). The results are shown in Figure 3-25 through Figure 3-28. As expected from the crack growth models, fatigue reliability indices by the bi-linear equivalent stress range are formed in upper levels, whereas those by the linear equivalent stress range are in lower levels. For given target reliability levels, $\beta_{target,1} = 1.0$ and $\beta_{target,2} = 2.0$, the ratios of the predicted fatigue lives are investigated for the well-fitted distributions in the details (see Table 3-10). As a result, the fatigue lives increased from 19% to 86% as presented in Table 3-10.

3.3.6 Summary

A reliability approach for useful estimation of fatigue life below the CAFT of steel bridges by adopting a bi-linear *S-N* was researched. The proposed approach was used to estimate effectively fatigue life under uncertainty. For the current AASHTO fatigue categories, the bi-linear *S-N* addressed in Crudele & Yen (2006) were established considering two different slopes (i.e., $m_1 = 3.0$, $m_2 = 4.0$). In the fatigue reliability assessment, the bi-linear *S-N* approach for the category classified at a detail was used to estimate structural capacity, whereas the stress-range bin histogram data from the long-term SHM were used to estimate the bi-linear equivalent stress range in terms of load demand. Several PDFs (i.e., Lognormal, Weibull, or Rayleigh) were used for the prediction of the bi-linear equivalent stress range under uncertainty. The stress-range bin histogram data collected from the SHM of an existing bridge, the Neville Island Bridge, were used to illustrate the proposed approach.

3.4 CONCLUDING REMARKS

In this chapter, reliability approaches for fatigue performance assessment and prediction of steel bridges by incorporating SHM data were presented based on (i) the linear *S-N* approach and (ii) the bi-linear *S-N* approach.

The following conclusions are drawn from this study:

1. The field monitoring data can be reliably used to estimate load effect for the time-dependent fatigue performance assessment and lifetime prediction of existing steel bridges. Based on the stress-range bin histogram obtained from

SHM, several PDFs can be employed to estimate the linear and bi-linear equivalent stress ranges under uncertainty.

2.   The upper and lower bounds of stress range cut-off thresholds from the established stress-range bin histogram can be reasonably determined considering fatigue criteria associated with the CAFT and the frequency limit.

3.   According to the predefined stress range cut-off levels and the assumed PDFs, the mean and standard deviation of the equivalent stress ranges can be computed. Thus, uncertainty associated with fatigue loading is reduced by using the estimated statistical information.

4.   Probabilistic treatments of two important parameters, which are the fatigue detail coefficient, A, and equivalent stress range, S_{re}, can improve the fatigue reliability assessment. Consequently, the remaining fatigue life of a structure can be reliably predicted by using the proposed probabilistic approach.

5.   The application of the bi-linear S-N approach with two different slopes leads to additional fatigue life than that estimated by using the direct extension provided in the AASHTO S-N approach.

6.   The bi-linear equivalent stress range can be effectively used to estimate probabilistic fatigue life associated with the propagation of fatigue cracks derived from a fracture mechanics model.

7.   In assessment phase, the bi-linear S-N, which is developed by the analytical derivations using the concept of decreasing the CAFT (Crudele & Yen 2006), can be applied for the useful fatigue life of respective fatigue details.

Table 3-1   The *S-N* values according to the AASHTO Categories (2002) for two existing bridges.

S-N values	Neville Island Bridge		Birmingham Bridge	
	CH-9	CH-17	CH-7	CH-11
Category	C	E	A	B
Fatigue retail coefficient, A, MPa^3 (ksi^3)	14.4E+11 (44.0E+08)	36.1E+10 (11.0E+08)	81.9E+11 (25.0E+09)	39.3E+11 (12.0E+09)
*Intercept, mean value, E(log A)	10.085	9.292	11.121	10.870
*Intercept, lower bound, E(log A)-2·σ(log A)	9.775	9.094	10.688	10.582
Constant amplitude fatigue threshold, CAFT, MPa (ksi)	68.9 (10.0)	31.0 (4.5)	165.5 (24.0)	110.3 (16.0)

* The Values are based on regression analyses of test results for steel bridge details performed by Keating and Fisher (1986). These values are used to calculate E(A) and σ(A) for fatigue reliability analysis using following transformation:

$E(A) = \exp(\lambda_A + \zeta_A^2 / 2)$ and $\sigma(A) = \sqrt{E(A)^2 \cdot (\exp(\zeta_A^2) - 1)}$, where $\lambda_A = \ln(10) \times E(\log A)$ and $\zeta_A = \ln(10) \times \sigma(\log A)$.

Table 3-2   Summary of deterministic parameters and random variables for fatigue reliability assessment.

Parameter	Notation	Distribution	Reference
Fatigue detail coefficient	A	Lognormal (see Table 3-1)	AASHTO Specifications (2002), Keating & Fisher (1986)
Equivalent stress range	S_{re}	Lognormal (see Table 3-4 and Table 3-6)	Field monitoring data
Miner's critical damage accumulation index	Δ	Lognormal LN (1.0, 0.3)	Wirsching (1984)
Measurement error	e	Lognormal LN (1.0, 0.03)	Frangopol et al. (2008)
Material constant	m	Deterministic $m = 3.0$	AASHTO Specifications (2002)
Average daily number of cycles	N_{avg}	Deterministic	Field monitoring data

Table 3-3 Effect of PDFs on equivalent stress range, S_{re}, for the details of the Neville Island Bridge.

Channel	Cut-off stress range, S_c MPa (ksi)	*S_{re} MPa (ksi)	Lognormal		Weibull		Gamma	
			**S_{re} MPa (ksi)	***S_{re} MPa (ksi)	**S_{re} MPa (ksi)	***S_{re} MPa (ksi)	**S_{re} MPa (ksi)	***S_{re} MPa (ksi)
CH-9	10.34 (1.50)	24.52 (3.56)	24.39 (3.54)	26.87 (3.90)	23.63 (3.43)	25.05 (3.63)	23.88 (3.46)	24.84 (3.60)
	13.79 (2.0)	31.01 (4.50)	31.09 (4.51)	32.39 (4.70)	30.51 (4.42)	31.36 (4.55)	30.78 (4.46)	31.37 (4.55)
	17.24 (2.5)	34.92 (5.07)	34.94 (5.07)	35.70 (5.18)	34.54 (5.01)	35.08 (5.09)	34.77 (5.04)	35.14 (5.10)
	20.68 (3.0)	37.40 (5.42)	37.36 (5.42)	37.94 (5.50)	37.07 (5.38)	37.50 (5.44)	37.25 (5.40)	37.55 (5.45)
CH-17	3.45 (0.5)	8.54 (1.24)	8.11 (1.18)	8.75 (1.27)	7.89 (1.14)	8.27 (1.20)	7.97 (1.16)	8.23 (1.19)
	6.89 (1.0)	14.94 (2.17)	14.91 (2.16)	15.47 (2.24)	14.66 (2.13)	15.03 (2.18)	14.78 (2.14)	15.04 (2.18)
	10.34 (1.5)	18.39 (2.67)	18.38 (2.67)	18.66 (2.71)	18.24 (2.65)	18.45 (2.68)	18.33 (2.66)	18.47 (2.68)

* see $S_{re} = \left[\sum \dfrac{n_j}{N_{total}} \cdot S_{rj}^3 \right]^{\frac{1}{3}}$; ** $S_{re} = \left[\int_0^\infty [S^3 \cdot f_S(s)] \, ds \right]^{\frac{1}{3}}$ for 2-parameter PDFs; and *** $S_{re} = \left[\int_{s_c}^\infty s^3 \cdot f_S(s) \cdot ds \right]^{\frac{1}{3}}$ for the

3-parameter PDFs (s_c = stress range cut-off level).

Table 3-4   Mean value and standard deviation of S_{re} by PDFs and N_{avg} for the details of the Neville Island Bridge.

Channels	Parameter	PDF		
		Lognormal	Weibull	Gamma
CH-9	$E(S_{re})$, MPa (ksi)	31.94 (4.63)	31.44 (4.56)	31.67 (4.59)
	$\sigma(S_{re})$, MPa (ksi)	4.90 (0.71)	5.08 (0.74)	5.05 (0.73)
	N_{avg} (cycles per day)	3674	3878	3782
CH-17	$E(S_{re})$, MPa (ksi)	13.80 (2.00)	13.60 (1.97)	13.70 (1.99)
	$\sigma(S_{re})$, MPa (ksi)	4.26 (0.62)	4.29 (0.62)	4.30 (0.62)
	N_{avg} (cycles per day)	6417	6723	6573

Table 3-5   Effect of PDFs on equivalent stress range, S_{re}, for the details of the Birmingham Bridge.

Channel	Cut-off Stress Range, S_c MPa (ksi)	*S_{re} MPa (ksi)	Lognormal		Weibull		Gamma	
			**S_{re} MPa (ksi)	***S_{re} MPa (ksi)	**S_{re} MPa (ksi)	***S_{re} MPa (ksi)	**S_{re} MPa (ksi)	***S_{re} MPa (ksi)
CH-7	6.89 (1.0)	14.65 (2.13)	14.38 (2.09)	15.12 (2.19)	14.11 (2.05)	14.58 (2.11)	14.24 (2.06)	14.56 (2.11)
	10.34 (1.5)	18.47 (2.68)	18.27 (2.65)	18.91 (2.74)	18.07 (2.62)	18.47 (2.68)	18.18 (2.64)	18.47 (2.68)
	13.79 (2.0)	22.35 (3.24)	22.21 (3.22)	22.64 (3.28)	22.05 (3.20)	22.35 (3.24)	22.15 (3.21)	22.36 (3.24)
	17.24 (2.5)	25.68 (3.73)	25.57 (3.71)	25.85 (3.75)	25.46 (3.69)	25.66 (3.72)	25.54 (3.70)	25.68 (3.72)
	20.68 (3.0)	28.40 (4.12)	28.30 (4.10)	28.51 (4.14)	28.22 (4.09)	28.38 (4.12)	28.28 (4.10)	28.39 (4.12)
	24.13 (3.5)	30.96 (4.49)	30.87 (4.48)	31.09 (4.51)	30.80 (4.47)	30.96 (4.49)	30.85 (4.47)	30.96 (4.49)
	27.58 (4.0)	34.59 (5.02)	34.51 (5.01)	34.70 (5.03)	34.46 (5.00)	34.59 (5.02)	34.50 (5.00)	34.59 (5.02)
CH-11	3.45 (0.5)	8.99 (1.21)	8.38 (1.21)	9.10 (1.32)	8.13 (1.18)	8.55 (1.24)	8.21 (1.19)	8.50 (1.23)
	6.89 (1.0)	15.15 (2.15)	14.84 (2.15)	15.78 (2.29)	14.52 (2.11)	15.10 (2.19)	14.66 (2.13)	15.05 (2.18)
	10.34 (1.5)	19.47 (2.82)	19.27 (2.79)	20.01 (2.90)	19.01 (2.76)	19.49 (2.83)	19.15 (2.78)	19.48 (2.18)
	13.79 (2.0)	23.05 (3.34)	22.91 (3.32)	23.49 (3.41)	22.71 (3.29)	23.10 (3.35)	22.83 (3.31)	23.10 (3.35)

*, **, and *** see Table 3-3.

Table 3-6   Mean value and standard deviation of S_{re} by PDFs and N_{avg} for the details of the Birmingham Bridge.

Channels	Parameter	PDF		
		Lognormal	Weibull	Gamma
CH-7	E(S_{re}), MPa (ksi)	24.87 (3.61)	24.74 (3.59)	24.82 (3.60)
	σ(S_{re}), MPa (ksi)	6.57 (0.95)	6.64 (0.96)	6.61 (0.96)
	N_{avg} (cycles per day)	202	206	204
CH-11	E(S_{re}), MPa (ksi)	16.35 (2.37)	16.09 (2.33)	16.21 (2.35)
	σ(S_{re}), MPa (ksi)	5.42 (0.79)	5.44 (0.79)	5.45 (0.79)
	N_{avg} (cycles per day)	1067	1128	1098

Table 3-7   The bi-linear *S-N* values based on the AASHTO fatigue categories (2008).

| *S-N* category | CAFT MPa (ksi) | Design value of constant *A* | |
		A_1 above the CAFT with $m_1 = 3.0$, MPa^3 (ksi^3)	A_2 below CAFT with $m_2 = 4.0$, MPa^4 (ksi^4)
A	165 (24)	82.0×10^{11} (250×10^8)	135.0×10^{13} (60.0×10^{10})
B	110 (16)	39.3×10^{11} (120×10^8)	43.2×10^{13} (19.0×10^{10})
B'	82.7 (12)	20.0×10^{11} (61×10^8)	16.5×10^{13} (7.3×10^{10})
C	69 (10)	14.4×10^{11} (44×10^8)	9.94×10^{13} (4.4×10^{10})
C'	82.7 (12)	14.4×10^{11} (44×10^8)	11.9×10^{13} (5.3×10^{10})
D	48.3 (7)	7.21×10^{11} (22×10^8)	3.48×10^{13} (1.5×10^{10})
E	31 (4.5)	3.61×10^{11} (11×10^8)	1.12×10^{13} (0.5×10^{10})
E'	17.9 (2.6)	1.28×10^{11} (3.9×10^8)	0.23×10^{13} (0.1×10^{10})

Table 3-8   Probabilistic characteristics associated with fatigue crack growth.

Random variables		Distribution	Reference
Fatigue exponent, B		Deterministic 3.0	Crudele & Yen (2006)
Geometric factor, G		Deterministic 1.0	
Final crack size, a_f mm (in)		Lognormal $E(a_f) = 12.7$ (0.5), $COV(a_f) = 0.10$	
Stress intensity threshold, ΔK_{th} MPa $\sqrt{m}$ (ksi $\sqrt{in}$)		Deterministic 2.75 (2.50)	Barsom & Rolfe (1999)
Crack growth parameter, C MPa $\sqrt{m}$ (ksi $\sqrt{in}$)		Lognormal $E(C) = 2.50E-13$ (4.13E-10), $COV(C) = 0.54$	Righiniotis (2004)
*Initial crack size, a_i mm (in)	category A	$E(a_i) = 0.088$ (0.00346)	Crudele & Yen (2006)
	category B	$E(a_i) = 0.198$ (0.00779)	
	category B'	$E(a_i) = 0.352$ (0.01384)	
	category C	$E(a_i) = 0.506$ (0.01994)	
	category C'	$E(a_i) = 0.352$ (0.01384)	
	category D	$E(a_i) = 1.033$ (0.04069)	
	category E	$E(a_i) = 2.501$ (0.09845)	
	category E'	$E(a_i) = 7.491$ (0.29491)	

* For lognormal PDF, the mean values are calculated by using Eq. 3-15 (Crudele & Yen 2006) and corresponding $COV(a_i) = 0.50$ (Zhang & Mahadevan 2001) for all fatigue categories.

Table 3-9   Equivalent stress ranges S_{re} and S_{re}^* computed by the linear and bi-linear S-N approaches, respectively.

PDF		Lognormal		Rayleigh		Weibull	
Equivalent stress range		S_{re} MPa (ksi)	S_{re}^* MPa (ksi)	S_{re} MPa (ksi)	S_{re}^* MPa (ksi)	S_{re} MPa (ksi)	S_{re}^* MPa (ksi)
Channel (Category)	CH-37 (A)	73.30 (10.63)	69.04 (10.01)	78.80 (11.43)	76.45 (11.09)	76.96 (11.16)	74.21 (10.76)
	CH-21 (B)	45.41 (6.59)	35.90 (5.21)	49.26 (7.14)	43.87 (6.36)	47.28 (6.86)	38.85 (5.64)
	CH-16 (C)	39.16 (5.68)	35.16 (5.10)	39.93 (5.79)	36.43 (5.28)	38.99 (5.66)	34.64 (5.02)
	CH-18 (E)	12.38 (1.80)	9.84 (1.43)	14.01 (2.03)	11.93 (1.73)	14.02 (2.03)	11.94 (1.73)

Note: $S_{re} = \left[\int_0^\infty s^3 \cdot f_S(s) \cdot ds \right]^{\frac{1}{3}}$ and $S_{re}^* = \left[\int_0^{CAFT} CAFT \cdot s^4 \cdot f_S(s) \cdot ds + \int_{CAFT}^\infty s^3 \cdot f_S(s) \cdot ds \right]^{\frac{1}{3}}$.

Table 3-10   Effect of the linear and bi-linear *S-N* approaches on fatigue life.

Channel (Category)	*PDF	Target reliability index, $\beta_{target,1} = 1.0$			Target reliability index, $\beta_{target,2} = 2.0$		
		Fatigue life predicted by the linear *S-N* approach, t_1 (years)	Fatigue life predicted by the bi-linear *S-N* approach, t_2 (years)	Ratio of predicted fatigue lives, t_2/t_1	Fatigue life predicted by the linear *S-N* approach, t_1 (years)	Fatigue life predicted by the bi-linear *S-N* approach, t_2 (years)	Ratio of predicted fatigue lives, t_2/t_1
CH-37 (A)	Lognormal	71.4	85.8	+1.20	37.8	44.9	+1.19
CH-21 (B)	Weibull	13.8	24.9	+1.80	7.2	13.4	+1.86
CH-16 (C)	Lognormal	14.1	19.3	+1.37	7.1	10.2	+1.44
CH-18 (E)	Weibull	6.2	9.8	+1.58	2.8	4.5	+1.61

* PDF indicates a best fit obtained from goodness-of-fit tests.

97
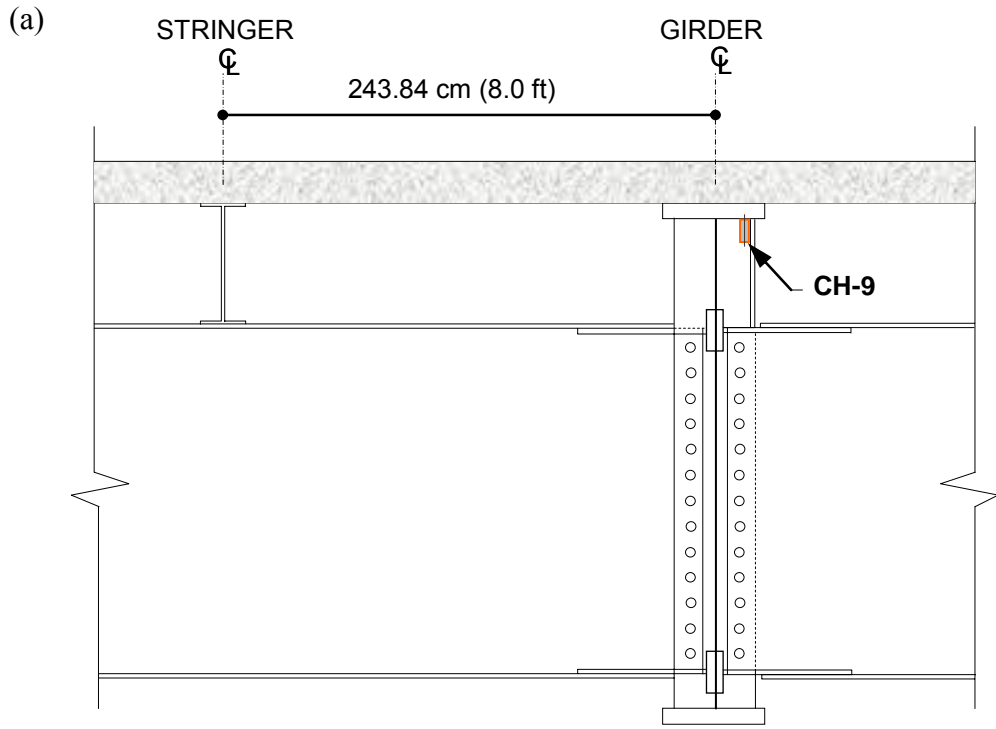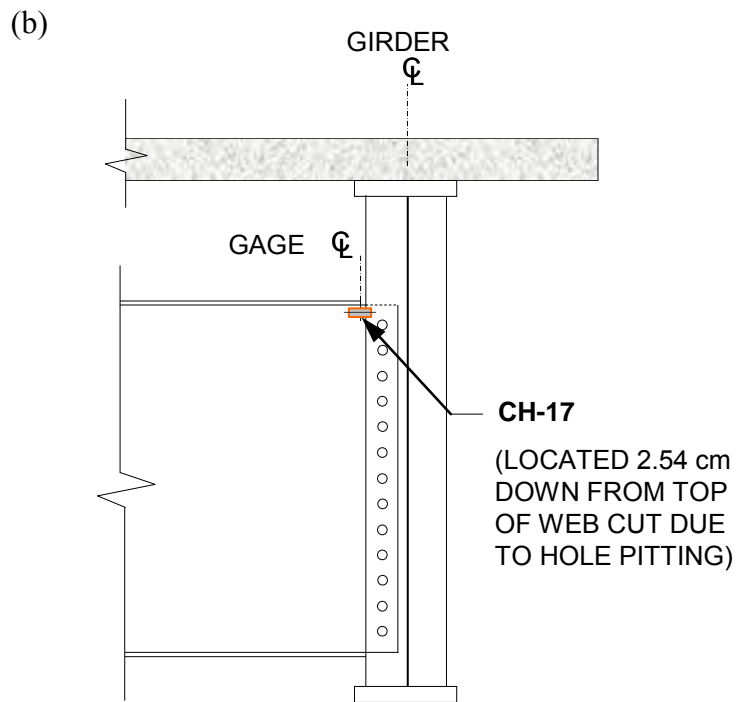
(a) at the channel CH-9

(b) at the channel CH-17

Figure 3-1   Detail of the Neville Island Bridge (adapted from Connor et al. 2005).

(a)

(a) at the channel CH-9

(b)
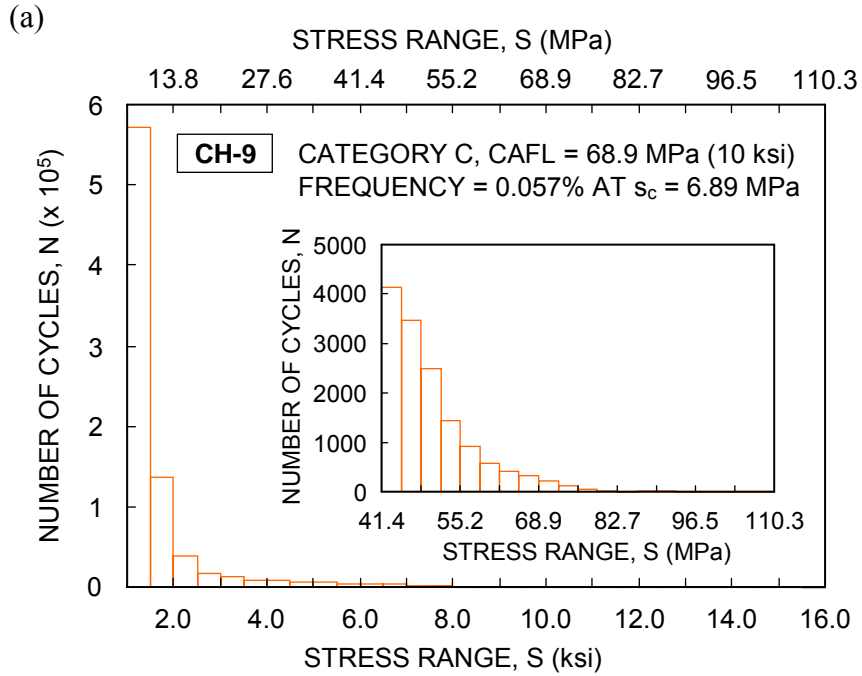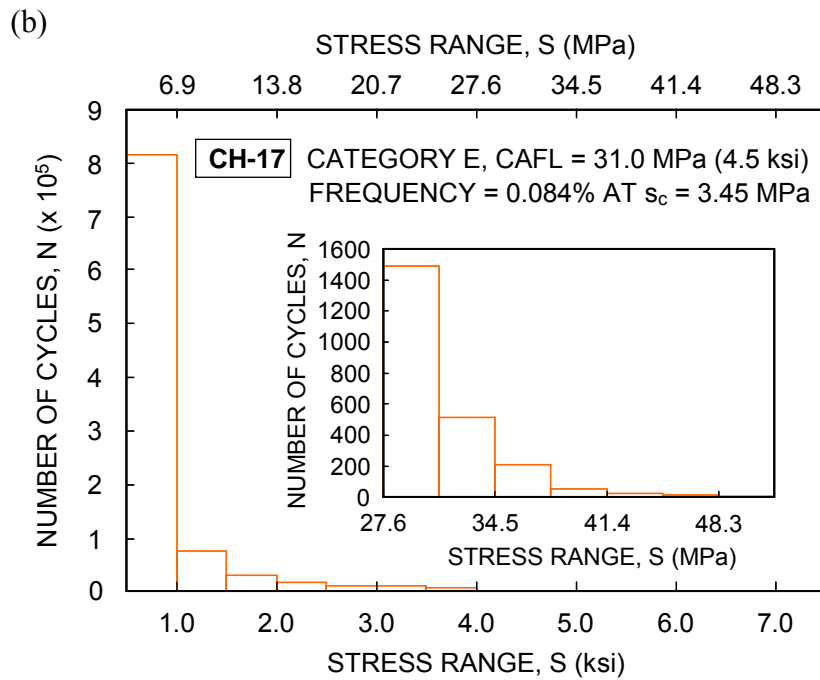
(b) at the channel CH-17

Figure 3-2   Stress-range bin histogram of the Neville Island Bridge (based on data
from Connor et al. 2005).
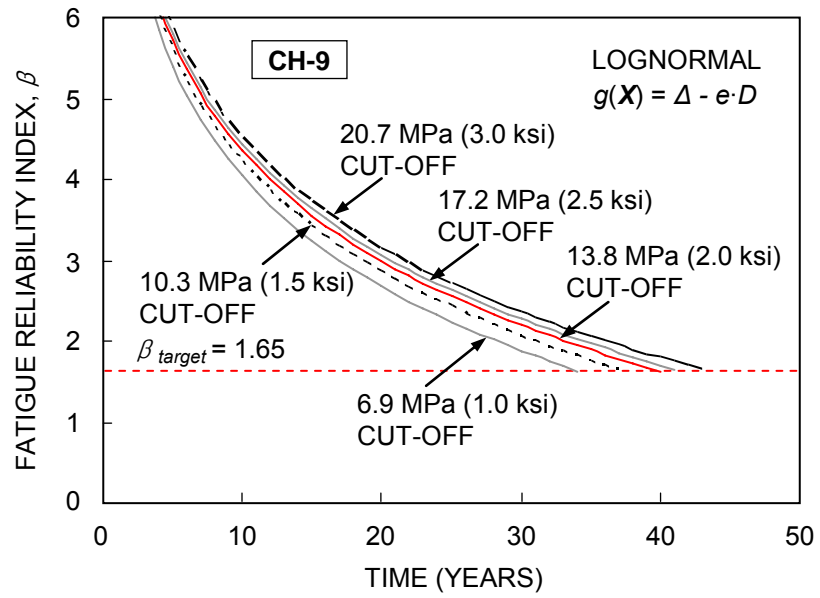
Figure 3-3   Effect of the predefined cut-off thresholds on fatigue reliability.
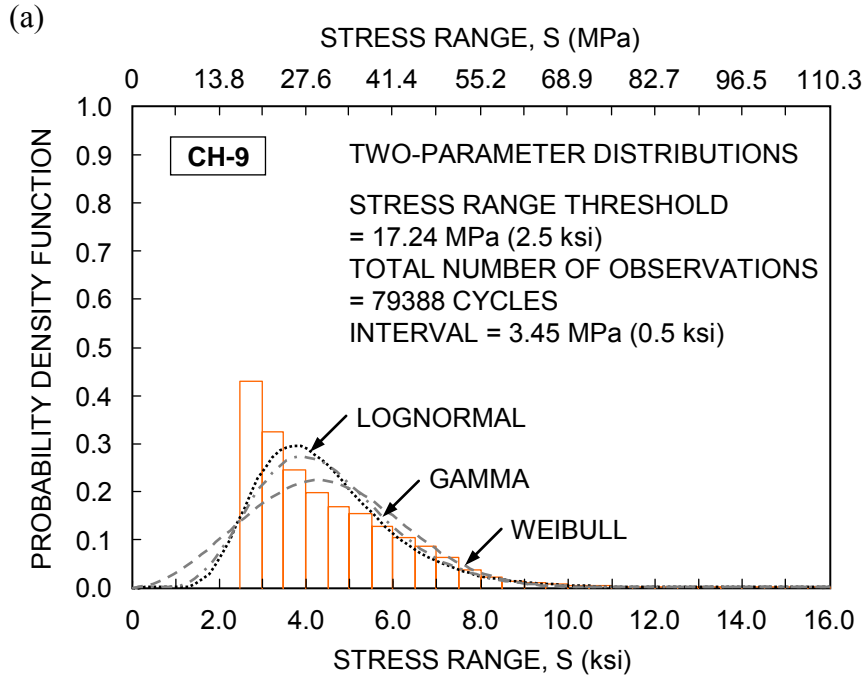
(a) using two-parameter PDFs
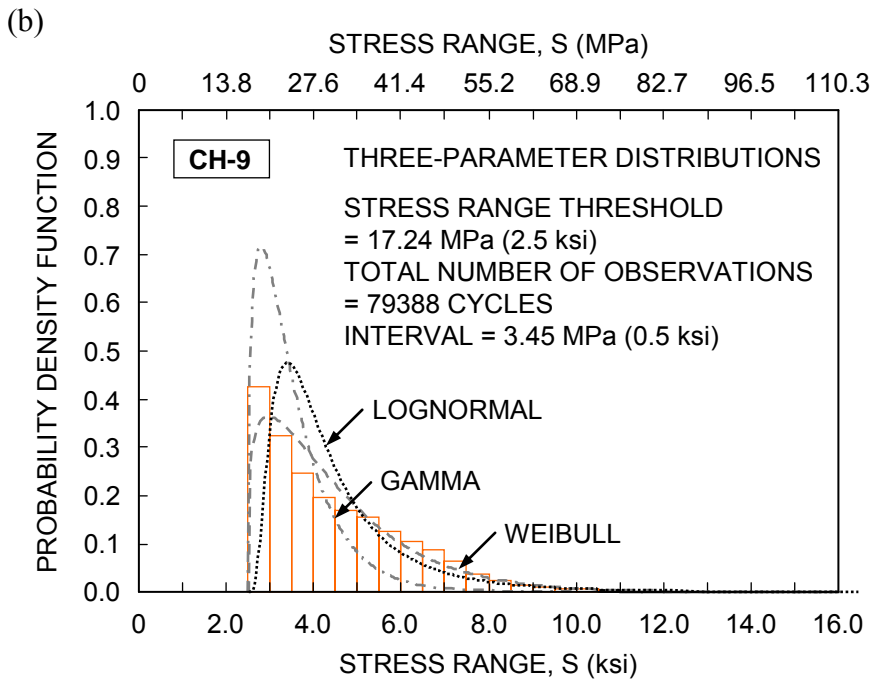
(b) using three-parameter PDFs

Figure 3-4   Stress-range bin histogram and PDFs at CH-9 of the Neville Island Bridge
(based on data from Connor et al. 2005).
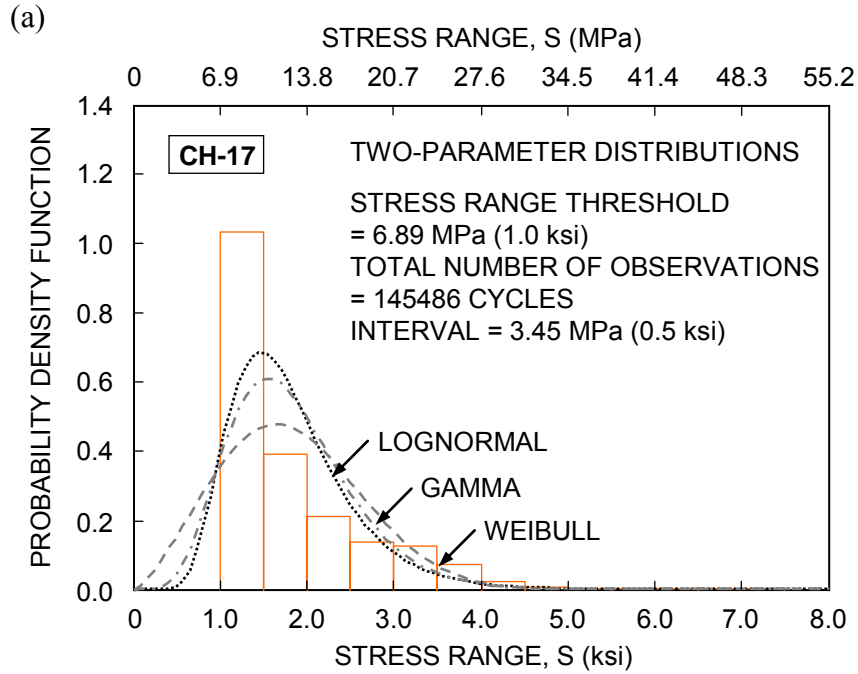
(a) using two-parameter PDFs
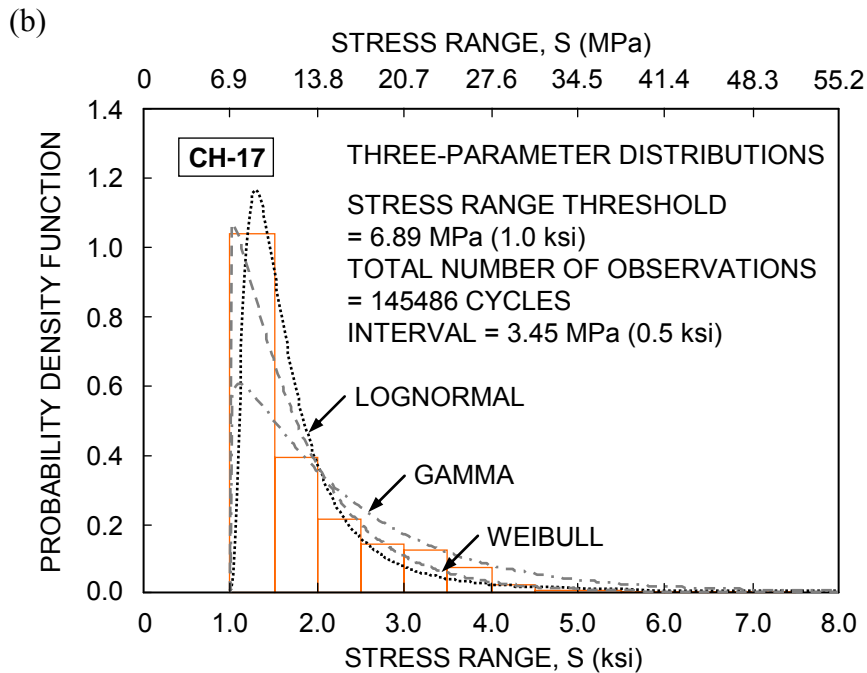
(b) using three-parameter PDFs

Figure 3-5   Stress-range bin histogram and PDFs at CH-17 of the Neville Island
Bridge (based on data from Connor et al. 2005).

(a)

(a) at the channel CH-9

(b)
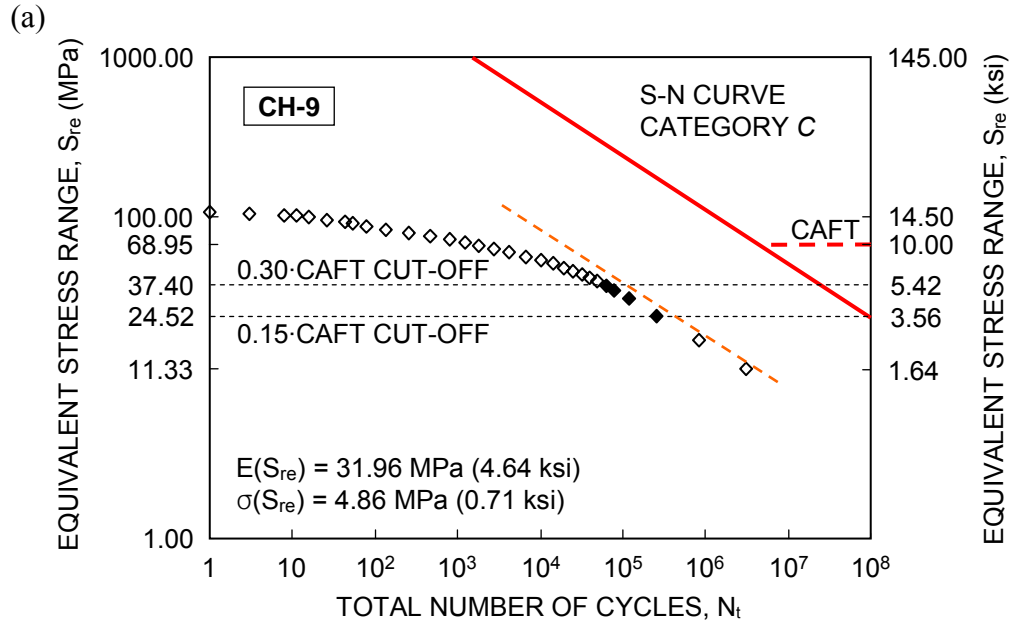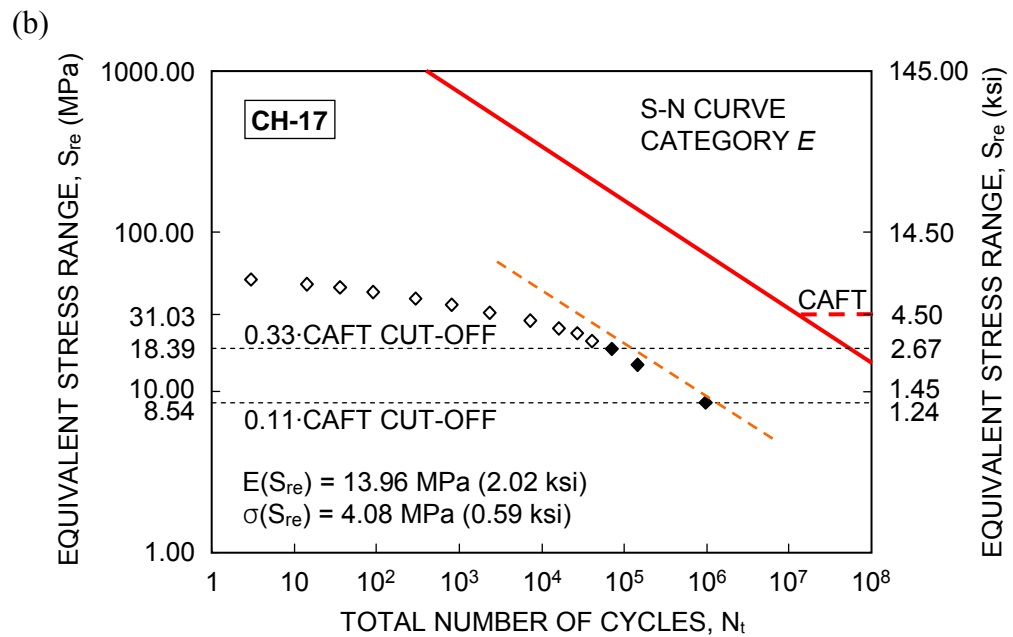
(b) at the channel CH-17

Figure 3-6   Equivalent stress range and total number of cycles according to the applicable stress range cut-off thresholds.

(a)

STRESS RANGE, S (MPa)

(a) lognormal PDF

(b)

STRESS RANGE, S (MPa)

(b) Weibull PDF

104

(c)

STRESS RANGE, S (MPa)

PROBABILITY DENSITY FUNCTION

CH-9

GAMMA
$E(S_{re})$ = 31.67 MPa (4.59 ksi)
$\sigma(S_{re})$ = 5.05 MPa (0.73 ksi)

CUT1
CUT2
CUT3
CUT4

STRESS RANGE, S (ksi)
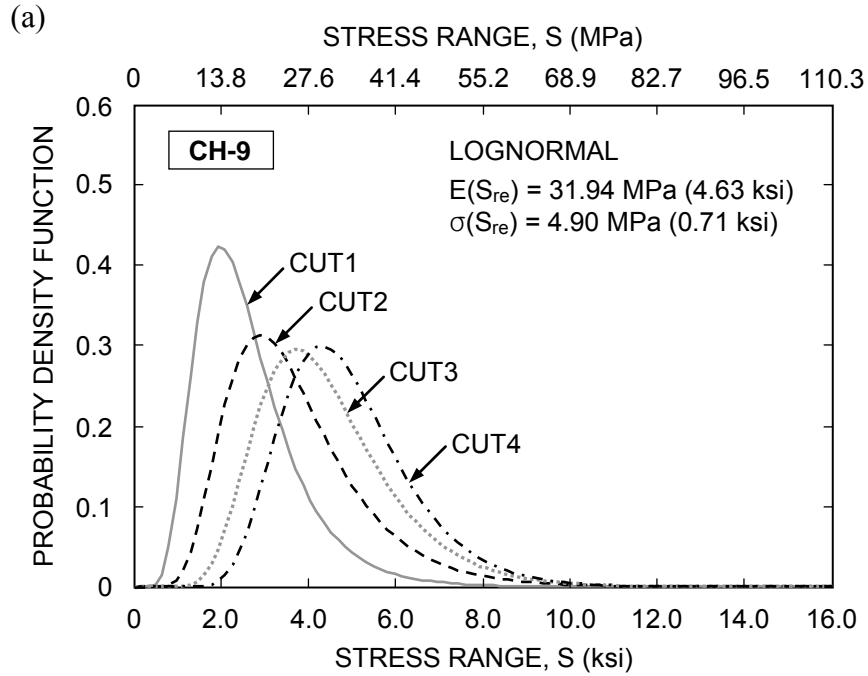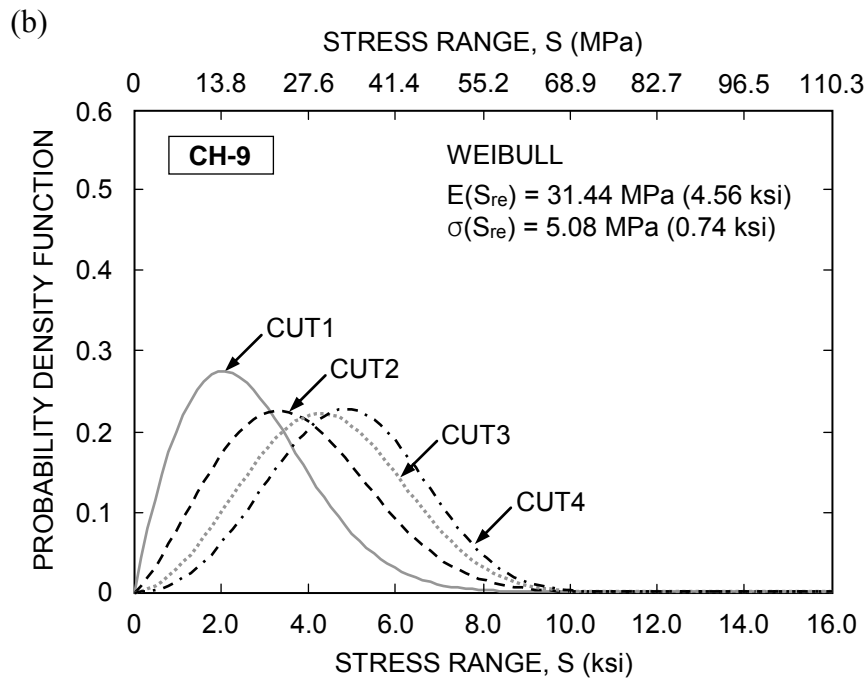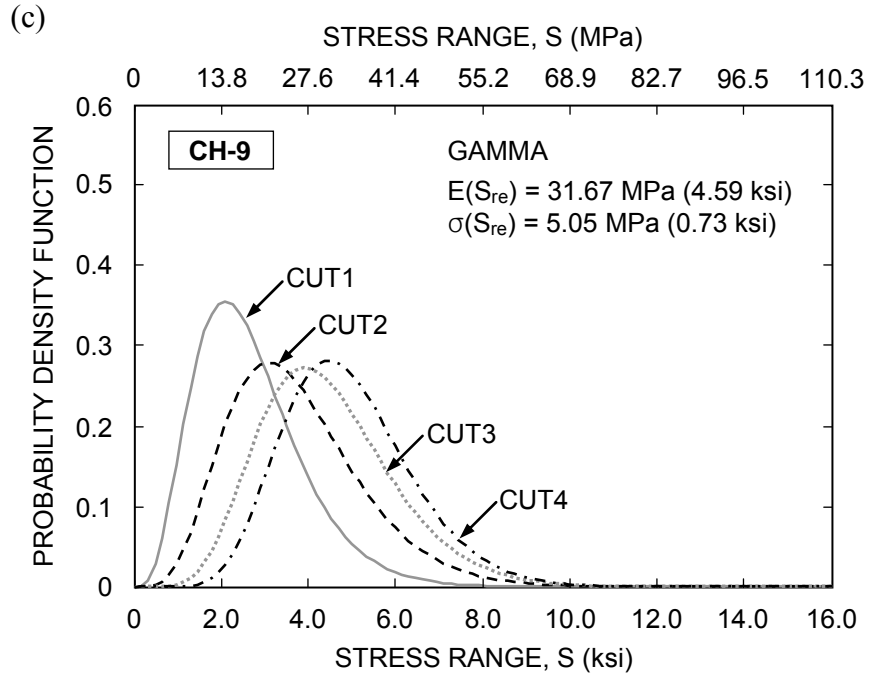
(c) Gamma PDF

Figure 3-7   PDFs according to the predefined cut-off thresholds.
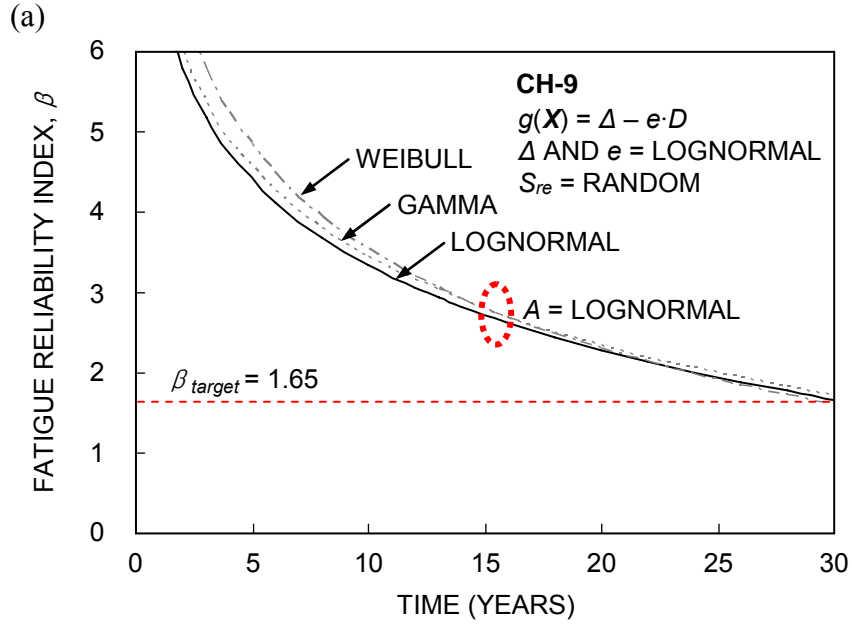
(a) at the channel CH-9
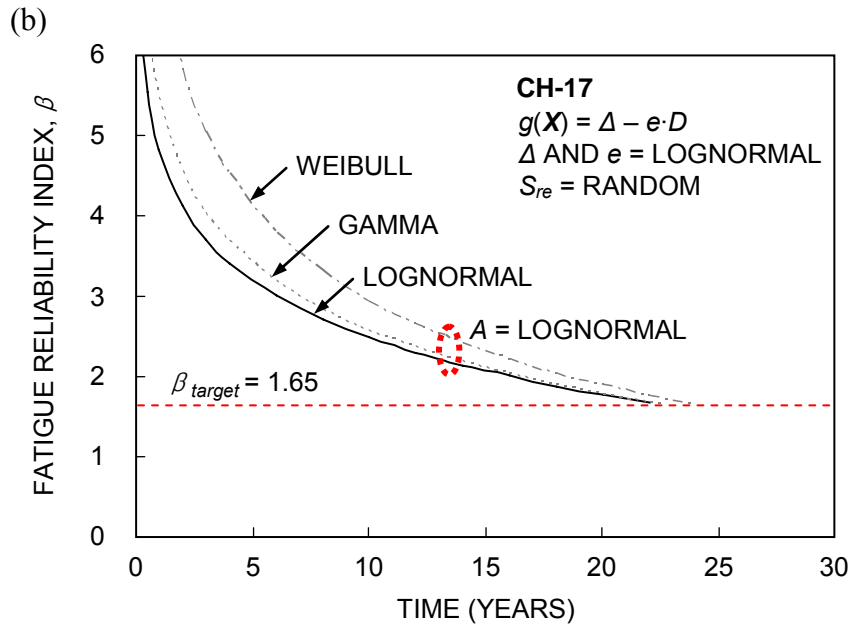
(b) at the channel CH-17

Figure 3-8   Effect of the PDF of S_{re} on fatigue reliability of the details.

(a)

STRESS RANGE, S (MPa)

LOGNORMAL OF CH-9

STRESS RANGE, S (ksi)

(a) lognormal PDF

(b)

STRESS RANGE, S (MPa)

WEIBULL OF CH-9

STRESS RANGE, S (ksi)

(b) Weibull PDF

107

(c)

STRESS RANGE, S (MPa)
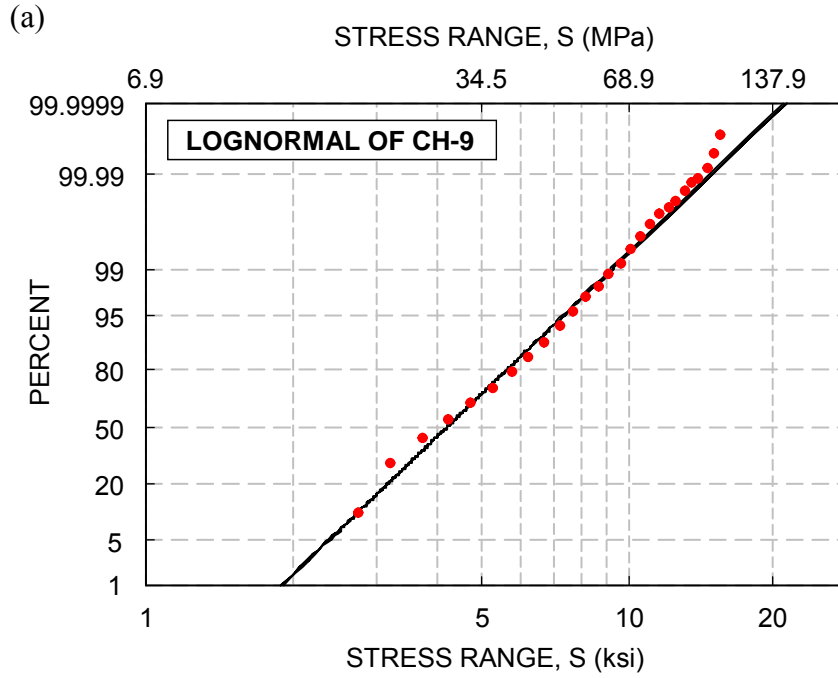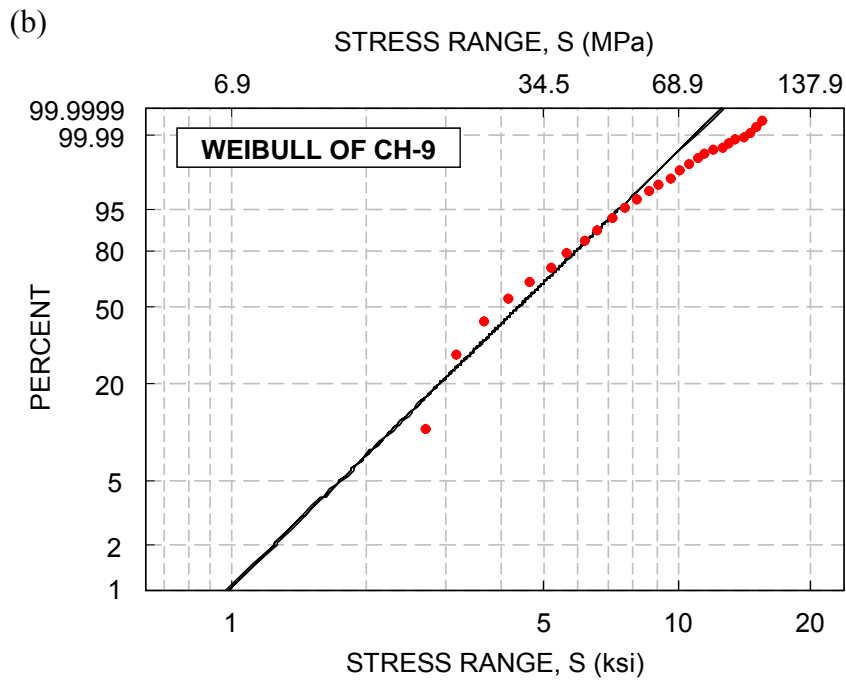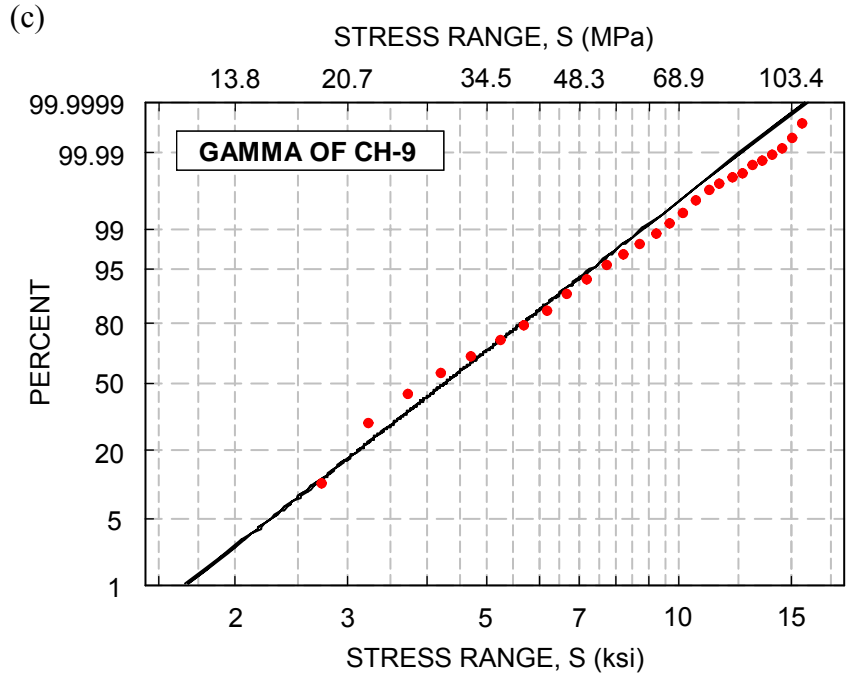
(c) Gamma PDF

Figure 3-9   Goodnees-of-fit tests at the channel CH-9.

(a)

(a) at the channel CH-9

(b)
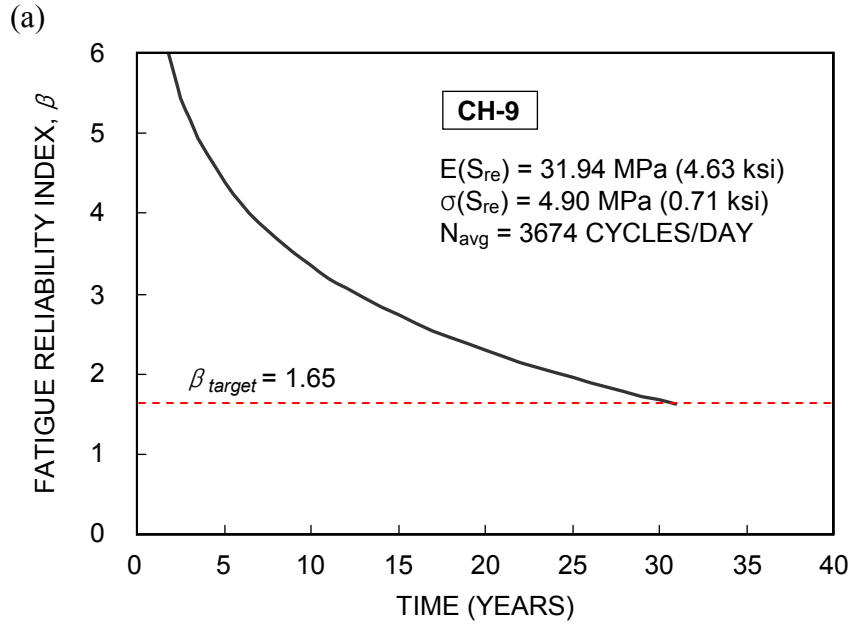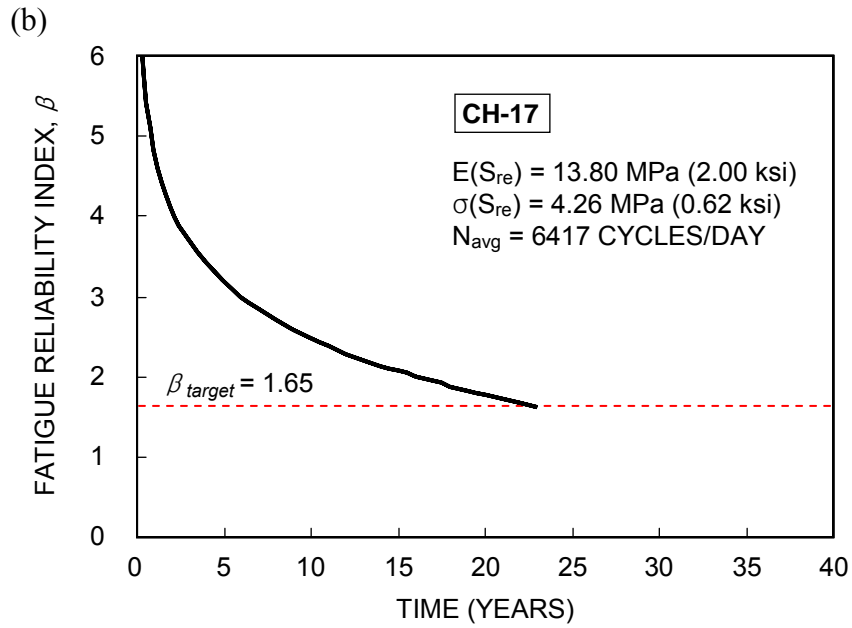
(b) at the channel CH-17

Figure 3-10   Fatigue reliability evaluation in the details of the Neville Island Bridge.
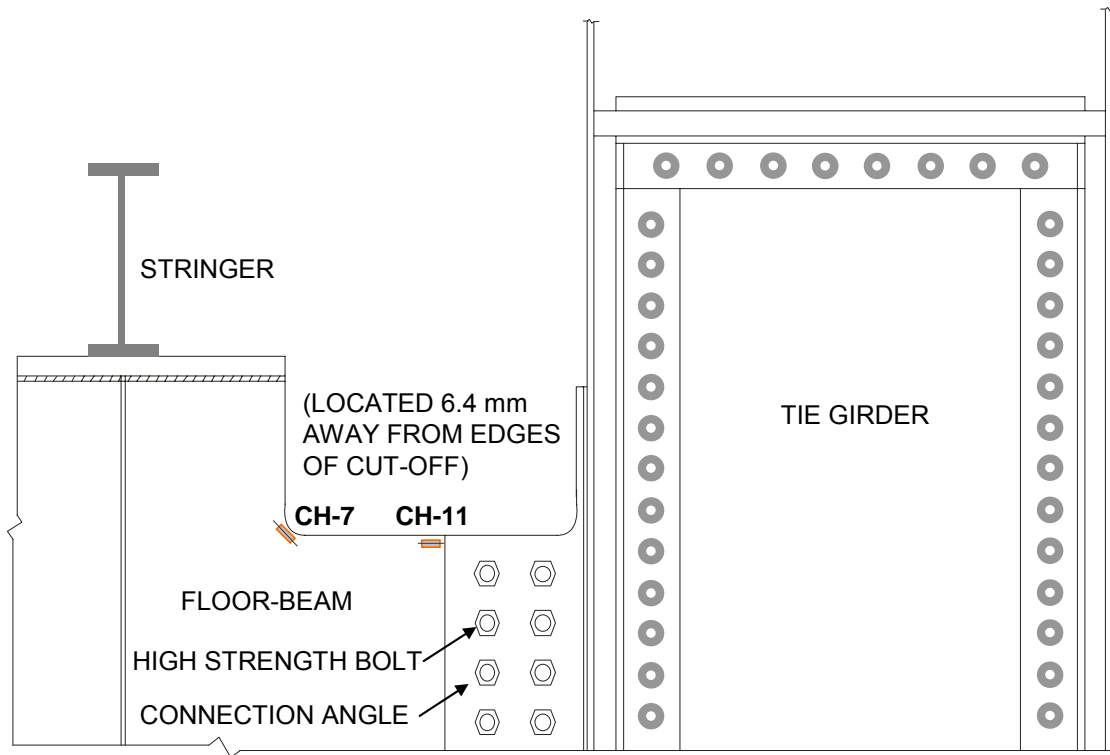
Figure 3-11   Detail of the Birmingham Bridge (adapted from Connor et al. 2004).

(a)

(a) at the channel CH-7

(b)
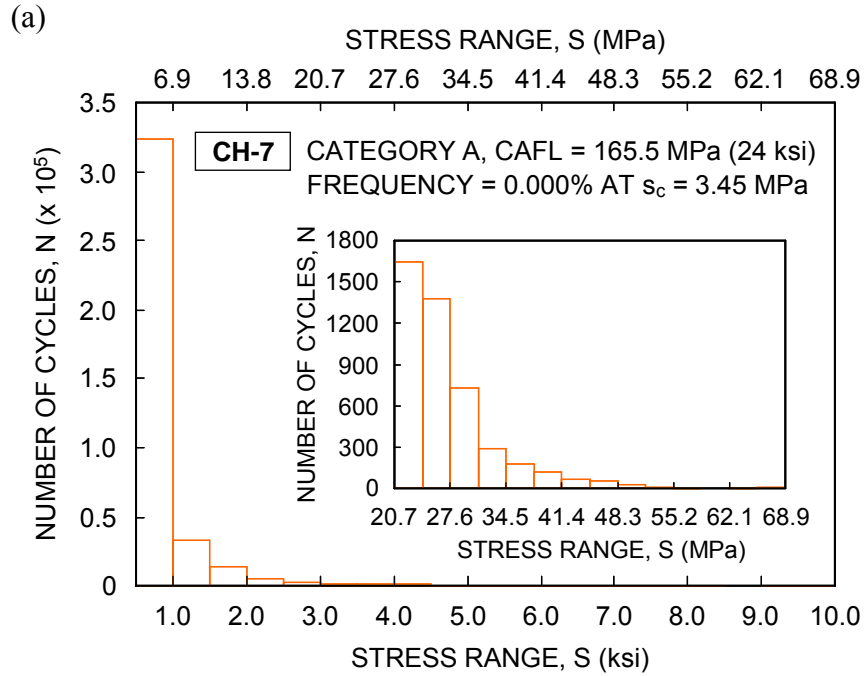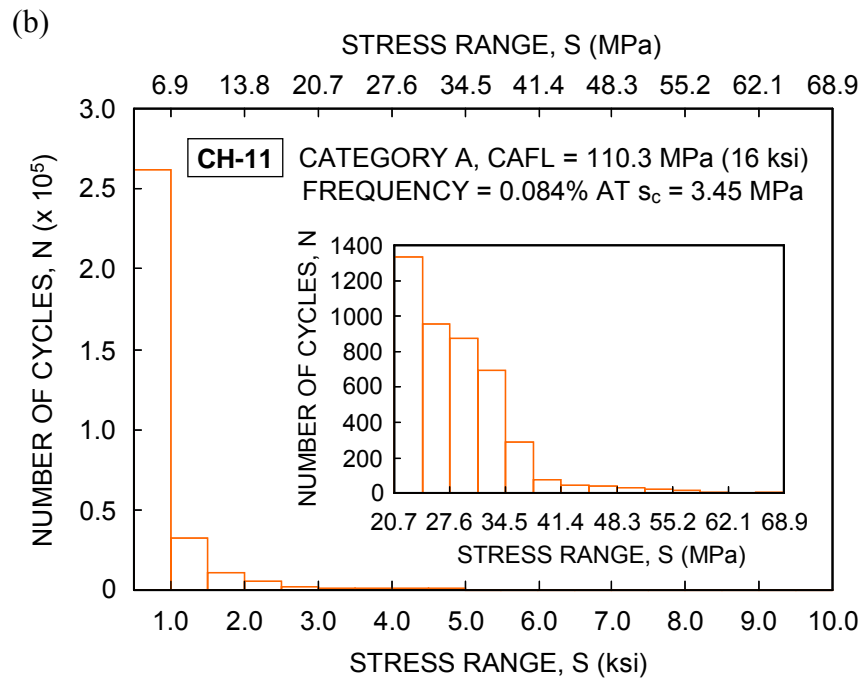
(b) at the channel CH-11

Figure 3-12 Stress-range bin histogram of the Birmingham Bridge (based on data from Connor et al. 2004).
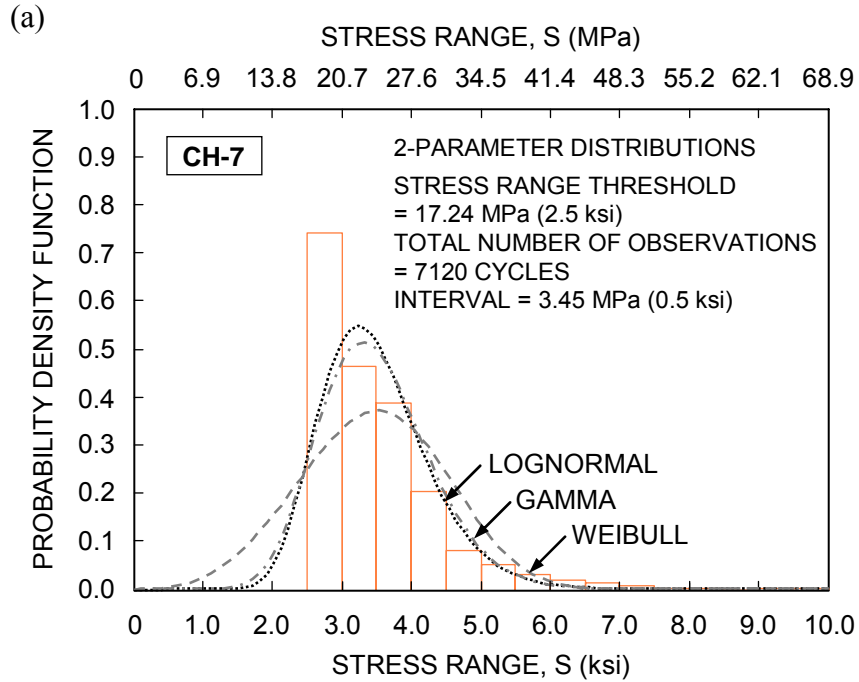
(a) using two-parameter PDFs
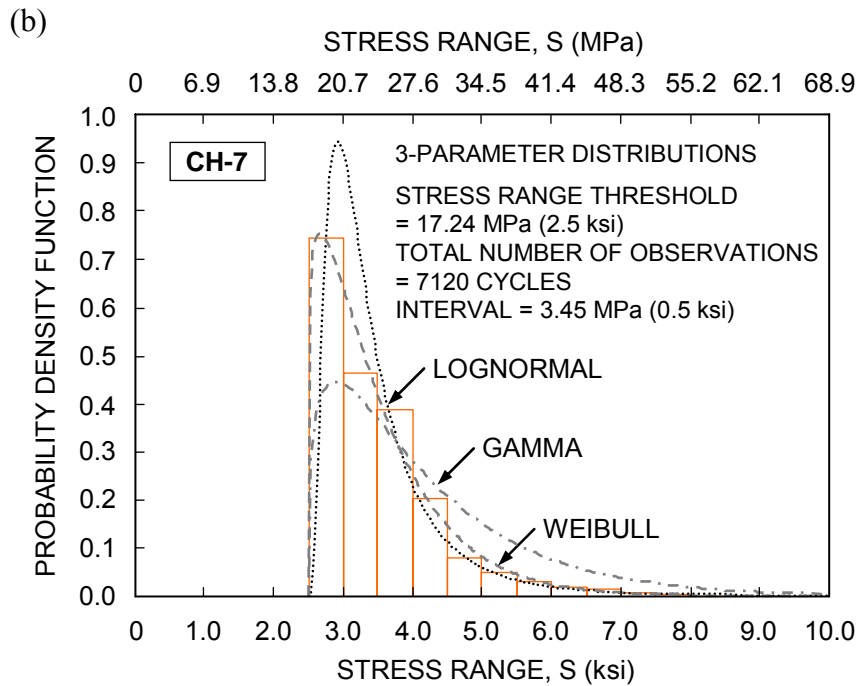
(b) using three-parameter PDFs

Figure 3-13   Stress-range bin histogram and PDFs at CH-7 of the Birmingham Bridge
(based on data from Connor et al. 2005).

(a)

(a) using two-parameter PDFs

(b)
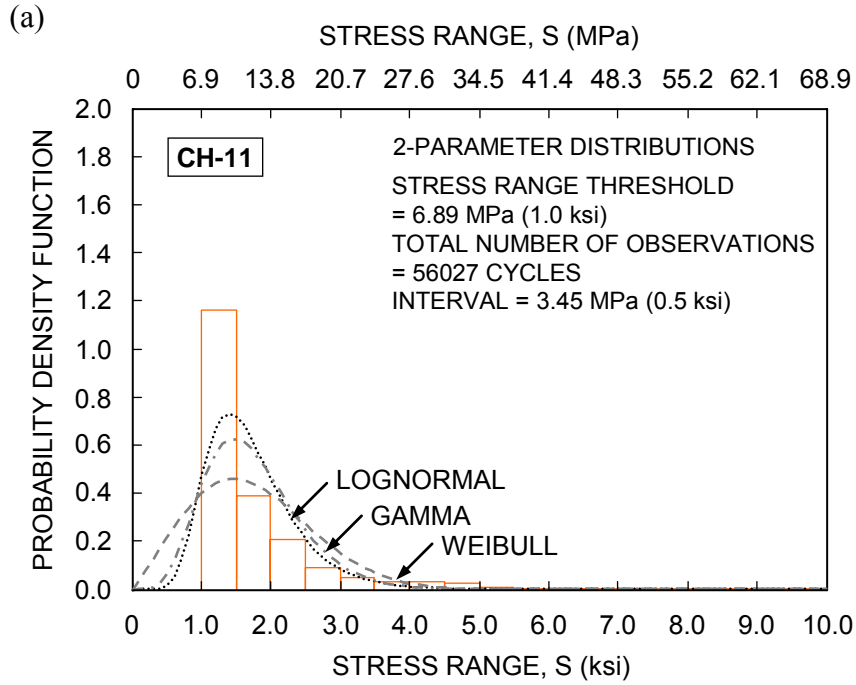
(b) using three-parameter PDFs

Figure 3-14   Stress-range bin histogram and PDFs at CH-11 of the Birmingham
Bridge (based on data from Connor et al. 2005).

(a)

(a) at the channel CH-7

(b)
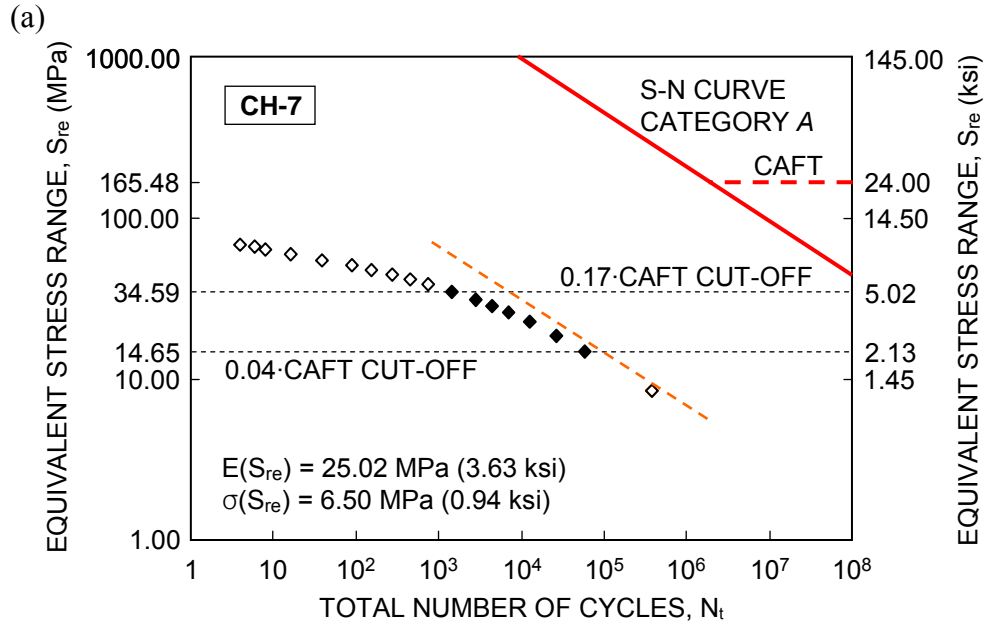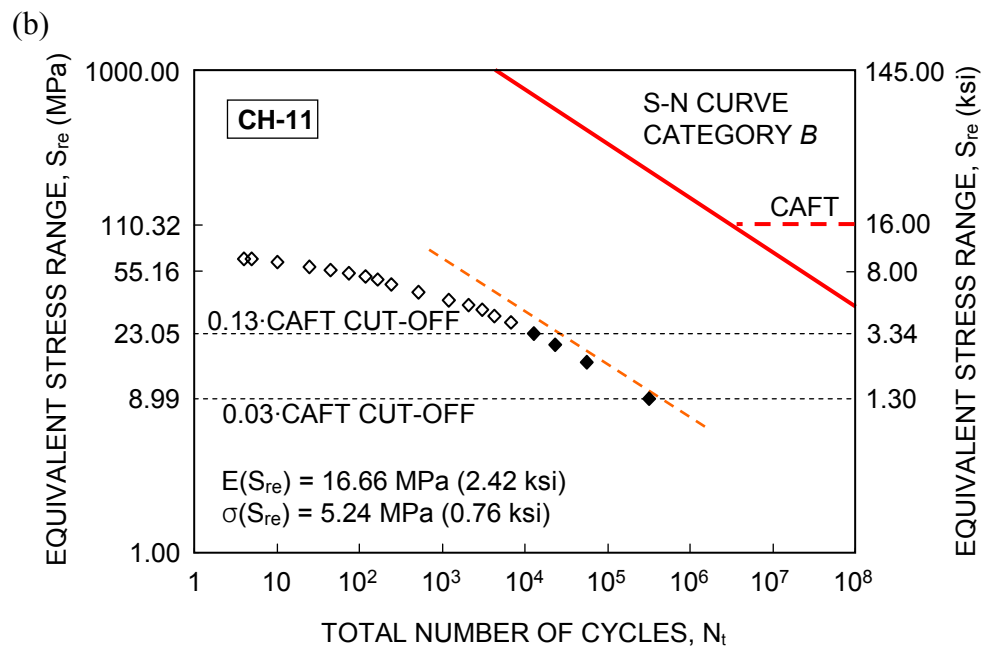
(b) at the channel CH-11

Figure 3-15   Equivalent stress range and total number of cycles according to the applicable stress range cut-off thresholds.

114

(a)

(a) at the channel CH-7

(b)
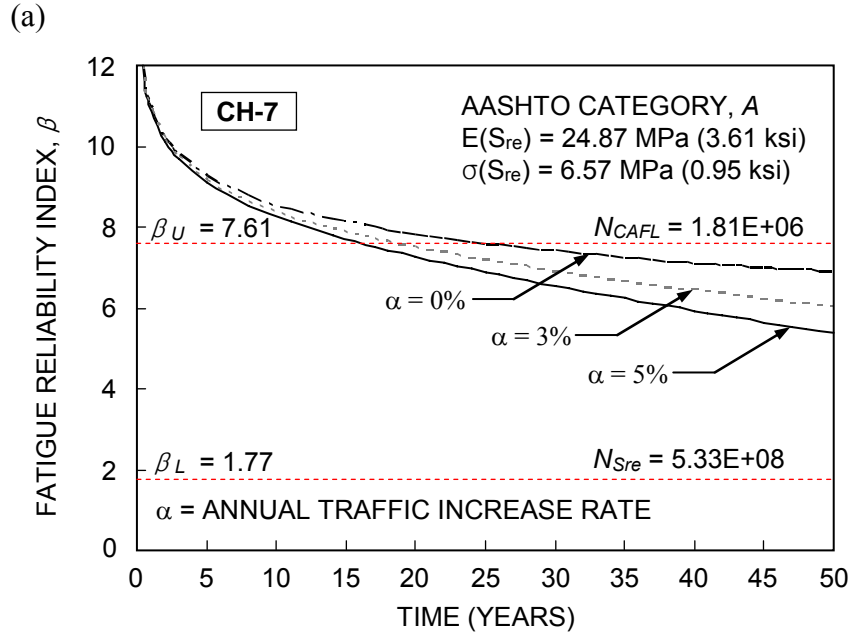
(b) at the channel CH-11

Figure 3-16   Fatigue reliability evaluation in the details of the Birmingham Bridge.
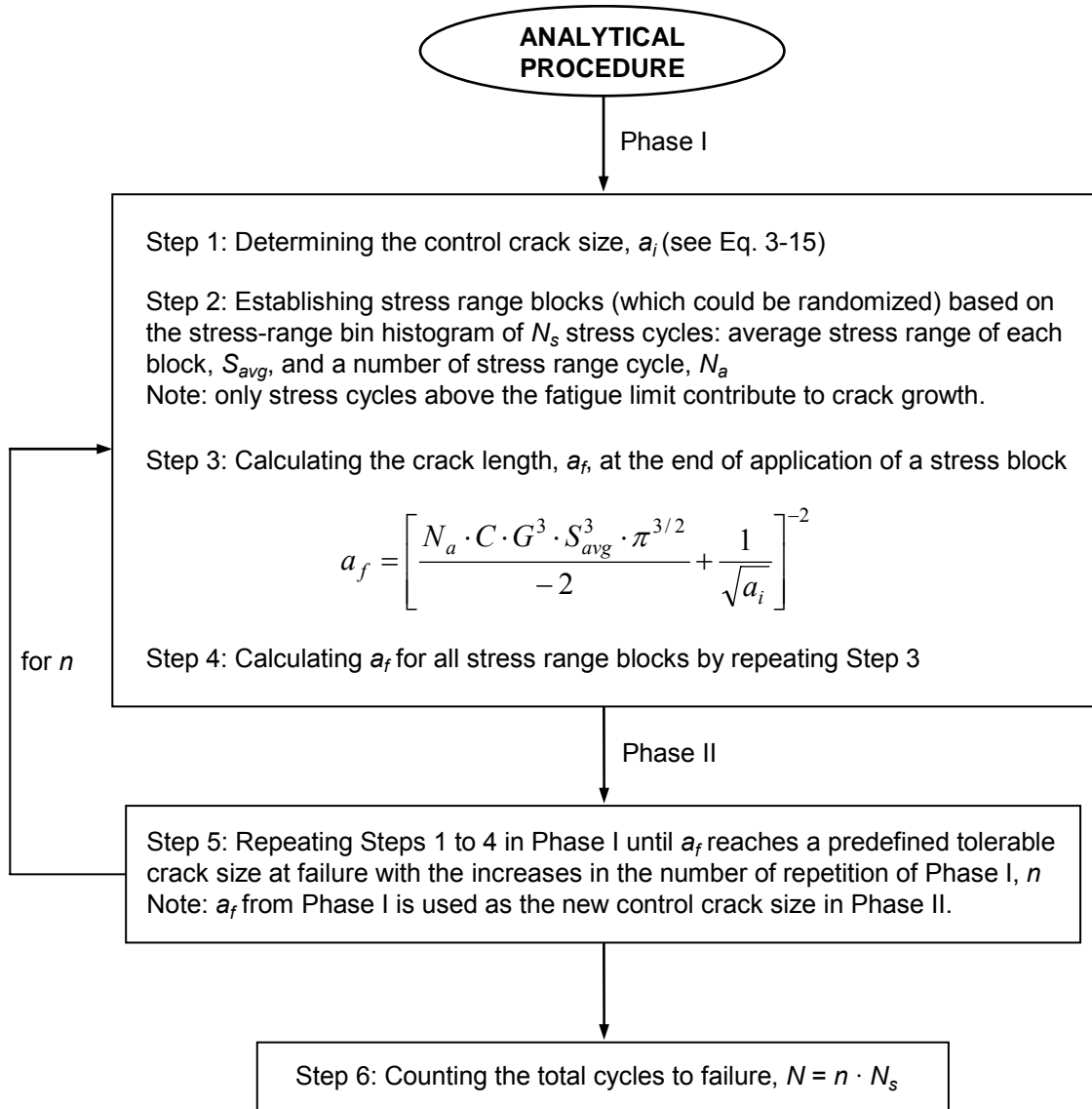
Figure 3-17 Analytical procedure using the concept of decreasing the CAFT (adapted from Crudele & Yen 2006).
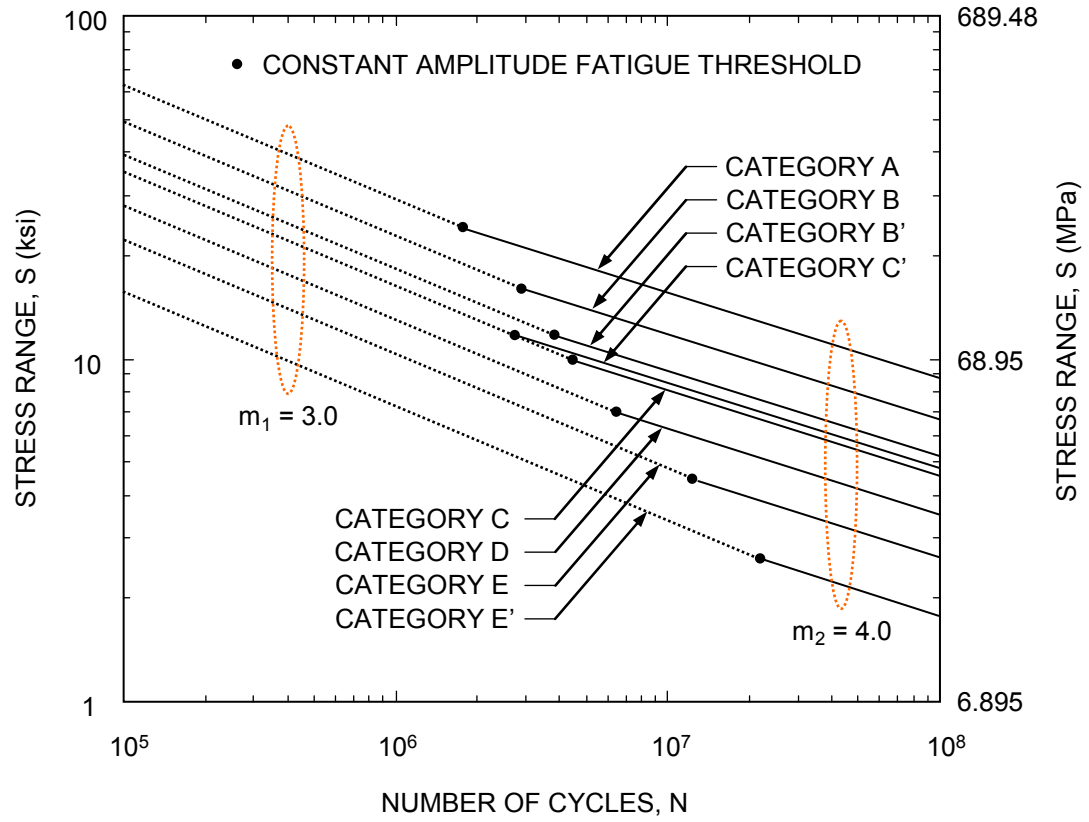
Figure 3-18   Bi-linear *S-N* lines using $m_1 = 3.0$ and $m_2 = 4.0$ for all fatigue categories.

Pier 25

Pier 26

5 @ 7.6 m = 38 m

GIRDER
G1

13.74 m

FB 17

FB 18

FB 19

FB 20

5@2.432=12.16 m

13.97 m

GIRDER
G2

A

A

GIRDER
G3

B

B

2.58 m

16.44 m

FB 38

FB 39

FB 40

FB 41

7@2.432=17.02m

19.61 m

GIRDER
G4

W 24 x 68
STRINGERS TYP.

(a) plan of span 25

118

(b)

GIRDER G2
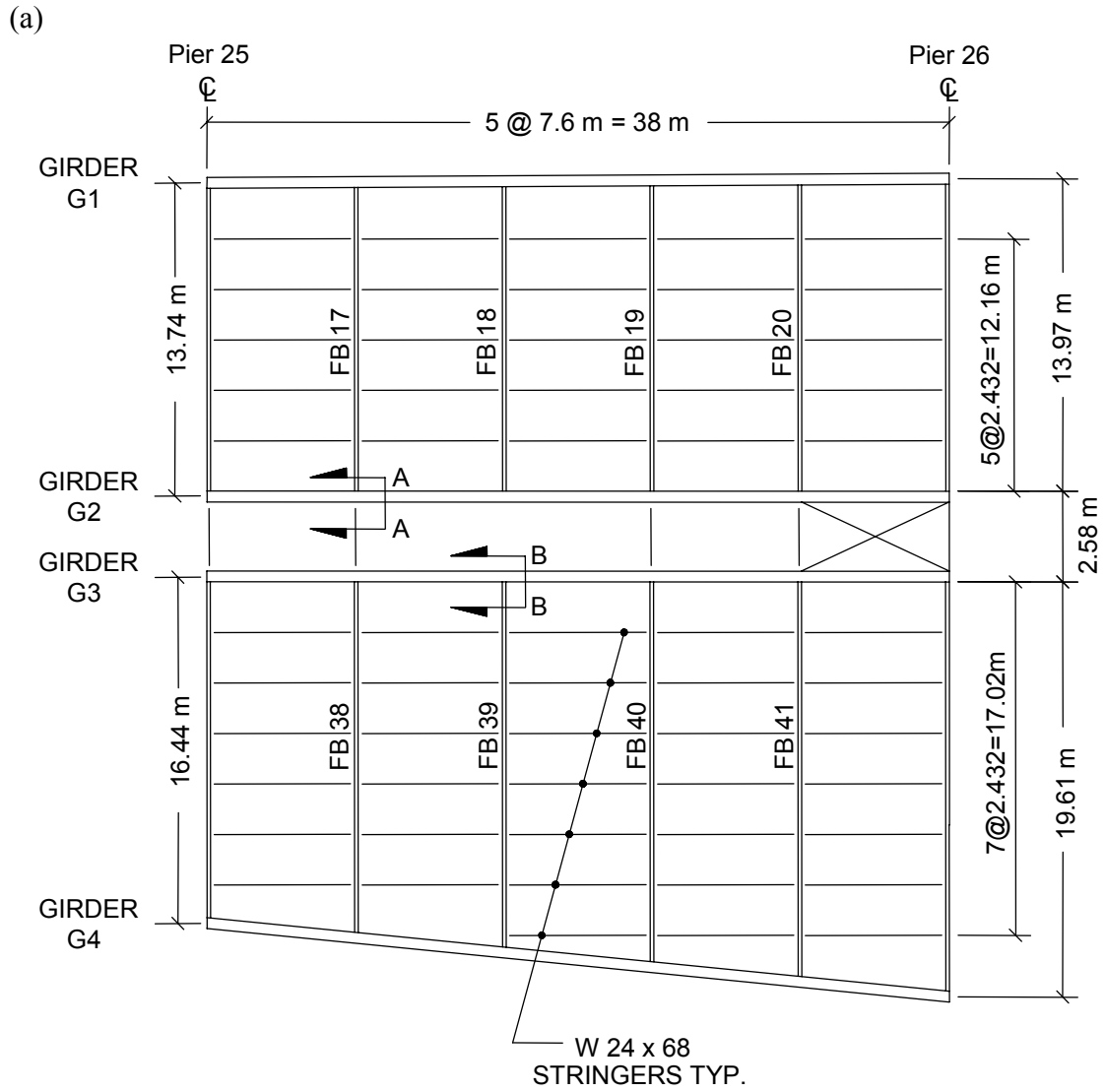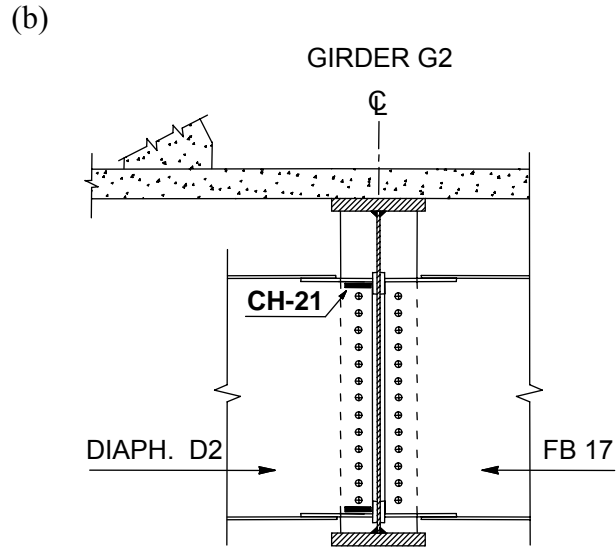
(b) at the channel CH-21 in section A-A

(c)

GIRDER G3
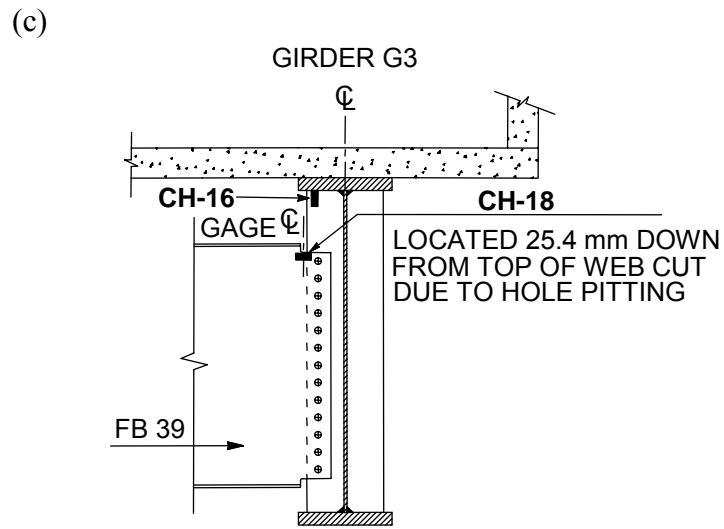
(c) at the channels CH-16 and CH-18 in section B-B

Figure 3-19   Fatigue details of the Neville Island Bridge (adapted from Connor et al. 2005).

(a)

STRESS RANGE, S (MPa)

CH-37: **CATEGORY A**

HISTOGRAM AND PDFs
N = 8,053 CYCLES
MAX (S) = 3.5 ksi (24.1 MPa)

LOGNORMAL PDF
$\lambda = 2.214$, $\zeta = 0.316$

SCALED PDFs
MAX (S) = 35 ksi

RAYLEIGH PDF
$S_{ro} = 7.350$

WEIBULL PDF
$\alpha = 10.897$, $\beta = 2.602$

PROBABILITY DENSITY FUNCTION

STRESS RANGE, S (ksi)

(a) stress-range bin histogram and PDFs

(b)

STRESS RANGE, S (MPa)

CH-37
LOGNORMAL PDF

PERCENT
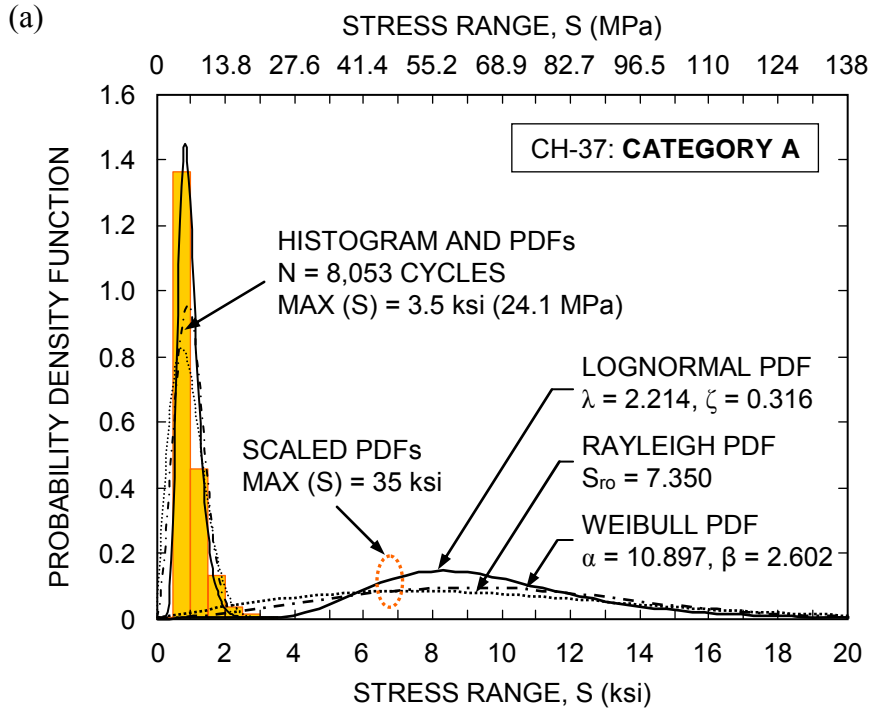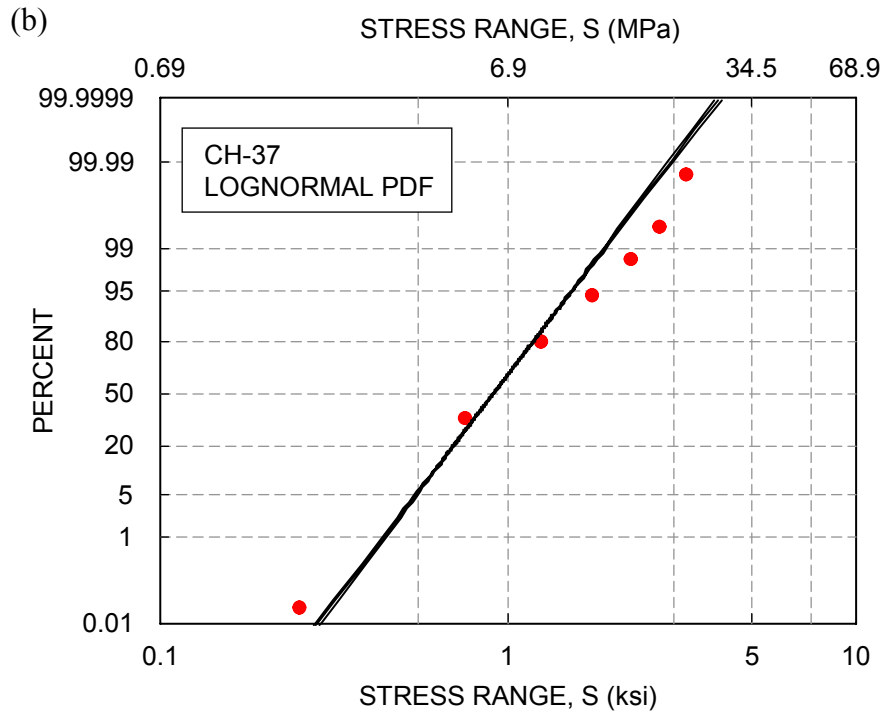
STRESS RANGE, S (ksi)

(b) a goodness-of-fit test of lognormal PDF

Figure 3-20   Fatigue loading at CH-37 for the *S-N* category *A*.

120

(a)

STRESS RANGE, S (MPa)

CH-21: **CATEGORY B**

HISTOGRAM AND PDFs
N = 95,413 CYCLES
MAX (S) = 3.5 ksi (24.1 MPa)

LOGNORMAL PDF
$\lambda = 1.792$, $\zeta = 0.249$

SCALED PDFs
MAX (S) = 23 ksi

RAYLEIGH PDF
$S_{ro} = 4.594$

WEIBULL PDF
$\alpha = 6.901$, $\beta = 3.145$

STRESS RANGE, S (ksi)

(a) stress-range bin histogram and PDFs

(b)
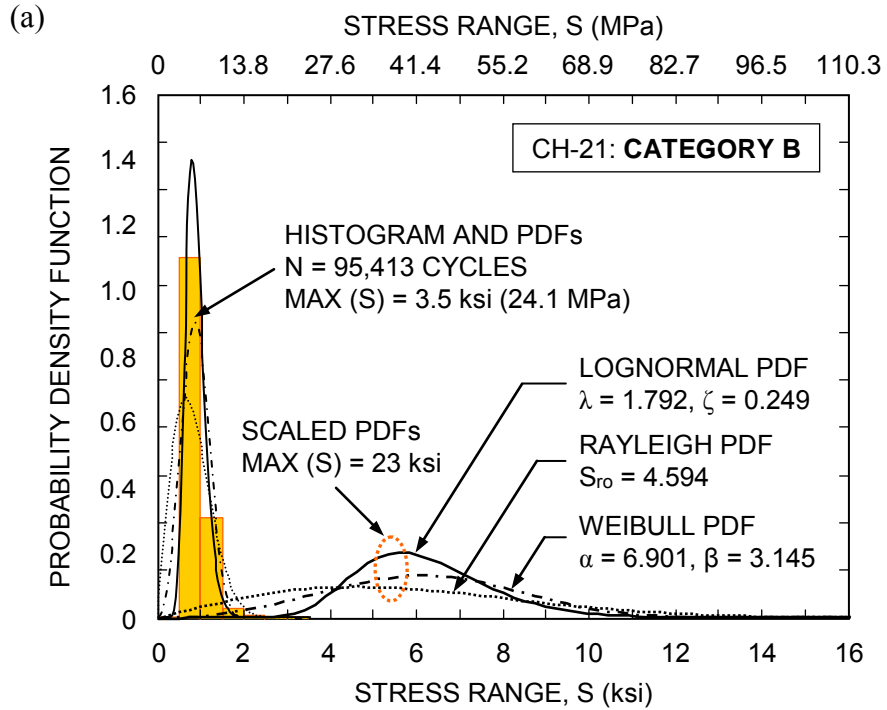
STRESS RANGE, S (MPa)

CH-21
WEIBULL PDF
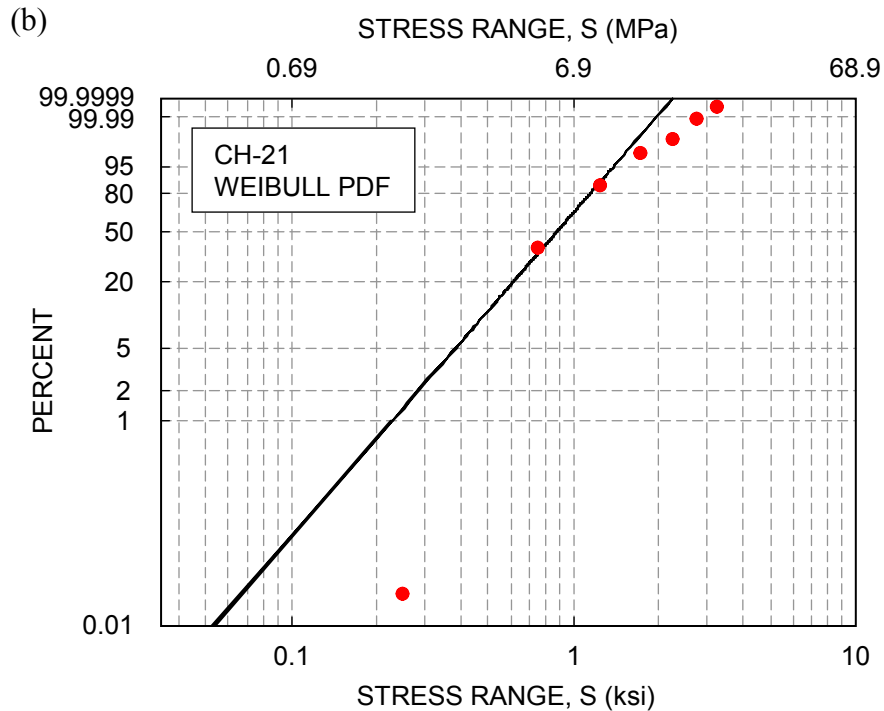
STRESS RANGE, S (ksi)

(b) a goodness-of-fit test of Weibull PDF

Figure 3-21   Fatigue loading at CH-21 for the *S-N* category *B*.

121

(a)

STRESS RANGE, S (MPa)

CH-16: **CATEGORY C**

HISTOGRAM
N = 96,157 CYCLES
STRESS BIN = 0.5 ksi (3.45 MPa)
MAX(S) = 16 ksi (110.3 MPa)

LOGNORMAL PDF
$\lambda = 1.498$, $\zeta = 0.399$

RAYLEIGH PDF
$S_{ro} = 3.725$

WEIBULL PDF
$\alpha = 5.488$, $\beta = 2.527$

PROBABILITY DENSITY FUNCTION

STRESS RANGE, S (ksi)

(a) stress-range bin histogram and PDFs

(b)

STRESS RANGE, S (MPa)

CH-16
LOGNORMAL PDF

PERCENT
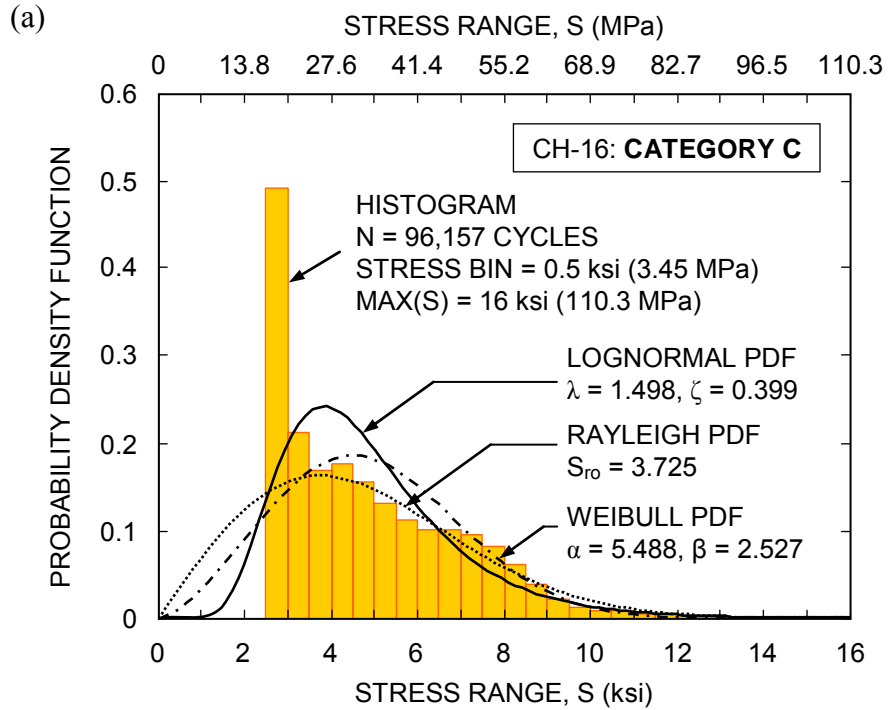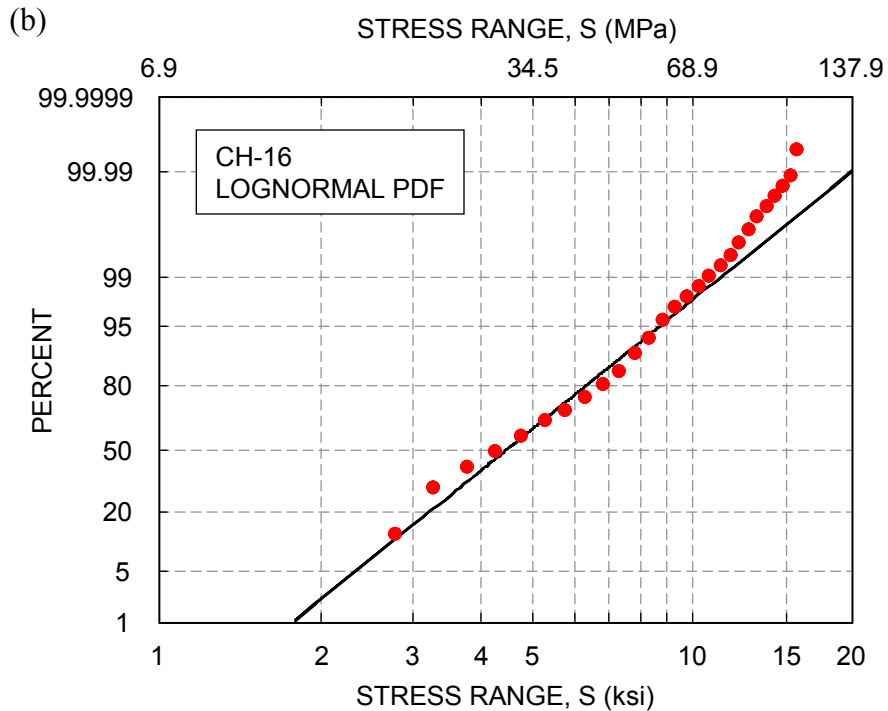
STRESS RANGE, S (ksi)

(b) a goodness-of-fit test of lognormal PDF

Figure 3-22   Fatigue loading at CH-16 for the *S-N* category *C*.

122

(a)

STRESS RANGE, S (MPa)

CH-18: **CATEGORY E**

HISTOGRAM
N = 1,409,424 CYCLES
STRESS BIN = 0.5 ksi (3.45 MPa)
MAX (S) = 12 ksi (82.7 MPa)

LOGNORMAL PDF
$\lambda = 0.414$, $\zeta = 0.338$

RAYLEIGH PDF
$S_{ro} = 1.307$

WEIBULL PDF
$\alpha = 1.846$, $\beta = 1.992$

STRESS RANGE, S (ksi)

(a) stress-range bin histogram and PDFs

(b)

STRESS RANGE, S (MPa)

CH-18
WEIBULL PDF

PERCENT
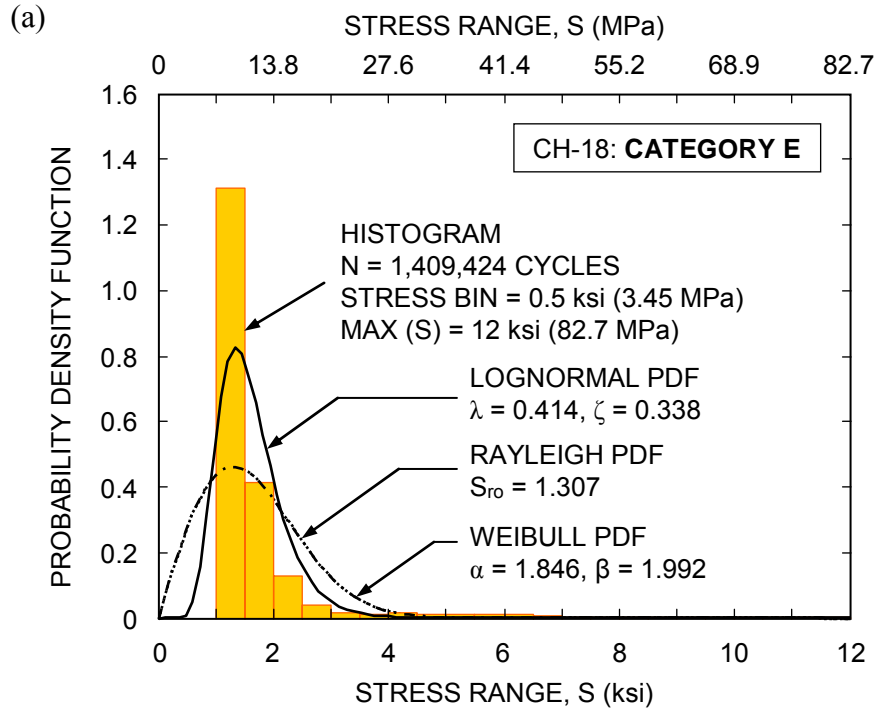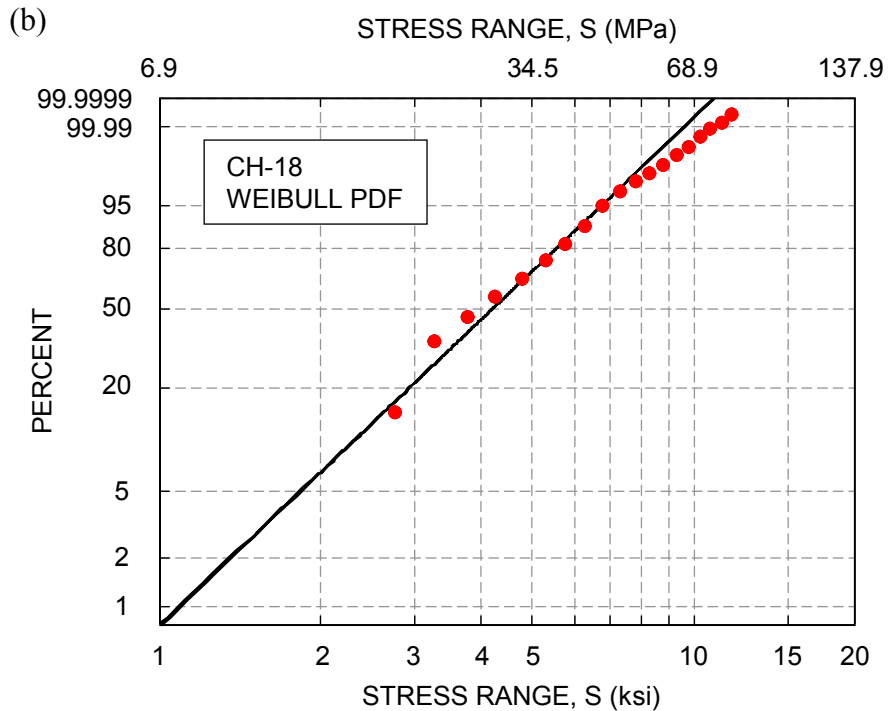
STRESS RANGE, S (ksi)

(b) a goodness-of-fit test of Weibull PDF

Figure 3-23   Fatigue loading at CH-18 for the *S-N* category *E*.

123
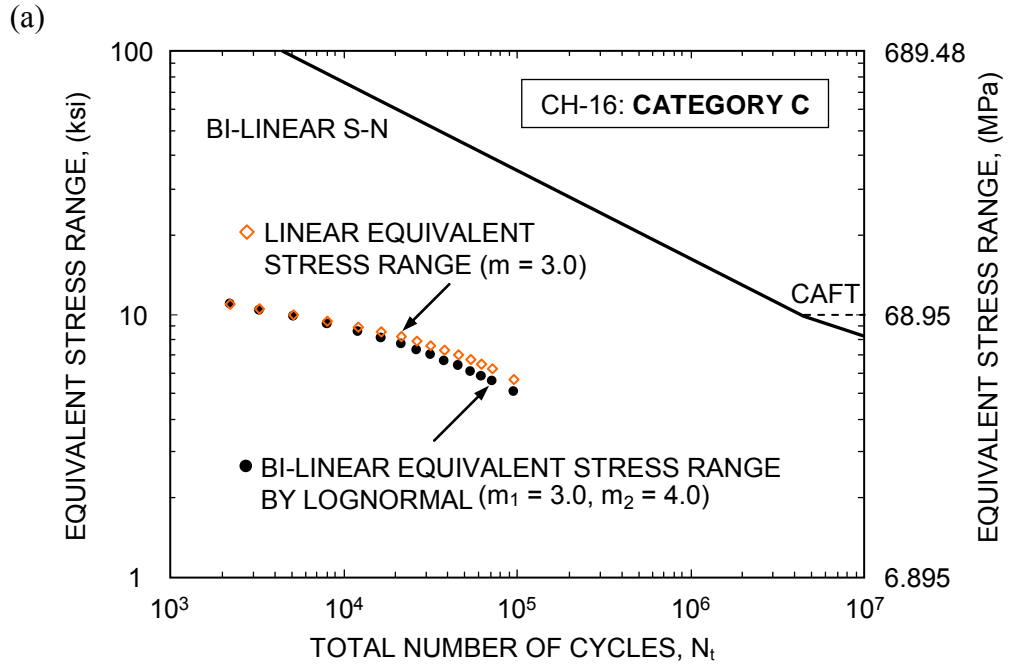
(a) for category C at CH-16
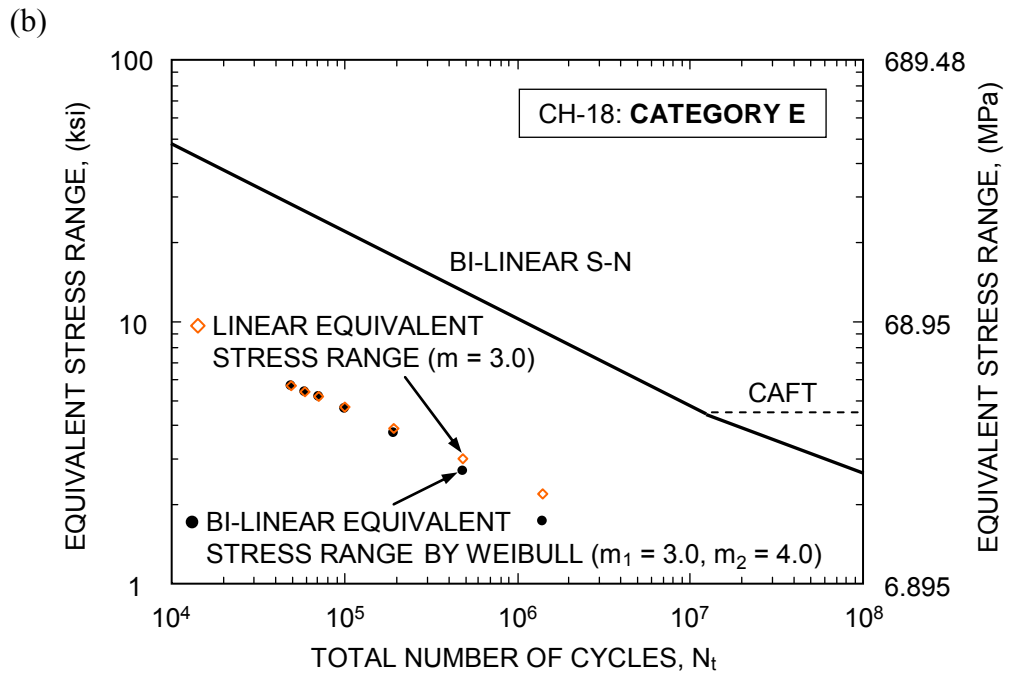
(b) for category E at CH-18

Figure 3-24   Equivalent stress ranges by the linear and bi-linear *S-N* approaches.

(a)

CH-37: **CATEGORY A**

- - - - $m_1 = m_2 = 3.0$
—— $m_1 = 3.0, m_2 = 4.0$

RAYLEIGH

WEIBULL

LOGNORMAL

CRACK SIZE, a (in)

CRACK SIZE, a (mm)

TIME, (YEARS)

(a) crack growth model

(b)

RELIABILITY INDEX, β

LOGNORMAL PDF

BI-LINEAR S-N
($m_1 = 3.0, m_2 = 4.0$)

LINEAR S-N (m = 3.0)

TIME, (YEARS)

(b) fatigue reliability profile for Lognormal PDF

125

(c)

WEIBULL PDF

BI-LINEAR S-N
($m_1 = 3.0$, $m_2 = 4.0$)

LINEAR S-N ($m = 3.0$)

(c) fatigue reliability profile for Weibull PDF

(d)

RAYLEIGH PDF

BI-LINEAR S-N
($m_1 = 3.0$, $m_2 = 4.0$)

LINEAR S-N ($m = 3.0$)

(d) fatigue reliability profile for Rayleigh PDF

Figure 3-25   Time-dependent fatigue life estimation at CH-37 for the *S-N* category A.

CH-21: **CATEGORY B**

$m_1 = m_2 = 3.0$

RAYLEIGH

WEIBULL

LOGNORMAL

$m_1 = 3.0$
$m_2 = 4.0$

CRACK SIZE, a (in)

CRACK SIZE, a (mm)

TIME, (YEARS)

(a) crack growth model

(b)

LOGNORMAL PDF

BI-LINEAR S-N
($m_1 = 3.0$, $m_2 = 4.0$)

LINEAR S-N ($m = 3.0$)

RELIABILITY INDEX, β

TIME, (YEARS)

(b) fatigue reliability profile for Lognormal PDF

(c)

(c) fatigue reliability profile for Weibull PDF

(d)

(d) fatigue reliability profile for Rayleigh PDF

Figure 3-26   Time-dependent fatigue life estimation at CH-21 for the *S-N* category B.
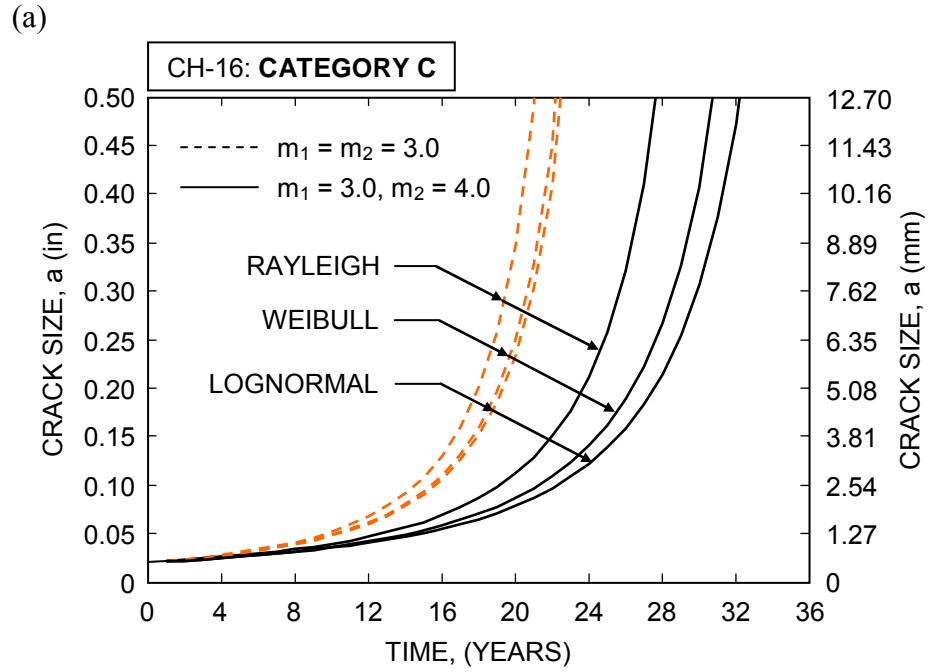
(a)
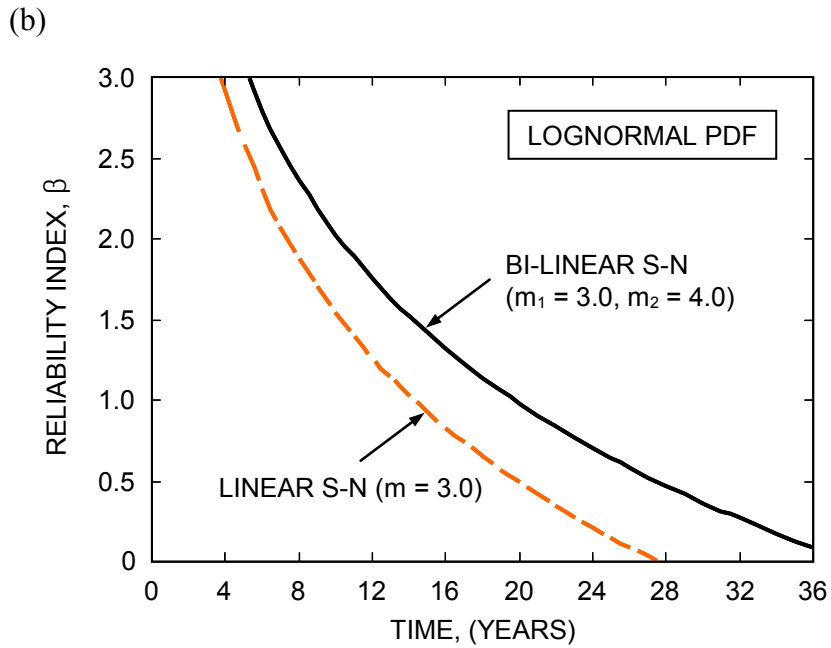
(a) crack growth model

(b)

(b) fatigue reliability profile for Lognormal PDF

(c)

(c) fatigue reliability profile for Weibull PDF

(d)
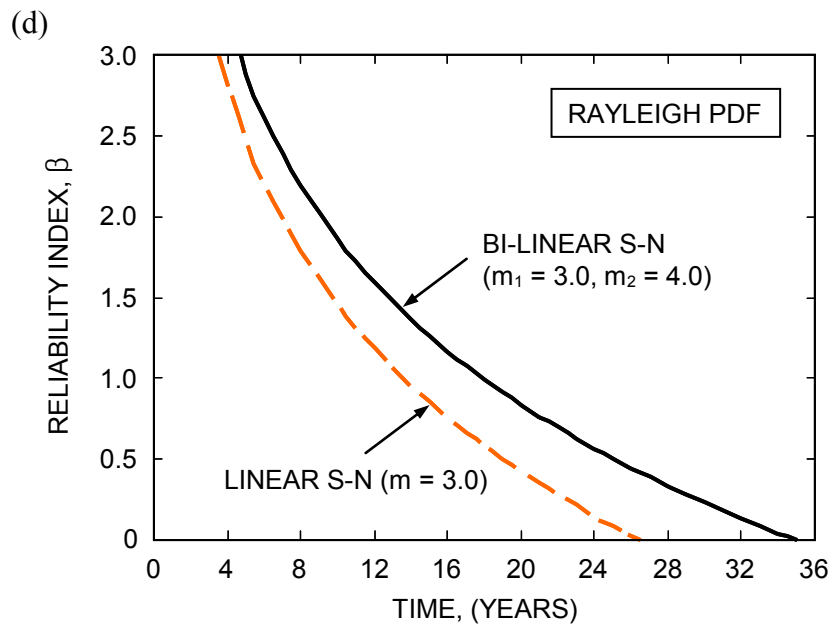
(d) fatigue reliability profile for Rayleigh PDF

Figure 3-27 Time-dependent fatigue life estimation at CH-16 for the *S-N* category C.

(a)
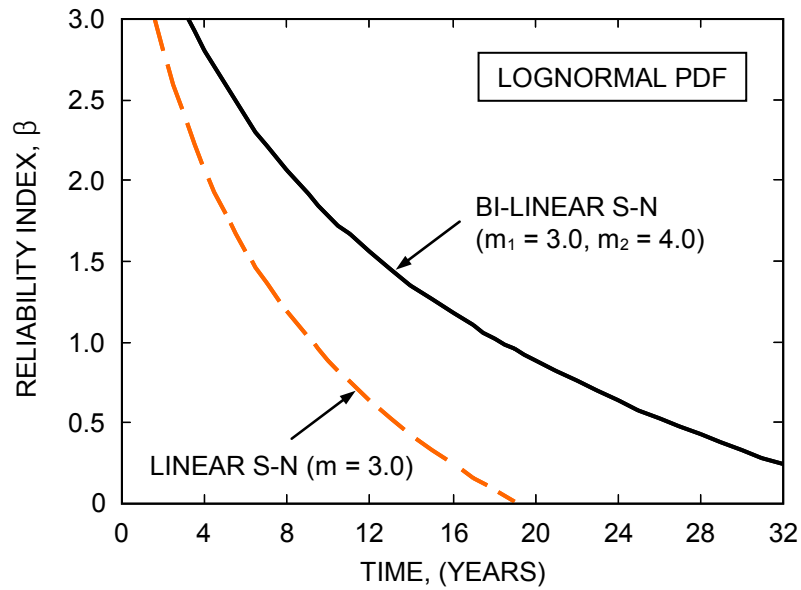
CH-18: **CATEGORY E**

LOGNORMAL

WEIBULL

RAYLEIGH

$m_1 = m_2 = 3.0$

$m_1 = 3.0, m_2 = 4.0$

CRACK SIZE, a (in)

CRACK SIZE, a (mm)

TIME, (YEARS)

(a) crack growth model

(b)

LOGNORMAL PDF

BI-LINEAR S-N
($m_1 = 3.0, m_2 = 4.0$)

LINEAR S-N (m = 3.0)

RELIABILITY INDEX, β

TIME, (YEARS)

(b) fatigue reliability profile for Lognormal PDF

131

(c) fatigue reliability profile for Weibull PDF
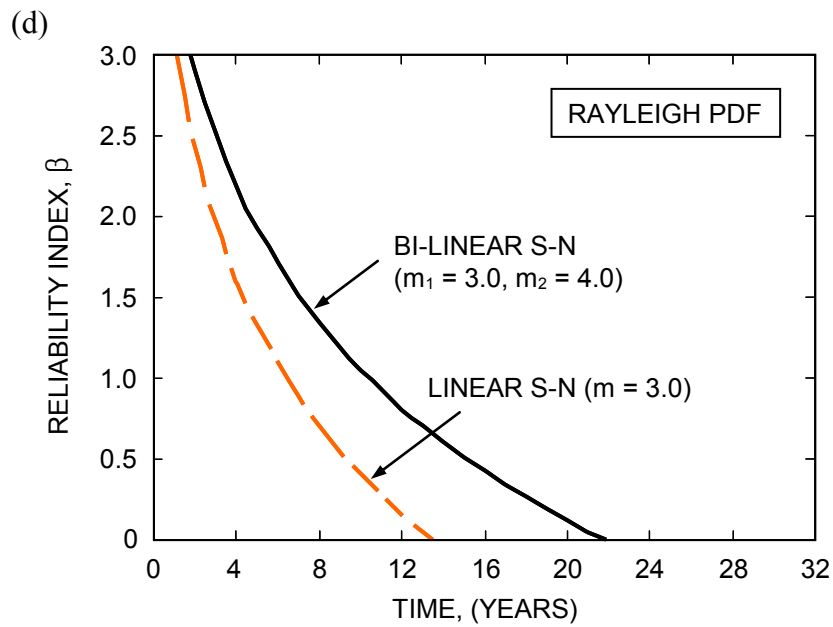
(d) fatigue reliability profile for Rayleigh PDF

Figure 3-28   Time-dependent fatigue life estimation at CH-18 for the *S-N* category E.

CHAPTER 4

TIME-DEPENDENT RELIABILITY ASSESSMENT OF

SHIP STRUCTURES

4.1 INTRODUCTION

This chapter describes the time-dependent reliability assessment of ship structures that is mainly focused on the prediction of lifetime fatigue performance of steel-based and aluminum-based ship structures, by using a probabilistic approach considering various uncertainties associated with sea environmental and ship operating conditions as well as errors in design, fabrication or construction.

For anticipated fatigue failure mode, the linear and bi-linear *S-N* approaches are employed to estimate fatigue resistance of steel and aluminum ship structures, respectively, while loading data from model test and/or SHM are used to estimate load effect affected by three important parameters that are significant wave height, relative wave heading, and ship speed for a given sea state. Under uncertainties associated with fatigue resistance and load effect, a reliability method considering probabilistic distributions is proposed for lifetime fatigue performance assessment. In particular, probabilistic lifetime sea loads for ship structures are estimated based on available loading data and integrated into fatigue performance assessment and service life prediction. The proposed approach is illustrated on both steel and aluminum ship structures.

Section 4.2 addresses the time-dependent fatigue reliability assessment and prediction of high-speed naval ships based on probabilistic lifetime sea loads in

consideration. Fatigue life estimation of aluminum ship structures is described in Section 4.3, by incorporating the bi-linear *S-N* approach and SHM into the time-dependent fatigue reliability assessment. In Section 4.4, the associated summaries and conclusions are presented.

4.2 FATIGUE RELIABILITY ASSESSMENT OF HIGH-SPEED STEEL SHIP STRUCTURES BASED ON LIFETIME PROBABILISTIC SEA LOADS

4.2.1 Introduction

Ship structures subjected to various sea loads during operations experience strength degradation due to fatigue over their service life. For this reason, structural performance assessment and service life prediction for fatigue have to be carried out in design and assessment phases. In general, fatigue life can be assessed based on (i) the stress–life (*S-N*) relationship as a model of fatigue resistance and (ii) the action of sea waves and the sea environment as a model of fatigue loading suggested by Ayyub et al. (2002b). If the *S-N* category of the structural detail is correctly classified, the necessary information regarding fatigue resistance can be easily obtained. However, the accurate estimation of fatigue lifetime sea loads may be more challenging in time-dependent fatigue deterioration processes due to various uncertainties. These uncertainties are associated with still water loading, wave-induced loading, and transient impact-slamming, among others. Clearly, in fatigue design, experiments or simulations are useful for predicting potential lifetime sea loads. Similarly, in fatigue assessment, SHM during voyages provides real-time fatigue loadings that can be integrated into lifetime fatigue performance assessment. However, continuous SHM

up to the anticipated service life may not be feasible because of many restrictions including budgetary, environmental, and operational constraints. Alternatively, a probabilistic approach for fatigue life estimation can be used to effectively predict potential lifetime sea loads based on available data from model tests, simulations, and/or monitoring.

To date, the use of simulations, model tests, and SHM programs has been widely accepted for the estimation of lifetime sea loads. Kaplan et al. (1974) conducted a study with the computer program SCORES in order to estimate wave loads on the SL-7 container ship. The key factors of their study were ship speeds, wave lengths, headings, and sea states. Similarly, Sikora et al. (1983) used the computer program SPECTRA for predicting primary load fatigue spectra for small waterplane area twin hull (SWATH) ships. Response amplitude operators for desired operating speeds and headings were used as input parameters as well as occurrence probabilities of sea state, heading, and speed. As a result of these computer simulations, it was concluded that ship operational and wave conditions are important factors for the estimation of lifetime wave loads.

Ship model tests can be performed to provide various ship structural responses considering wave conditions, ship speeds, and relative wave headings. In general, performance measures obtained from model tests as well as SHM programs can be used to provide more reliable structural responses, and to improve the decision making process for ship maintenance management. The measured data from SHM or model tests have been successfully used for structural performance assessment (Chiou & Chen 1990, Frangopol et al. 2008, and Okasha et al. 2010a and 2010b). Available sea

loading information from model tests may allow not only the assessment of current ship structural performance but also the development of lifetime sea load prediction models using probabilistic methods.

This study focuses on estimating probabilistic lifetime sea loads based on model test and on integrating them into fatigue performance assessment and service life prediction. As an illustration, potential lifetime sea loads including low frequency wave-induced loading and high frequency slam-induced whipping loading are investigated, and the probabilistic approach for fatigue life evaluation is conducted. Occurrence probabilities associated with potential sea states are used to estimate probabilistic lifetime sea loads. Loading information is provided from the scaled test measurements of joint high-speed sealift ship (JHSS) monohull structural seaways loads test (Devine 2009). Based on all necessary information from the *S-N* approach for resistance and model test data for load effect, a fatigue reliability analysis is conducted by using the reliability software RELSYS (Estes & Frangopol 1998).

4.2.2 Fatigue Resistance Based on the S-N Approach

In many ship structures, the structural deterioration process due to fatigue significantly diminishes their service life. Based on the *S-N* approach, the time-dependent fatigue strength of steel ships can be possibly assessed as that case applied for fatigue life estimation of steel bridges.

As mentioned in previous sections, the *S-N* approach has been widely used and adopted by all standards and specifications. Fatigue strength of a structural detail is characterized in the relationship between stress range (nominal applied stresses) and

136

cycles to failure for classified detail categories. The characteristic *S-N* curves corresponding to the mean life of a detail are represented as sloping straight lines in logarithmic scale. For steel ship structures, a typical set of *S-N* curves representing the eight categories (i.e., *B*, *C*, *D*, *E*, *F*, *F*2, *G* and *W*), as that shown in Figure 4-1, can be established based on the BS 5400 (1980). It is found that three different values of material constant (i.e., $m = 4.0$ at *B*, $m = 3.5$ at *C*, and $m = 3.0$ at others) are used in the classified categories, whereas the AASHTO *S-N* curves are established with a single value only (i.e., $m = 3.0$).

4.2.3 Probabilistic Lifetime Sea Loads

Reliable information on sea loadings, which is primarily associated with the action of sea waves and the sea environment, can be obtained from simulations, sea trial tests, segmented structural seakeeping model tests, and/or real-time SHM. In this section, real model test data obtained from the scaled test measurements of JHSS (Devine 2009) are used to estimate probabilistic lifetime sea loads.

4.2.3.1 Estimation of Sea Loads Based on Simulation and SHM

In the design phase, accurate estimates of potential sea loadings are important to ensure the desired structural performance during the entire service life of ship structures, especially for high speed vessels. Primary structural loads on a ship result from its own weight, cargo, buoyancy, and operation (Ayyub et al. 2002c). In assessing the reliability of ship structures, load effects may be estimated by finite element analysis, simulation, and/or SHM.

According to Paik and Frieze (2001), ship hull girder loads can be classified into three types: still water loads, low and high frequency wave-induced loads, and thermal loads. Still water loads are due to the difference between the weight and buoyancy distributions along the length of the ship. The low frequency wave-induced loads consist of vertical, horizontal, and torsional wave loads, whereas the high frequency dynamic loads are due to slamming or whipping and springing (Devine 2009). Wave and dynamic loads are affected by many factors such as ship characteristics, ship speed, relative wave heading, and sea states associated with significant wave heights (Ayyub et al. 2002c). Significant wave height is usually treated as a random variable that requires statistical analyses of ship response data collected from simulation, experiment, or monitoring. For various sea states, efforts to estimate wave-induced load effects more accurately have been made (Glen et al. 1999, Wu & Moan 2006, and Pedersen & Jensen 2009). For various ship speeds, Aalberts & Nieuwenhuijs (2006) analyzed one-year full scale measurements from a general cargo/container vessel in order to determine the effect of whipping (high frequency) and wave-induced (low frequency) loads on fatigue. Maximum wave-induced and dynamic bending moments that the ship may encounter during its service life should be taken into account in performance assessment and life prediction.

In recent years, the development of effective SHM systems for naval ships, especially for lightweight high speed ships, has been an important issue (Hess III 2007, and Salvino & Brady 2008). The SHM systems can be used to obtain prompt responses in terms of structural diagnosis and prognosis, and to offer possibilities for supporting operational and maintenance decisions. The use of available information

from SHM is the most effective tool for the decision making process. However, there are many restrictions to the adoption of this kind of SHM systems to high speed and high performance ships. In fact, these systems are still in an early stage of their development (Salvino & Brady 2008). Alternatively, ship model tests (e.g., segmented scaled model) or simulation analyses by using SPECTRA (Sikora et al. 1983) or LAMP (Lin & Yue 1990) can be employed to estimate lifetime sea loads considering various wave conditions. The simulation program SPECTRA developed by Sikora et al. (1983), is useful for computing vertical, lateral, and torsional moments applied to the hull girder of a monohull ship, and for creating a stress-range bin histogram to evaluate fatigue life considering ship characteristics and wave conditions associated with specific sea routes (Michaelson 2000). In more reliable manner, ship model tests can be preferred when estimating various ship responses (e.g., stress, strain) for given sea states (e.g., moderate, high, hurricane), ship speeds, and relative wave headings. In addition, sea loads obtained from these model tests can be possibly integrated into probabilistic lifetime sea loads prediction models. Consequently, probabilistic lifetime sea loads estimated from model tests can be used effectively for the time-dependent fatigue reliability assessment.

4.2.3.2 Stress-Range Bin Histogram and PDF

As described previously, in terms of fatigue resistance, the *S-N* approach may be useful for estimating the total fatigue life including both crack initiation and crack propagation. On the other hand, in terms of fatigue load effects, variable amplitude loadings (i.e., stress range) must be appropriately taken into account for fatigue life

evaluation. Cycle counting methods can be used to establish a stress-range bin histogram (i.e., stress range vs. number of cycles). The ASTM Standard E 1049 (1997) addresses the following cycle counting techniques: level-crossing counting, peak counting, rain-flow counting, among others. In this study, the bending stress-range bin histogram of a typical ship structure is computed by means of the peak counting technique. To consider the whole stress cycle (positive and negative), the values of the absolute peak stresses are doubled for the purpose of the histogram computation. This results in a more conservative estimation of sea loads.

The procedure for creating a stress-range bin histogram using peak counting method is summarized as follows:

(i) determine the mean value of all time records

(ii) filter all peak values (i.e., stresses) above the determined mean value

(iii) set the stress range at two times the peak stress

(iv) set the bin size (e.g., 0.5 ksi, 1.0 ksi) and count the assigned stress ranges

(v) establish a histogram of stress range occurrences.

Based on the established stress-range bin histogram, equivalent stress range, S_{re}, and average daily number of cycles, N_{avg}, can be computed. Most importantly, an appropriate PDF for the prediction of lifetime sea loads should be determined. As addressed in previous sections, the probabilistic approach can be used to predict both resistance, R, and stress range, S, during fatigue life and eventually to perform fatigue reliability evaluation. The applicable PDFs associated with R and S are usually assumed to be lognormal and Weibull, respectively, for evaluating ship fatigue life.

140

The parameters of the lognormal distribution can be easily obtained from fatigue resistance data (Keating & Fisher 1986), while those of the Weibull distribution are derived from the stress-range bin histogram data. The equivalent stress range, S_{re}, could be derived as the qth moment of the Weibull PDF as follows:

$$ S_{re} = \left[\int_0^\infty s^q \cdot \left(\frac{\beta}{\alpha} \cdot \left(\frac{s}{\alpha} \right)^{\beta-1} \cdot \exp\left(-\left(\frac{s}{\alpha} \right)^\beta \right) \right) \cdot ds \right]^{\frac{1}{q}} \qquad \text{for s} > 0 \qquad (4\text{-}1) $$

where α = scale parameter, β = shape parameter, and $\alpha > 0$, $\beta > 0$. This can be also computed directly from the stress-range bin histogram and Miner's rule (Miner 1945 and Fisher et al. 1998), as defined in Eq. 3-17.

4.2.3.3 Probabilistic Lifetime Sea Loads Prediction for Fatigue

A probabilistic approach to potential sea loads prediction for fatigue is herein addressed. This approach considers both equivalent stress range at a specified sea wave condition (e.g., sea state 7, ship speed of 35 knots, and heading of 0° for following seas) and number of cycles in its observed time period. As described previously, sea loads are function of ship characteristics, ship speeds, relative wave headings, and sea states associated with significant wave heights (wave conditions). If ship model test data for certain wave conditions are provided, probabilistic lifetime sea loads can be estimated by considering both S_{re} and N_{avg}.

Based on given information (e.g., stress vs. time), wave-induced and whipping responses can be separately obtained by filtering. Wave-induced loadings are produced by the low-pass filtering, whereas wave impacts causing global hull girder

whipping are collected using high-pass filtering (Brady 2004 and Hildstrom 2007). Based on the filtering processes of raw data, individual stress-range bin histograms for the given wave conditions are established using the peak counting method. Then, S_{re} and N_{avg} for an observed time period are calculated from the stress-range histogram data. To estimate fatigue lifetime sea loads considering all possible wave conditions, the predicted equivalent stress range, S_{re}^*, can be derived under consideration of probabilistic ship operational profiles at a specific seaway. As an approximation, in this study it will be assumed that sea state, ship speed, and relative wave heading are independent variables. The various probabilities of occurrence are considered to be the continuous representations of the relative frequencies n_i / N_{total}. Therefore, the resulting equation is

$$S_{re}^* = \left[\sum_{i=1}^{ss} \sum_{j=1}^{sp} \sum_{k=1}^{wh} P_{SS,i} \cdot P_{SP,j} \cdot P_{WH,k} \cdot S_{re,ijk}^m \right]^{\frac{1}{m}} \tag{4-2}$$

where S_{re} = equivalent stress range; m = material constant (i.e., $m = q$); and $P_{SS,i}$ = probability of occurrence of the i-th sea state ($i = 1, 2, \ldots, ss$), $P_{SP,j}$ = probability of occurrence of the j-th ship speed ($j = 1, 2, \ldots, sp$) and $P_{WH,k}$ = probability of occurrence of the k-th relative wave heading ($k = 1, 2, \ldots, wh$) for the applicable sea events. The corresponding schematic for estimating S_{re}^* is shown in Figure 4-2(a) and (b). Figure 4-2(a) is associated with the three occurrence probabilities $P_{SS,i}$, $P_{SP,j}$, and $P_{WH,k}$, for the computation of corresponding equivalent stress ranges, while Figure 4-2(b) shows the estimation of the predicted equivalent stress range in consideration. As indicated, a new equivalent stress-range bin histogram can be established by the

computed individual equivalent stress ranges from each histogram and the occurrence probability associated with wave conditions.

Similarly, the predicted average daily number of cycles, N_{avg}^*, may be derived using the three occurrence probabilities which are associated with all potential sea wave conditions, that is,

$$N_{avg}^* = \sum_{i=1}^{ss} \sum_{j=1}^{sp} \sum_{k=1}^{wh} P_{SS,i} \cdot P_{SP,j} \cdot P_{WH,k} \cdot N_{avg,ijk} \qquad (4\text{-}3)$$

The computed N_{avg}^* is used to estimate the cumulative number of stress cycles for future years, $N_t(t)$, considering annual ship operation rate, α, in anticipated seaways. Therefore, $N_t(t)$ is estimated from the linear relationship to ship service life as

$$N_t(t) = 365 \cdot \alpha \cdot N_{avg}^* \cdot t \qquad (4\text{-}4)$$

where t = number of years, and α = ship operation rate per year (e.g, α = 50% for six months of operation, 75% or 90%).

4.2.4 Fatigue Reliability Assessment

Performance assessment and service life prediction for fatigue are herein addressed. As mentioned previously, ship fatigue life can be assessed more reliably based on both the *S-N* curve for ship capacity and the test data for load effects under uncertainties. It is noted that the predicted equivalent stress range, S_{re}^*, derived from Eq. 4-2 is used for the prediction of lifetime load effect for fatigue.

4.2.4.1 Limit-State Function for Fatigue

Under the repeated or fluctuating application of stresses, ship performance assessment and service life prediction for fatigue can be performed by fatigue reliability analysis with a well-defined fatigue limit-state function consisting of fatigue resistance, R, and load effect, S. This is important because maintenance-management actions including inspection, monitoring, and repair can be better planned if based on the well quantified ship reliability. For fatigue reliability evaluation, the limit-state functions of structural details are established with the assumed PDFs for resistance and stress range. Typically, the safety of any structure would be preserved when its resistance, R, is larger than the predicted equivalent stress range, S_{re}^*.

For the time-dependent fatigue reliability assessment, the limit-state function defined in Eq. 3-6 is re-expressed using S_{re}^* as follows:

$$g(t) = \Delta - D = \Delta - \left(\frac{N_t(t)}{A} \right) \cdot \left(e \cdot S_{re}^* \right)^m = 0 \qquad (4\text{-}5)$$

where e is a typical measurement error factor which may include potential fatigue stress damage in steel ship details, and m is a constant defined in the BS 5400 (1980). The total number of cycles, $N_t(t)$, which is obtained from Eq. 4-4, is treated as random in consideration of $COV(N_{avg}) = 0.2$ and A is also considered random. Complete details for all random variables are presented in Table 4-1.

4.2.4.2 Fatigue Reliability Analysis

Based on the function $g(t)$, the fatigue reliability analysis is performed by using

the reliability software RELSYS (Estes & Frangopol 1998). S_{re}^* is treated as Weibull PDF with COV(S_{re}^*) = 0.2, while other random variables (i.e., $\varDelta$, A, N_{avg} and e) are Lognormal (see Table 4-1).

The flowchart for the fatigue reliability evaluation is shown in Figure 4-3, and the corresponding steps are summarized as follows:

Step 1: *Details of structural members based on the S-N approach*

Based on the BS 5400 (1980), the *S-N* approach in terms of fatigue resistance, *R*, provides relevant information including the *S-N* category, material constant, *m*, constant amplitude fatigue threshold (CAFT), and fatigue detail coefficient, *A*.

Step 2: *Low-pass and high-pass filtering based on the collected unfiltered data*

From the unfiltered (raw) data, wave-induced and slamming-induced whipping responses are obtained by filtering at low and high frequency levels, respectively, in order to provide separately useful responses for ship fatigue life evaluation.

Step 3: *Stress-range bin histogram and PDFs*

The stress-range bin histograms are established by using peak counting method from the unfiltered or filtered data at the selected locations (stations) of structural members. Based on the stress-range bin histogram, the equivalent stress range, S_{re}, and the average daily number of cycles, N_{avg}, from a monitoring time period, T_{shm}, can be computed. Mean modal wave period, T_w, which is different at each sea state, is used to estimate N_{avg} by multiplying the ratio (i.e., T_{shm} / T_w) by the counted number of occurrences during T_{shm}. An appropriate PDF for predicting sea loads is used

considering uncertainty during fatigue lifetime. In ship fatigue reliability evaluation, lognormal and Weibull PDFs can be used for resistance and load effects, respectively.

Step 4: *Probabilistic lifetime sea loads prediction*

The probabilistic approach to potential sea loads prediction for fatigue life evaluation is developed considering ship speeds, relative wave headings, and sea states associated with wave heights. The calculated S_{re} and N_{avg} according to the sea states (e.g., 0 ~ 9) or applicable sea events are used to estimate both the predicted equivalent stress range, S_{re}^*, and the predicted average daily number of cycles, N_{avg}^*. All possible ship operational conditions through anticipated seaways are taken into account.

Step 5: *Total number of cycles, $N_t(t)$*

By using Eq. 4-4, $N_t(t)$ is estimated for the time-dependent fatigue reliability evaluation. In this study, $N_t(t)$ does not reflect instantaneous but progressive time effect for fatigue life of ship, meaning that the number of cycles up to a specific year has been accumulated since the first ship operation year.

Step 6: *Fatigue reliability analysis*

For a given service year, the fatigue reliability analysis is performed with all necessary information from steps 1 to 5. For the assumed PDFs (lognormal and Weibull), the reliability software RELSYS (Estes & Frangopol 1998) is used to compute the fatigue reliability index. This program uses the First-Order Reliability Method (FORM) to compute the reliability index.

4.2.5   Application Example

As an illustration, probabilistic lifetime sea loads of the JHSS for fatigue are estimated based on model test data and integrated into the fatigue performance assessment and service life prediction. Potential lifetime load effects, which are associated with low frequency wave-induced and high frequency slam-induced whipping loadings due to vertical bending moment, are investigated. For fatigue reliability analysis, the collected sea loadings from the scaled test measurements of a JHSS monohull structural seaways loads test (Devine 2009) are used together with the *S-N* curve provided by the BS 5400 (1980).

4.2.5.1   Segmented Model Test

A full-scaled JHSS monohull length was scaled down to reach the value of 6.1 m (20 ft) in the segmented model (Devine 2009). It is noted that appropriate scale factors for the involved quantities (e.g., length, time, moment of inertia, bending moment) were obtained based on Froude scaling laws.

The segmented model approach was used to measure detailed hull response using a simple internal backspline (see Figure 4-4). The vertical, lateral and torsional stiffness and vibrational characteristics of the hull were modeled by using the internal backspline (Devine 2009). During each test run, realistic vibrational response, including hull primary and secondary loads, was collected from the installed strain gages on the Froude-scaled structural component at Stations 4, 7, 10, 13 and 16 (see Figure 4-4). As shown in Figure 4-4, the shell sections were connected with a continuous backspline beam and strain gages were installed at each segment cut to

measure the vertical, lateral and torsional bending moments and vertical/lateral shear forces. It is noted that section modulus at the identified stations on the backspline varies along the beam length. Description of the JHSS segmented model tests and further details can be found in Devine (2009).

4.2.5.2   Fatigue Resistance and Load Effect

Details of fatigue resistance and the scaled test data, which are associated with the strain gages installed on the top flanges of the backspline at five stations (i.e., Stations 4, 7, 10, 13 and 16 in Figure 4-4), are used to illustrate the fatigue reliability assessment and service life prediction based on the estimated probabilistic lifetime sea loads. For fatigue resistance, the *S-N* curves based on the BS 5400 (1980) are used and the corresponding *S-N* parameters (i.e., category, CAFT, and fatigue detail coefficient, *A*) are investigated at the respective structural details. Typically, the rational procedure to find the *S-N* parameters is to identify the worst weld detail in the design and assessment phases. In this study, for illustrative purposes, the *S-N* category *F*, which may be the worst case, is assumed for all the details, for illustrative purposes. The material constant, *m*, is 3.0, while the mean value of *A* is 6.29E+11 MPa^3 (1.92E+09 ksi^3) with coefficient of variation COV(*A*) = 0.54. The corresponding constant amplitude fatigue limit is CAFT = 39.78 MPa (5.77 ksi).

In this study, two sets of test data provided by Devine (2009) are used: (i) sea state 7 (SS7), 35 knots and heading of 0˚; and (ii) Hurricane Camille (HC), 15 knots and heading of 0˚. Based on the given model test data, primary vertical hull-girder bending moments are investigated at the gage stations. At midship (i.e., Station 10),

vertical bending moments due to SS7 and HC are presented in Figure 4-5. Hogging moment is positive and sagging is negative. Ship speeds in SS7 and HC were 35 knots and 15 knots, respectively, in the same heading of 0° (i.e., following seas). It is noted that the Froude scale factor with respect to the bending moment is $1.025 \cdot \lambda_F^4$ where λ_F = 47.5255 (Devine 2009). In both wave conditions, the filtering procedure has been applied to data, using low-pass and high-pass filtering to extract separately wave-induced moment and slamming-induced whipping moment (see Figure 4-5(b) and (d)).

For the wave conditions SS7 and HC, stress-range bin histograms using peak counting are established based on unfiltered (wave-induced and slam-induced) and filtered (wave-induced) data. To convert bending moment, M, to stress, σ (i.e., $\sigma = M / S_m$), the Froude scale factor $0.346 \cdot \lambda_F^4$ for section modulus, S_m, was used (Devine 2009). Weibull PDF, which is widely accepted for lifetime sea loads prediction, is used for the probabilistic approach. As shown in Figure 4-6(a) to (d), Weibull PDFs of full scaled stress range are fitted on the established stress-range bin histograms, for illustrative purposes. The parameters α and β indicate scale and shape of the Weibull PDF, respectively, while $E(S_r)$ and $\sigma(S_r)$ denote the mean value and standard deviation of the stress range, respectively. It is found that the $E(S_r)$ from the filtered data (i.e., neglecting high frequency load effect) is larger than that from the unfiltered data (i.e., including high frequency) at both loading conditions (see Figure 4-6). This is because the contribution of lower stress ranges to fatigue damage is diminished in the filtered data, as shown in Figure 4-5(b) or (d). However, since the number of cycles for high frequency can be large, the cumulative effect of these numbers can be important.

For each test run of SS7 and HC at Stations 10 and 13, S_{re} and N_{avg} in the

149

observed time period are computed and presented in Figure 4-7(a) to (d). With the sampling rate for this primary hull response data of 200 Hz, full scaled observed time periods for the total concatenated runs of SS7 and HC are about 42.4 minutes and 66.6 minutes, respectively. As shown in Figure 4-7, S_{re} and N_{avg} are fluctuating through individual test runs. For the lifetime fatigue assessment and prediction, these two parameters are herein treated as random variables considering loading uncertainty associated with the limited test runs.

4.2.5.3   Fatigue Reliability Assessment Using Probabilistic Lifetime Sea Loads

As described previously, under uncertainty associated with wave loading, a probabilistic approach for potential sea loads prediction is necessary to be developed based on given information (e.g., model tests, simulations, SHM). In particular, if model test data for each sea state is available, lifetime sea loads for fatigue life evaluation can be reliably estimated using occurrence probability of sea states in a seaway, and the computed S_{re} and N_{avg} from applicable operational conditions. As a result, the probabilistic lifetime sea loads of JHSS monohull from model test data can be computed by using the proposed approach.

The established histograms from low frequency wave-induced data of SS7 and HC, which are filtered from total concatenated runs, are used to estimate S_{re} and N_{avg} at the five stations. In the calculation of S_{re}, Eqs. 3-17 and 4-1 are employed considering Miner's rule and Weibull PDF, respectively. The calculated S_{re} and N_{avg} at the five stations are presented in Table 4-2. The maximum value of S_{re} was observed at Station 13, not at midship (i.e., Station 10) for both SS7 and HC, whereas the

maximum bending moment was recorded at Station 10 (see Figure 4-8). This is because the section modulus on the backspline varies along the length of JHSS monohull. By using Eqs. 4-2 and 4-3, the predicted equivalent stress range, S_{re}^*, and predicted average daily number of cycles, N_{avg}^*, considering potential sea states at the worst area (i.e., North Atlantic Ocean) as presented in Table 4-3 (Brady et al. 2004), are estimated to perform the fatigue reliability assessment. Due to the lack of information, occurrence probability of sea state is only considered in order to estimate probabilistic lifetime sea loads. Occurrence probabilities of ship speed and relative wave heading are ignored in this application.

All necessary information for the fatigue reliability analysis is obtained from steps 1 to 5 (see also Figure 4-3). The established *S-N* curve based on the BS 5400 (1980) is herein used and predicted lifetime loads are estimated based on the low frequency wave-induced data filtered. The fatigue reliability at each station is obtained using RELSYS (Estes & Frangopol 1998). Furthermore, fatigue reliability evaluation at the identified critical location (station) is performed for investigating (i) the effect of annual ship operation rate, α, of 50%, 75% and 90% on fatigue life, and (ii) the effect of low frequency wave-induced moment and complete history including high frequency slam-induced whipping moment on fatigue life. Target reliability, β_{target}, is assumed to be 3.0. This target is in the range of target reliability indices for fatigue (i.e., $2.0 \leq \beta_{target} \leq 4.0$) recommended in Mansour et al. (1996).

The identified critical location of JHSS monohull is shown in Figure 4-9(a). At Station 13, fatigue reliability attains its lower bound, whereas the upper bound is at

Station 4. Fatigue reliability analyses at the critical location (i.e., Station 13) are performed considering both cases (i) and (ii). The result for case (i) is shown in Figure 4-9(b). As expected, fatigue life of JHSS decreases significantly when the ship operation rate increases. For the predefined β_{target} of 3.0, the predicted fatigue life was only about 9 years in the case of $\alpha = 90\%$, whereas it was 16 years in the case of $\alpha = 50\%$. The result of the fatigue reliability analysis for case (ii) is presented in Figure 4-9(c). It is found that the effect of high frequency slam-induced whipping moment on fatigue life could not be neglected when considering operations in the worst areas.

4.2.6 Summary

A probabilistic approach for fatigue reliability assessment and service life prediction of high-speed naval ships based on the probabilistic lifetime sea loads estimated from model test data was presented. The linear *S-N* approach in the identified steel-based details was used to assess structural capacity in the fatigue reliability evaluation, whereas model test data were used to estimate probabilistic lifetime sea loads in terms of load effects. Under uncertainties associated with fatigue resistance and loading history, two PDFs (i.e., Lognormal, Weibull) were used. The unfiltered (raw) data collected on a scaled JHSS monohull was used to establish the stress-range bin histogram using peak counting method and to illustrate the proposed approach.

4.3 FATIGUE RELIABILITY ASSESSMENT AND PREDICTION OF ALUMINUM SHIP STRUCTURES

4.3.1 Introduction

In recent years, the development of aluminum ship structures has been promoted in the context of the rapid evolution of high-speed and light-weight vessels. Under the repeated and/or fluctuating application of stresses during voyages, fatigue damage of aluminum ship members is accumulated. For this reason, fatigue reliability evaluation has to be conducted for assessing and predicting lifetime performance of aluminum ships. Furthermore, this need can offer the opportunity to plan lifetime ship structural management in an optimal way. A probabilistic approach for the time-dependent fatigue reliability evaluation of aluminum ship structures is proposed in this section.

As addressed in previously, ship fatigue life can be assessed by using a fatigue reliability method based on the *S-N* approach and available loading information. Several approaches have been proposed to assess the time-dependent fatigue performance under uncertainty (Paik & Frieze 2001, Frangopol et al. 2008, Liu et al. 2010a, and Kwon & Frangopol 2009 and 2010a). However, these approaches have been limited to fatigue life estimation of steel structures which is based on the linear S-N approach (i.e., AASHTO, BS 5400). Since aluminum is more susceptible to fatigue cracking than steel (Sielski 2007b), steel-based fatigue approaches are being used with reservation for aluminum structures. Application of the fatigue reliability approach to aluminum ship structures is still in its infancy. A probabilistic approach predicting the time-dependent structural performance of aluminum structures is herein

153

addressed. It uses the bi-linear *S-N* approach provided in Eurocode 9 (1999) for
fatigue resistance and available stress-range bin histogram data for sea loading. The
estimated fatigue reliability in this section is incorporated into the life-cycle cost
optimization for efficient structural maintenance management which will be addressed
in Chapter 6.

4.3.2 The Bi-Linear S-N Approach

For fatigue life evaluation of aluminum structures, the bi-linear *S-N* approach
can be used. Based on current specifications, fatigue strength of aluminum details is
characterized by the relationship between stress range (nominal applied stresses) and
cycles to failure for the classified detail categories. The characteristic *S-N* curves are
based on numerous fatigue test data. An *S-N* curve derived from a mean *S-N* curve that
is shifted two standard deviations lower is commonly used for design purposes and
associated with a 2.3 % probability of failure assuming the life logarithms to be
normally distributed (Fisher et al. 1998 and Maddox 2003). For assessment purposes,
a mean curve has to be used to realize the true life. The bi-linear *S-N* equations in two
phases are defined as

$$R_1 = \left(\frac{A_1}{N}\right)^{1/m_1} \qquad \text{for } N \leq N_D = 5 \times 10^6 \text{ cycles} \qquad (4\text{-}6a)$$

$$R_2 = \left(\frac{A_2}{N}\right)^{1/m_2} \qquad \text{for } N > N_D = 5 \times 10^6 \text{ cycles} \qquad (4\text{-}6b)$$

where R_1, R_2 = nominal fatigue resistance (stress range); A_1, A_2 = fatigue detail
coefficient above and below the constant amplitude fatigue limit, S_D, respectively, and

$A_2 = (S_D{}^{m_2-m_1}) \cdot A_1$. It is noted that S_D corresponds to the CAFT defined in the AASHTO Specifications (2008); N_D = number of cycles corresponding to S_D; and m_1, m_2 = material constant. Typical *S-N* curves can be established based on Eurocode 9 (1999) as those shown in Figure 4-10(a) for welded joints between members and in Figure 4-10(b) for members with welded attachments-transverse welded toe. After the number of applied stress cycles reaches five-million ($N_D = 5 \times 10^6$), the *S-N* curves are extended using the slope $m_2 = m_1 + 2$ (see Figure 4-10). The classified *S-N* categories are designated by the reference fatigue strength, S_C (in MPa unit), corresponding to $N_C = 2 \times 10^6$ cycles and m_1 (e.g., *S-N* categories 55-6, 44-5, 39-4, and so on).

In terms of fatigue resistance, the *S-N* approach is useful for estimating the total fatigue life including both crack initiation and crack propagation. On the other hand, in terms of fatigue load effects, variable amplitude fatigue loadings (i.e., stress range) can be converted into an equivalent constant amplitude stress range by using Miner's rule. The equivalent stress range, S_{re}, is available for equivalent estimation of fatigue damage (Fisher et al. 1998). Cycle counting methods such as peak counting or rain-flow counting, which are techniques based on extracting extrema from a continuous time history to identify individual and/or nested cycles, can be used to establish a stress-range bin histogram (ASTM Standard, 1997). Lifetime sea loads associated with ship characteristics, ship speed, relative wave heading and sea states can be treated as random variables (e.g., equivalent stress range for fatigue). In this context, an appropriate PDF can be assumed for predicting potential lifetime sea loads under uncertainty, as described previously. The probabilistic approach is used to reliably predict both fatigue resistance, R, and representative load effect, S_{re}, during

155

the fatigue life and to evaluate the time-dependent fatigue reliability. For fatigue life estimation of ship structures, the applicable PDFs associated with R and S_{re} are usually assumed to be lognormal and Weibull, respectively (Ayyub et al. 2002 and Munse et al. 1983).

Typically, S_{re} is computed by using Eq. 3-17 or 4-1 based on the linear S-N approach and Miner's rule. However, this general form (i.e., Eq. 3-17) has to be re-expressed for the calculation of S_{re} of aluminum fatigue details using the bi-linear S-N approach, as addressed in Section 3.3 (see Eq. 3-18). Based on Eurocode 9 (1999), S_{re} in aluminum structures that may experience two slopes (i.e., $m_1 = m$, $m_2 = m+2$) of the S-N curve is calculated from stress-range bin histogram data as (Kosteas 1999)

$$S_{re} = \left[\frac{\sum(n_i \cdot S_i^{m_1}) + (S_D^{m_1-m_2}) \cdot \sum(n_j \cdot S_j^{m_2})}{\sum n_i + \sum n_j} \right]^{\frac{1}{m_1}} \tag{4-7}$$

where n_i = number of cycles in the stress-range bin S_i greater than S_D; n_j = number of cycles in the stress-range bin S_j which is less than S_D and greater than a cut-off limit S_L corresponding to N_L = 100 million cycles; and $\sum n_i + \sum n_j$ = total number of cycles to failure that corresponds to N_t as defined previously. It is noted that Eq. 4-7 can be restricted to application of stress cycles from one source of loading only (e.g., overall wave bending) not from several sources.

When considering a probabilistic distribution associated with stress ranges, the corresponding S_{re} is obtained by

$$S_{re} = \left[\int_0^{S_D} (S_D^{m_1-m_2}) \cdot s^{m_2} \cdot f_S(s) \cdot ds + \int_{S_D}^{\infty} s^{m_1} \cdot f_S(s) \cdot ds \right]^{\frac{1}{m_1}} \tag{4-8}$$

As mentioned above, S_{re} for fatigue reliability evaluation is in this study treated as Weibull PDF with COV(S_{re}) = 0.1.

To predict fatigue life, the average daily number of cycles, N_{avg}, is calculated from stress-range bin histogram data. The computed N_{avg} is used to estimate the annual cumulative number of cycles, $N_t(t)$, considering annual ship operation rate, α, in anticipated seaways. Based on N_{avg} and α, $N_t(t)$ for future years is

$$N_t(t) = 365 \cdot \alpha \cdot N_{avg} \cdot t \tag{4-9}$$

where t = number of years, α = ship operation rate per year at sea exposed to the sea states from which the stress-range histogram data have been determined.

4.3.3 Fatigue Reliability Assessment

For fatigue life assessment of aluminum ships, the time-dependent reliability analysis is performed with a well-defined fatigue limit-state function. As noted previously, applicable maintenance-management interventions can be effectively planned based on the well-quantified ship reliability profiles. Based on the *S-N* approach and Miner's rule (1945), the limit-state function is defined as:

$$g_1(t) = \Delta - \left(\frac{N_t(t)}{A_1} \right) \cdot (e \cdot S_{re})^{m_1} = 0 \quad \text{for } N_t(t) \leq N_D = 5 \times 10^6 \text{ cycles} \tag{4-10a}$$

$$g_2(t) = \Delta - \left(\frac{N_t(t)}{A_2} \right) \cdot (e \cdot S_{re})^{m_2} = 0 \quad \text{for } N_t(t) > N_D = 5 \times 10^6 \text{ cycles} \tag{4-10b}$$

where Δ = Miner's critical damage accumulation index in terms of resistance which is assumed as lognormal with E(Δ) = 1.0 and COV(Δ) = 0.3 (Wirsching 1984). It should

be noted that these values typically applicable to steel structures are used with reservation for aluminum structures; D = Miner's damage accumulation index; e = typical measurement error factor to consider uncertainty associated with fatigue stress damage (Ayyub et al. 2002); m_1 , m_2 = material constants defined in Eurocode 9 (e.g., m_1 = 3.2 and m_2 = 5.2 for a *S-N* category 22-3.2); and A_1 , A_2 = fatigue detail coefficients which are considered random. Complete descriptions for all deterministic parameters and random variables are presented in Table 4-4 and Table 4-5. Based on the functions $g_1(t)$ or $g_2(t)$, the fatigue reliability analysis is obtained by using the reliability software RELSYS (Estes & Frangopol 1998). S_{re} is treated as a Weibull random variable with $COV(S_{re})$ = 0.1, while other random variables (i.e., Δ, A, and e) are considered lognormal (see Table 4-4).

4.3.4   Application Example

A fatigue detail of a 42.67 meter 32 knot aluminum crew boat (Sielski 2007a) is investigated as an illustration for fatigue life estimation of aluminum ship structures. As shown in Figure 4-11, the ship detail is a type of welded attachment provided in Eurocode 9 (1999). The associated *S-N* categories depend fully on the length of attachment, L, and thickness of base plate, T. Since the detail consists of a cover plate with length L = 40 mm and thickness T = 8 mm, its *S-N* curve is identified by the 22-3.2 curve as shown in Figure 4-10(b). The *S-N* values for all categories are presented in Table 4-5.

For fatigue loading, the stress-range bin histogram data provided in Sielski (2007a), as shown in Figure 4-12, are used together with the identified S-N curve for fatigue resistance. It is assumed that for a service life of 30 years the loading data was obtained from one-year measurement with the annual ship operation rate $\alpha = 0.8$. Thus, all necessary information on both the fatigue resistance and the loading data are collected for evaluating lifetime fatigue reliability.

For the fatigue reliability evaluation, the established S-N curve in the 22-3.2 category provides its associated S-N values (i.e., S_D, A_1, A_2, m_1, m_2). Equivalent stress range, S_{re}, and average daily number of cycles, N_{avg}, are obtained based on the stress-range bin histogram data. For the ship detail considered, the material constant, m, is 3.2 (therefore, $m_1 = 3.2$ and $m_2 = 5.2$). Fatigue detail coefficients $\log A_1$ and $\log A_2$ for design purposes are 10.597 and 13.033, respectively (Eurocode 9, 1999), whereas the mean values of $\log A_1$ and $\log A_2$ being 11.597 and 14.033, respectively, are used for assessment purposes with COV(A) = 0.45 (Wirsching 1987). The defined units and type of stress are MPa and stress range, respectively. The constant amplitude fatigue limit, S_D, is 16.5 MPa at N_D = five-million cycles, while the cut-off limit, S_L, is 9.3 MPa at N_L = 100 million cycles (Eurocode 9, 1999). As noted previously, if the fatigue life is less than N_D, the S-N curve characterized by the slope $m_1 = 3.2$ is used for fatigue resistance. Otherwise, the S-N values m_2 and A_2 are used. For lifetime sea loads prediction, the widely accepted Weibull PDF is assumed. As shown in Figure 4-12, Weibull PDF is fitted to the established stress-range bin histogram representing all stress cycles from one-year measurement. However, fatigue reliability may be significantly affected by an assumed PDF of stress range. For this reason, goodness-

of-fit tests have to be conducted to find the best fit. A goodness-of-fit test by using the

Anderson and Darling (1952) method was conducted to find the best fit of the PDF.

The test results of Weibull, lognormal, and Gumbel are presented in Figure 4-13(a),

(b), and (c), respectively. As shown in Figure 4-13(a), Weibull PDF was the best fit

for the stress range data as compared to lognormal and Gumbel PDFs. Therefore, the

ship fatigue life is predicted by using Weibull PDF. S_{re} and N_{avg} in the observed time

period are computed by using Eqs. 4-8 and 4-9, respectively, with $\Sigma n_i = 87,808$ cycles

and $\Sigma n_j = 526,000$ cycles. The computed values are $S_{re} = 13.08$ MPa (1.90 ksi) and

$N_{avg} = 2102$ cycles per day. S_{re} is herein assumed as Weibull PDF with COV(S_{re}) = 0.1

considering loading uncertainty. Based on all necessary information, the time-

dependent fatigue reliability analysis is conducted using reliability software RELSYS

(Estes & Frangopol 1998). The evaluated fatigue reliability is shown in Figure 4-14.

After 30 years, the fatigue reliability index is expected to drop below 2.43. According

to the target reliability index considered (e.g., $\beta_{target} = 3.0$), relevant repair

interventions during the service life of 30 years may be required. Moreover, it is

interesting that a transition gap of fatigue reliability exists at 8.15 years when N

reaches N_D (i.e., five-million cycles).

4.3.5   Summary

A reliability approach for fatigue life estimation of aluminum ship structures

was presented. The proposed approach was used to estimate effectively fatigue life

under uncertainty. It was based on the bi-linear *S-N* approach within 100-million

cycles (Eurocode 9, 1999) and the stress-range bin histogram data from SHM.

Lognormal and Weibull PDFs were used for fatigue resistance and sea load effect, respectively.

4.4   CONCLUDING REMARKS

From the analyses of the time-dependent fatigue reliability assessment and performance prediction of ship structures, the following conclusions are drawn:

1. The model test data can be effectively used for estimating probabilistic lifetime sea loads representative of the equivalent stress range and the average daily number of cycles.

2. Using filtering process, low frequency wave-induced and high frequency slam-induced whipping moments can be extracted from unfiltered test data in order to identify structural responses separately.

3. Based on the established stress-range bin histogram, individual equivalent stress ranges for given ship operational and wave conditions (which are related to ship characteristics, ship speeds, relative wave headings, and sea states) can be computed and used to estimate the predicted equivalent stress range, S_{re}^*, considering all possible occurrences.

4. Based on the estimated probabilistic lifetime sea loads and the *S-N* approach, fatigue reliability and service life prediction of ship structures can be investigated up to the anticipated service life.

5. The time-dependent fatigue life of aluminum ship structures can be reliably assessed and predicted by using the probabilistic approach based on the bi-linear S-N approach and the histogram data from SHM. The quantified lifetime

structural performance can be effectively used to plan life-cycle maintenance interventions in an optimal way.

Table 4-1   Summary of random variables for fatigue reliability evaluation.

Random variables	Notation	Distribution	Source
Critical damage accumulation index	Δ	Lognormal, $E(\Delta) = 1.0$ $COV(\Delta) = 0.3$	Wirsching (1984)
Fatigue detail coefficient	A	Lognormal, $*E(A) = 6.29E{+}11\ MPa^3$ $(1.92E{+}09\ ksi^3)$ $*COV(A) = 0.54$	BS 5400 (1980)
Measurement error factor	e	Lognormal, $E(e) = 1.0$ $COV(e) = 0.1$	Ayyub et al. (2002) and Frangopol et al. (2008)
Predicted effective stress range	S_{re}^*	Weibull (see Table 4-2) $COV(S_{re}^*) = 0.2$	Based on model test data
Predicted average daily number of cycles	N_{avg}^*	Lognormal (see Table 4-2) $COV(N_{avg}^*) = 0.2$	Based on model test data

* The values E(A) and COV(A) assigned by the S-N category F.

Table 4-2 Lifetime prediction of sea loads for fatigue at each station.

Station	Sea state 7			Hurricane Camille			Predicted value		
	S_{re}, MPa (ksi)		N_{avg} (cycles)	S_{re}, MPa (ksi)		N_{avg} (cycles)	S_{re}^{*}, MPa (ksi)		N_{avg}^{*} (cycles)
	Weibull	Miner		Weibull	Miner		Weibull	Miner	
Station 4	5.83 (0.85)	5.93 (0.86)	187	10.99 (1.59)	10.70 (1.55)	703	5.43 (0.79)	5.48 (0.79)	143
Station 7	12.43 (1.80)	12.34 (1.79)	175	19.88 (2.88)	19.41 (2.81)	656	11.40 (1.65)	11.29 (1.64)	134
Station 10	16.93 (2.45)	16.82 (2.44)	164	23.81 (3.45)	23.39 (3.39)	652	15.40 (2.23)	15.27 (2.21)	126
Station 13	18.77 (2.72)	18.55 (2.69)	163	24.17 (3.50)	23.85 (3.46)	653	17.01 (2.47)	16.83 (2.44)	125
Station 16	13.19 (1.91)	13.10 (1.90)	162	15.43 (2.23)	15.29 (2.22)	668	11.91 (1.73)	11.86 (1.72)	125

Note: Eqs. 3-17 and 4-1 are used in the calculation of S_{re} by Miner's rule and Weibull PDF, respectively.

Table 4-3   Modal wave period and probability of occurrence according to sea states of North Atlantic Ocean (Brady et al. 2004).

Sea state	Mean value of significant wave height		Mean modal wave period (seconds)	* Probability of occurrence (%)
	(ft)	(m)		
0 - 1	0.16	0.05	-	1.0
2	0.98	0.30	6.9	6.6
3	2.87	0.87	7.5	19.6
4	6.15	1.87	8.8	29.7
5	10.66	3.25	9.7	20.8
6	16.40	5.00	12.4	14.1
7	24.61	7.50	15.0	6.8
8	37.73	11.50	16.4	1.3
> 8	> 45.90	> 13.99	20.0	0.1

* Probabilities reported for the North Atlantic annual.

Table 4-4   Deterministic and random variables for fatigue reliability assessment.

Random variables	Notation	Distribution	Reference
Critical damage accumulation index	Δ	Lognormal LN (1.0, 0.3)	Wirsching (1984)
Fatigue detail coefficients	A_1, A_2	Lognormal COV(A_1) = 0.45, COV(A_2) = 0.45	Eurocode 9 (1999), Wirsching et al. (1987)
Measurement error factor	e	Lognormal LN (1.0, 0.1)	Ayyub et al. (2002)
Material constant	m	Deterministic $m_1 = m$ $m_2 = m+2$	Eurocode 9 (1999)
Equivalent stress range	S_{re}	Weibull E(S_{re}) = 13.08 MPa COV(S_{re}) = 0.1	Stress-range bin histogram data (Sielski, 2007a)
Average daily number of cycle	N_{avg}	Deterministic 2102 cycles per day	

Table 4-5   The S-N values for members with welded attachments–transverse weld toe (Eurocode 9, 1999).

Detail category ($N_C = 2,000,000$)		$N \leq 5,000,000$		$N > 5,000,000$		$N_D = 5,000,000$
Reference stress range, S_C (MPa)	m	$\log A_1$	Mean value of $\log A_1$	$\log A_2$	Mean value of $\log A_2$	Constant amplitude fatigue limit, S_D (MPa)
31	3.2	11.074	12.074	13.809	14.809	23.2
28	3.2	10.932	11.932	13.577	14.577	21.0
25	3.2	10.775	11.775	13.323	14.323	18.8
22	3.2	10.597	11.597	13.033	14.033	16.5
20	3.2	10.464	11.464	12.818	13.818	15.0
18	3.2	10.318	11.318	12.580	13.580	13.5
16	3.2	10.154	11.154	12.314	13.314	12.0
14	3.2	9.969	10.969	12.012	13.012	10.5

Note: log A is assumed to follow a normal distribution and obtained using following transformation: $E(A) = \exp\left(\lambda_A + \zeta_A^2 / 2\right)$ and $\sigma(A) = \sqrt{E(A)^2 \cdot \left(\exp(\zeta_A^2) - 1\right)}$, in which $\lambda_A = \ln (10) \times E(\log A)$ and $\zeta_A = \ln (10) \times \sigma(\log A)$. Therefore, standard deviation of log A of 0.186 is calculated and used for all detail categories.
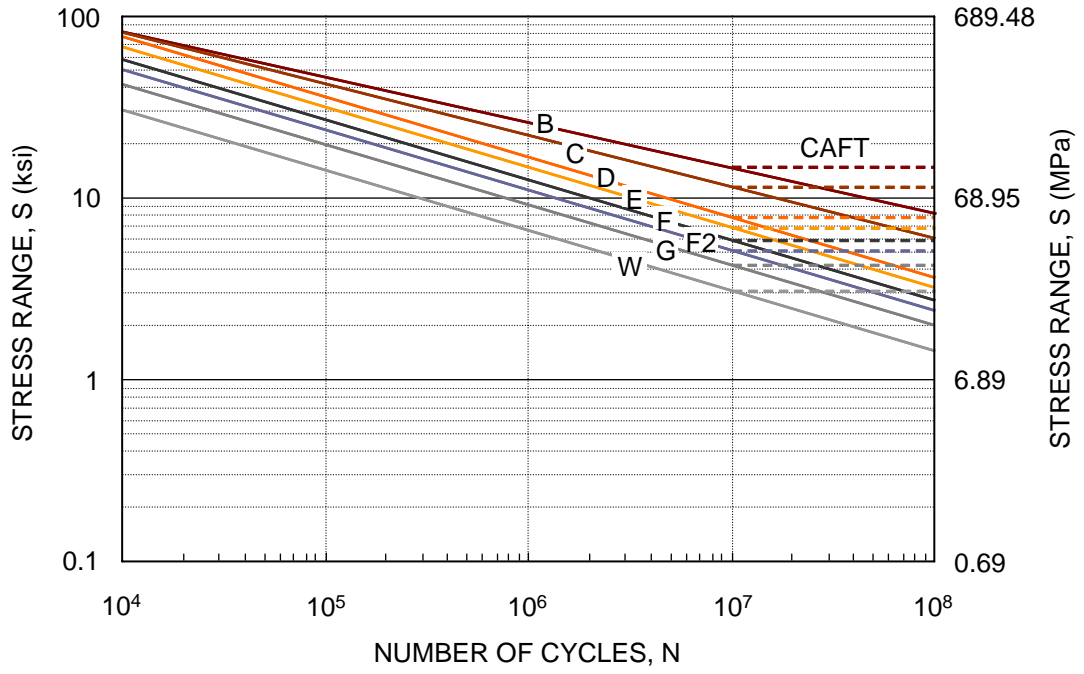
Figure 4-1   The S-N curves based on the BS 5400 (1980).

$P_{SS,1}$

$P_{SP,1}$

$P_{WH,1}$ .... $S_{re,111}$
$P_{WH,2}$ .... $S_{re,112}$

$P_{WH,k}$ .... $S_{re,11k}$

$P_{SP,2}$

$P_{SP,j}$

$P_{SS,2}$

$P_{SS,i}$

$P_{SP,1}$

$P_{WH,1}$ .... $S_{re,i11}$
$P_{WH,2}$ .... $S_{re,i12}$

$P_{WH,k}$ .... $S_{re,i1k}$

$P_{SP,2}$

$P_{SP,j}$

$P_{WH,1}$ .... $S_{re,ij1}$
$P_{WH,2}$ .... $S_{re,ij2}$

$P_{WH,k}$ .... $S_{re,ijk}$
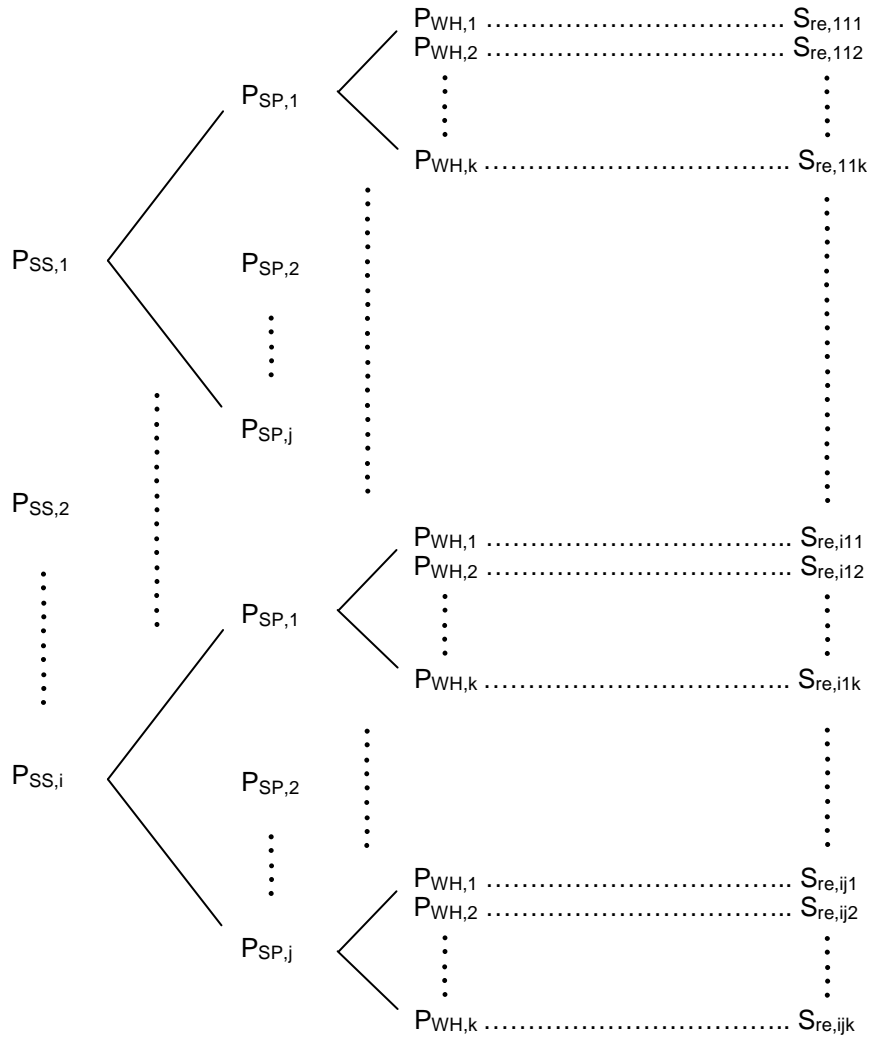
(a) the relationship of individual equivalent stress ranges and occurrence probabilities

(b)
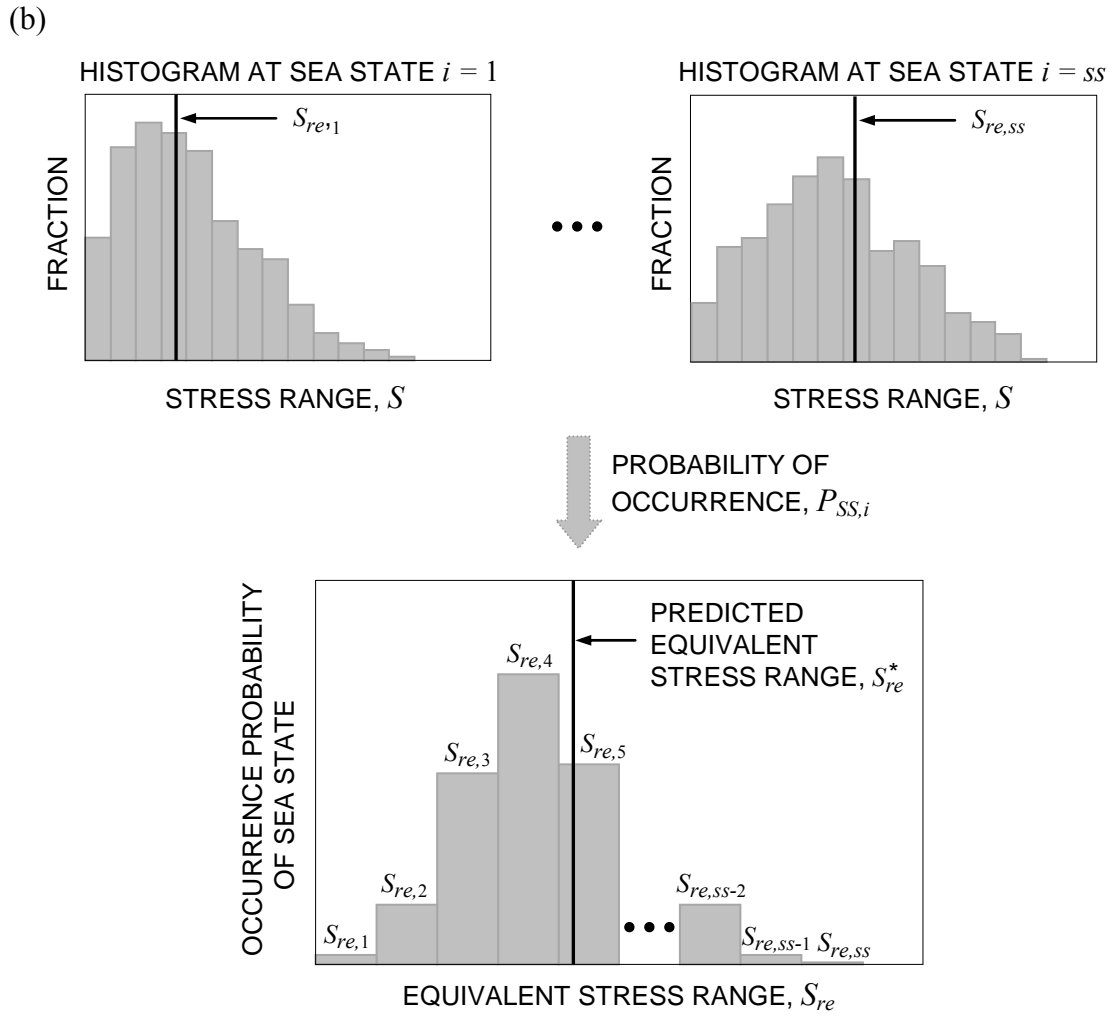
(b) the relationship of predicted and individual equivalent stress ranges

Figure 4-2   Schematic for estimation of the predicted equivalent stress range, S_{re}^*.
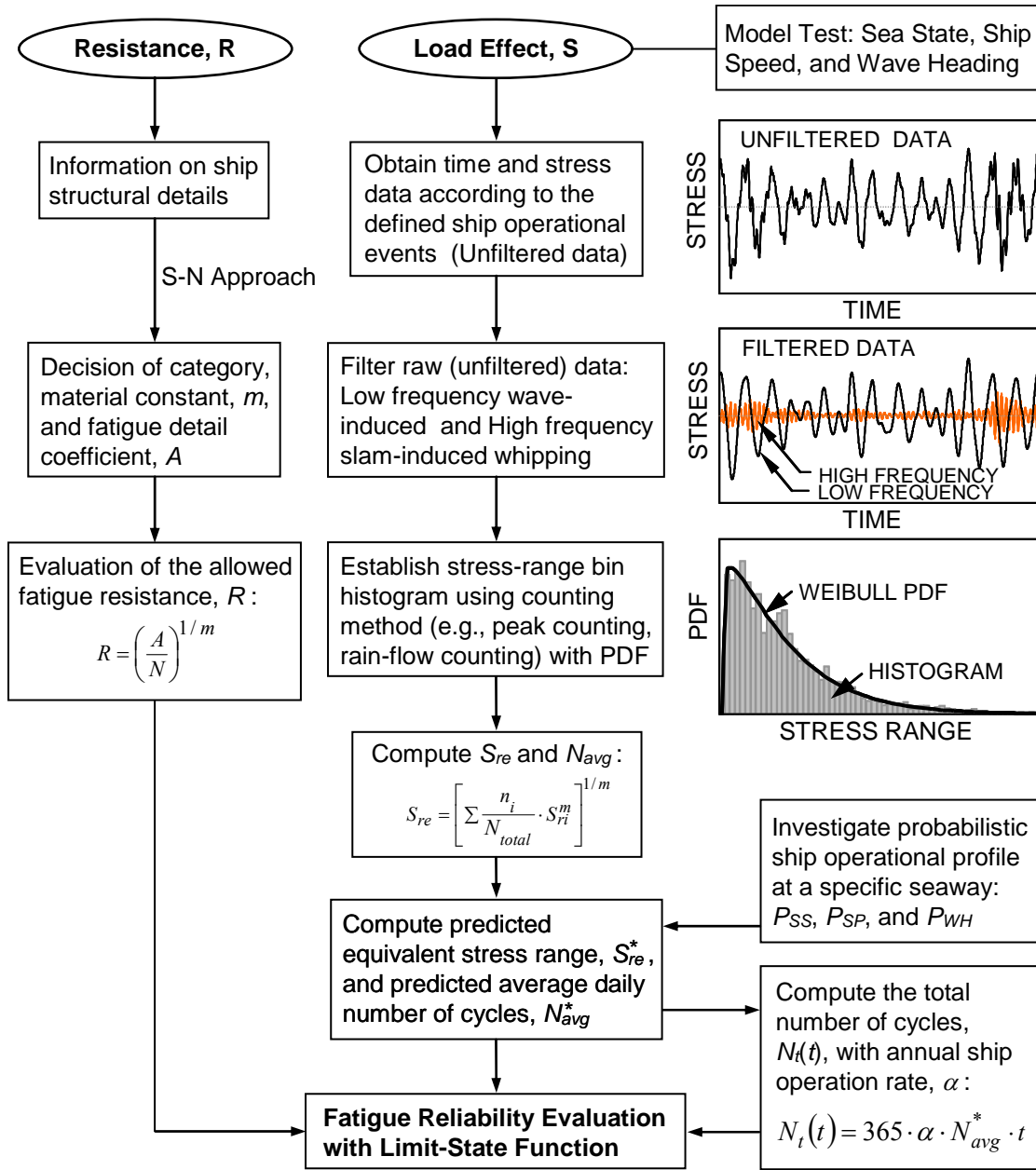
Figure 4-3   Flowchart for the fatigue reliability evaluation.

Resistance, R

Information on ship structural details

S-N Approach

Decision of category, material constant, m, and fatigue detail coefficient, A

Evaluation of the allowed fatigue resistance, R :

$$R = \left(\frac{A}{N}\right)^{1/m}$$

Load Effect, S

Model Test: Sea State, Ship Speed, and Wave Heading

Obtain time and stress data according to the defined ship operational events (Unfiltered data)

Filter raw (unfiltered) data: Low frequency wave-induced and High frequency slam-induced whipping

Establish stress-range bin histogram using counting method (e.g., peak counting, rain-flow counting) with PDF

Compute S_{re} and N_{avg} :

$$S_{re} = \left[\Sigma \frac{n_i}{N_{total}} \cdot S_{ri}^m\right]^{1/m}$$

Investigate probabilistic ship operational profile at a specific seaway: P_{SS}, P_{SP}, and P_{WH}

Compute predicted equivalent stress range, S_{re}^*, and predicted average daily number of cycles, N_{avg}^*

Compute the total number of cycles, $N_t(t)$, with annual ship operation rate, α :

$$N_t(t) = 365 \cdot \alpha \cdot N_{avg}^* \cdot t$$

Fatigue Reliability Evaluation with Limit-State Function

UNFILTERED DATA

STRESS

TIME

FILTERED DATA

STRESS

HIGH FREQUENCY
LOW FREQUENCY

TIME

PDF

WEIBULL PDF

HISTOGRAM

STRESS RANGE

171

Figure 4-4   JHSS model (adapted from Devine 2009).
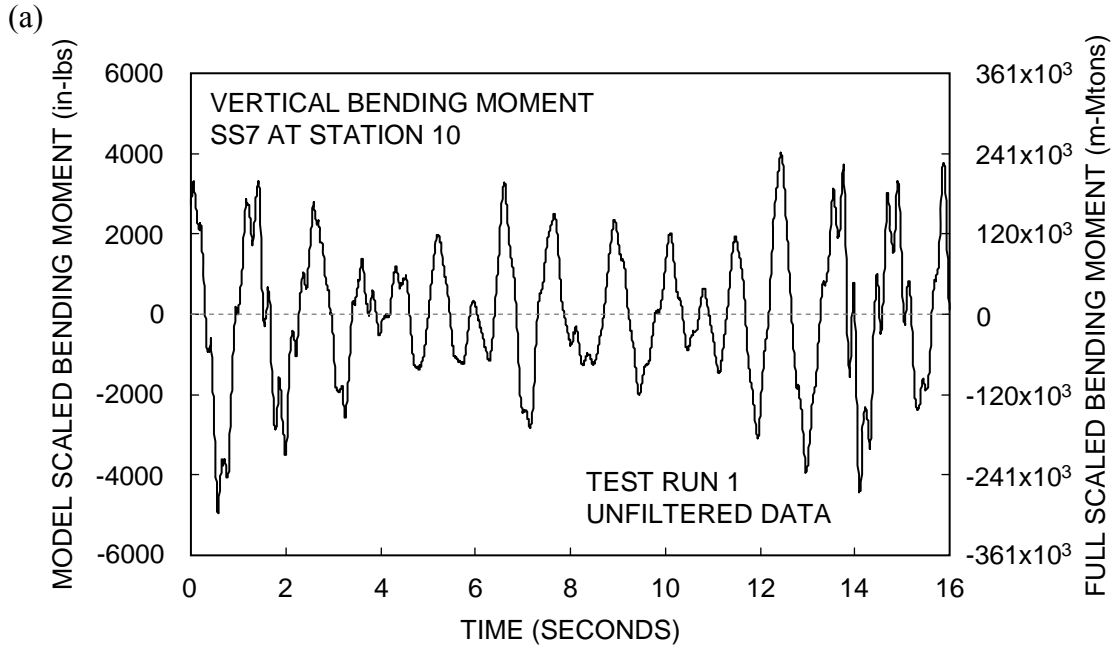
(a) unfiltered data at Station 10, 35 knots, SS 7 and heading of 0˚
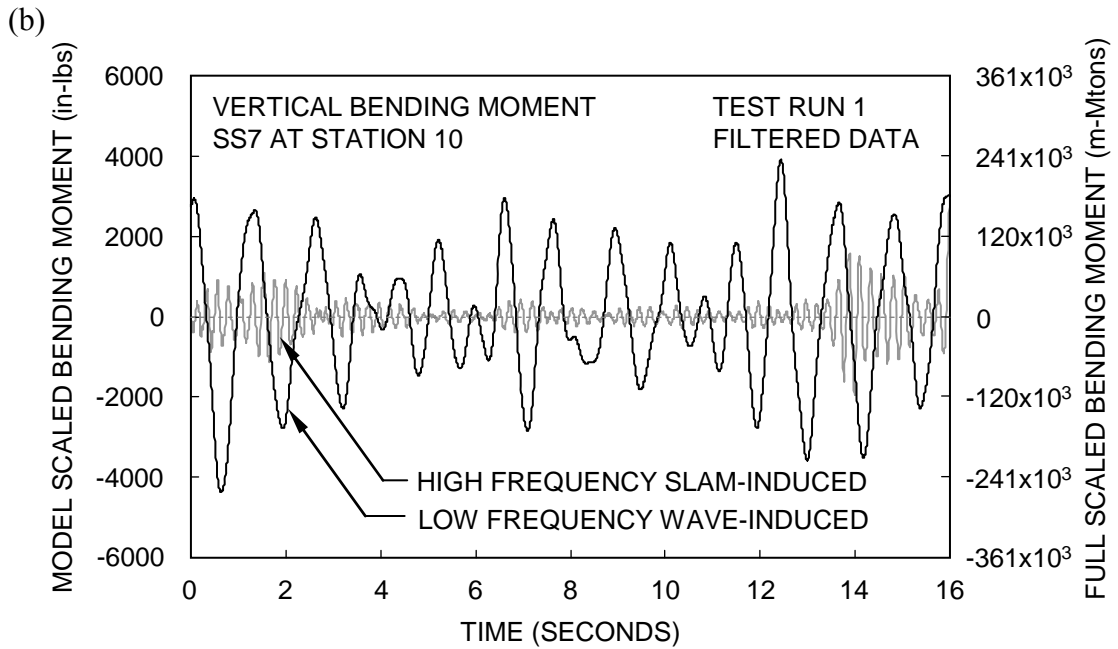
(b) low and high frequency filtered data at Station 10, 35 knots, SS 7 and heading of 0˚

173

(c)

(c) unfiltered data at Station 10, 15 knots, HC and heading of 0°

(d)
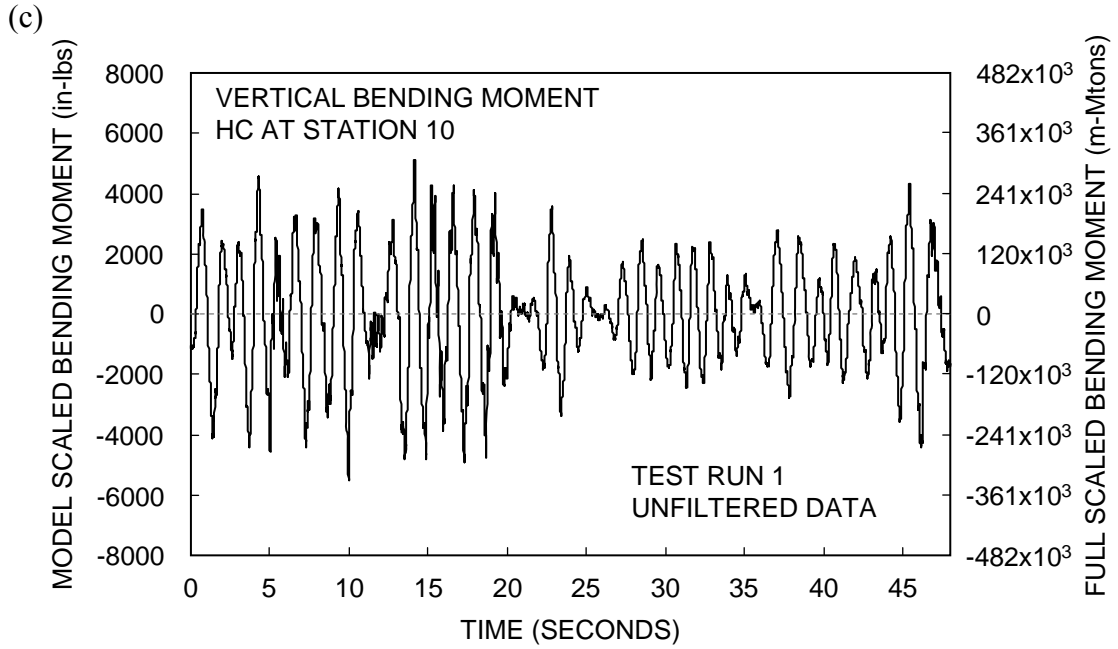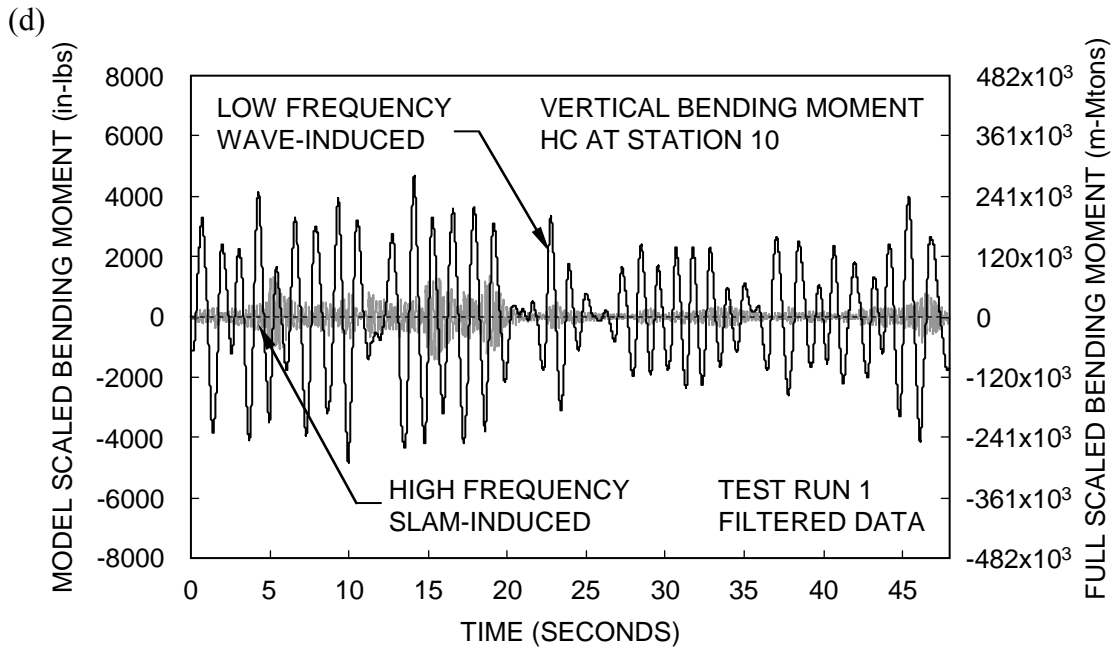
(d) low and high frequency filtered data at Station 10, 15 knots, HC and heading of 0°

Figure 4-5   JHSS primary vertical bending moment.
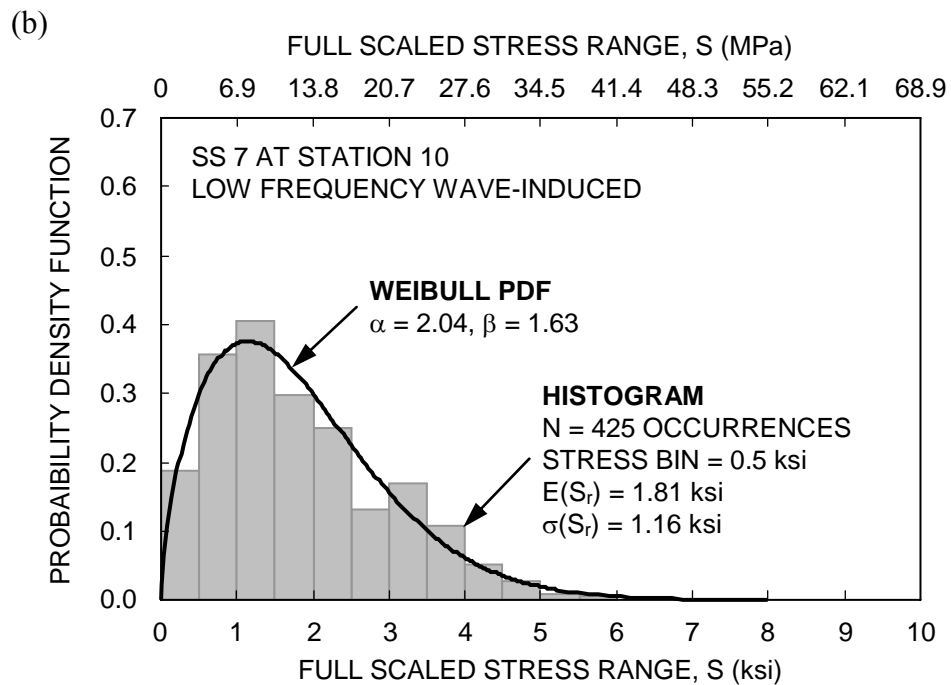
174

(a) unfiltered data at Station 10, 35 knots, SS 7 and heading of 0˚

(b) low frequency wave-induced data at Station 10, 35 knots, SS 7 and heading of 0˚

(c)

FULL SCALED STRESS RANGE, S (MPa)

(c) unfiltered data at Station 10, 15 knots, HC and heading of 0°

(d)

FULL SCALED STRESS RANGE, S (MPa)
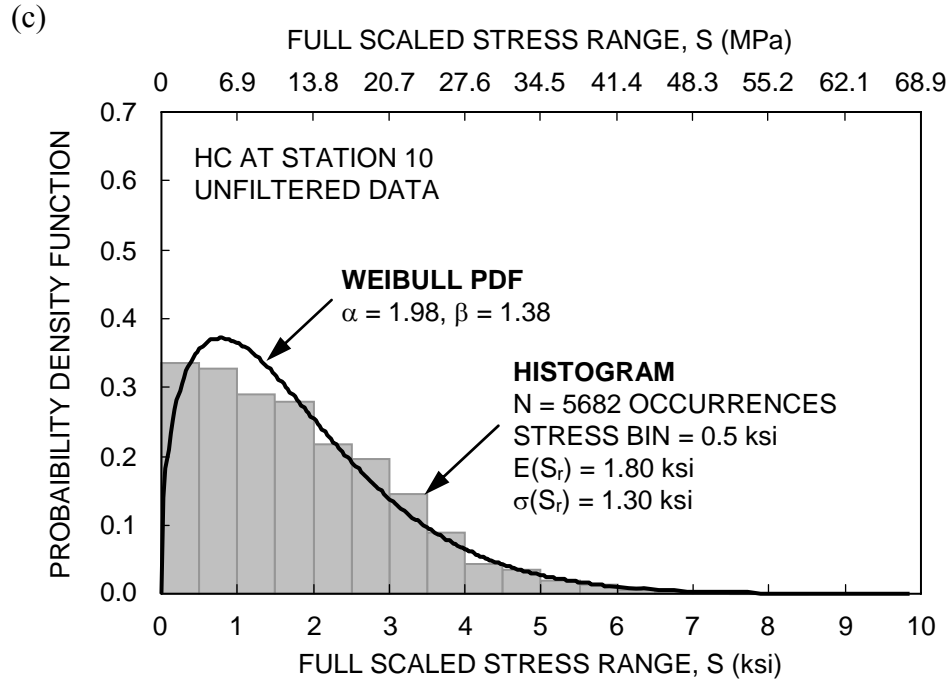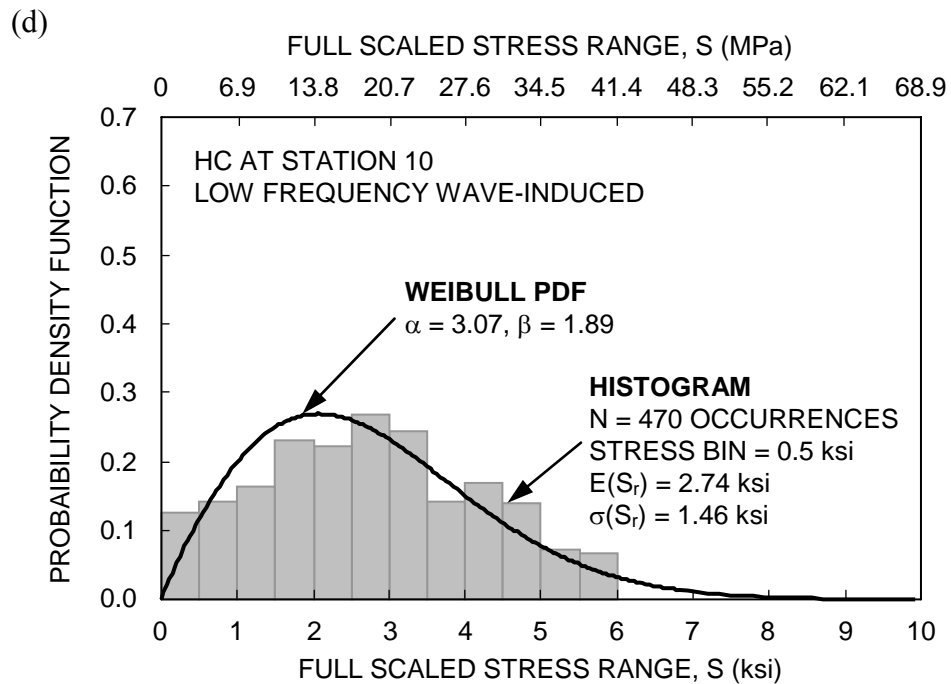
(d) low frequency wave-induced data at Station 10, 15 knots, HC and heading of 0°

Figure 4-6   Stress-range bin histogram and Weibull PDF.

176

(a)
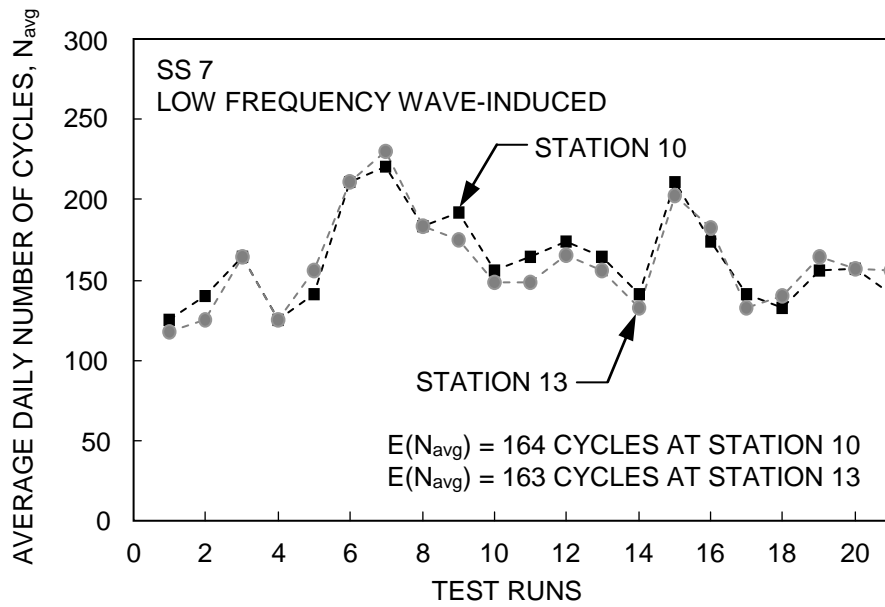
(a) N_{avg} of SS 7

(b)
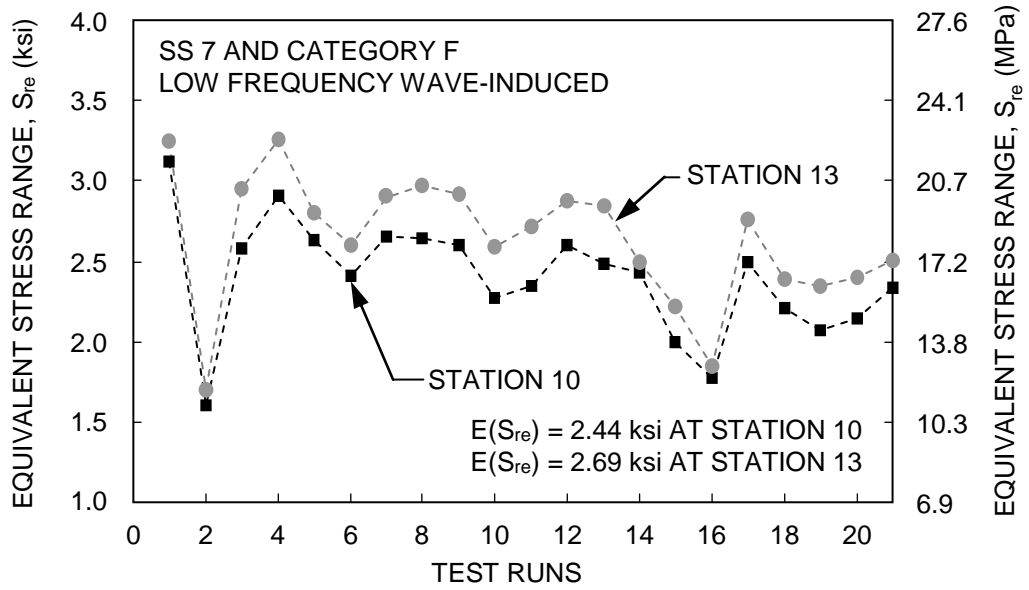
(b) S_{re} of SS7

177

(c)
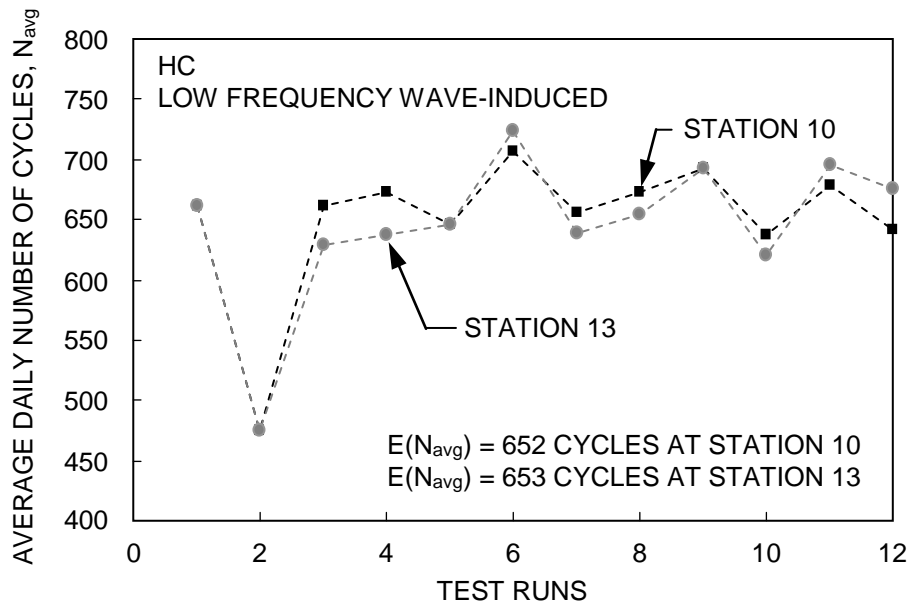
(c) N_{avg} of HC

(d)
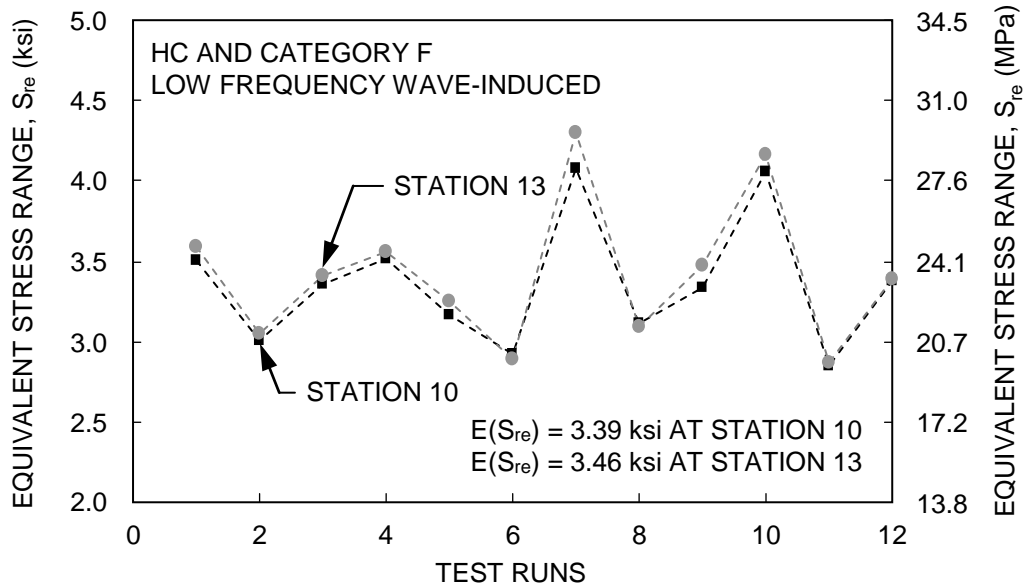
(d) S_{re} of HC

Figure 4-7 S_{re} and N_{avg} at Stations 10 and 13 for each test run based on low frequency wave-induced moment.
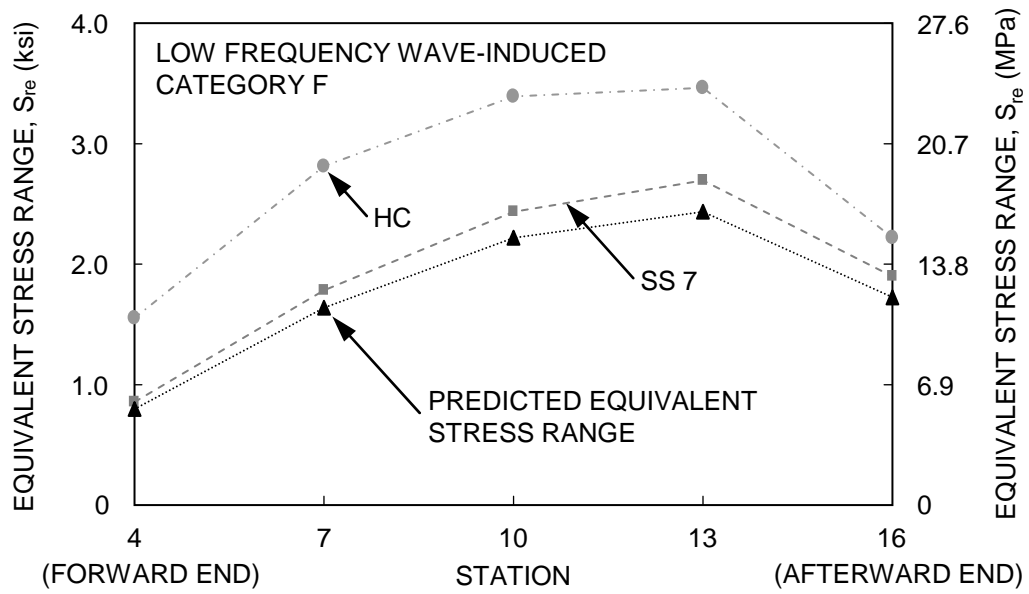
Figure 4-8   Predicted equivalent stress range, S_{re}^{*}, at the five stations of the JHSS.

(a)
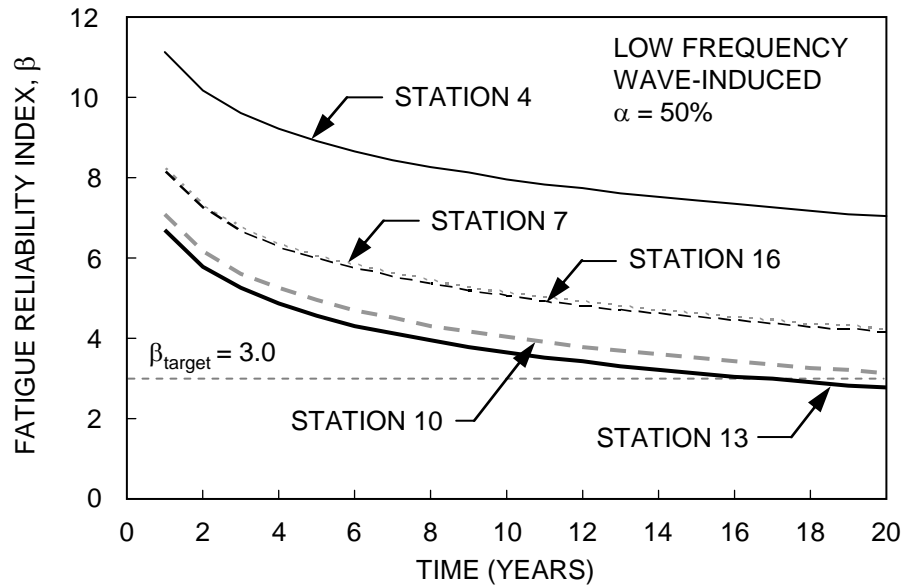
(a) at the five stations with annual operation rate, $\alpha = 50\%$

(b)
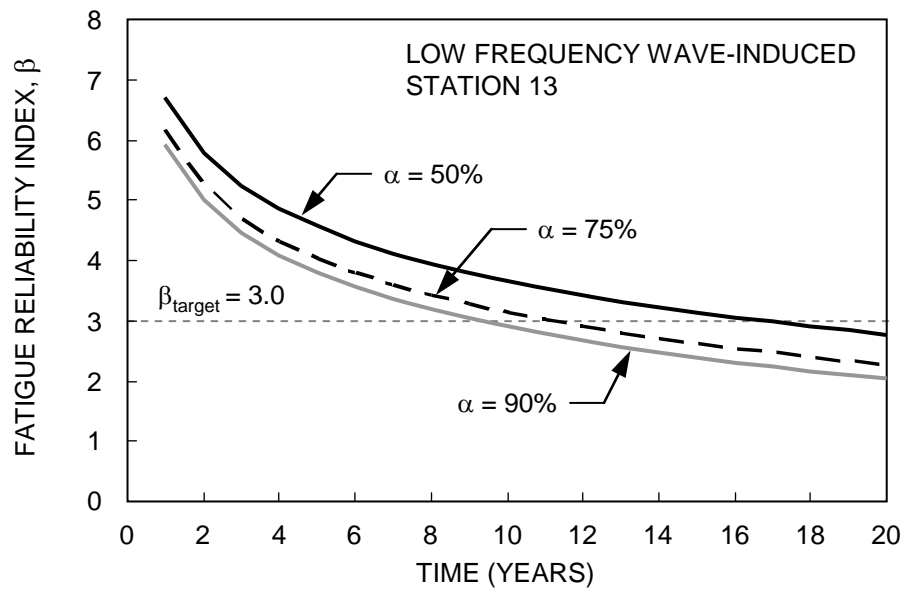
(b) at Station 13 according to $\alpha = 50\%$, 75% and 90%

180

(c)
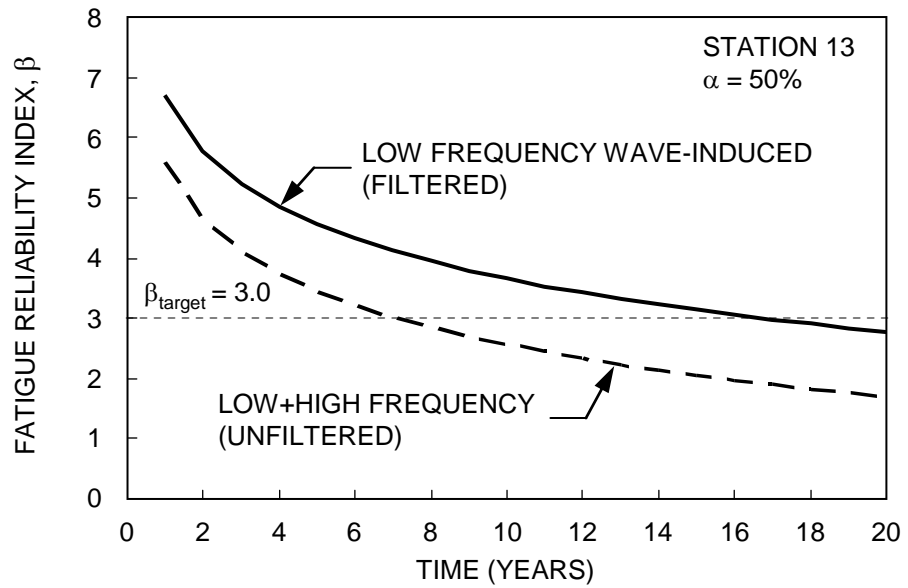
(c) using low frequency wave-induced filtered data and unfiltered data at Station 13

Figure 4-9   Fatigue performance assessment and service life prediction of the JHSS based on the predicted lifetime sea loads.
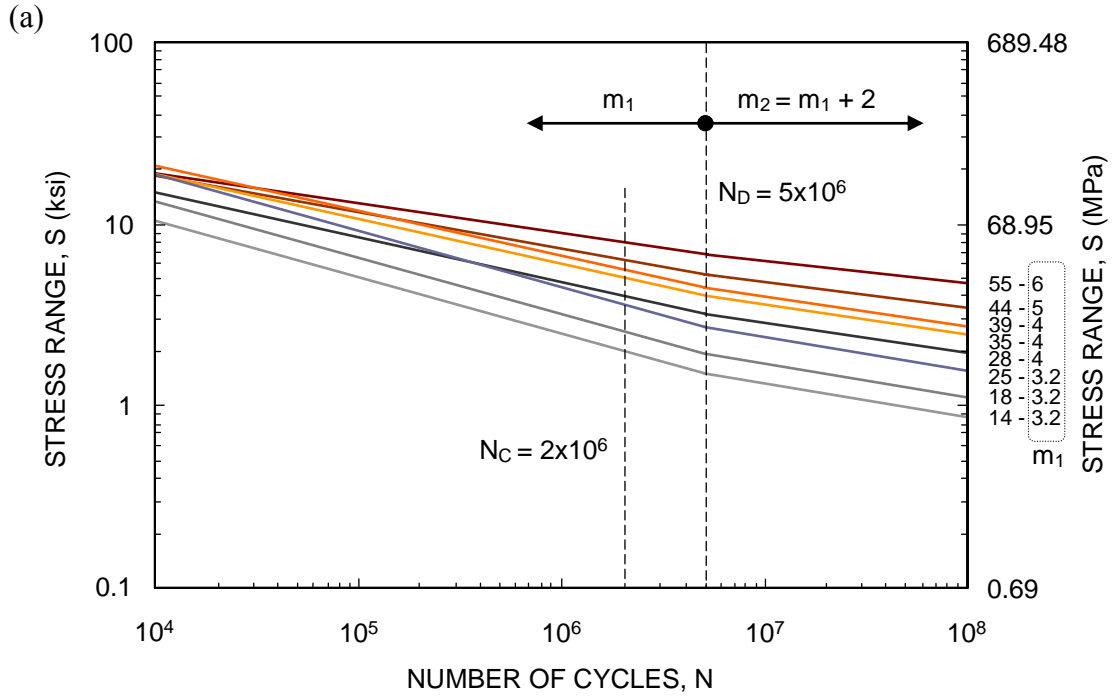
(a) for welded joints between member
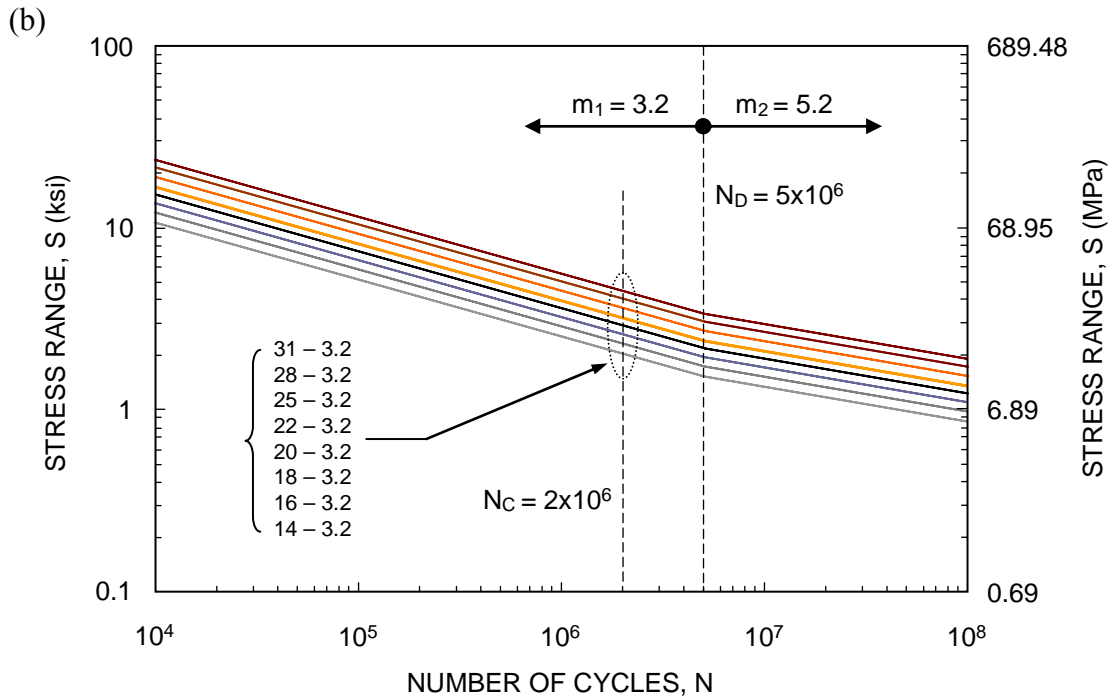
(b) for members with welded attachments-transverse welded toe

Figure 4-10   The *S-N* Curves representing two slopes m_1 and m_2 (Eurocode 9, 1999).
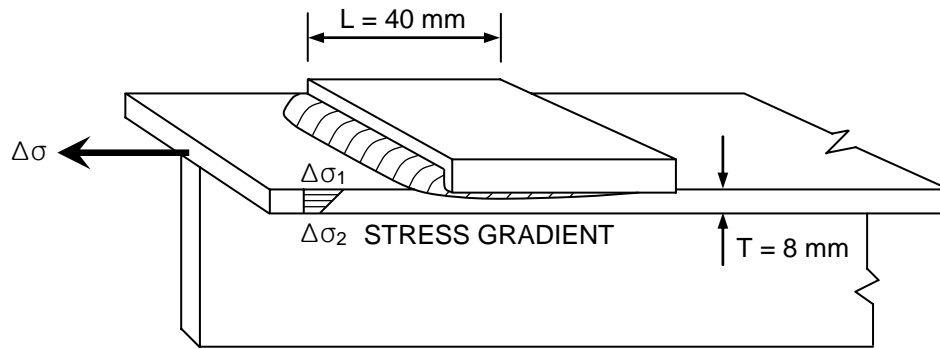
Note: L = length of attachment (mm), T = thickness of base plate (mm)

Figure 4-11   Aluminum welded attachment detail (adapted from Sielski 2007a).

HISTOGRAM
N = 3,148,808 CYCLES
STRESS BIN = 2.71 MPa
MAX (S) = 67.75 MPa
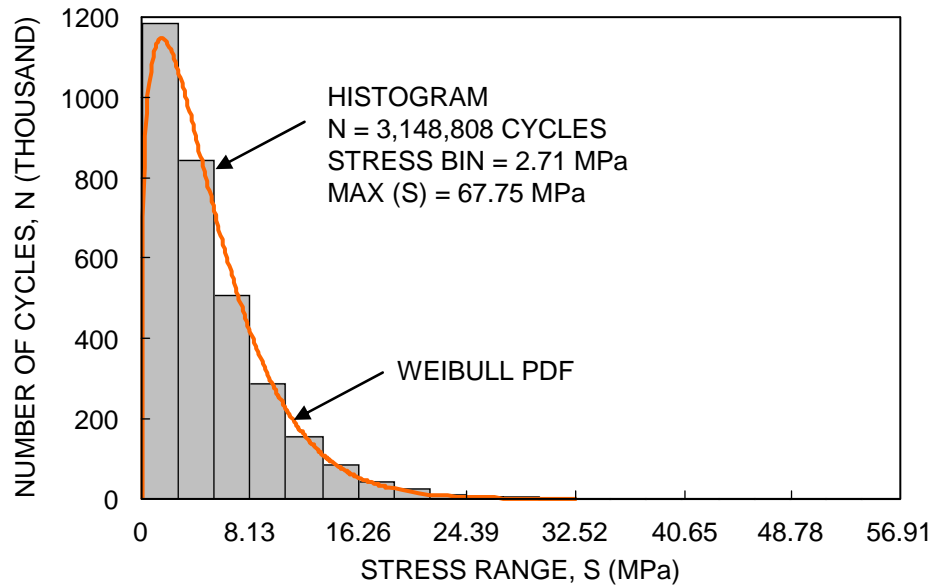
WEIBULL PDF

Figure 4-12   Stress-range bin histogram and Weibull PDF for fatigue loading.

(a)
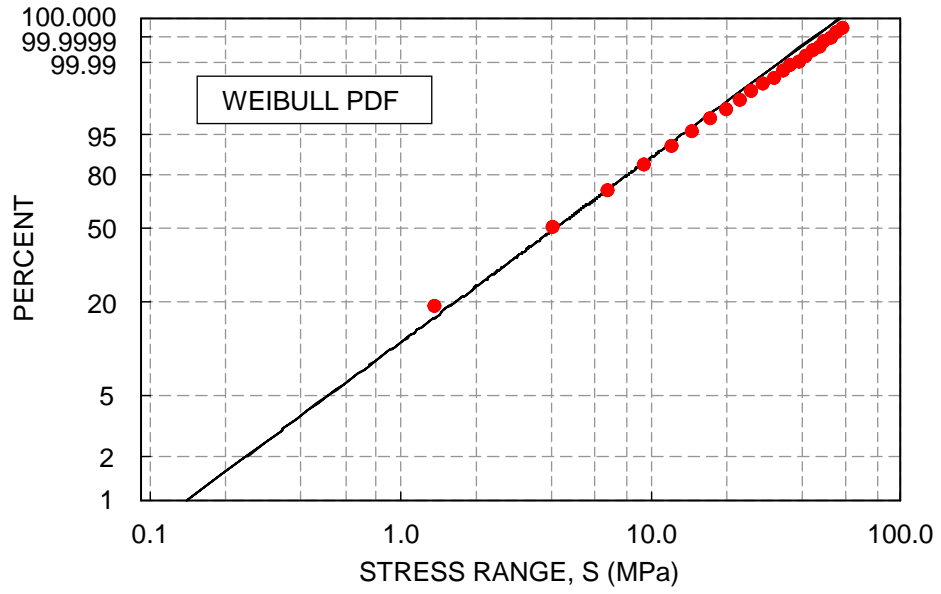
(a) Weibull PDF

(b)

(b) lognormal PDF

184

(c)
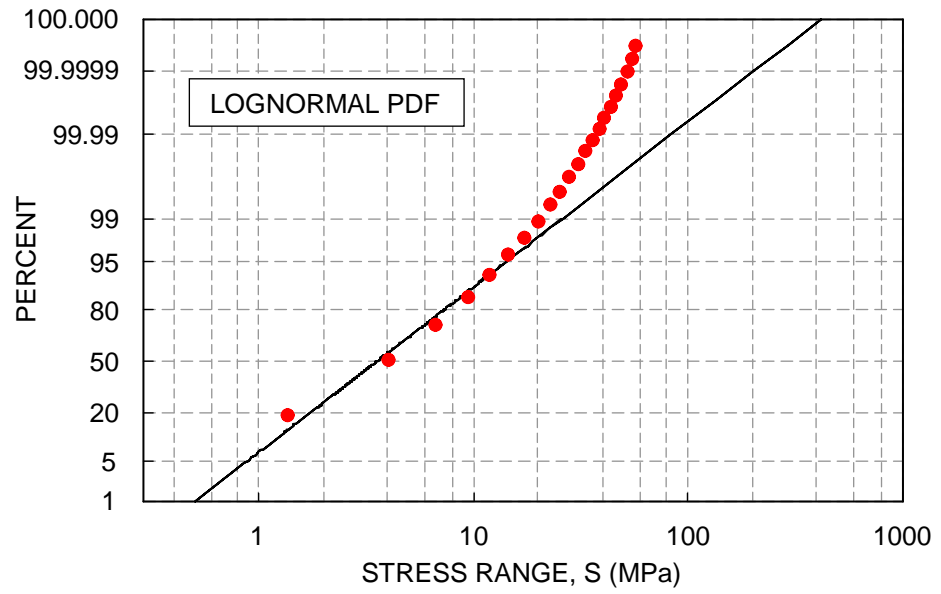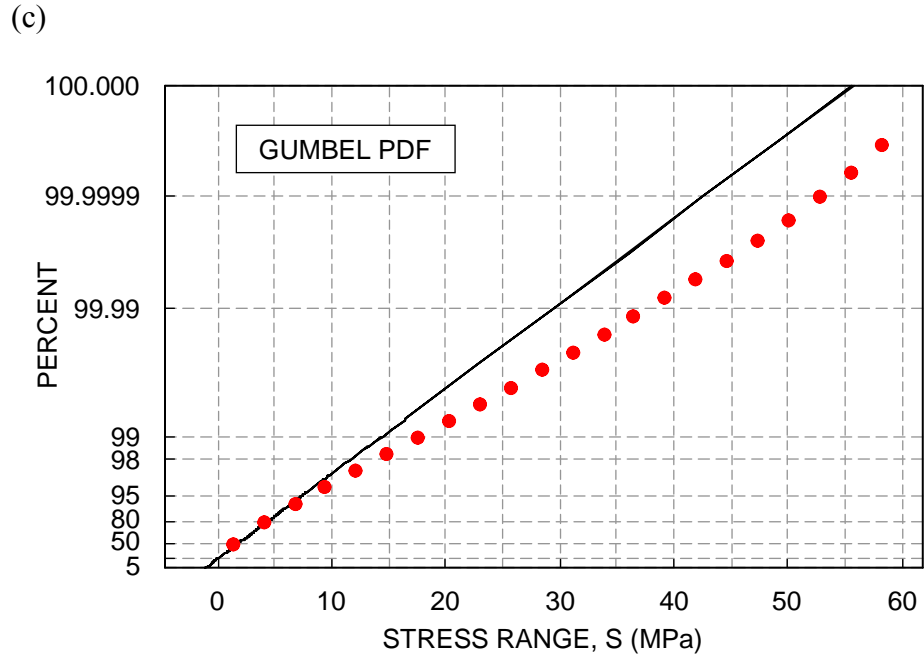
(c) Gumbel PDF

Figure 4-13   Goodness-of-fit tests for each PDF.
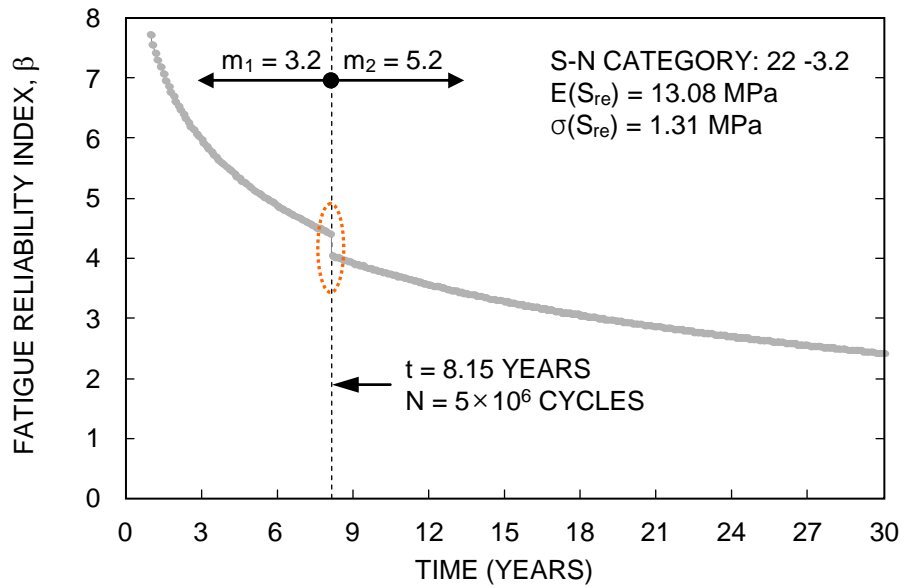
Figure 4-14   Time-dependent fatigue reliability assessment.

CHAPTER 5

BRIDGE RELIABILITY-BASED LIFE-CYCLE MANAGEMENT

5.1 INTRODUCTION

This chapter describes the reliability-based life-cycle structural management of steel bridges associated with inspection, monitoring, and repair/retrofit. In this study, a series of analyses are performed to evaluate the time-dependent reliability and to find optimal solutions in the formulated optimization problems. All detail information for the reliability analysis considering uncertainties associated with structural resistance and load effects was previously addressed in Chapters 2 and 3.

In this study, lifetime structural performance assessment and management of steel bridges under fatigue were performed by integrating three prediction models: fatigue reliability model (FRM), crack growth model (CGM), and probability of detection model (PDM). Bridge retrofit design optimization for single-objective and bi-objective was carried out based on (a) objective function, (b) fatigue stress constraint, (c) fatigue reliability constraint, and/or (d) geometrical constraint.

Section 5.2 describes efficient bridge fatigue assessment and management by using a combined approach from three prediction models (i.e., FRM, CGM and PDM) that are developed based on loading information from field monitoring and cracking information from NDE. Section 5.3 describes bridge retrofit design optimization to find the optimal cut-off area (size) in the floor-beam connection details, by applying the single-objective (i.e., minimization of the cut-off area) only and the bi-objective (i.e., maximization of the fatigue reliability and minimization of the cut-off area).

5.2 LIFETIME STRUCTURAL MANAGEMENT OF STEEL BRIDGES

5.2.1 Introduction

Many steel bridges are deteriorating due to fatigue that may cause critical damage locally or globally. As a result, bridge fatigue performance may not be preserved safely up to the anticipated service life. For this reason, bridge performance has to be steadily assessed during the entire service life. If necessary, interventions have to be applied to improve fatigue performance. Various strategies for assessing and managing steel bridges have to be considered in order to identify structural deficiencies due to fatigue. Fatigue assessment of steel bridges may be reliably performed based on long-term monitoring program and non-destructive evaluation (NDE). A long-term monitoring program is used to collect structural response data (e.g., stress or strain) associated with load effects, while NDE is used to detect fatigue cracks causing structural degradation in potential critical regions. Continuous monitoring and NDE are useful for finding time-dependent fatigue damage which may be mitigated or removed by taking proper repair actions. However, since it is not practically possible to continuously monitor and to conduct NDE during the entire service life of steel bridges, a combined approach is proposed to assess and manage effectively bridge safety under fatigue by using three prediction models: fatigue reliability model (FRM), crack growth model (CGM), and probability of detection model (PDM).

Modern concepts for structural health monitoring (SHM) as well as maintenance of bridges under uncertainty have been developed (Frangopol & Estes 1997, Frangopol & Messervey 2007, and Frangopol & Liu 2007). Based on long-term

monitoring data, various applications to bridge fatigue reliability assessment and prediction have been studied (Pourzeynali & Datta 2005, Frangopol et al. 2008, and Liu et al. 2010a). However, these approaches do not include cracking information associated with the time-dependent crack growth since they are only based on the AASHTO stress-life (S-N) approach. In this study, the FRM is developed to provide not only fatigue reliability to number of cycles (i.e., service years) but also cracking information by integrating the CGM. Rummel and Matzkanin (1997) addressed the PoD concept and methodology as a useful metric for quantifying and assessing NDE capabilities. For many crack patterns, they carried out the NDE by using various techniques such as Ultrasonic, Eddy current and Dye-penetrant testing, and provided the relationship between PoD and actual crack depth or length. Harlow and Wei (1999) concluded that the accurate assessment of structures may depend on the development of a quantitative methodology that integrates necessary information from NDE with validated methods for structural integrity assessment and prediction of damage accumulation. Accordingly, the PDM associated with NDE has to be used in conjunction with other quantitative prediction models (e.g., FRM and CGM) for assessing, predicting and eventually extending bridge fatigue life with proper maintenance management. This approach is similar to that for crack-growth-based maintenance scheduling reported by Berens (1996).

Typically, the fatigue CGM, which is generated to estimate the cumulative number of cycles according to cracks sizes, is used as an efficient method for estimating fatigue life. This model can be combined with the FRM and PDM. The interrelationship among the three prediction models is represented in the flowchart

188

shown in Figure 5-1. Based on this flowchart, a combined approach using the three prediction models is proposed. This approach for bridge fatigue assessment and management is useful for quantifying and restoring the time-dependent structural deficiencies associated with crack growth by using inspection and repair strategies, respectively. Interventions according to crack sizes can be determined by imposing the predefined PoD levels with respect to a specified flaw size. For welding defects of steel components, various experiments have been carried out to investigate applicable repair methods according to flaw sizes. For welding defects of steel components, various experiments have been carried out to investigate applicable repair methods according to flaw sizes. The typical repair methods (Fisher et al. 1998 and Miki 2007) are: (a) Peening; (b) Gas Tungsten Arc Remelting; (c) Rewelding; and (d) Bolted Splices.

As previously indicated, a combined approach integrating the FRM, CGM, and PDM is developed for lifetime structural performance assessment and management associated with fatigue cracks. Field monitoring data and the AASHTO *S-N* approach are used to develop the FRM for the time-dependent fatigue reliability evaluation, while cracking information from NDE and fracture mechanics is used to develop the CGM and PDM. Bridge fatigue performance according to the identified crack sizes is quantified and the corresponding repair option is employed. The proposed approach is illustrated on an existing bridge, the Yellow Mill Pond Bridge in Bridgeport, Connecticut, USA.

5.2.2 Inspection and Monitoring

The use of inspection, monitoring, repair and maintenance programs has been widely accepted for lifetime performance assessment and management of aging steel bridges under fatigue. In particular, bridge inspection and monitoring are extremely important in order to obtain current loading and cracking information and provide support for interventions considering time-dependent bridge deterioration process due to fatigue. PDM, which assess the NDE capabilities, is useful to schedule inspection time as well as repair time. Loading and resistance data collected during monitoring can be used to assess current structural performance and to predict remaining service life. Information from monitoring and/or NDE offers the opportunity to develop a combined approach for efficient bridge assessment and management.

Field monitoring is used to gain useful information on the current condition of a structure, with the ultimate goal being the prognosis of the load capacity of the structure and providing a decision making basis to repair/retrofit, maintenance, or rebuild. Monitoring has to be implemented to provide stress-range bin histogram data and eventually to reliably perform fatigue life assessment.

There are two typical test methods to investigate load effects: controlled and uncontrolled (Mahmoud et al. 2005). The controlled live load tests are fulfilled to find the effects of both vehicle speed and vehicle position on the bridge deck, whereas the uncontrolled live load testing is conducted to investigate the overall influence of real traffic. Commonly, the long-term uncontrolled live load test is used to collect stress-range bin histogram data which offer an opportunity for developing a random variable-amplitude stress range spectrum. The long-term monitoring system will

automatically record and store data obtained in installed strain gages whenever heavy vehicles cross a bridge. In particular, it is necessary to compute equivalent stress ranges and average daily truck traffic (*ADTT*) from the stress-range bin histogram established by long-term monitoring program for bridge fatigue reliability assessment and prediction (i.e., FRM). Stress range spectrum and number of cycles from the monitoring program can be effectively used by FRM or CGM.

For assessing the integrity of structural components, various NDE methods are available for in-service structures. Common NDE methods include visual testing (VT), magnetic particle testing (MT), dye-penetrant testing (PT), eddy current testing (ET), ultrasonic testing (UT), and X-radiographic testing (RT). An efficient NDE may be selected according to the type of degradation being detected. For instance, while the UT can be utilized for nearly all steel components in a bridge, the PT may be applied to aluminum and stainless steel members (Ghorbanpoor 2003). It is essential to take into account the accuracy of inspection, consequences of detection failures, frequency, accessibility, and cost when selecting the appropriate NDE methods (Chung 2006). In particular, the cost levels associated with the NDE methods are important to be considered. The inspection cost is usually proportional to the NDE equipment cost (Rummel & Matzkanin 1997). Typically, NDE capability is associated with PoD with respect to fatigue cracks. The results from NDE may be used to plan efficient bridge inspection strategies.

5.2.3 Combined Approach for Fatigue Cracking

A combined approach is proposed to perform efficient bridge assessment and management for fatigue cracking by using three prediction models: fatigue reliability model (FRM), crack growth model (CGM), and probability of detection model (PDM). Based on all necessary information from field monitoring and/or non-destructive evaluation (NDE), the FRM is developed to quantify time-dependent bridge performance. An appropriate crack growth curve from the CGM is selected from the cracking data collected by the NDE and the target reliability index in the FRM is determined. The purpose of the PDM, which depends on crack sizes and performance of NDE methods, is to find proper repair options according to the predefined target probability of detection. Determining the target PoD is an important issue in order to implement proper maintenance-management. Consequently, the three prediction models are combined to assess, predict, and eventually extend bridge fatigue life using inspection, repair and maintenance strategies.

5.2.3.1 Fatigue Reliability Model (FRM)

Bridge performance assessment and prediction for fatigue can be performed by using FRM, with a well-defined fatigue limit-state consisting of fatigue resistance, R, and load effect, S. In the combined approach, the FRM is integrated with the CGM and PDM in order to determine an appropriate crack growth curve and schedule bridge inspection and repair interventions. This is important because bridge management actions including inspection, monitoring and repair can be taken based on fatigue reliability information.

192

In general, the stress-range bin histogram data collected by rain-flow counting method (Downing & Socie 1982) from monitoring data provide the load effect, S, while the AASHTO S-N curve (AASHTO 2002) and the Miner's rule (1945) provide necessary information associated with resistance, R. Typically, the fatigue reliability of any structure is preserved when its resistance, R, is larger than the stress range, S. Based on AASHTO Specifications (2002) and Miner's rule (1945), the performance function employed in fatigue reliability analysis is represented as:

$$g(\boldsymbol{X}) = \Delta - e \cdot D \quad \text{where } D = \sum n_i / N_i = \frac{N}{A} \cdot (S_{re})^m \tag{5-1a}$$

Therefore,

$$g(\boldsymbol{X}) = \Delta - e \cdot \frac{N}{A} \cdot (S_{re})^m \tag{5-1b}$$

where Δ = Miner's critical damage accumulation index assumed lognormal with the mean value $E(\Delta) = 1.0$ and coefficient of variation $COV(\Delta) = 0.3$ for resistance of metallic materials (Wirsching 1984); e = measurement error factor; D = Miner's damage accumulation index for load effect; N = number of stress range cycles; A = random variable representing the fatigue details coefficient for each category, the mean value and standard deviation of the A are presented in Table 5-1 (Wirsching et al. 1987); m = material constant representing the slope of the S-N curves, which may be assigned as 3.0 (i.e., $m = q = 3.0$); and $\boldsymbol{X}$ = vector of random variables. The equivalent stress range, S_{re}, is calculated from stress-range bin histogram as (Miner 1945):

$$S_{re} = \left(\sum_{i=1}^{k} \frac{n_i}{N_{total}} \cdot S_{ri}^{m} \right)^{1/m} \qquad (5\text{-}2)$$

where n_i = number of observations in the i-th predefined stress-range bin, S_{ri}, and N_{total} = total number of observations up to the k-th range during the monitoring period.

Lognormal distributions for both S and R can be used (Kwon & Frangopol 2009 and Liu et al. 2010a). In addition, measurement error factor in monitoring and traffic increase rate per year can be included in fatigue reliability assessment (Frangopol et al. 2008).

Based on Eq. 5-1(b), the fatigue reliability index, β, is derived with lognormal distributions in both terms as follows (Kwon & Frangopol 2009 and 2010a):

$$\beta = \frac{\lambda_\Delta + \lambda_A - \left(\lambda_e + m \cdot \lambda_{S_{re}} + \ln N \right)}{\sqrt{\zeta_\Delta^{2} + \zeta_A^{2} + \zeta_e^{2} + \left(m \cdot \zeta_{S_{re}} \right)^{2}}} \qquad (5\text{-}3)$$

where N = accumulated number of stress cycles related to the traffic volume, $m = 3.0$, and e = measurement error factor considered lognormal with $E(e) = 1.0$ and COV $(e) = 0.04$ (Frangopol et al. 2008). The parameters, λ_Δ, ζ_Δ, and λ_A, ζ_A are the mean value and standard deviation of $\ln \Delta$ and $\ln A$, respectively, while the λ_e, ζ_e, and λ_{Sre}, ζ_{Sre} are those of $\ln e$ and $\ln S_{re}$, respectively.

5.2.3.2 Crack Growth Model (CGM)

Fatigue is the initiation and propagation of microscopic cracks into macro cracks by the repeated application of stresses (Fisher et al. 1998). For existing steel

bridges, examination of fatigue cracking must be an essential consideration because of repeated loading such as traffic. The majority of fatigue life may fully rely on propagation of the initiated cracks under uncertainties including loading history of environmental and mechanical stressors, human errors in fabrication, and unexpected traffic increases. Accordingly, crack growth curves (i.e., CGM) are generated for evaluating fatigue life associated with crack propagation and for planning proper inspections and repairs by integrating the FRM and PDM (see Figure 5-1). The CGM is useful for estimating the cumulative number of cycles (time) according to crack sizes and remaining fatigue life.

For estimating fatigue crack growth curves, the Paris equation is used (Paris & Erdogan 1963):

$$\frac{da}{dN} = C \cdot (\Delta K)^B \tag{5-4}$$

where a = crack size, N = number of cycles, and ΔK = stress intensity factor range while C and B are the fatigue coefficient and the fatigue exponent (i.e., $B = 3.0$), respectively. The estimation of ΔK is especially complex in common use of welded structures. It can be expressed in terms of crack size as (Bannantine et al. 1990):

$$\Delta K(a) = G(a) \cdot S_{re} \cdot \sqrt{\pi \cdot a} \tag{5-5}$$

where $\Delta K(a)$ = generalized stress intensity factor range, and $G(a)$ = a non-dimensional function of the geometry including various factors (i.e., finite width factor, non-uniform stresses factor, free surface effect factor, and crack shape factor). Values for these factors provided in the literature are associated with the flaw types caused in

critical structural members (Tada et al. 1973). Case studies conducted by Fisher (1984) present proper application of correction factors according to various crack patterns.

By using Eqs. 5-4 and 5-5, the equation for estimating the cumulative number of cycles, $N(a)$, is (Fisher 1984):

$$N(a) = \frac{1}{C \cdot S_{re}{}^{B}} \cdot \int_{a_i}^{a_f} \frac{da}{\left(G(a) \cdot \sqrt{\pi \cdot a}\right)^{B}}$$ (5-6)

where a_i = initial crack size and a_f = final (critical) crack size.

The final crack size, a_f, depends on the parameters, C, S_{re}, and a_i, which can be treated as random variables. Under these conditions, numerous crack growth curves can be generated by simulation. A sufficiently large number of samples should be employed to identify an appropriate crack growth curve based on field monitoring and NDE. For bridge fatigue assessment and management, the CGM representing the cumulative number of cycles and crack sizes can be effectively used to provide cracking information at any given time.

5.2.3.3   Probability of Detection Model (PDM)

Inspection is an essential step for bridge management not only to identify possible structural deficiencies but also to plan appropriate repair strategies. A PoD curve is used as an accepted metric for characterizing the NDE performance capability (Rummel and Matzkanin 1997). The PoD depends on both the NDE methods and the defected flaw sizes. In 1973, the PoD functions were introduced and have been

accepted in aerospace industry (Rummel and Matzkanin 1997). To date, PDM has been used in many engineering fields as a common method for quantifying and assessing the NDE capabilities. As a function of the flaw size a, the PDM can be used to quantify the detective capability of specified inspection methods.

There are two general statistical models for the estimation of the PoD: (a) hit & miss data; and (b) signal response data (Rummel 1982). The PoD curves from hit & miss data are usually developed based on log-logistic distributions. The NDE conducted by PT, MT and UT is only characterized by hit & miss of binary data. The log-logistic PoD function is defined as (Berens and Hovey 1981):

$$PoD\ (a) = \frac{\exp[\gamma + \delta \cdot \ln(a)]}{1 + \exp[\gamma + \delta \cdot \ln(a)]} \tag{5-7}$$

where γ and δ are statistical parameters estimated by the maximum likelihood method dependent on NDE, $\gamma = -\delta \cdot m_e$ and $\delta = \pi/(\sqrt{3} \cdot \sigma)$, in which m_e and σ are the median and standard deviation, respectively.

The signal response data model provides an estimate, $\hat{a}$, of the discontinuity size, a, when a discontinuity is found during an inspection. An appropriate linear relationship between $\ln(\hat{a})$ and $\ln(a)$ is (Berens 1997):

$$\ln(\hat{a}) = \delta_0 + \delta_1 \cdot \ln(a) + \varepsilon \tag{5-8}$$

where δ_0 and δ_1 are regression parameters, and ε is normally distributed with zero mean value and constant standard deviation, σ_ε. The term $\delta_0 + \delta_1 \cdot \ln(a)$ in Eq. 5-8 is the mean value E(a) of the probability density function (PDF) of $\ln(\hat{a})$.

The PoD function from signal response data is (Crawshaw and Chambers 1984):

$$PoD\ (a) = \Phi\left[\frac{\ln(a) - \mu}{\sigma}\right] \quad \text{for } \mu = \frac{\ln(y_{th}) - \delta_0}{\delta_1} \text{ and } \sigma = \frac{\sigma_\varepsilon}{\delta_1} \qquad (5\text{-}9)$$

where $\Phi(\cdot)$ = standard normal cumulative distribution function, y_{th} = value of the signal response data $\hat{a}$ at the decision threshold, and μ and σ are the mean value and standard deviation of flaw size, a, respectively.

In most field applications, inspection data are usually recorded as hit & miss data. Based on Eq. 5-7, inspection times can be computed for various PoD levels such as PoD(a_{50}) or PoD(a_{60}) which indicates crack detection probability of 50% or 60%, respectively. Decision on applicable welded repair methods (e.g., peening, GTA remelting) is usually made according to the propagated maximum crack sizes (Fisher et al. 1998). If a crack size exceeds a certain critical value, all welded repairs are not efficient in that case. For this reason, PoD inspection model is necessary to be developed. This model is useful to assign the most efficient repair option associated with the flaw sizes which are detected by using the predefined target PoD levels.

5.2.4 Structural Management Using Combined Approach

A novel approach using three prediction models is herein proposed for bridge fatigue assessment and maintenance including inspection and repair. Basically, this approach takes into account three important time-dependent factors: structural performance level, crack growth rate, and crack detection probability. The CGM offers useful information regarding crack propagation with respect to the number of

cycles, while the FRM estimates reliability of structural components with respect to the number of cycles. The PDM (PoD vs. crack sizes) is integrated into the FRM and CGM using the same parameter (crack sizes) for inspection planning. If field monitoring data and NDE outcomes are provided, a combined approach can be used for the time-dependent fatigue performance assessment and management.

Clearly, FRM quantifies safety of structural components, while CGM and PDM offer useful information regarding crack propagation and crack detection probability, respectively. In the FRM, the number of cycles, $N(y)$, is

$$N(y) = 365 \cdot ADTT \cdot \int_0^y (1+\alpha)^y \, dy = 365 \cdot ADTT \cdot \frac{(1+\alpha)^y - 1}{\ln(1+\alpha)} \qquad (5\text{-}10)$$

where $ADTT$ is average daily truck traffic considering single stress cycle per truck passage (cycles per day), y is the number of years, and α is annual traffic increase rate. By using Eqs. 5-6 and 5-10, the number of years, y, is obtained as:

$$y = \ln[N(a) \cdot \ln(1+\alpha) + 365 \cdot ADTT] - \ln(365 \cdot ADTT) - \ln(1+\alpha) \qquad (5\text{-}11)$$

In the following, PDM assessing NDE capability is used to schedule inspection times according to the predefined PoD levels. This model is combined with the developed fatigue reliability-based CGM for efficient bridge assessment and management.

The combined approach using the three prediction models (see Figure 5-1) is summarized as follows:

(a) The necessary information from monitoring and NDE inspection is available for developing three prediction models;

(b) Based on the monitoring data and the AASHTO Specifications (2002), FRM is developed (see Figure 5-2);

(c) Fatigue crack growth curves are generated by simulation. An appropriate crack growth curve is selected based on both cracking information from NDE and the number of cycles (years) from monitoring;

(d) Final (critical) crack size, a_f, and target reliability index, β_{target}, are determined in the CGM and FRM, respectively;

(e) Fatigue reliability-based CGM is developed to provide detailed information regarding time-dependent fatigue reliabilities and crack growth. This model is used as a decision making tool for inspection and repair;

(f) PDM is developed by using general statistical models (i.e., hit & miss, signal response). Target PoD(a_i) levels are determined considering available repair options with respect to the allowable maximum flaw sizes (Fisher et al. 1998);

(g) In every inspection, target reliability index, β_{target}, is used as a threshold for a decision with respect to repair. If the predicted fatigue reliability level during the 75 years service life is lower than β_{target}, bridge is repaired. When repair is undertaken, fatigue reliability-based CGM is updated based on the improved fatigue resistance using AASHTO (Fisher et al. 1998 and Miki 2007); and

(h) All above steps are repeated in order to provide the anticipated service life of 75 years.

Schematic of the combined approach is presented in Figure 5-3. Expected general relationship among the three prediction models is presented in Figure 5-4, in

terms of fatigue reliability index, β, PoD and crack size, a. It is expected that as crack size increases, fatigue reliability index will decrease, whereas PoD will increase.

5.2.5   Application Example

As an illustration of the combined approach, the fatigue life of a cover plate welded detail is investigated in an existing highway bridge, the Yellow Mill Pond Bridge, which is located in Bridgeport, Connecticut (Fisher 1984). Based on the NDE and monitoring, all necessary information associated with fatigue cracks and loading (i.e., equivalent stress range and number of cycles) is collected and used for developing prediction models (Fisher et al. 1979 and 1981, and Fisher 1984). For welding defects at the toe of a cover plate, time-dependent performance assessment and management are performed by using the proposed approach.

5.2.5.1   Bridge Description and Cause of Fatigue Cracks

The Yellow Mill Pond Bridge opened in January 1958 carries Interstate I-95 over the Yellow Mill Channel in Connecticut. This structure consists of 14 consecutive simple span cover-plated steel and concrete composite beam bridges. Details of the plan and elevation can be found in Fisher (1984).

In many existing steel bridges, a cover plate beam, which may be commonly classified in the AASHTO categories *D*, *E*, *E'* or *F*, has been welded to the flange for enhancing the structural capacity. However, the increase of the moment capacity of the section can cause additional stress concentrations due to bending moment in a beam and at the ends of the cover plate weld (Ghorbanpoor et al. 2003). Between 1970

201

and 1981 the Yellow Mill Pond multi-beam structures have developed extensive numbers of fatigue cracks at the end of cover plates. According to Fisher (1984), the cracking was the result of the unexpected large volume of truck traffic and the anticipated low fatigue resistance of the large-sized cover-plated beam members. The non-destructive inspections for the fatigue cracks were conducted from 1970 by magnetic particle, dye-penetrant, and ultrasonic techniques (Fisher et al. 1979 and 1981, and Fisher 1984). In span ten of the bridge, the deepest crack depth indications of 13 mm (0.5 in.) were found in beams 3 and 7, and measured by the ultrasonic inspection in June 1976 (Fisher et al. 1979 and 1981). It is noted that cracks smaller than 2.5 mm (0.1 in.) deep could not be detected reliably by the ultrasonic probe. Most of the cracks were developed at the toe of the transverse fillet weld connecting the cover plate to the tension flange of the beam (Fisher 1984).

5.2.5.2   Fatigue Reliability Evaluation

Fatigue reliability evaluation of the Yellow Mill Pond Bridge in Connecticut is carried out by using the monitoring data and the AASHTO specifications (2002) with reliability software RELSYS (Estes & Frangopol 1998). All necessary data for estimating fatigue reliability are presented in Table 5-2. As indicated, all random variables are assumed lognormal. Based on the strain history of traffics (Fisher et al. 1981), $ADTT$ of 4430 cycles per day and annual traffic increase rate $\alpha = 2\%$ are estimated (see Figure 5-5(a)). This agrees well with the record of around 35 millions cycles accumulated from 1958 to 1976 reported by Fisher (1984). Total cumulative

number of cycles of 279 millions is predicted in 2033 at the end of the service life (i.e., 75 years, see Figure 5-5).

The cover plate in beam 7 of the span ten can be classified by AASHTO as Category E' under consideration of the worst case. The equivalent stress range, S_{re}, and fatigue detail coefficient, A, are treated as random with lognormal probability density functions (PDFs). Based on the estimated number of cycles, fatigue reliability evaluation is performed (see Figure 5-5(b)). Fatigue reliability index of 2.77 is reached in 1976, and it drops significantly to 0.52 at the end of the life of 75 years. Therefore, relevant repair interventions for preventing fatigue failure in the detail should be applied. When a repair action is taken, it is important that the FRM is updated by means of the improvement of fatigue strength (Fisher et al. 1998). Updating of the FRM associated with repair methods is described in the application using the combined approach. Before and after repair, the FRM is useful for estimating quantitatively time-dependent structural performance as well as envisioning possible repair scenarios.

5.2.5.3 Fatigue Reliability-Based CGM

As noted previously, fatigue cracks in the Yellow Mill Pond Bridge were caused by bending stresses concentrated at the large-sized cover-plated beam members. The non-dimensional function $G(a)$ (see Eq. 5-5) considering four geometry factors is (Fisher 1984):

$$G(a) = F_e(a) \cdot F_s(a) \cdot F_w(a) \cdot F_g(a) \tag{5-12}$$

where $F_e(a)$ = crack shape factor = 0.952; $F_s(a)$ = free surface effect factor =

$1.211 - 0.186 \cdot \sqrt{a/c}$ for $c = 5.462 \cdot a^{1.133}$; $F_w(a)$ = finite width factor = 1.0; and

$F_g(a)$ = non-uniform stresses factor = $K_{tm} \cdot [1 + 6.7889 \cdot (a/t_f)^{0.4348}]^{-1}$ where K_{tm} =

stress concentration factor = $-3.539 \cdot \ln(Z/t_f) + 1.981 \cdot \ln(t_{cp}/t_f) + 5.798$; a = depth

crack size, c = width crack size, Z = weld size, t_f = flange thickness and t_{cp} = cover

plate thickness. The deterministic parameters and random variables included in CGM

are presented in Table 5-3. Initial crack depth, a_i, and fatigue coefficient, C, are

treated as lognormal PDFs with COV of 0.4 and 0.51, respectively (Righiniotis &

Chryssanthopoulos 2003 and Moan et al. 1993).

By using Eqs. 5-6, 5-11 and 5-12, fatigue crack growth curves are generated by

simulation using 500 samples. This relative small number of samples is enough to

identify an appropriate crack growth curve based on field monitoring and NDE. As

shown in Figure 5-6(a), a crack growth curve is selected based on the monitoring and

NDE undertaken in 1976. The crack growth curve is used to determine target

reliability level in the FRM (see Figure 5-6(b)). The target reliability index, β_{target}, is

2.16 which corresponds to the final (critical) crack depth of 25.4 mm (1.0 in.). For a

service life of 75 years, the crack propagation approaches final crack depth after

almost 30 years, meaning that the cover-plated region has to be repaired in order to

extend its service life up to the anticipated target time (i.e., 75 years) before reaching

the critical reliability level. When a repair strategy is undertaken to improve fatigue

resistance, the selected target reliability index is used to identify a new crack growth

curve. Thus, updating of the CGM can be conducted based on the FRM.

Consequently, fatigue reliability-based CGM provides efficient information for making bridge repair decisions with well-quantified performance levels in the FRM and crack growth rate in the CGM.

5.2.5.4   PDM for Fatigue

The log-logistic PoD function of Eq. 5-7 is used to develop inspection PDM. As an illustration of the combined approach, the parameters γ and δ are assumed as 1.895 and 0.897, respectively (Chung et al. 2006 and Berens & Hovey 1981). As shown in Figure 5-7(a), the PDM in Eq. 5-7 shows the various depth crack sizes (i.e., a_{50}, a_{60}, a_{70}, or a_{80}) according to the predefined PoD levels. The notation, PoD(a_p) (p = 50, 60, 70 and 80), indicates predictable PoD of p % and its corresponding crack depth, a_p. During the entire service life, the predefined PoD levels are used for planning bridge inspection times to detect the identified fatigue cracks. As noted previously, the inspection PoD levels have to be determined considering maximum allowable depth crack sizes for application of repair methods (e.g., peening, GTA remelting). For instance, if a depth crack detected in an inspection PoD(a_p) exceeds 3 mm, peening repair is not a good strategy to cure effectively the defected detail (Fisher et al. 1998).

Based on the developed fatigue reliability-based CGM, the relationship between fatigue reliability and crack depth is plotted in Figure 5-7(b). By incorporating the PDM, fatigue reliabilities corresponding to the identified depth crack sizes (i.e., a_p) are estimated in the fatigue reliability-based CGM. This information can be used in the decision making process for bridge inspection as well as repair.

Consequently, relevant repair options to remove fatigue cracks propagated in the detail can be determined based on the target inspection PoD levels.

5.2.5.5   Bridge Fatigue Assessment and Management Using Combined Approach

The proposed combined approach is used for bridge fatigue reliability assessment and management. As an initial step, bridge performance assessment was performed using FRM and crack propagation was investigated using CGM. All necessary information collected from records of the inspection NDE and monitoring (field survey) in 1976 was used (Fisher 1984). As shown in Figure 5-6(a) and (b), it is predicted that the detail would be driven into finite fatigue life after almost 30 years without repair actions. For this reason, bridge inspection and repair strategies by using the combined approach should be planned and employed in certain time in order to extend service life. Clearly, the combined approach for bridge management will assist scheduling inspection time and finding proper repair methods associated with propagated cracks.

Based on the predefined PoD levels (see Figure 5-7(a)), inspection and repair strategies are first scheduled. Then, analyses using the combined approach for bridge lifetime management are conducted to find applicable inspection/repair solutions satisfying β_{target} = 2.16 during the entire service life of 75 years. As illustrations, several single or multiple repair methods are considered, and the associated inspection/repair solutions are provided.

The first inspection from PoD level of 50% (i.e., p = 50) is assumed to be

scheduled and applicable inspection/repair strategies are determined by two possible outcomes (i.e., whether fatigue crack is detected or not). When fatigue crack is detected, a proper repair action is taken and the developed fatigue reliability-based CGM is updated. If the predicted reliability level during 75 years of service time is larger than β_{target} = 2.16, a bridge management scenario is completed without any additional repair actions. Based on the scheduled target repair methods, bridge inspection and repair are carried out and fatigue reliability is updated whenever repair actions are applied.

As indicated previously, four repair methods of the cover plate beam are herein employed (Fisher et al. 1998 and Miki 2007): (a) Peening; (b) Gas Tungsten Arc Remelting; (c) Rewelding; and (d) Bolted Splices. For welding defects at the toe of a cover plate, these repair options are used to update the FRM and the CGM for a given inspection PoD(a_p).

Peening repair is a very efficient repair method to eliminate shallow surface cracks and increases fatigue resistance by one AASHTO Category (Fisher et al. 1998). Typically, peening can be effectively employed when crack size is less than 3.0 mm (0.12 in.) deep. Therefore, this repair option can be used in all inspection PoD(a_{50}) levels to improve fatigue performance. As shown in Figure 5-8(a) and (b), fatigue reliability-based CGM considering peening repair only is developed. When the number of inspections, k, and the number of repairs, n, are $k = n = 2$, it is observed that bridge reliabilities after peening do not drop below the predefined target reliability index, β_{target} = 2.16 during the entire lifetime. Associated inspection and repair times are also presented in Figure 5-8(a) and (b), respectively.

Gas Tungsten Arc (GTA) remelting repair can be employed in the predefined target crack depth, a_{60}, of 5.0 mm (0.20 in.). After this repair, the updating of the fatigue reliability-based CGM is performed resulting in all improved fatigue resistance by one AASHTO Category, as shown in Figure 5-9(a) and (b). GTA remelting repair was completed after four inspections and two repairs, since fatigue reliability was higher than the target reliability index. During the second and fourth inspections, fatigue cracks were detected.

Rewelding repair is assumed to be conducted when the detected crack depth exceeds 5.0 mm (0.20 in.) with the inspection PoD (a_{70}), as shown in Figure 5-10 (Miki 2007). In updating of fatigue reliability-based CGM, the accumulated fatigue damage before repair is considered to be completely recovered since fatigue life by rewelding can be completely restored (Fisher et al. 1998). As a result, several rewelding repairs were undertaken (see Figure 5-10). The number of inspections and repairs were 9 and 3, respectively, during the service life of 75 years.

For the large crack of 14.5 mm deep corresponding to the inspection PoD (a_{80}), Bolted Splices repair option can be employed. Typically, this repair is always better than welded repair since it improves significantly fatigue resistance up to AASHTO Category of *B* (Fisher et al. 1998). For this reason, it is recommended as a permanent repair method of damaged structural members. However, it is important to keep in mind that extensive construction time for the bolt splicing can be required due to fastening high tension bolts (Miki 2007). Up to 75 years of service life, bridge fatigue life can be preserved safely with only one time Bolted Splices repair action.

As presented in Figure 5-8 to Figure 5-10, bridge lifetime management was

208

successfully performed by the application of single repair method only. However, multiple repair strategies may provide better solutions in order to extend bridge fatigue life. For this reason, several multiple repair methods are considered as follows: (i) peening and GTA remelting; (ii) GTA remelting and rewelding; and (iii) peening, GTA remelting and rewelding. For case (i), it is assumed that two different repair methods are employed when improving bridge performance level. To extend bridge service life, these repairs were effectively applied with $k = 3$ and $n = 2$ at the first and third inspection times scheduled (see Figure 5-11). When considered GTA remelting and rewelding repairs (see Figure 5-12), seven inspections were conducted resulting in cracking detection of three times (i.e., $n = 3$). The associated fatigue reliability-based CGM is shown in Figure 5-12(a) and (b) for inspections and repairs, respectively. Three different repair methods are considered in case (iii). When cracks are detected, repair actions are taken. As shown in Figure 5-13(a) and (b), the performed number of inspections and repairs were six and three, respectively. Consequently, various solutions for bridge performance assessment and lifetime management can be obtained according to the imposed inspection and repair strategies. Details regarding possible inspection time as well as repair are presented in Table 5-4. All inspection/repair solutions satisfy the minimum target reliability level (i.e., $\beta_{target} = 2.16$) during the entire service life of 75 years.

5.2.6 Conclusions

This study presented a novel approach to perform bridge fatigue assessment and management by integrating three prediction models: FRM, CGM, and PDM. The

FRM was used to quantify bridge performance levels during the entire service life, while the CGM and the PDM were used to predict crack growth rate and to schedule inspection time associated with probability of cracking detection, respectively. The application of the combined approach was illustrated on an existing highway bridge, the Yellow Mill Pond Bridge in Connecticut.

The following conclusions are drawn:

1. For bridge fatigue assessment and maintenance, the PDM representing NDE capabilities can be combined with CGM and FRM in order to schedule inspection interventions according to the probability of detection with respect to the propagated flaw sizes.

2. For the welding defects of steel bridges, the combined approach offers the possibility for establishing reliability-based inspection and repair scenarios.

3. All necessary information including cracking data from NDE and S_{re} from field monitoring can be used to develop the FRM, CGM, and PDM.

4. Based on the AASHTO S-N approach, the FRM can provide lifetime fatigue performance in terms of reliability and number of cycles.

5. Fatigue life evaluation associated with crack propagation can be evaluated by the CGM. This prediction model is useful for estimating the remaining fatigue life.

6. As a further study, life-cycle cost analysis can be performed in order to formulate an optimal cost-based bridge maintenance management strategy under uncertainty. The proposed combined method can be used as a novel approach to schedule inspection, repair, and maintenance for keeping bridge

fatigue reliability above the target level during the anticipated service life.

5.3   BRIDGE RETROFIT DESIGN OPTIMIZATION

By formulating either single- and bi-objective optimization problems (Kwon & Frangopol 2010b and Liu et al. 2010b), optimized retrofit design for preventing distortion-induced fatigue cracking of steel bridges is addressed in this section.

5.3.1   Introduction

In the United States, many existing steel bridges were built from the late 1950s through the 1970s. Due to the lack of in-depth research on the fatigue performance of connection details (Roddis & Zhao 2001), a considerable number of these bridges have developed fatigue cracks caused by out-of-plane distortion. Thus, the connection details of steel bridges subjected to out-of-plane distortions are recognized as the largest category of fatigue cracking nationwide (Fisher 1984, Fisher et al. 1989 and 1990). Even if the magnitude of out-of-plane distortions is only 0.5 mm (0.02 in), it may induce high cyclic stress ranges up to 276 MPa (40 ksi) in small welded web gaps (Fisher et al. 1990). Due to tensile stress concentrations, the fatigue cracking initiated in the small web gaps propagates parallel to the flange along the flange-web connection of the floor-beam (Demers and Fisher 1989).

The typical retrofit methods include (a) drilling a crack arrest hole at the crack tip to stop the crack propagation, (b) providing a positive attachment between the tie-girder and the top flange of the floor-beam to eliminate the relative movements, (c) stiffening the entire bridge to prevent the large deformations of the bridge, and (d)

softening the connection by cutting off portions of its upper end to allow the relative movements to effectively occur over a longer length of the web without the restraint of the top flange and the connection plate or angles (Connor et al. 2004; see also Figure 5-14). Drilling a crack arrest hole is the most economical retrofit method, but only provides a temporary solution because re-initiation of the distortion-induced fatigue cracks often occurs around the drilled hole. Rigidly connecting the top flange of the floor-beam to the tie girder is expensive, and may shift the cracking locations to the floor-beam web near the stringer-to-floor-beam connections (Roeder et al. 2000). Obviously, stiffening the entire bridge is a costly retrofit option, and constructability on existing steel bridges presents a great challenge for this retrofit method (Kulicki et al. 1989). On the other hand, softening the connection is a cost-efficient and effective alternative among all potential retrofit methods. This softening connection retrofit has been used in existing steel bridges such as the Des Moines Bridge (Fisher 1984), the Midland County Bridge (Keating et al. 1996), and the Birmingham Bridge (Connor and Fisher 2002). It is the shape and size of the cut-off portion that hold the key for a successful retrofit operation, under consideration of anticipated fatigue life. However, it is not simple to design relevant retrofit shape and size since fatigue cracks may move into other regions due to the retrofits. For this reason, optimization problems regarding shape and/or size can be formulated to provide optimal solutions associated with the softening retrofit strategies.

Shape optimization may be used to find the optimal shape of the cut-off in terms of the required stress field after retrofit, while cut-off size (area) optimization may be used to find the optimal size of the retrofit considering remaining service life.

In this study, the cut-off size optimization for a rectangular shape used in an existing bridge, the Birmingham Bridge (see Figure 5-15), is considered in order to (a) determine optimal sizes according to anticipated service life of the bridge after retrofit, (b) use the monitoring data collected from the rectangular cut-off retrofit for fatigue reliability evaluation, and (c) compare the optimized areas with the actual cut-off area. The rectangular shape, obtained by using a plasma or saw for cutting, is recommended as the most common and economic for the efficient dispersion of stresses locally concentrated in potential critical locations of the specified retrofit detail (Connor & Fisher 2002). The rectangular cut-off region is usually smoothed in the corners to increase fatigue strength by providing a smooth transition with grinding hole edges. The transition radius associated with fatigue details can be determined based on the American Association of State Highway and Transportation Officials (AASHTO) Specifications (1996).

This study focuses on the size optimization of the cut-off area of the softening connection retrofit by formulating (a) single-objective optimization problem and (b) bi-objective optimization problem with the design variables (height and length) of the retrofit cut-off size.

For the single-objective optimization, the objective is the minimization of the cut-off area (Kwon & Frangopol 2010b). The constant amplitude fatigue threshold (CAFT) associated with the S-N category is imposed as the stress constraints. The optimal solutions are computed by linking the finite element (FE) analysis software ABAQUS (version 6.7.1, 2007) with the optimization software VisualDOC (2006). Fatigue reliability assessment of the optimal cut-off retrofit design is performed at

critical locations based on field monitoring data and FE analysis. The proposed approach in section 4.3.2 is illustrated on an existing bridge.

When considering the bi-objective optimization (Liu et al. 2010b), two competing objectives including (a) the maximization of the fatigue reliability of the connection details after retrofit and (b) the minimization of the cut-off area are established. Multiple constraints include geometrical restrictions, predefined maximum tensile stresses, and minimum remaining fatigue life of the connection details after retrofit. The retrofit cut-off size is determined based on FE analysis and the CAFT (Connor et al. 2004). The proposed bi-objective optimization problem is performed in Section 5.3.4.

To preserve bridge performance, the fatigue limit criterion (i.e., maximum stresses developed at potential critical locations after retrofit should not exceed the CAFT) has to be satisfied. However, under uncertainties, bridge remaining lifetime after retrofit can be overestimated or underestimated. The proposed optimization approaches (i.e., single- and bi-objective) taking into consideration uncertainties and the constraint related to the remaining fatigue life restriction provides a more realistic and cost-effective method for determining the retrofit cut-off size of steel bridges under distortion-induced cracking.

In this study, the fatigue reliability of the connection detail is evaluated, based on the field monitoring data and the approach used in the AASHTO Guide Specifications for Fatigue Evaluation of Existing Steel Bridges (AASHTO, 1990) and Standard Specifications for Highway Bridges (AASHTO, 2002). In the bi-objective optimization, the original monitoring data may be modified by using a cut-off size

adjustment factor (SAF) to represent the fatigue stress ranges at the identified critical locations after retrofit (Liu et al. 2010a and b). This is similar to the method of applying a scale factor to the stress ranges in order to produce a new stress-range bin histogram for finite fatigue life of a detail (Crudele & Yen 2006). The proposed approaches are illustrated on an existing steel tied-arch bridge monitoring in 2003 by the Advanced Technology for Large Structural Systems (ATLSS) Engineering Research Center at Lehigh University.

5.3.2   Bridge Description and Cause of Fatigue Cracks

The Birmingham Bridge is located in Pittsburgh, Pennsylvania. The main span of the structure is a 189.0 m (620 ft) tied arch designed in 1973 and built in 1976. Multi-girder approach spans flank each side of the tied arch. The floor-beams are spaced at 9.45 m (31 ft) and are 2.84 m (111 in) deep. The complete description of the bridge can be found in Connor & Fisher (2002).

In 2002 fatigue cracks have been found in nearly all of the transverse floor-beams at the connection to the tie girders. According to Connor & Fisher (2002), the cracking was the result of relative longitudinal displacement that occurred between the floor system and the tie girder, as shown in Figure 5-14 . The displacement produces out-of-plane movement within the web gap above the connection angles. This is because the flanges of the floor-beams are not directly connected to the tie girder. It was proposed to soften the connection by removing a portion of the floor-beam flange and web near the tie girder to prevent stresses within the web gap from concentrating (Connor & Fisher 2002). Softening the connection allows the displacement to

215

effectively occur over a longer length of the web without the restraint of the top flange or connection angles (Connor et al. 2004).

5.3.3   Single-Objective Optimization for Retrofit

The softening connection retrofit method is used to extend bridge service life by removing distortion-induced fatigue cracks. It is important to find the proper cut-off size for a successful retrofit. Too small cut-off size results in re-initiation of the fatigue cracks soon after retrofit, as evidenced on the Poplar Street Bridge in East St. Louis (Connor et al. 2004). On the other hand, it is expected that too large cut-off size may greatly reduce the shear capacity of the connection details. In addition, remaining service life of a bridge has to be considered in a cost-effective manner. An appropriate cut-off retrofit size can be determined by a single-objective optimization strategy considering remaining service life (Kwon & Frangopol 2010b).

5.3.3.1   Formulation of Single-Objective Optimization Problem

The design variables are cut-off height (h) and length (l), and the objective is to minimize the cut-off area $h \times l$. The *S-N* CAFTs for each category are employed as upper and lower stress constraints. Accordingly, the single-objective optimization problem for finding the optimal cut-off retrofit solution can be formulated as follows:

Find the design variables: h and l

Objective function: *minimize $h \times l$*   (5-13)

Subjected to inequality constraints:

$$-\text{CAFT} \leq \sigma_{yy,i} \leq \text{CAFT} \tag{5-14}$$

$$-\text{CAFT} \leq (\sigma_{yy,i}{}^2 + \sigma_{zz,i}{}^2)^{0.5} \leq \text{CAFT} \tag{5-15}$$

$$-\text{CAFT} \leq \sigma_{zz,i} \leq \text{CAFT} \tag{5-16}$$

Subjected to equality constraints:

$$\sigma_{yy,i} = (1 - \alpha_{target}) \cdot \text{CAFT} \tag{5-17}$$

$$(\sigma_{yy,i}{}^2 + \sigma_{zz,i}{}^2)^{0.5} = (1 - \alpha_{target}) \cdot \text{CAFT} \tag{5-18}$$

$$\sigma_{zz,i} = (1 - \alpha_{target}) \cdot \text{CAFT} \tag{5-19}$$

where α_{target} = target stress parameter considering remaining fatigue life of a bridge, and $\sigma_{yy,i}$, $\sigma_{zz,i}$ = maximum vertical stress and maximum longitudinal stress in the cut-off region of the floor-beam, respectively, for $i = 1, 2, 3 \ldots. k$ (identified critical locations within cut-off region). The values of the design variables h and l can be restricted considering geometrical conditions of a bridge. Two software programs (ABAQUS 2007 and VisualDOC 2006) are used to conduct the cut-off retrofit design optimization based on Eqs. 5-13 to 5-19.

The procedure for finding the optimal solution is summarized as follows:

Step 1: *Identifying the critical locations after retrofit*

Critical locations, where potential re-initiation of fatigue cracking after retrofit can occur, are identified based on FE models calibrated using field monitoring data.

Step 2: *Defining the design variables*

The cut-off sizes h and l are defined as design variables, and their product is the objective to be minimized.

Step 3: *Establishing the stress constraints*

Based on the AASHTO Specifications (2002), the CAFTs associated with the classified fatigue categories are determined and used in order to impose inequality stress constraints (Eqs. 5-14 to 5-16). Equality stress constraints (Eqs. 5-17 to 5-19) are established to find the optimal solution taking into account remaining fatigue life after retrofit.

Step 4: *Solving the optimization problem*

The two software programs (ABAQUS 2007, VisualDOC 2006) are linked. For given conditions, design iterations are performed for finding the optimal cut-off retrofit area.

5.3.3.2 Fatigue Reliability Assessment

The fatigue reliability assessment at critical locations is performed to estimate remaining fatigue life associated with the optimal solutions for retrofit design. According to Kwon & Frangopol (2008 and 2010a), lognormal PDFs of both resistance, *R*, and loading, *S*, are assumed. The AASHTO approach to fatigue reliability assessment is based on the *S-N* curves (AASHTO 2002) and the Miner's rule (Miner 1945). As shown in Table 5-5, fatigue detail coefficient, *A*, for each category and material constant, *m*, which is assumed 3.0 for all categories, are provided in AASHTO Specifications (2002). Based on the assumed distributions for resistance and the stress range, the performance function defined in Eq. 5-1 is used for the fatigue reliability assessment. S_{re} at each critical location is computed by using Eq. 5-2. For a given service year, fatigue reliability index, *β*, is evaluated by using the

reliability software RELSYS (Frangopol & Estes 1998; see also Eq. 5-3) for the assumed distribution types. The procedure for fatigue reliability evaluation is also presented in the flowchart of Figure 5-2.

In this study, fatigue reliability analysis is performed to estimate remaining fatigue life associated with the optimal cut-off solutions obtained from the bridge retrofit design optimization. The complete procedure including the single-objective optimization is presented in the flowchart of Figure 5-15.

5.3.3.3 FE Modeling Verification

Fatigue performance assessment for the actual retrofit cut-off size was performed by the ATLSS Engineering Research Center at Lehigh University (Connor & Fisher 2002, Connor et al. 2004). The actual (trial) cut-off size was h_0 = 29.8 cm (11.75 in) in height and l_0 = 52.1 cm (20.5 in) in length. A total of 32 uniaxial strain gages were installed symmetrically on retrofit cutout regions both upstream and downstream of the bridge. The triggered time history data and stress-range bin histograms were collected for a total of 39.95 days. All details are provided in Connor & Fisher (2002) and Connor et al. (2004).

The critical locations CL-I (CH-2), CL-II (CH-7), and CL-III (CH-11) among the measured locations are selected from FE modeling stress results, as shown in Figure 5-16 and Figure 5-17. Linear-elastic 3-D FE modeling was developed for the connection details with the software ABAQUS (version 6.7.1, 2007). The largest peak longitudinal relative displacement recorded in field was about 2.54 mm (0.1 in), and the corresponding stress ranges were 44.8 MPa (6.5 ksi), 37.2 MPa (5.4 ksi) and 48.3

MPa (7.0 ksi) at sensor locations CH-2, CH-7, and CH-11, respectively. The stresses represented at CH-2, CH-7, and CH-11 are the vertical stress $\sigma_1 = \sigma_{yy,1}$ at the intersection of the top flange and web of the floor-beam (i.e., CL-I), the resultant stress $\sigma_2 = \sqrt{\sigma_{yy,2}^2 + \sigma_{zz,2}^2}$ near the bottom of the cut-off (i.e., CL-II), and the longitudinal stress $\sigma_3 = \sigma_{zz,3}$ at web near the connection angles (i.e., CL-III), respectively. These measurements are used to validate the stresses obtained from FE analysis subjected to same relative displacement (i.e., 2.54 mm) and the corresponding horizontal forces of 0.98 kN (0.22 kips). As shown in Figure 5-17(b), the stress results agree well. For the retrofit design optimization, FE models can be effectively used to investigate stress distributions at the three critical locations CL-I, CL-II, and CL-III.

5.3.3.4   Retrofit Design Optimization

For different cut-off areas A_1, A_2, A_3, and A_4 (see Figure 5-18(a)), sensitivity to the maximum stress distributions is first investigated by using FE analysis at the identified critical locations CL-I, CL-II, and CL-III classified as the AASHTO categories of C, A, and B, respectively. Stress results associated with the cut-off areas A_1, A_2, A_3, and A_4 are shown in Figure 5-18(b). It is observed that increase in the cut-off area decreases the maximum stress at a same location.

Bridge retrofit design optimization considering the single-objective is performed to find the optimal cut-off size according to the anticipated remaining fatigue life. Applicable ranges of the design variables h and l are imposed considering geometrical restrictions of the floor-beam connection detail as follows: 10.2 cm $\leq h \leq$ 82.2 cm and 26.8 cm $\leq l \leq$ 69.8 cm. When the inequality stress constraints are

considered only (see Eqs. 5-14 to 5-16), the relationship between design iterations and maximum stresses is obtained by linking ABAQUS (version 6.7.1, 2007) with VisualDOC (2006). The result is shown in Figure 5-19. There exist two active stress constraints by $\sigma_{yy,1}$ at CL-I and $\sigma_{zz,3}$ at CL-III. For given target stress parameters (i.e., α_{target} = 0, 25%, and 50%), retrofit design optimization is performed. It is noted that the imposed target stress constraints at the three critical locations CL-I, CL-II, and CL-III represent σ_{yy}, $(\sigma_{yy}^2 + \sigma_{zz}^2)^{0.5}$, and σ_{zz}, respectively. The minimized cut-off retrofit areas by using the target equality constraints are presented in Figure 5-20(a). The corresponding design space is shown in Figure 5-20(b). It is observed that the actual retrofit was designed for a safety level corresponding to the AASHTO CAFT of 46%.

5.3.3.5 Reliability-Based Remaining Fatigue Life

Fatigue reliability evaluation is performed to estimate remaining fatigue life associated with the optimized retrofit solutions (i.e., cut-off areas) with all necessary information (see Table 5-5 and Table 5-6). Original monitoring data obtained from the actual retrofit size (h = 29.8 cm and l = 52.1 cm) are used to estimate equivalent stress range, S_{re}, and average daily number of cycles, N_{avg}, corresponding to the optimal cut-off areas, by using FE analysis and random number generation technique (Liu et al. 2010a).

FE analysis is used to investigate stress distributions at critical locations due to the applied horizontal displacements. The stress distributions are proportional to the magnitude of imposed horizontal displacements. Based on the linear stress relationship established from FE modeling, new stress-range bin histograms associated with the

optimal cut-off sizes are established. Since the typical stress-range bin in the rain-flow cycle counting method is rather narrow (i.e. 3.45 MPa (0.5 ksi) in this example), the newly produced stress ranges are generated by using random number generation assuming uniform distribution of the individual stress ranges. As a result, S_{re} and N_{avg} associated with the optimal solutions are calculated based on the new stress-range bin histograms. Table 5-6 shows the computed mean value and standard deviation of S_{re}, and N_{avg} at the critical locations. Based on N_{avg} and annual traffic increase rate, the cumulated number of stress cycles, $N(y)$, for increased years is estimated by using Eq. 5-10. It is noted that when considering single stress cycle per truck passage (cycles per day), $ADTT$ is equivalent to N_{avg}. In this study, the annual traffic increase rate is considered to be 3%. The relationship between S_{re} and N_{total} at the identified critical locations CL-I, CL-II, and CL-III is presented in Figure 5-21(a), Figure 5-22(a), and Figure 5-23(a), respectively. It is observed that the increases in the optimal cut-off sizes lead to decreases in S_{re}.

The fatigue reliability profiles for the optimized retrofit solutions is computed by using the reliability software RELSYS (Frangopol & Estes 1998). For the optimal sizes 1, 2, and 3 as well as the actual retrofit size, the computed fatigue reliabilities at CL-I, CL-II, and CL-III are plotted in Figure 5-21(b), Figure 5-22(b), and Figure 5-23(b), respectively, with the target reliability index β_{target} = 3.72. The reliability indices associated with the optimal cut-off sizes 1 and 3 represent lower and upper bound, respectively, while the fatigue reliabilities associated with the actual retrofit design are near the upper bound.

Based on the reliability profiles, remaining fatigue life associated with the

222

optimal cut-off sizes is estimated. As presented in Table 5-7, remaining lifetime varies in the optimized retrofit sizes. Remaining lifetime corresponding to the optimal size 1 of CL-III is 51 years, while that at CL-I and CL-II is 54 years and 89 years, respectively. Consequently, the most critical location in the floor-beam connection detail after retrofit will be CL-III when applying the optimal size 1 obtained from the single-objective optimization strategy.

5.3.3.6   Conclusions

The following conclusions are drawn from this study:

1. An optimization for retrofit design can be formulated and solved to find the optimal cut-off size of connection details for retrofitting distortion-induced fatigue cracking of steel bridges under uncertainty.

2. SHM data and FE stress outputs can be used to perform the single-objective optimization as well as fatigue reliability assessment.

3. Based on the predefined stress constraints associated with the *S-N* CAFT of each category, various optimal cut-off retrofit solutions can be obtained from the single-objective optimization.

4. Remaining fatigue lifetime of candidate optimal retrofit solutions can be possibly predicted by incorporating fatigue reliability evaluation.

5.3.4   Bi-Objective Optimization for Retrofit

In this section, bi-objective optimization of retrofitting distortion-induced fatigue cracking using monitoring data under uncertainty (Liu et al. 2010b) is

223

presented. The optimization problem has two competing objectives: (i) maximization of the fatigue reliability of the connection details after retrofit and (ii) minimization of the cut-off area. The geometrical restrictions and predefined maximum tensile stresses (as the single-objective optimization problem imposed in previous section) as well as minimum remaining fatigue life of the connection details after retrofit are all taken into account as constraints. The fatigue reliability assessment with monitoring data is based on the formulation used in the AASHTO Specifications (2002). The original monitoring data may be modified by using a proposed cut-off size adjustment factor (SAF) to represent the fatigue stress ranges at the identified critical locations after retrofit. The nonlinear relationships between the cut-off size and SAF are established.

5.3.4.1   Fatigue Reliability Assessment with SHM

The AASHTO approach to fatigue reliability assessment is based on the *S-N* curves in the AASHTO Specifications (AASHTO, 2002) and the Miner's rule (Miner, 1945). When integrated the field monitoring data, the limit-state equation, $g(X) = 0$, where X is a vector of random variables, can be expressed for fatigue reliability analysis of the connection details as (Liu et al. 2010a and Kwon & Frangopol 2010a)

$$g(X) = \Delta - e \times D = 0 \tag{5-20a}$$

where $D = [N(t) \times (S_{re})^{m}] / A = N_s(t) / A$ (5-20b)

In Eq. 5-20(a), Δ = Miner's critical damage accumulation index which is assumed as a lognormal distributed random variable with parameters $\lambda_{\Delta} = \overline{\ln \Delta}$ and ζ_{Δ} = COV($\ln \Delta$) × $\overline{\ln \Delta}$ representing the mean value and standard deviation of $\ln \Delta$,

respectively (Wirsching 1984; see also Table 5-8); e = measurement error factor in structural health monitoring (SHM) which may be considered as lognormal (Frangopol et al. 2008); and D = Miner's damage accumulation index in terms of loading. In Eq. 5-20(b), A = fatigue detail coefficient, a lognormal distributed random variable with the mean value, $\overline{A}$, that is based on the category of the connection details under consideration, and the standard deviation of ln A, $\sigma(\ln A) = 0.429$ (Wirsching et al. 1987); and $N_S(t) = N(t) \times S_{re}^m$ where $N(t)$ is the total number of stress cycles within a period of time T under consideration, S_{re} is the equivalent stress range during T which can be estimated from field monitoring data, and $m = 3.0$ is a material constant representing the slope of the S-N curve (AASHTO 2002). Thus, $N_S(t)$ is a stochastic process. According to previous studies based on field monitoring data (Liu et al. 2010a), $N_S(t)$ can be treated, in a simplified way, as a lognormal random variable with a coefficient of variation (COV) usually less than 0.30. The random variables for fatigue reliability analysis are presented in Table 5-8.

The time-dependent reliability index $\beta(t)$ associated with Eq. 5-20(a) is used to estimate fatigue life. The random variables, Δ, A, e, and $N_s(t)$, are assumed to be statistically independent. Correlations can, of course, be taken into account if data are available. Unfortunately, this is not the case. Reliability of a structural component or system is defined as the probability of safe performance, $P(g(X) > 0)$. Based on the performance function, $g(X) = R - S$, including resistance, R, and load effect, S, the limit-state formulation (see Eqs. 5-20(a) and (b)), will have $R = \Delta \times A$ and $S = e \times N_s(t)$. Since Δ, A, e, and $N_s(t)$ are considered to be lognormal random variables, the equivalent performance function adopted is expressed as

$$g(X) = \ln (R / S) = \ln R - \ln S = \ln (\Delta \times A) - \ln [e \times N_s(t)]$$

$$= \ln \Delta + \ln A - \ln e - \ln N_S(t) \tag{5-21}$$

Therefore, the time-dependent reliability index $\beta(t)$, defined as the mean value of $g(X)$ divided by the standard deviation of $g(X)$, is

$$\beta(t) = \frac{\left(\lambda_\Delta + \lambda_A\right) - \left(\lambda_e + \lambda_{N_S(t)}\right)}{\sqrt{\varsigma_\Delta^2 + \varsigma_A^2 + \varsigma_e^2 + \varsigma_{N_S(t)}^2}} = 1.67 \ln\left[\frac{\overline{A}}{1.10 \overline{N}_s(t)}\right] \tag{5-22}$$

where λ and ζ denote the mean value and standard deviation of each random variable, and $\overline{N}_S(t)$ denotes the mean value of $N_S(t)$. This value may be obtained from the original monitoring data which may be modified by using a SAF. This factor represents the fatigue stress ranges and corresponding number of stress cycles at the identified critical locations after retrofit. To identify critical locations in the retrofit detail (i.e., a cut-off region of rectangular shape), the AASHTO category corresponding to each location along the edges is first defined and classified. Then, the most critical location within the same category is identified by using FE modeling.

5.3.4.2   Formulation of Optimization Problem

In many practical optimization applications, two or more objective functions can be optimized at the same time. These are referred to, respectively, as bi-objective or multi-objective optimization problems (Arora, 2004). In this study, a bi-objective optimization approach is proposed for retrofitting distortion-induced fatigue cracks in steel bridges in order to obtain the optimal retrofit solutions associated with the softening connection detail which is cost-efficient and technical effective. The design

variables considered are the cut-off height (h) and length (l), where the objective functions are (a) the maximization of the computed fatigue reliability of the connection details after retrofit and (b) the minimization of the cut-off area. Accordingly, the proposed approach is a bi-objective optimization since both objectives have to be achieved simultaneously under predefined constraints.

Typically, this approach is different from the classical optimization under uncertainty in that a single-objective (e.g., usually the expected total cost) is considered and the decision maker has a single choice to implement the optimum solution. If the cost associated with the optimum solution is not affordable, the decision maker has to choose another non-optimal solution. However, if a bi-objective optimization approach is alternatively used, multiple optimal solutions will be provided for decision makers. Therefore, the two objective functions are herein considered to provide multiple optimal cut-off sizes for retrofit of the bridge connection details while satisfying all pre-imposed constraints.

Failure modes at the critical locations are considered to be perfectly correlated. This is because the structural responses at the softening connection details are fully dependent when a relative horizontal displacement is applied to the floor-beam system. Accordingly, this assumption supports that the fatigue reliability computed in the connection details after retrofit can be defined as the minimum of the fatigue reliabilities of the identified critical locations. The constraints associated with the bi-objective optimization problem can be imposed considering the geometrical restraints, predefined maximum tensile stresses at each of the identified critical locations, and

minimum remaining fatigue life of the connection details after retrofit. As a result, the bi-objective optimization problem can be formulated as follows:

Find the design variables: h and l

Objective functions: (i) maximize $\{$minimum $(\beta_1, \beta_2 \ldots \beta_p)\}$ $\qquad$ (5-23)

(ii) minimize $h \times l$ $\qquad$ (5-24)

Subjected to: $h_{min} \leq h \leq h_{max}$ $\qquad$ (5-25a)

$l_{min} \leq l \leq l_{max}$ $\qquad$ (5-25b)

$\sigma_i \leq \sigma_{max,i}$ $\quad$ ($i = 1, 2, \ldots\ldots, p$) $\qquad$ (5-26)

$T_i \geq T_{min}$ $\quad$ ($i = 1, 2, \ldots\ldots, p$) $\qquad$ (5-27)

where β_i = fatigue reliability index at the i-th identified critical location ($i = 1, 2, \ldots\ldots, p$); p = number of the identified critical locations after retrofit; h_{min} and h_{max} = minimum and maximum cut-off height due to the geometrical restrictions, respectively; l_{min} and l_{max} = minimum and maximum cut-off length associated with the geometrical restrictions, respectively; σ_i and T_i = tensile stress and remaining fatigue life at the i-th identified critical location, respectively; $\sigma_{max,i}$ = predefined maximum tensile stress at the i-th identified critical location, and T_{min} = predefined minimum remaining fatigue life of the connection details after retrofit. It is noted that $\sigma_{max, i}$ should be related to the fatigue category classified by the AASHTO Specifications (2002). Thus, $\sigma_{max, i}$ may vary at different critical locations.

The procedure for solving the optimization problem formulated by Eqs. 5-23 to 5-27 includes the following steps.

Step 1: *Identifying the critical locations after retrofit*

The critical locations for potential re-initiation of fatigue cracking after retrofit may be identified by developing the validated FE modeling and/or from field monitoring data.

Step 2: *Collecting the stress range histogram data at the identified critical locations*

Since the optimal cut-off size is not available at this step, the sensors for collecting fatigue stress ranges and number of stress cycles may be installed for a trial cut-off size only. However, the collected stress range data at these sensor locations may be modified by using the proposed SAF to estimate new stress range histogram data at the identified critical locations after optimal retrofit.

Step 3: *Establishing the relationship between SAF and $N_S(t)$ at the identified critical locations*

The proposed SAF_i at the i-th identified critical location is defined as the ratio of σ_i to the stress ranges collected at the corresponding sensor location. The mean values of $N_S(t)$ associated with different values of SAF_i may be obtained from the collected stress range histogram data (Liu et al. 2010a).

Step 4: *Developing the formulation to calculate σ_i based on design variables h and l*

The formulation to calculate σ_i based on the design variables h and l is developed at each of the identified critical locations (see Appendix B). These developed formulations are validated by comparing the computed results with those from the corresponding FE modeling (see Table 5-10).

Step 5: *Re-formulating the developed optimization problem in Eqs. 5-23 to 5-27*

Eqs. 5-23 to 5-27 can be re-formulated by using the results from Steps 1 to 4, where the design variables *h* and *l* are explicitly included in both objective functions and constraints.

Step 6: *Solving the optimization problem*

The design optimization software VisualDOC (2006) may be used to solve the re-formulated optimization problem.

To find multiple optimal cut-off retrofit solutions, the proposed approach is illustrated on the same bridge connection detail (see Figure 5-16) which was applied in the single-objective optimization (see Section 5.3.3), by following the steps described above.

Steps 1 and 2: As shown in Figure 5-16 and Figure 5-17(b), the potential fatigue cracking re-initiation after retrofit is identified at the three critical locations (i.e., CL-I, CL-II, and CL-III) based on the FE modeling stress results and the AASHTO *S-N* category. As described the previous section, the fatigue stress range data at the critical locations CL-I, CL-II, and CL-III are $\sigma_1 = \sigma_{yy,1}$, $\sigma_2 = \sqrt{\sigma_{yy,2}^2 + \sigma_{zz,2}^2}$, and $\sigma_3 = \sigma_{zz,3}$, respectively, while the *S-N* categories are classified as C, A, and B, respectively. Figure 5-24(a) through (c) present the original monitoring stress-range bin histograms at CL-I, CL-II, and CL-III, respectively (Connor et al., 2004). It is noted that these histogram data can be used to establish new stress-range bin histograms by using the proposed SAF.

Step 3: For given annual traffic increase rate (i.e, α = 0%, 2%, and 5%) and service life (i.e., t = 1 year, 5 years, and 10 years), the mean values of $N_S(t)$ associated with different values of SAF at CL-I, CL-II, and CL-III are estimated as shown in Figure 5-25(a) to (c), respectively. Because the original monitoring data only contain the stress-range bin histograms at sensor locations directly obtained by the rain-flow cycle counting method, but the SAF needs to be applied to individual stress ranges, the random number generator has to be adopted to reproduce the individual stress ranges in the modification procedures (Liu et al. 2010a). Since the typical stress range bin from the rain-flow cycle counting method is rather narrow (i.e., 3.45 MPa (0.5 ksi) in this study; Connor et al. 2004), the uniform distribution of the individual stress ranges can be assumed in the corresponding stress range bins. Only stress ranges greater than 3.45 MPa (0.5 ksi) in the original monitoring data are used because those less than 3.45 MPa (0.5 ksi) make no contributions to fatigue damages accumulated (Fisher 1977). The effect of the annual traffic increase rate, α, on the mean values of $N_S(t)$ is indicated well in Figure 5-25(a) through (c).

The newly generated stress-range bin histograms based on the randomly simulated individual stress ranges and SAFs are used to calculate the corresponding S_{re} with m = 3.0 (see Eq. 5-2). When the mean value of $N_S(t)$ with the SAF during the monitoring period, $\overline{N}_{shm}$, is considered, $\overline{N}_{shm}$ can be expressed as

$$\overline{N}_{shm} = N_{total} \times S_{re}^3 = \Sigma (n_j \times S_{rj}^3) \tag{5-28}$$

It is emphasized that the predefined stress range threshold must be established in the computation of $\overline{N}_{shm}$ by using Eq. 5-28. This is because the low magnitude stress

cycles make no contributions to fatigue damage, but, when included in Eq. 5-28, yield

larger values of $\overline{N}_{shm}$ which results in unnecessary conservative estimations of $\beta(t)$ by

using Eq. 5-22. This is in contrast to the estimation of the fatigue resistance of the

connection details field monitoring data where the higher predefined stress range

thresholds result in higher S_{re} and lower (conservative) fatigue resistance from the

corresponding AASHTO S-N curves (Zhou 2006 and Alampalli & Lund 2006).

From a large number of laboratory experiments under the constant amplitude

cyclic loading, the constant amplitude fatigue threshold (CAFT) is established for each

category as presented in Table 5-9, indicating that no fatigue cracks appear if the

applied stress cycles have the constant amplitude smaller than the corresponding

CAFT. For the variable-amplitude stress cycles, the predefined stress range thresholds

may be lowered to a quarter of the CAFT (Connor & Fisher 2006). In this study, 10%

of the corresponding CAFT is used as the predefined stress range threshold (see Table

5-9). This is because the curves representing the relationship between the computed S_{re}

and N_{total} become asymptotic to the applicable S-N curves after the predefined

threshold is set to be lower than 10% of the CAFT (Connor et al. 2004, Liu et al.

2010a, and Kwon & Frangopol 2010a). As a result, the relationship between SAF (i.e.,

S_1, S_2, …, and S_p) and $\overline{N}_{shm}$ can be established by using the regression models of the q-

order polynomial functions as

$$\overline{N}_{shm,i} = \sum_{j=0}^{q} a_{ij} \times S_i^j \qquad (i = 1, 2, \ldots, p) \qquad (5\text{-}29)$$

where a_{ij} = coefficients that can be obtained from monitoring. The quadratic polynomial functions (i.e., $q = 2$) are adopted in this study where the regression models of $\overline{N}_{shm}$ in MPa unit can be described as

$$\overline{N}_{shm,1} = (1.03S_1^2 - 1.21S_1 + 0.38) \times 10^8 \qquad (5\text{-}30a)$$

$$\overline{N}_{shm,2} = (7.87S_2^2 - 10.50S_2 + 3.66) \times 10^8 \qquad (5\text{-}30b)$$

$$\overline{N}_{shm,3} = (9.69S_3^2 - 12.80S_3 + 4.56) \times 10^8 \qquad (5\text{-}30c)$$

Furthermore, the regression models with the quadratic polynomial function for any targeted time period T_g in years, that is, $\overline{N}_{S_i}(T_g)\,(i = 1, 2, 3)$, can be expressed as

$$\overline{N}_{S_i}(T_g) = \frac{365}{T_{shm}} \times \overline{N}_{shm,i} \times \int_0^{Tg} (1+\alpha)^t \, dt \qquad (5\text{-}31)$$

where T_{shm} = monitoring period in days (i.e., T_{shm} = 40 days).

Step 4: After retrofit, the structural behavior of the floor-beam connection detail when subjected to the out-of-plane displacement loading is shown in Figure 5-26. It can be represented by the virtual beams where the vertical edge of the cut-off is restrained by the flange at the top and by portion of the web at the bottom, while the horizontal edge of the cut-off is restrained by the connection angles at one end and by portion of the web at the other end. Since the restraints provided by the portion of the web are relatively weak, the pinned end may be assigned at the bottom of the cut-off as shown in Figure 5-26 (Connor et al. 2004 and Liu et al. 2010a). Consequently, the analytical formulations to calculate σ_1, σ_2 and σ_3 can be expressed as

$$\sigma_1 = C_1 \frac{H^3 \times L_c^2 - (H + 2h) \times (H - h)^2 \times l^2}{H^3 \times L_c^2 \times h^2} \tag{5-32a}$$

$$\sigma_2 = \sqrt{(C_{21} \cdot \sigma_1)^2 + (C_{23} \cdot \sigma_3)^2} \tag{5-32b}$$

$$\sigma_3 = C_3 \frac{(H + 2h) \times (H - h)^2}{h \times l} \tag{5-32c}$$

where C_1, C_{21} and C_{23}, and C_3 = constants that are independent on h and l as listed in Table 5-9, H = height of the floor-beam that is $H = 2.85$ m (112.0 in), and L_c = length of the floor-beam affected by the end constraints under the out-of-plane loading condition which may be obtained from the FE modeling as $L_c = 0.64$ m (25.0 in).

Table 5-10 compares the computed stresses σ_1, σ_2, and σ_3 from Eq. 5-32 with those from the FE modeling (Liu et al. 2010a) where reasonable agreements can be observed for validating Eq. 5-32. Therefore, the nonlinear relationships between the SAF (i.e., S_1, S_2, and S_3) and the cut-off size (i.e, h and l) can be established as

$$S_1 = \frac{H^3 \times L_c^2 - (H + 2h) \times (H - h)^2 \times l^2}{H^3 \times L_c^2 - (H + 2h_0) \times (H - h_0)^2 \times l_0^2} \times \frac{h_0^2}{h^2} \tag{5-33a}$$

$$S_2 = \frac{h}{50.0} \times \sqrt{6.71\sigma_1^2 + 2.86\sigma_3^2} \tag{5-33b}$$

$$S_3 = \frac{(H + 2h) \times (H - h)^2}{(H + 2h_0) \times (H - h_0)^2} \times \frac{h_0 \times l_0}{h \times l} \tag{5-33c}$$

Step 5: Based on the analytical results from Steps 1 to 4 (see Table 5-9), the reliability indices $\beta_1(t)$, $\beta_2(t)$, and $\beta_3(t)$ at the critical locations CL-I (Category C), CL-

II (Category A), and CL-III (Category B), respectively, for any targeted time period T_g in years, can be expressed as

$$\beta_1(t) = 1.67\ln\left[\frac{1.44\times10^4}{1.03S_1^2 - 1.21S_1 + 0.38}\cdot\left(\int_0^{T_g}(1+\alpha)^t\,dt\right)^{-1}\right] \qquad (5\text{-}34a)$$

$$\beta_2(t) = 1.67\ln\left[\frac{8.20\times10^4}{7.87S_2^2 - 10.50S_2 + 3.66}\cdot\left(\int_0^{T_g}(1+\alpha)^t\,dt\right)^{-1}\right] \qquad (5\text{-}34b)$$

$$\beta_3(t) = 1.67\ln\left[\frac{3.93\times10^4}{9.69S_3^2 - 12.80S_3 + 4.56}\cdot\left(\int_0^{T_g}(1+\alpha)^t\,dt\right)^{-1}\right] \qquad (5\text{-}34c)$$

in which,

$$S_1 = \frac{9.29 - (2.85 + 2h)\times(2.85 - h)^2\times l^2}{36.3h^2} \qquad (5\text{-}35a)$$

$$S_2 = h\times\sqrt{4.82S_1^2 + 6.36S_3^2} \qquad (5\text{-}35b)$$

$$S_3 = \frac{(2.85 + 2h)\times(2.85 - h)^2}{143.6(h\times l)} \qquad (5\text{-}35c)$$

The geometrical constraints in this application example are h_{min} = 0.10 m (4.0 in), h_{max} = 0.43 m (17.0 in), l_{min} = 0.31 m (12 in), and l_{max} = 0.61 (24 in). The maximum tensile stresses after retrofit are predefined as the corresponding CAFT at each of the identified critical locations, that is, $\sigma_{max,1}$ = 69 MPa (10 ksi), $\sigma_{max,2}$ = 165 MPa (24 ksi), and $\sigma_{max,3}$ = 110 MPa (16 ksi). In addition, the remaining fatigue life of the connection detail after retrofit is defined as the period from the start of the fatigue

235

damage to the time when the reliability index $\beta(t)$ in Eq. 5-34 reaches the targeted minimum $\beta_{target} = 3.72$ (Chung 2004). Based on Eqs. 5-22 and 5-29 or 5-30, Eq. 5-27 can be expressed for $i = 1, 2,$ and 3 at CL-I, CL-II, and CL-III, respectively:

$$\beta(T_{\min}) = 1.67 \ln\left[\frac{\overline{A}}{1.10\overline{N}_S(T_{\min})}\right] \geq 3.72 \tag{5-36}$$

$$\text{where} \quad \overline{N}_S(T_{\min}) = \frac{365}{T_{shm}} \times \overline{N}_{shm,i} \times \int_0^{T_{\min}}(1+\alpha)^t\,dt \tag{5-37}$$

Therefore,

$$\int_0^{T_{\min}}(1+\alpha)^t\,dt \times \overline{N}_{shm,i} \leq 0.0107\overline{A} \tag{5-38}$$

Moreover, Eq. 5-26 can be re-formulated considering Eq. 5-32 as

$$\sigma_1 = C_1 \times \frac{9.29 - (2.85 + 2h)\times(2.85 - h)^2 \times l^2}{9.29h^2} \leq 69.0 \tag{5-39a}$$

$$\sigma_2 = h \times \sqrt{6.71\sigma_1^2 + 2.86\sigma_3^2} \leq 165.0 \tag{5-39b}$$

$$\sigma_3 = C_3 \times \frac{(2.85 + 2h)\times(2.85 - h)^2}{l \times h} \leq 110.0 \tag{5-39c}$$

Consequently, the optimization problem in Eqs. 5-23 through 5-27 can be re-formulated for any targeted time period T_g in years as follows:

Find the design variables: h and l

     Objective functions: (i) maximize $\{\beta(h, l)\}$ (5-40)

                            (ii) minimize $h \times l$ (5-41)

Subjected to:

(i) geometrical constraints

$$0.102 \leq h \leq 0.432 \tag{5-42a}$$

$$0.305 \leq l \leq 0.610 \tag{5-42b}$$

(ii) stress constraints

for the critical location CL-I,

$$\frac{9.29C_1 - 641.0h^2}{C_1 \times (2h^3 - 8.54h^2 + 23.0)} \leq l^2 \tag{5-43a}$$

for the critical location CL-II,

$$\left(C_1 \times \frac{9.29 - (2.85 + 2h) \times (2.85 - h)^2 \times l^2}{66.05h} \right)$$

$$+ \left(C_3 \times \frac{(2.85 + 2h) \cdot (2.85 - h)^2}{10.89l} \right)^2 \leq 80.27^2 \tag{5-43b}$$

for the critical location CL-III,

$$C_3 \times \frac{2h^3 - 8.54h^2 + 23.0}{110.0h} \leq l \tag{5-43c}$$

(iii) fatigue reliability constraints

for the critical location CL-I,

$$1.03S_1^2 - 1.21S_1 + 0.38 \leq 1.54 \times 10^3 \times \left(\int_0^{T_{\min}} (1 + \alpha)^t \, dt \right)^{-1} \tag{5-44a}$$

for the critical location CL-II,

237

$$7.87S_1^2 - 10.50S_1 + 3.66 \le 8.77 \times 10^3 \times \left(\int_0^{T_{\min}} (1+\alpha)^t \, dt \right)^{-1} \qquad (5\text{-}44b)$$

for the critical location CL-III,

$$9.69S_1^2 - 12.80S_1 + 4.56 \le 4.21 \times 10^3 \times \left(\int_0^{T_{\min}} (1+\alpha)^t \, dt \right)^{-1} \qquad (5\text{-}44c)$$

in which,

$$\beta(h,l) = \min \begin{Bmatrix} \beta_1(h,l) \\ \beta_2(h,l) \\ \beta_3(h,l) \end{Bmatrix} \qquad (5\text{-}45)$$

Step 6: The bi-objective optimization problem formulated in Eqs. 5-40 to 5-45 is solved by using the design optimization software VisualDOC (2006). The detail procedure is based on the flowchart presented in Figure 5-27.

5.3.4.3 Pareto Solution Sets for Bridge Retrofit Design

For decision makers, multiple optimal solutions for the cut-off retrofit design of the floor-beam connection details are provided by using the proposed bi-objective optimization approach. According to Pareto (1971), the dominant solution concept in defining solutions for bi-objective or multi-objective optimization problems is that of Pareto optimality. A point x^* in the feasible design space (FDS) is called Pareto optimal if there is no other point x in FDS, that reduces at least one objective function without increasing another one.

Figure 5-28(a), (b), (c), and (d) present the feasible regions of the cut-off sizes

for the minimum required fatigue life (i.e., target life) of 25, 50, 75, and 100 years,

respectively, when the out-of-plane displacement Δ_h = 2.54 mm (0.10 in) and the

annual traffic increase rate α = 5%. The actual and optimal cut-off sizes are also

indicated in Figure 5-28, where the three optimal cut-off sizes (i.e., optimal points 1,

2, and 3) are based on (i) maximization of the computed fatigue reliability of the

connection details after retrofit (see optimal point 1), (ii) minimization of the cut-off

area (see optimal point 2), and (iii) the combined objective function with the equal

weight on the objective functions (i) and (ii) (see optimal point 3), respectively. The

active lower bound constraints of the feasible regions are $\sigma_1 < \sigma_{max, 1}$ and $\sigma_3 < \sigma_{max, 3}$ up

to the minimum required fatigue life of 50 years, while $\{\sigma_1 < \sigma_{max, 1}$ and $T_3 > T_{min, 3}\}$

and $\{T_2 > T_{min, 2}$ and $T_3 > T_{min, 3}\}$ become the active lower bound constraints for the

minimum required fatigue life of 75 and 100 years, respectively. It is interesting to

note that the actual cut-off size is always in the feasible region, and the optimal cut-off

size based on the objective function (i) (i.e., maximization of $\beta(t)$) stays the same for

different minimum target lives of 25 and 50 years, with Δ_h = 2.54 mm (0.10 in) and α

= 5%. In addition, the optimal cut-off size based on the objective function (ii) (i.e.,

minimization of the cut-off area) always stays at the active lower bound constraints,

while the optimal cut-off size based on the objective function (iii) (i.e., combined

objective function) varies significantly. The combined objective function (iii) may

fully depend on the assigned weights on each of the objective functions.

For a given target life of 25 years with Δ_h = 3.175 mm (0.125 in), Figure

5-29(a), (b), and (c) compare the effects of the annual increase rate α = 0%, 2%, and

5% on the feasible regions and optimal solutions, while Figure 5-30(a), (b), (c), and (d) present the feasible regions and optimal solutions from different out-of-plane displacements Δ_h = 1.905 mm, 2.540 mm, 3.175 mm, and 3.810 mm, respectively. It can be concluded that the feasible regions and optimal solutions of the cut-off sizes are not sensitive to the annual increase rate of the stress cycles up to α = 5%, whereas they change significantly with different out-of-plane displacements. It is noted that the actual cut-off size is in the infeasible region due to the constraint $\sigma_3 > \sigma_{max,\,3}$ when the out-of-plane displacement is assigned as 3.810 mm (0.150 in), as shown in Figure 5-30(d). Therefore, it may be critical to verify the actual out-of-plane displacement before retrofitting the connection details.

Figure 5-31 and Figure 5-32 present the Pareto optimal solutions in both objective and design variable spaces, considering the out-of-plane displacements of 2.540 mm (0.100 in) and 3.175 mm (0.125 in), respectively. As shown in Figure 5-31(a) and Figure 5-32(a), the Pareto frontiers are clearly shown in the objective spaces, where the targeted levels of the objective functions can be determined according to the decision maker's preferences. The optimal cut-off sizes h and l associated with the objective spaces can be easily found in the corresponding design variable spaces (see Figure 5-31(b) and Figure 5-32(b)). It is very interesting to note that the actual cut-off area is always on the Pareto frontiers for different minimum required fatigue lives up to 100 years, which implies that no future re-retrofitting is necessary. However, it should be emphasized herein that this conclusion is based on the out-of-plane displacement up to 3.175 mm (0.125 in). Therefore, if the out-of-

plane displacement from field monitoring exceeds 3.175 mm (0.125 in), a larger cut-off size for retrofit has to be taken into account.

Finally, Figure 5-33 and Figure 5-34 present the time-dependent minimum cut-off areas and the time-dependent maximum fatigue reliability indices associated with the Pareto optimal solutions indicated in Figure 5-31 and Figure 5-32. These Pareto optimal solutions will provide the decision makers with the useful guidelines for their preference choices.

5.3.4.4 Conclusions

In this study a novel approach to finding the optimal cut-off size of the connection details for retrofitting distortion-induced fatigue cracking in steel bridges using monitoring data under uncertainty was presented. Two competing objectives indicating minimization of the cut-off area and maximization of the fatigue reliability of the connection details were used. The concept of the cut-off size adjustment factor (SAF) was introduced. This factor was used to develop the nonlinear relationship with respect to the cut-off size. The optimal cut-off size was found by integrating the stress range histogram data of an existing bridge monitored by the ATLSS Engineering Research Center. The following conclusions are drawn:

1. For retrofitting distortion-induced fatigue cracking of steel bridges under uncertainty, the optimal cut-off size of the connection details can be found from the proposed bi-objective optimization formulation using the field monitoring data.

2. The SHM data can be used (a) to represent the fatigue stress ranges at the

241

identified critical locations after retrofit based on the proposed SAF and (b) to find the mean values of $N_S(t)$.

3. The developed stress formulations, which are validated by FE stress outputs, can be used to impose stress constraints in respective fatigue details.

4. The geometrical constraints on connection details, stress constraints associated with the AASHTO CAFT, and fatigue reliability constraints defining structural service life after retrofit have to be used to provide practical solutions.

5. Further research is needed to develop the proposed size optimization approach for cost-oriented reliability-based shape optimization of retrofitting distortion-induced fatigue cracking in steel bridges.

Table 5-1   The *S-N* values according to the AASHTO Categories.

AASHTO category	Fatigue detail coefficient, A MPa^3 (ksi^3)		
	Design value, A	Mean value, $E(A)$	Standard deviation, $\sigma(A)$
B	3.93E+12 (1.20E+10)	3.93E+13 (1.20E+11)	1.77E+13 (5.40E+10)
C	1.44E+12 (4.40E+09)	1.44E+13 (4.40E+10)	6.49E+12 (1.98E+10)
D	7.21E+11 (2.20E+09)	7.21E+12 (2.20E+10)	3.24E+12 (9.90E+09)
E	3.61E+11 (1.10E+09)	3.61E+12 (1.10E+10)	1.62E+12 (4.95E+09)
E′	1.28E+11 (3.90E+08)	1.28E+12 (3.90E+09)	5.75E+11 (1.76E+09)
Reference	AASHTO Specifications (2002)	Wirsching et al. (1987)	Wirsching et al. (1987)

Table 5-2   Details of deterministic and random variables for fatigue reliability model.

Deterministic parameters and random variables	Distribution	Reference
Critical damage accumulation index, Δ	Lognormal $E(\Delta) = 1.0$, $COV(\Delta) = 0.3$	Wirsching (1984)
Fatigue detail coefficient, A MPa^3 (ksi^3)	Lognormal $E(A) = 1.28E+12$ ($3.90E+09$), $COV(A) = 0.45$	AASHTO Specifications (2002) for S-N category E′
Equivalent stress range, S_{re} MPa (ksi)	Lognormal $E(S_{re}) = 13.1$ (1.98), $COV(S_{re}) = 0.25$	Fisher et al. (1984)
Material constant, m	Deterministic 3.0	AASHTO Specifications (2002)
Average daily truck traffic, $ADTT$ (cycles per day)	Deterministic 4430	Fisher et al. (1981)
Annual traffic increase rate, α (%)	Deterministic 2.0	Frangopol et al. (2008)
Measurement error factor, e	Lognormal $E(e) = 1.0$, $COV(e) = 0.04$	Frangopol et al. (2008)

Table 5-3   Details of deterministic and random variables for crack growth model.

Deterministic parameters and random variables	Distribution	Reference
Initial crack depth, a_i mm (in.)	Lognormal $E(a_i) = 0.6$ (0.02362), $COV(a_i) = 0.4$	Righiniotis & Chryssanthopoulos (2003)
Fatigue coefficient, C MPa $\sqrt{m}$ (ksi $\sqrt{in.}$)	Lognormal $E(C) = 1.375E\text{-}13$ (2.271E-10), $COV(C) = 0.51$	Moan et al. (1993)
Weld size, Z mm (in.)	Deterministic 16.0 (0.63)	Fisher et al. (1984)
Flange thickness, t_f mm (in.)	Deterministic 32.0 (1.26)	
Cover plate thickness, t_{cp} mm (in.)	Deterministic 31.8 (1.25)	
Final crack depth, a_f mm (in.)	Deterministic 25.4 (1.00)	

Table 5-4 Inspection and repair solutions according to repair methods.

Repair method	Inspection and repair times (years)									Minimum reliability index, β
	T_1	T_2	T_3	T_4	T_5	T_6	T_7	T_8	T_9	
(1) Peening	4.9[+]	27.0[+]	-	-	-	-	-	-	-	2.52
(2) GTA Remelting	4.9	8.3[+]	26.6	33.6[+]	-	-	-	-	-	2.51
(3) Rewelding	4.9	8.3	12.6[+]	17.0	21.8	27.2[+]	37.8	41.5	45.4[+]	2.21
(4) Bolt-Splices	4.9	8.3	12.6	20.1[+]	-	-	-	-	-	2.75
(1) + (2)	4.9[+]	27.0	33.9[+]	-	-	-	-	-	-	2.51
(2) + (3)	4.9	8.3[+]	26.6	33.6	40.6[+]	51.1	54.8[+]	-	-	2.87
(1) + (2) + (3)	4.9[+]	27.0	33.9	40.4[+]	49.1	53.1[+]	-	-	-	2.88

Note: [+] indicates that a repair option follows an inspection.

246

Table 5-5   The *S-N* values according to categories (AASHTO Specifications, 2002).

S-N values	Channels		
	CL-I (CH-2)	CL-II (CH-7)	CL-III (CH-11)
Category	C	A	B
Fatigue retail coefficient, A, MPa^3 (ksi^3)	14.4E+11 (44.0E+08)	81.9E+11 (25.0E+09)	39.3E+11 (12.0E+09)
*Intercept, mean value, $E(\log A)$	10.085	11.121	10.870
*Intercept, lower bound, $E(\log A)$-2·σ($\log A$)	9.775	10.688	10.582
Constant amplitude fatigue threshold, CAFT, MPa (ksi)	68.9 (10.0)	165.5 (24.0)	110.3 (16.0)

* Keating & Fisher (1986)

Table 5-6 S_{re} and N_{avg} according to target parameter, α_{target}.

Critical locations	Parameters	Target stress constraint parameter, α_{target}			
		0 % Optimal size 1 (28.5cm, 32.2cm)	25 % Optimal size 2 (30.2cm, 47.2cm)	46 % Actual retrofit size (29.8cm, 52.1cm)	50 % Optimal size 3 (29.9cm, 53.2cm)
CL-I	N_{avg} (cycles per day)	253	208	307	277
	Mean value of S_{re}, MPa (ksi)	21.6 (3.13)	15.4 (2.23)	11.5 (1.67)	11.3 (1.64)
	Standard deviation of S_{re}, MPa (ksi)	6.0 (0.87)	4.3 (0.62)	3.2 (0.46)	3.1 (0.45)
CL-II	N_{avg} (cycles per day)	174	132	178	170
	Mean value of S_{re}, MPa (ksi)	35.3 (5.12)	29.2 (4.23)	25.7 (3.73)	25.5 (3.70)
	Standard deviation of S_{re}, MPa (ksi)	9.1 (1.33)	7.6 (1.10)	6.7 (0.97)	6.6 (0.96)
CL-III	N_{avg} (cycles per day)	1197	872	1403	1332
	Mean value of S_{re}, MPa (ksi)	28.2 (4.08)	19.7 (2.86)	15.1 (2.20)	14.7 (2.13)
	Standard deviation of S_{re}, MPa (ksi)	6.4 (0.93)	4.5 (0.65)	3.4 (0.50)	3.3 (0.48)

Note: optimal sizes h and l are indicated in parentheses.

Table 5-7 Remaining fatigue life according to target parameter, α_{target}.

Optimal sizes	Target stress constraint parameter, α_{target}	Optimal cut-off area, cm^2 (in^2)	Remaining fatigue life, years		
			CL-I	CL-II	CL-III
Optimal size 1 (28.5cm, 32.2cm)	0 %	919 (142)	54	89	51
Optimal size 2 (30.2cm, 47.2cm)	25 %	1429 (221)	90	116	92
Actual retrofit size (29.8cm, 52.1cm)	46 %	1555 (241)	105	119	102
Optimal size 3 (29.9cm, 53.2cm)	50 %	1589 (246)	110	121	107

Note: optimal sizes h and l are indicated in parentheses.

Table 5-8   Random variables for fatigue reliability analysis.

Parameter	Notation	Distribution	Reference
Miner's critical damage accumulation index	Δ	Lognormal LN (1.0, 0.3)	Wirsching (1984)
Fatigue detail coefficient	A	Lognormal COV(A) = 0.45 (see Table 5-9)	Wirsching et al. (1987)
Measurement error factor	e	Lognormal LN (1.0, 0.04)	Frangopol et al. (2008)
Product of $N(t)$ and S_{reff}^3	$N_s(t)$	Lognormal COV($N_s(t)$) = 0.30	Liu et al. (2010a)

Table 5-9   Basic information at critical locations CL-I, CL-II, and CL-III.

Critical location		CL-I (CH-2)	CL-II (CH-7)	CL-III (CH-11)
Fatigue category		C	A	B
*Mean value of coefficient A	MPa^3 (ksi^3)	14.4×10^{12} (44.0×10^9)	82.0×10^{12} (250.0×10^9)	39.3×10^{12} (120.0×10^9)
CAFT	MPa (ksi)	69.0 (10.0)	165.0 (24.0)	110.0 (16.0)
Predefined threshold	MPa (ksi)	6.9 (1.0)	16.5 (2.4)	11.0 (1.6)
**C_1 in Eq. 5-32(a)	$MPa \cdot m^2$ $(ksi \cdot in^2)$	10.89 (2.45×10^3)	σ_2 in MPa $(\sigma_2$ in ksi$)$	σ_3 in MPa $(\sigma_3$ in ksi$)$
C_{21} in Eq. 5-32(b)	h in m (in)	σ_1 in MPa $(\sigma_1$ in ksi$)$	$2.59 (0.066) \times h$	σ_3 in MPa $(\sigma_3$ in ksi$)$
C_{23} in Eq. 5-32(b)	h in m (in)	σ_1 in MPa $(\sigma_1$ in ksi$)$	$1.69 (0.043) \times h$	σ_3 in MPa $(\sigma_3$ in ksi$)$
**C_3 in Eq. 5-32(c)	$MPa \cdot m^{-1}$ $(ksi \cdot in^{-1})$	σ_1 in MPa $(\sigma_1$ in ksi$)$	σ_2 in MPa $(\sigma_2$ in ksi$)$	0.52 (0.002)

* See Wirsching et al. (1987) for computation procedures.
** Values are based on the out-of-plane displacement of 2.54 mm (0.1 in) applied to the top of the floor-beam flange only.

Table 5-10   Validation of equation 5-32 by FE modeling.

Cut-off size	Stress by Equation 5-32 (MPa)			Stress by FE modeling (MPa)			Ratio		
l (m) x h (m)	CL-I	CL-II	CL-III	CL-I	CL-II	CL-III	CL-I	CL-II	CL-III
0.61 x 0.43	7.886	32.372	42.598	10.247	36.365	51.541	0.770	0.890	0.826
0.61 x 0.41	8.495	31.962	44.589	8.670	37.260	51.700	0.980	0.858	0.862
0.61 x 0.30	12.984	33.050	62.304	13.000	44.341	53.000	0.999	0.745	1.176
0.52 x 0.41	23.943	43.922	52.202	23.858	37.207	56.999	1.004	1.180	0.916
0.52 x 0.30	42.376	49.995	74.571	45.000	45.320	62.100	0.942	1.103	1.201
0.41 x 0.30	73.373	73.941	93.456	78.013	63.949	94.094	0.941	1.156	0.993
0.41 x 0.25	100.735	81.779	110.742	95.905	73.348	104.543	1.050	1.115	1.059
0.30 x 0.30	94.509	97.542	127.391	111.783	86.841	160.895	0.845	1.123	0.792
0.30 x 0.25	130.163	107.673	150.954	144.936	103.632	186.284	0.898	1.039	0.810
0.30 x 0.20	202.902	125.535	190.220	201.257	136.075	222.599	1.008	0.923	0.855
0.30 x 0.15	360.039	157.049	255.242	318.288	170.979	301.395	1.131	0.919	0.847

Note: values are based on the out-of-plane displacement of 2.54 mm (0.1 in) applied to the top of the floor-beam flange only.

252
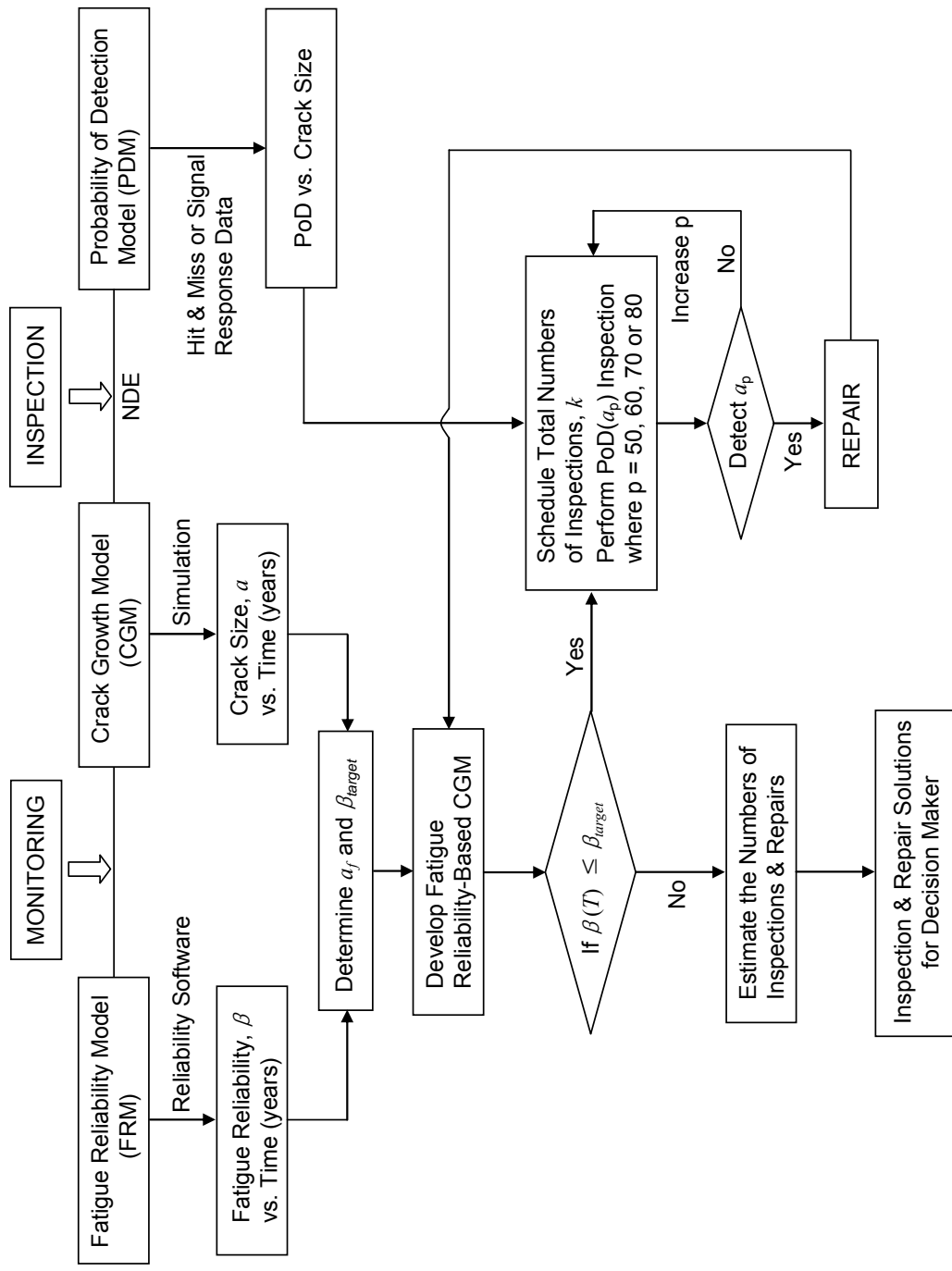
Figure 5-1 Flowchart of the combined approach.
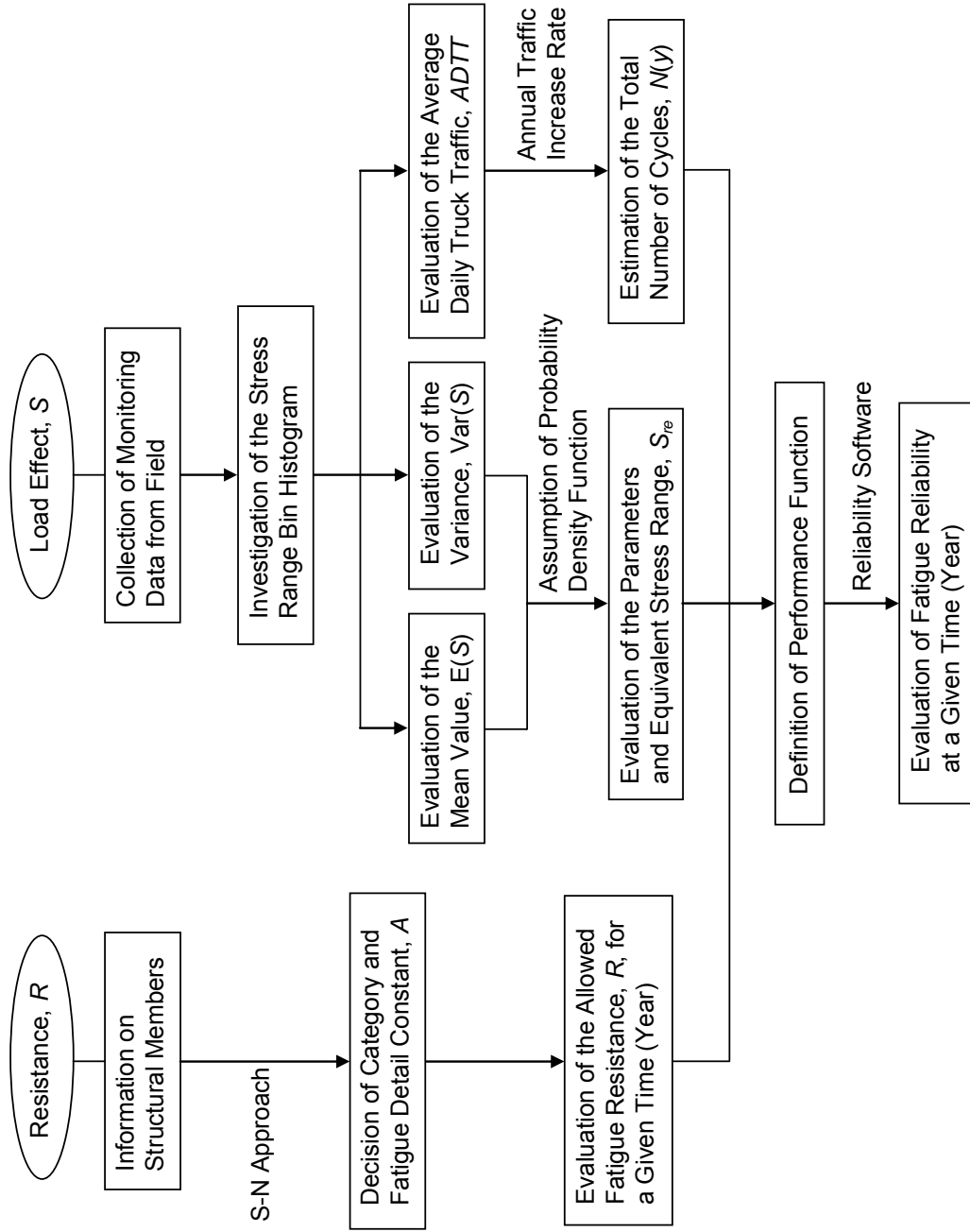
Figure 5-2 Flowchart for fatigue reliability evaluation.
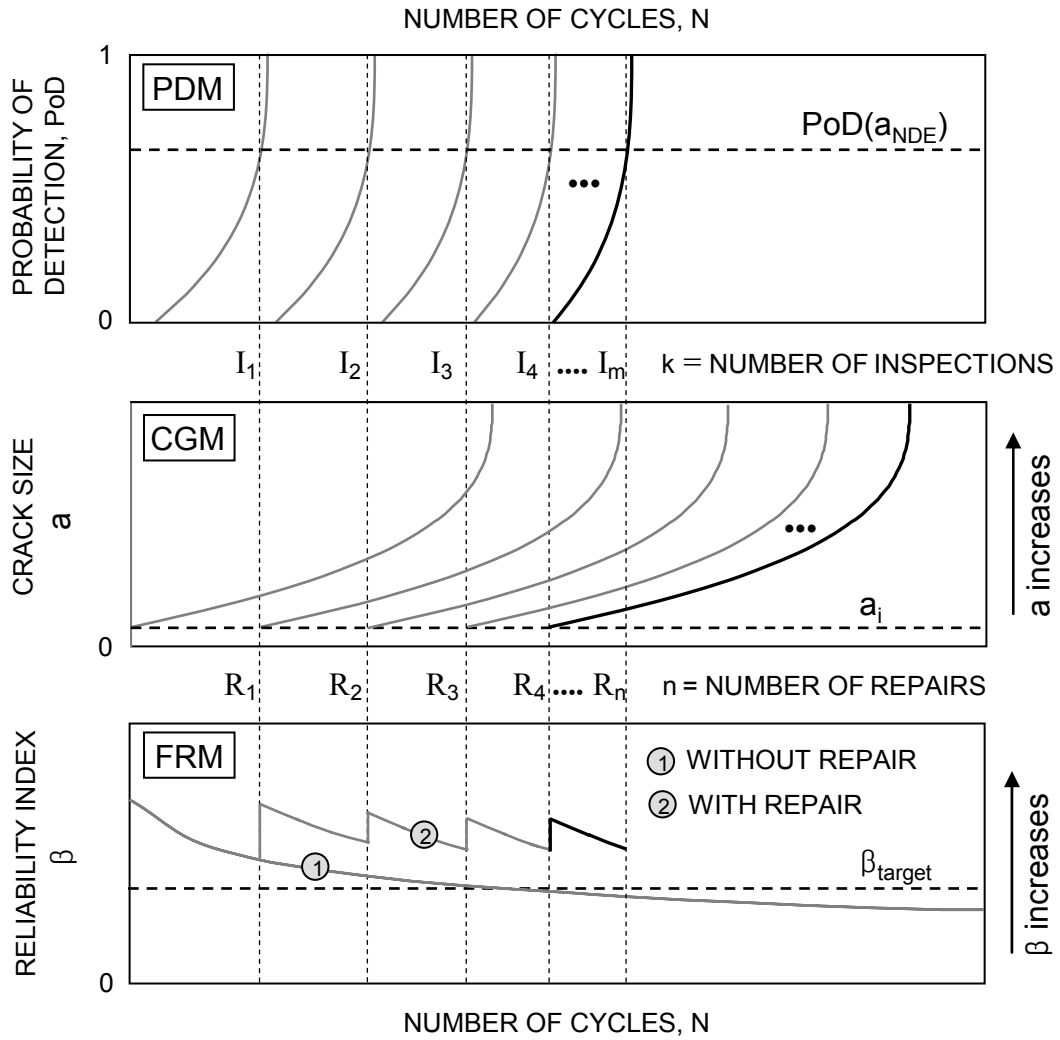
NUMBER OF CYCLES, N

Figure 5-3   Schematic of the three prediction models: FRM, CGM, and PDM.
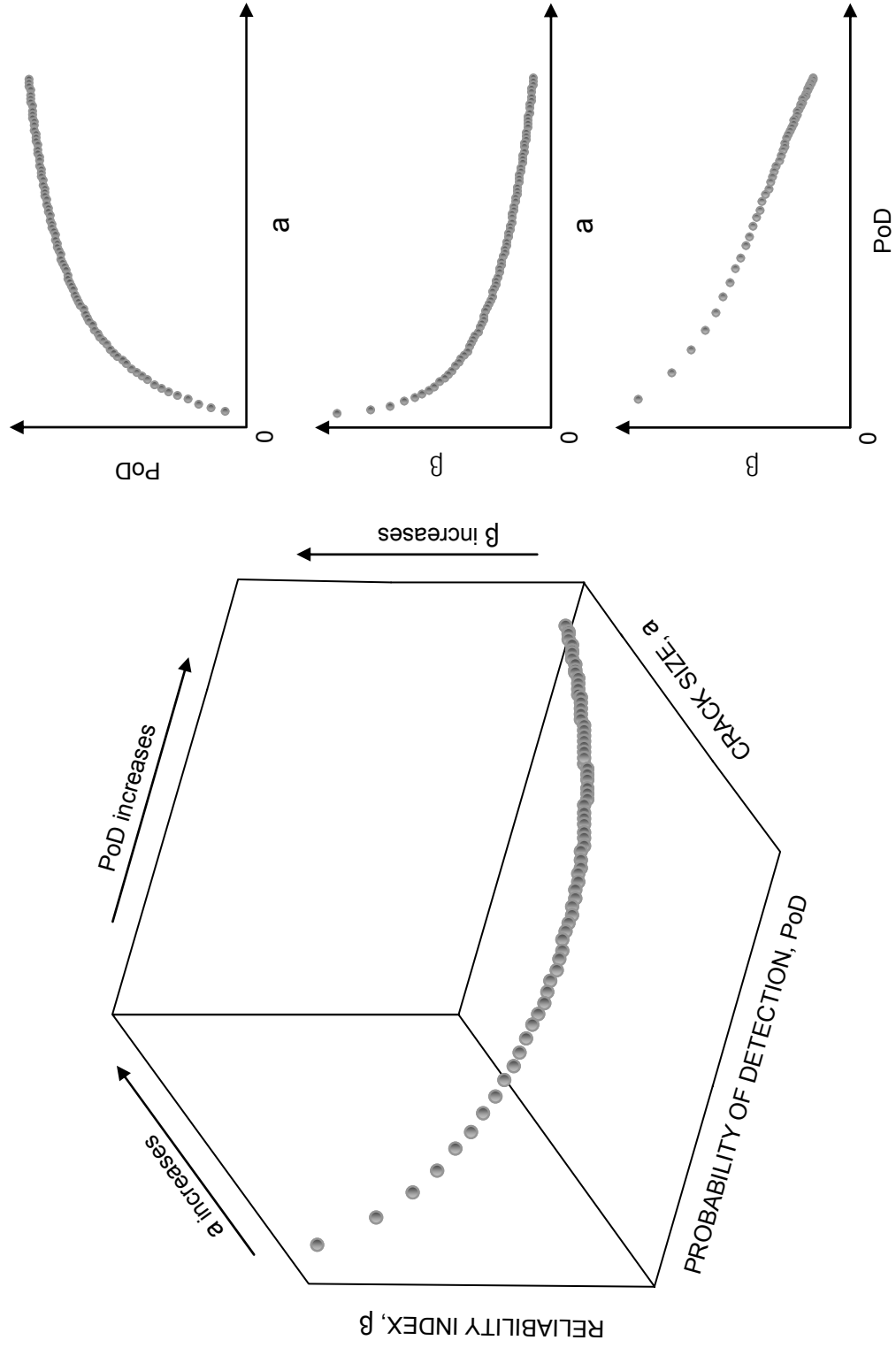
Figure 5-4   Schematic of the relationship among the combined models.
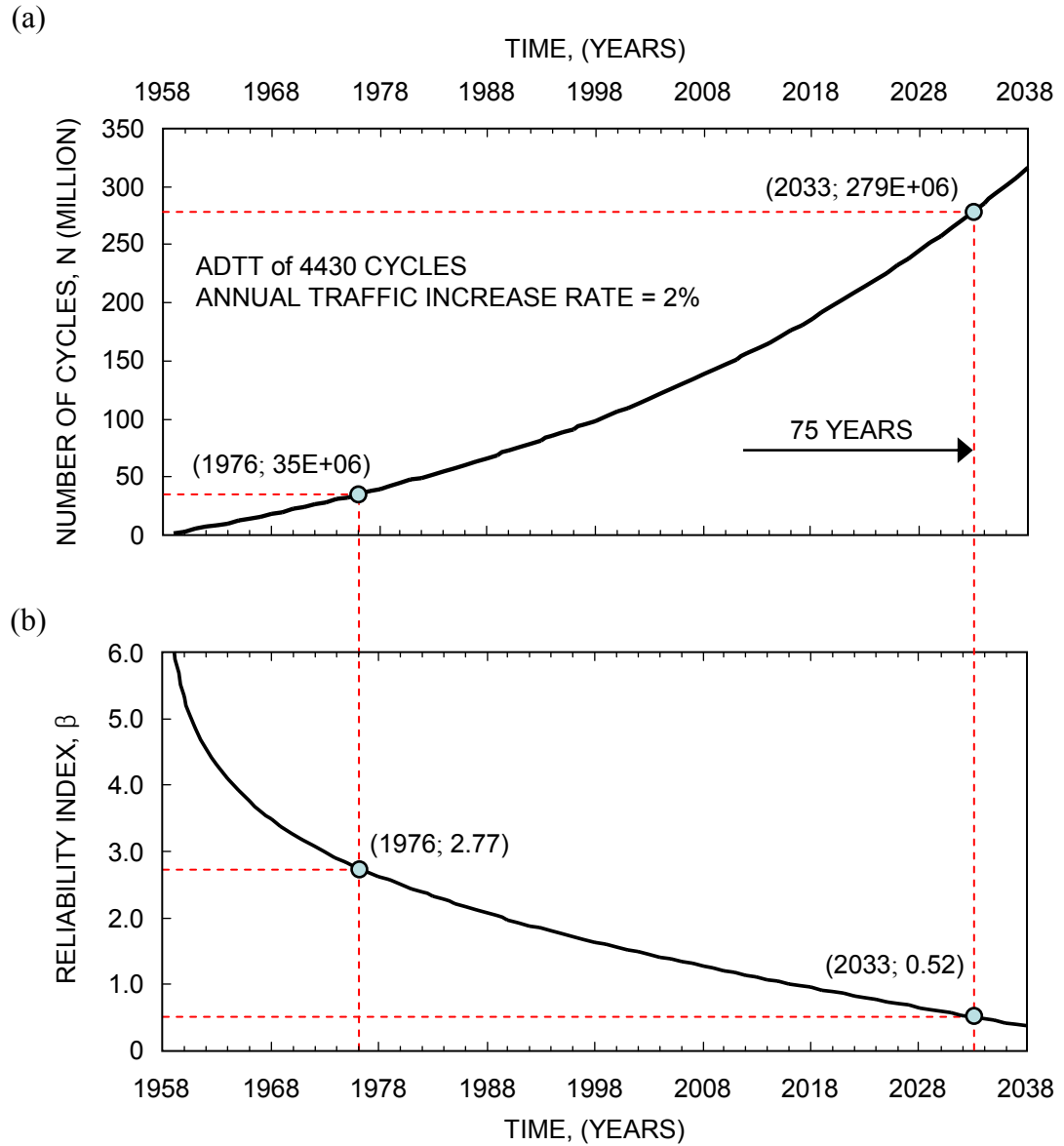
Figure 5-5   Fatigue reliability model (FRM): (a) estimation of the cumulative number of cycles, and (b) fatigue reliability evaluation

(a)

(b)
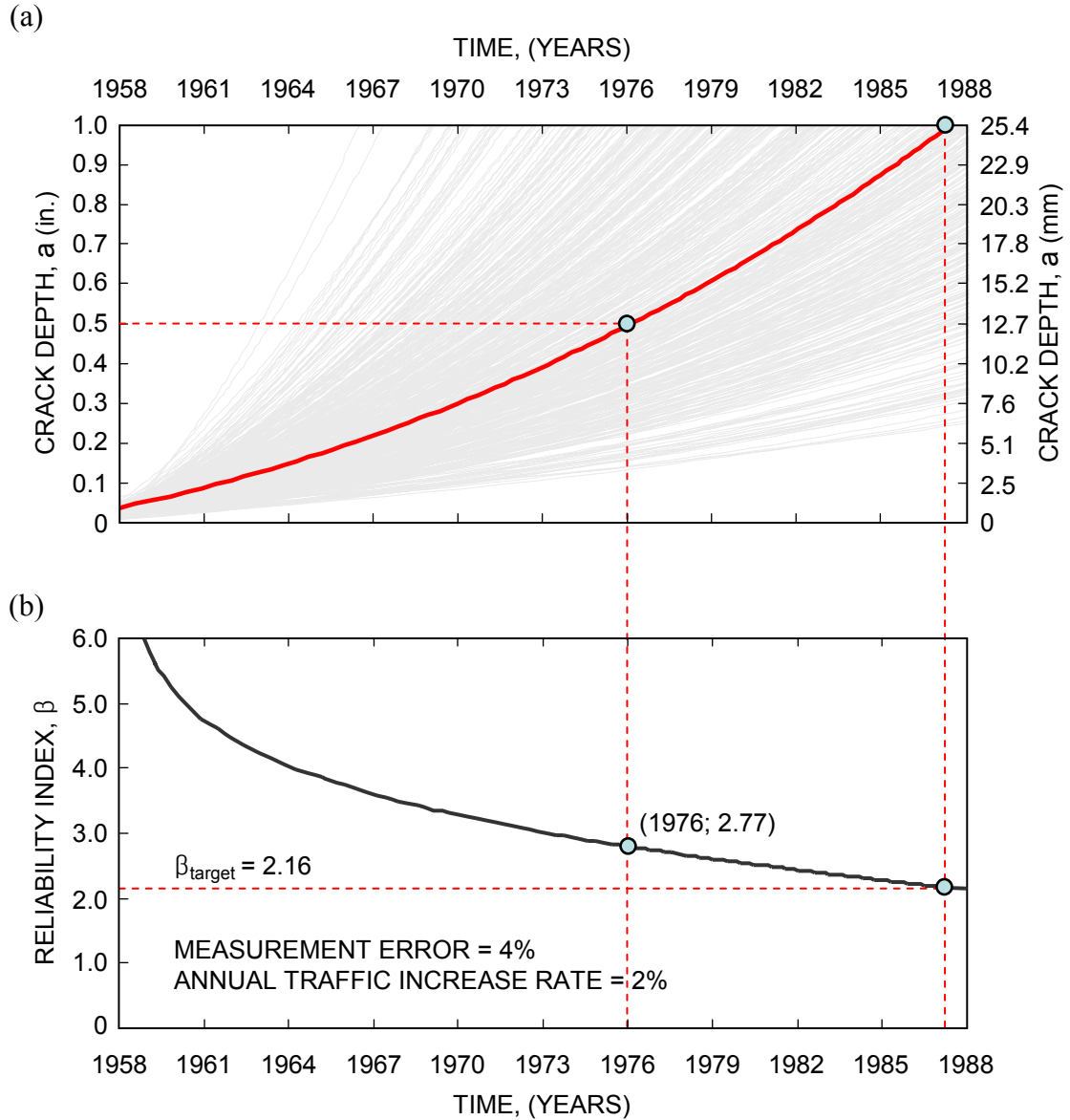
Figure 5-6: Fatigue reliability-based CGM: (a) CGM in the increase of years, and (b)
FRM in the increase of years.

(a)

(b)
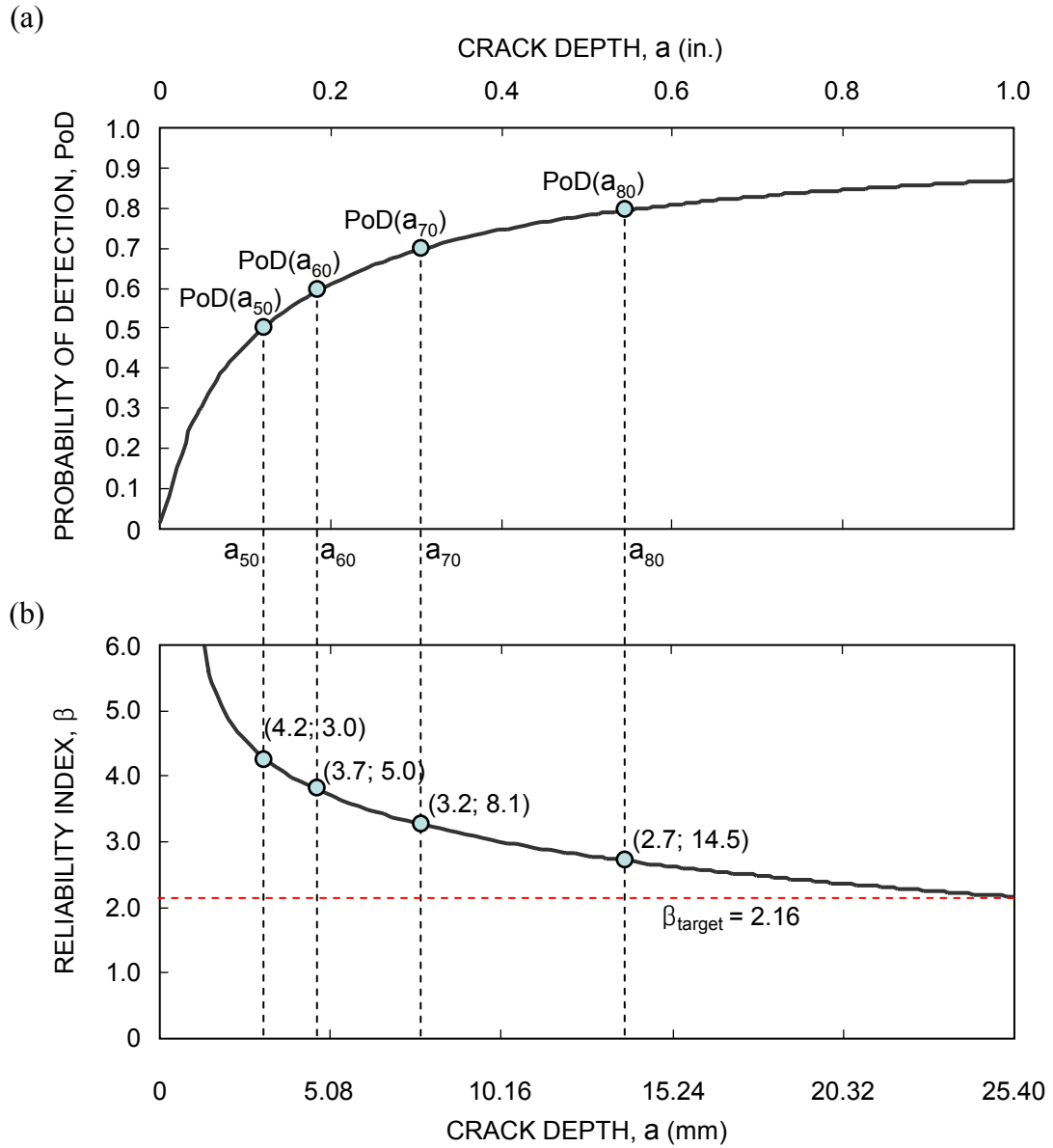
Figure 5-7   Probability of detection model (PDM): (a) PDM according to depth crack sizes, and (b) FRM according to depth crack sizes.
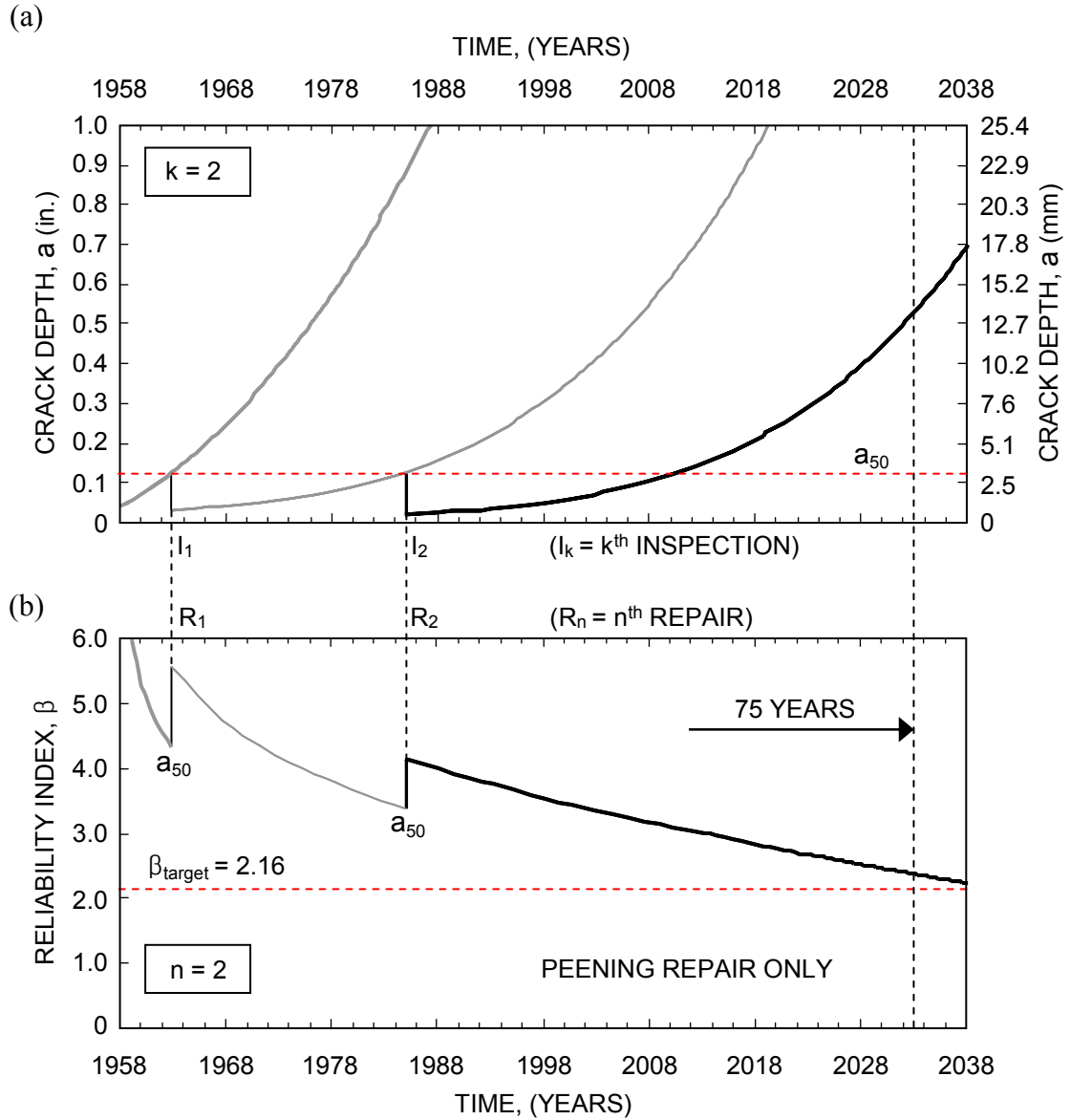
Figure 5-8   Peening repair performed by inspection PoD (a_{50}): (a) updating CGM, and (b) updating FRM.
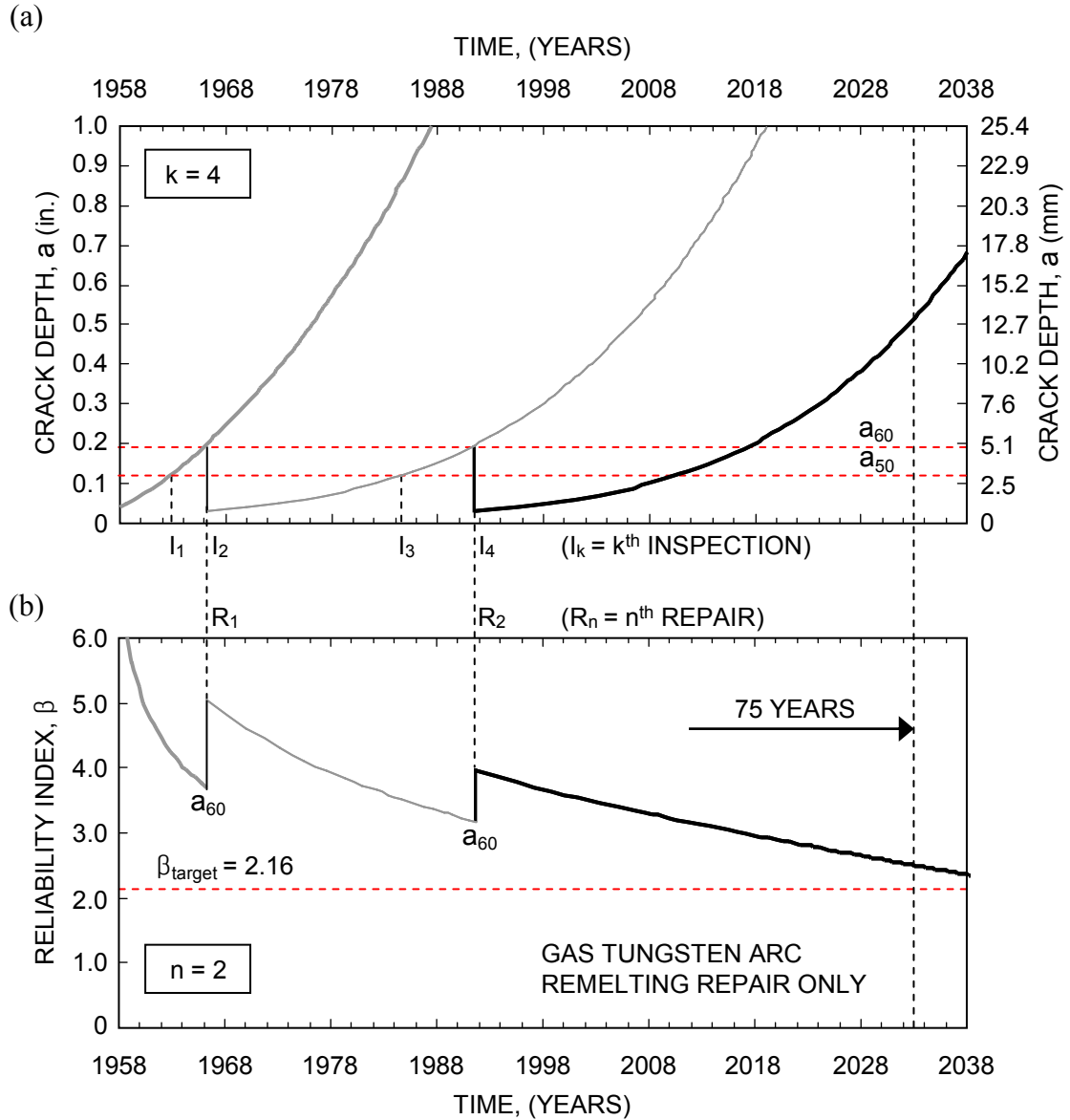
Figure 5-9 Gas Tungsten Arc (GTA) remelting repair performed by inspection PoD (a_{60}): (a) updating CGM, and (b) updating FRM.
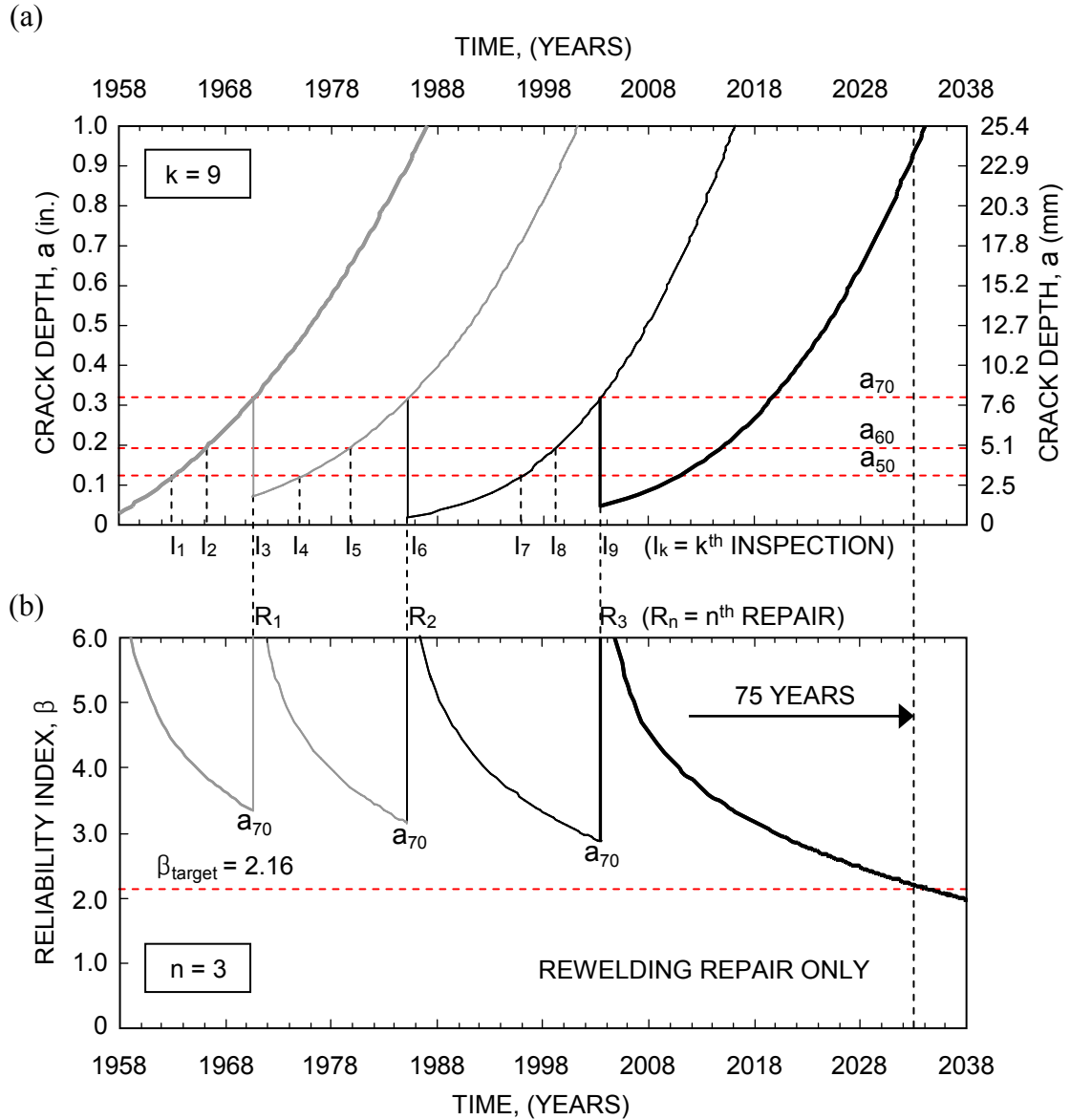
Figure 5-10   Rewelding repair performed by inspection PoD (a_{70}): (a) updating CGM, and (b) updating FRM.

(a)

TIME, (YEARS)

1958   1968   1978   1988   1998   2008   2018   2028   2038

k = 3

CRACK DEPTH, a (in.)

CRACK DEPTH, a (mm)

a_{60}
a_{50}

I_1 I_2 I_3 ($I_k = k^{th}$ INSPECTION)

(b)

R_1 R_2 ($R_n = n^{th}$ REPAIR)

RELIABILITY INDEX, β

75 YEARS

a_{50}

a_{60}

$β_{target} = 2.16$

n = 2

PEENING AT R_1 AND
GTA REMELTING AT R_2

1958   1968   1978   1988   1998   2008   2018   2028   2038

TIME, (YEARS)
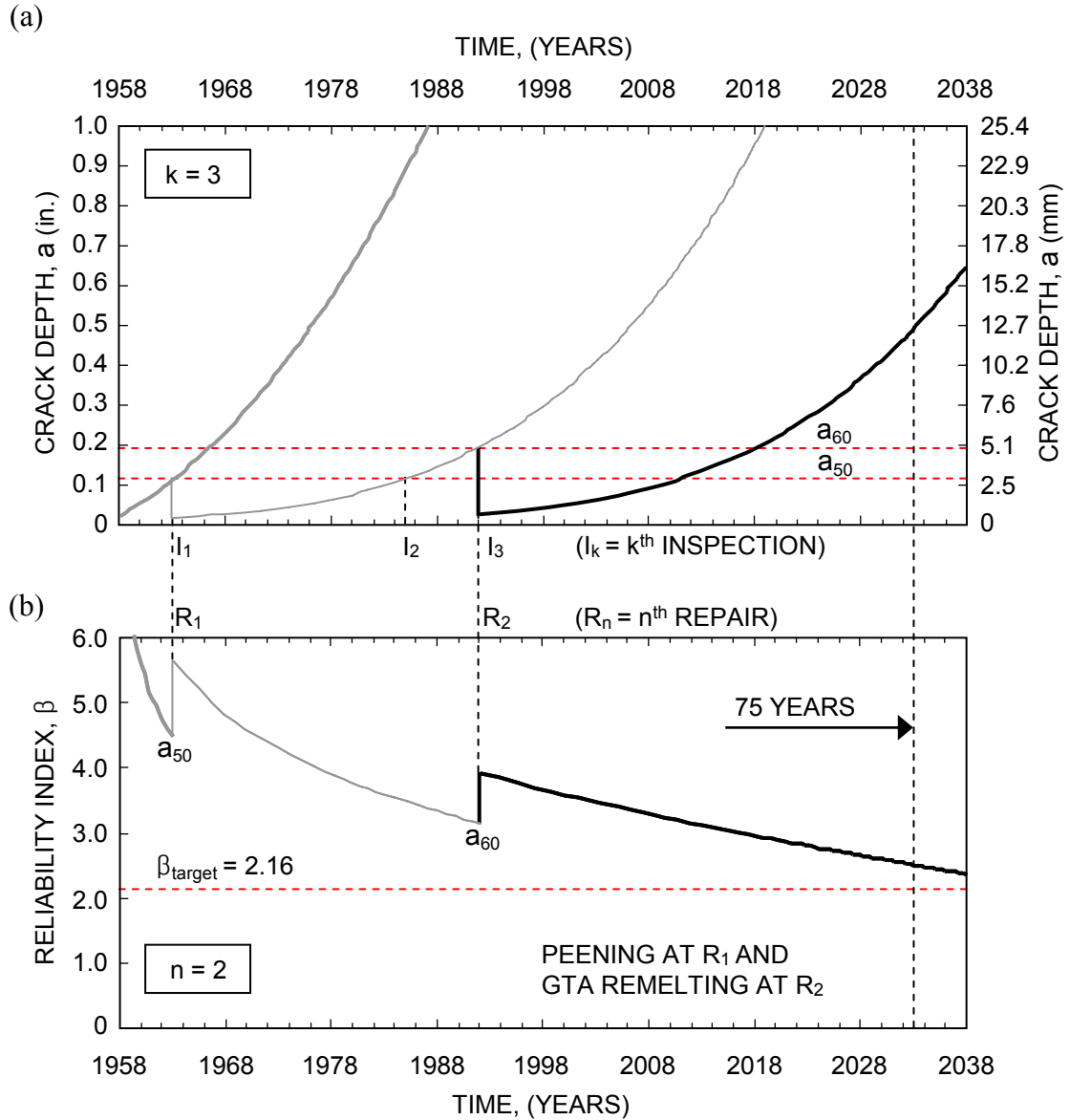
Figure 5-11   Peening and GTA remelting repairs: (a) updating CGM, and (b) updating FRM.

(a)
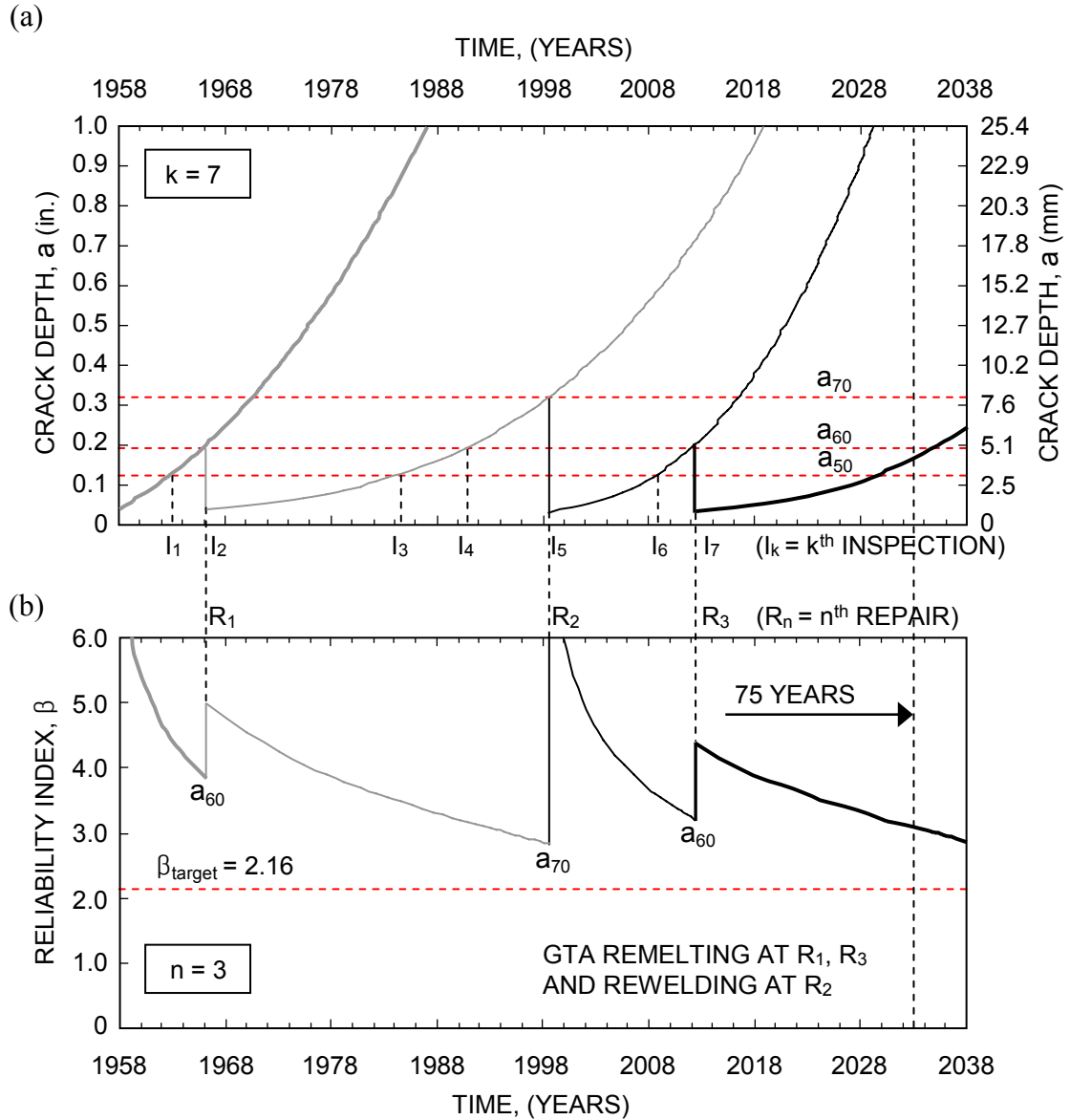
Figure 5-12   GTA remelting and rewelding repairs: (a) updating CGM, and (b) updating FRM.
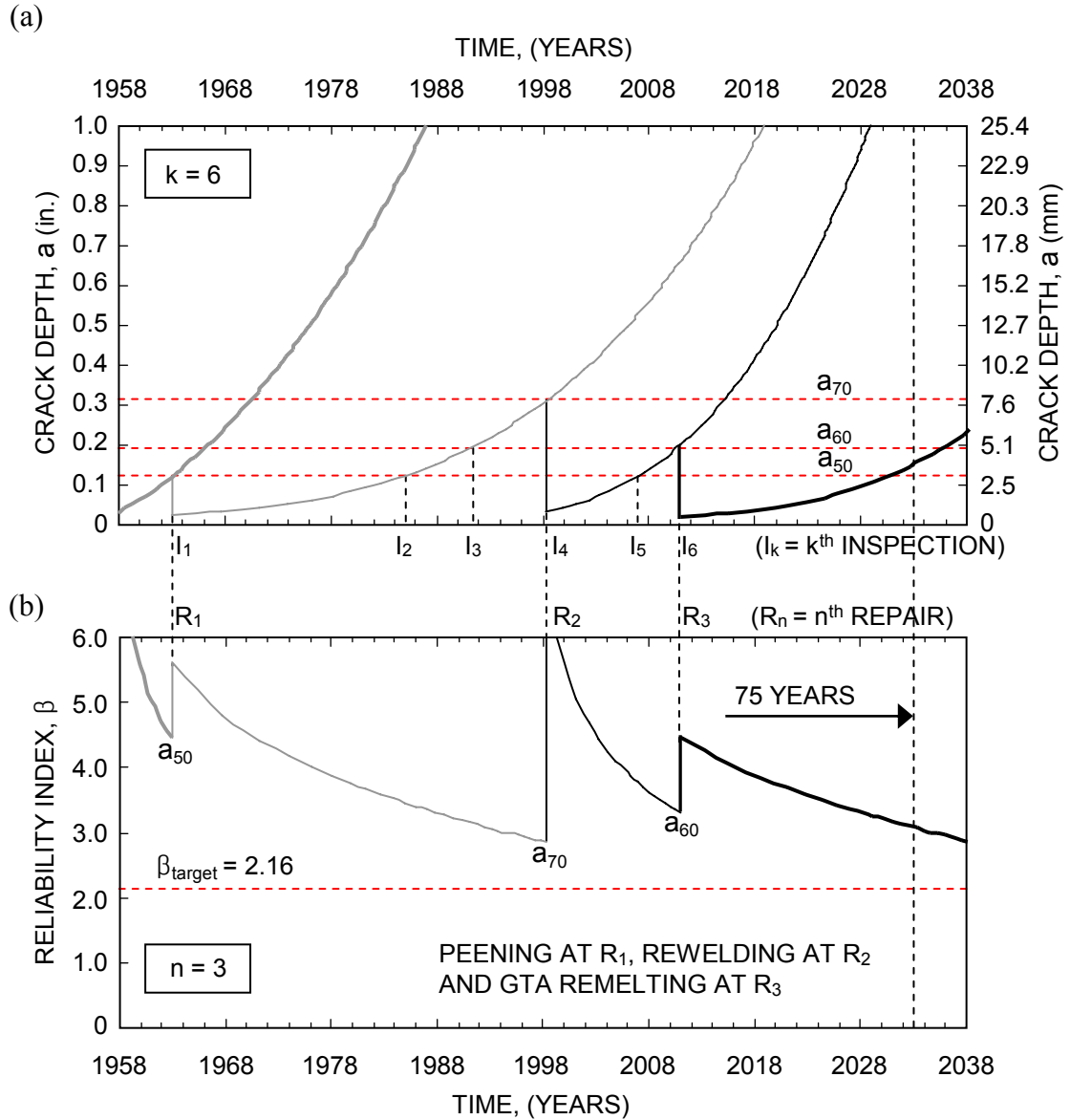
Figure 5-13   Peening, GTA remelting and rewelding repairs: (a) updating CGM, and (b) updating FRM.
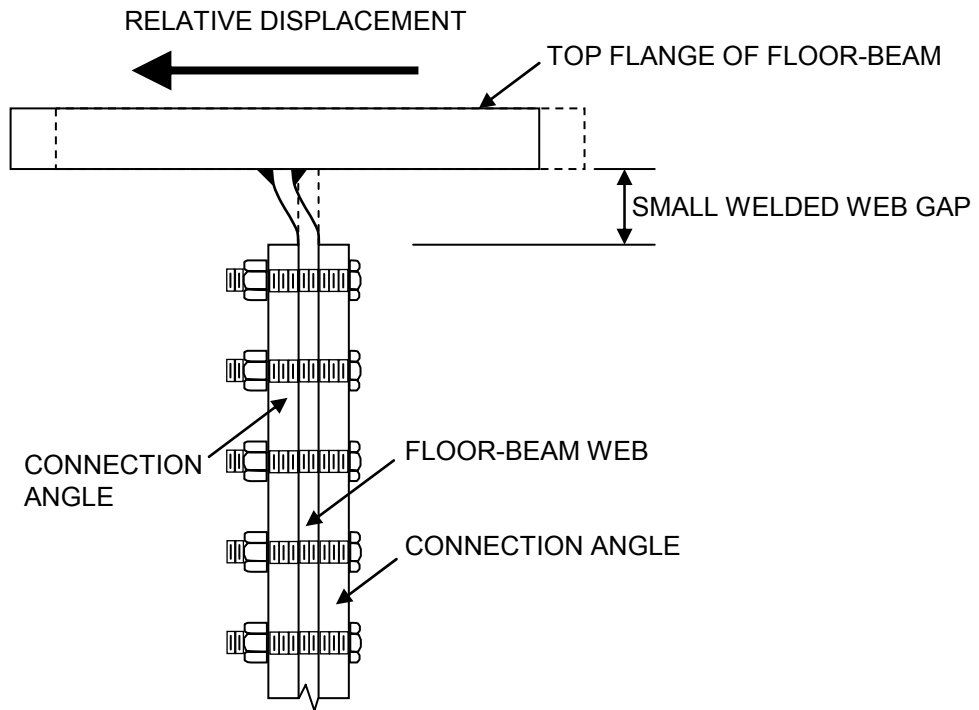
Figure 5-14   Schematic distortion of a floor-beam small welded web gap (adapted from Connor et al. 2004).

REQUIREMENTS → Collecting Information on Structural Members (i.e., material properties, geometric conditions etc.)

FE Analysis After Retrofit

Identifying Critical Locations and Validating FEM Stress Results with Field Measurements from Monitoring

AASHTO S-N Curve

Identifying S-N Category of Critical Locations and Investigating CAFT, Fatigue Detail Coefficient, A

OPTIMIZATION → Establishing Optimization Problem for Effective Cut-off Retrofit Design (i.e., Design variables, Objective functions, and Constraints: see Eqs. 5-13 to 5-19)

Software Programs (ABAQUS & Visual DOC)

Linking VisualDOC for Optimization and ABAQUS for FE Analysis with the Defined Input Variables (i.e., cut-off height and length)

Run VisualDOC

Obtaining Optimal Cut-off Sizes for Given Constraints

For α_{target}

RELIABILITY → Establishing New Stress Range Bin Histogram for Optimal Cut-off Size by using FE Analysis and Monitoring

Reliability Software (RELSYS)

Performing Fatigue Reliability Analysis

$\beta_{target} = 3.72$

Estimating Remaining Lifetime for Optimal Solution

For Other Cut-off Sizes

Figure 5-15   Flowchart for optimal retrofit design and fatigue reliability assessment.
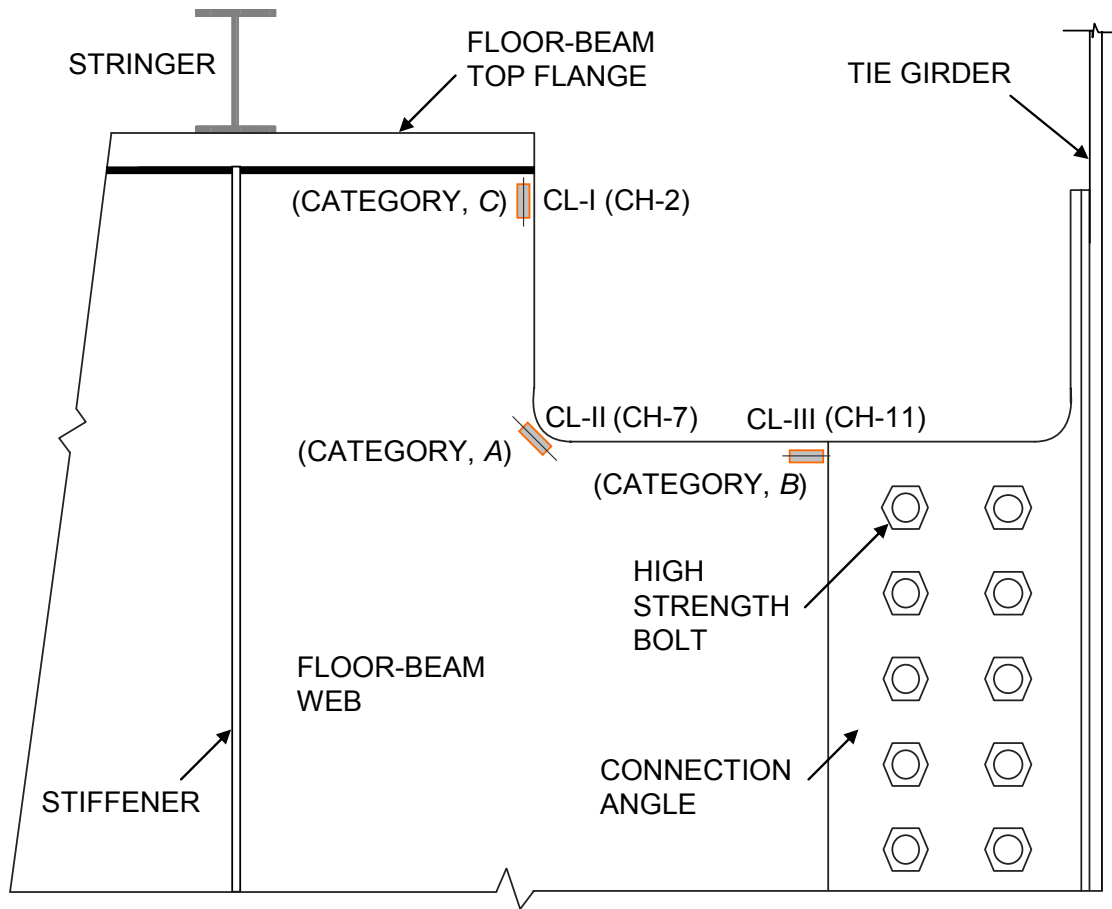
Figure 5-16   Floor-beam connection detail after retrofit with sensor locations.

0.521 m
(1.71 ft)

1.63 m
5.33 ft

1.63 m
5.33 ft

1.63 m
5.33 ft

1.63 m
5.33 ft

1.63 m
5.33 ft

1.63 m
5.33 ft

1.68 m
5.50 ft

1.68 m
5.50 ft

1.68 m
5.50 ft

1.68 m
5.50 ft

1.68 m
5.50 ft

16.07 m (52.71 ft)

0.71m
2.33 ft

0.02 m (0.06 ft)

FLOOR-BEAM WEB

STIFFENER

FLOOR-BEAM CONNECTION DETAIL
AFTER RETROFIT
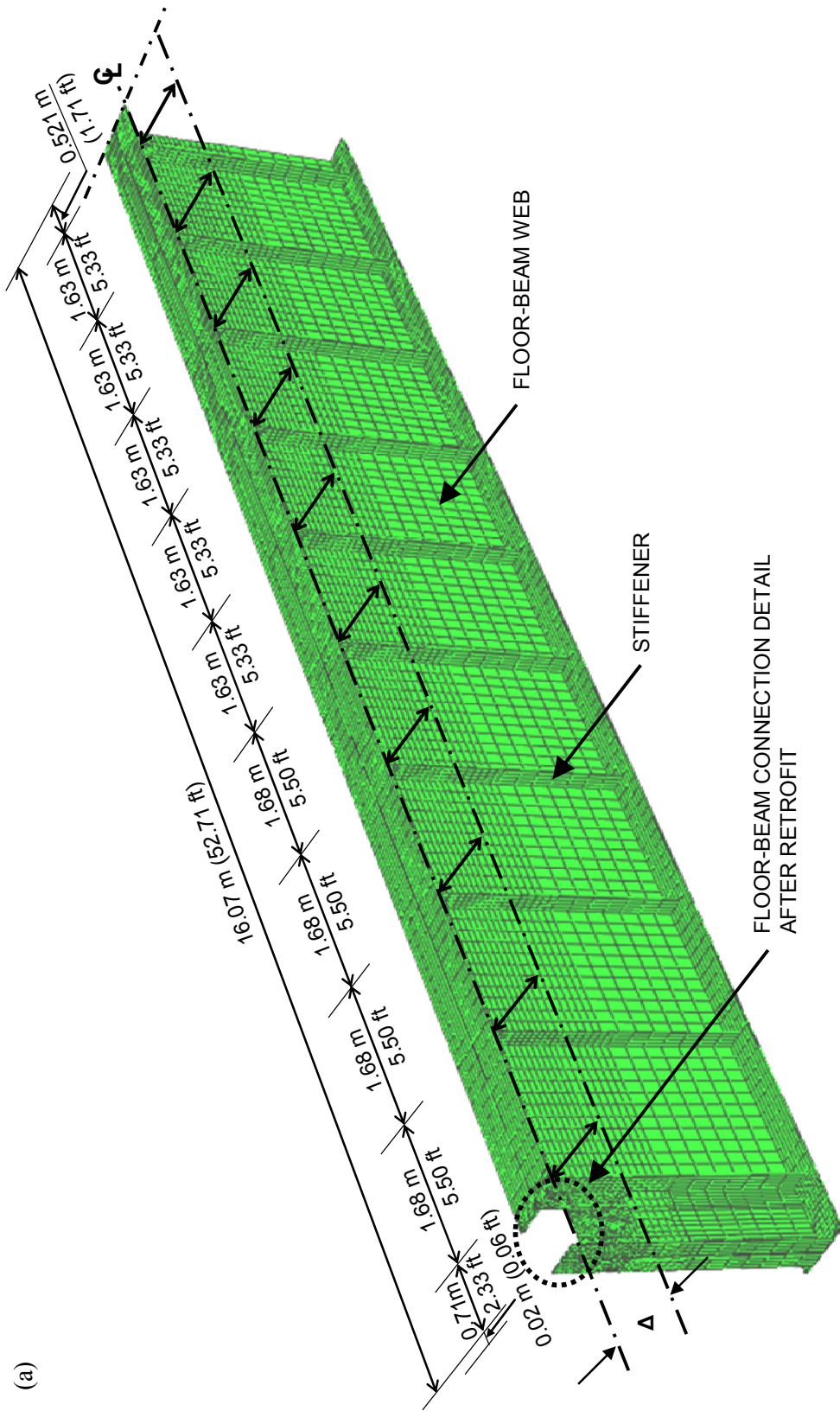
Note: HORIZONTAL DISPLACEMENT, Δ = 2.54 mm (0.1 in)

(a) FE modeling

(a)

269

(b)
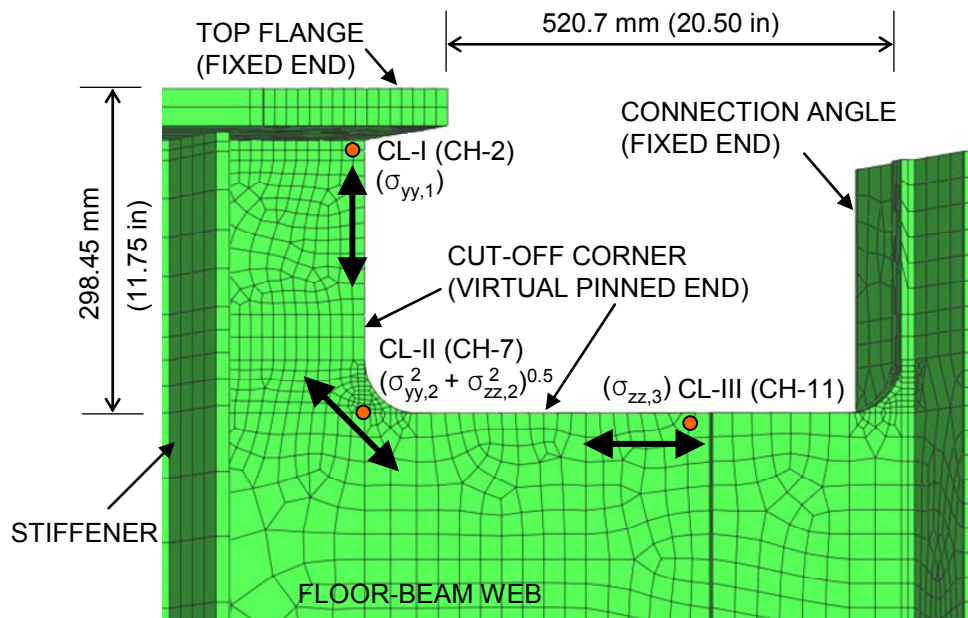
CH-2: FIELD = 44.8 MPa, FEM1 = 42.0 MPa, and FEM2 = 42.2 MPa
CH-7: FIELD = 37.2 MPa, FEM1 = 34.6 MPa, and FEM2 = 35.3 MPa
CH-11: FIELD = 48.3 MPa, FEM1 = 58.3 MPa, and FEM2 = 57.3 MPa

Note: FIELD and FEM1 results in relative displacement of 2.54 mm (0.1 in), and FEM2 results in corresponding horizontal force of 0.98 kN (0.22 kips)

(b) critical locations

Figure 5-17   FE modeling verification of a floor-beam connection detail after retrofit.
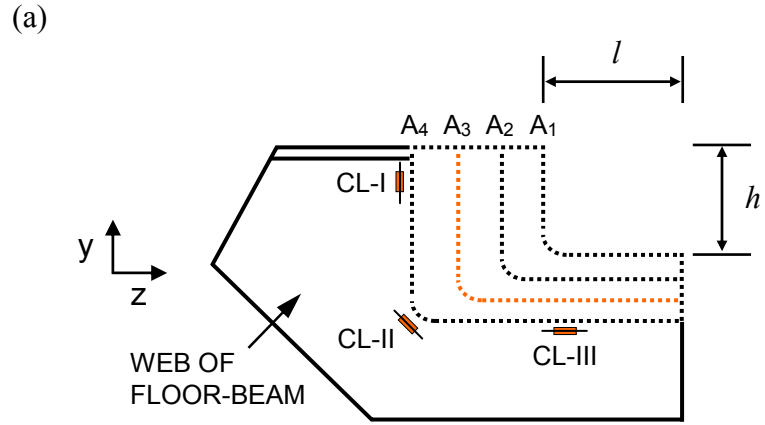
Note: A₃ is the actual retrofit size

(a) cut-off area details
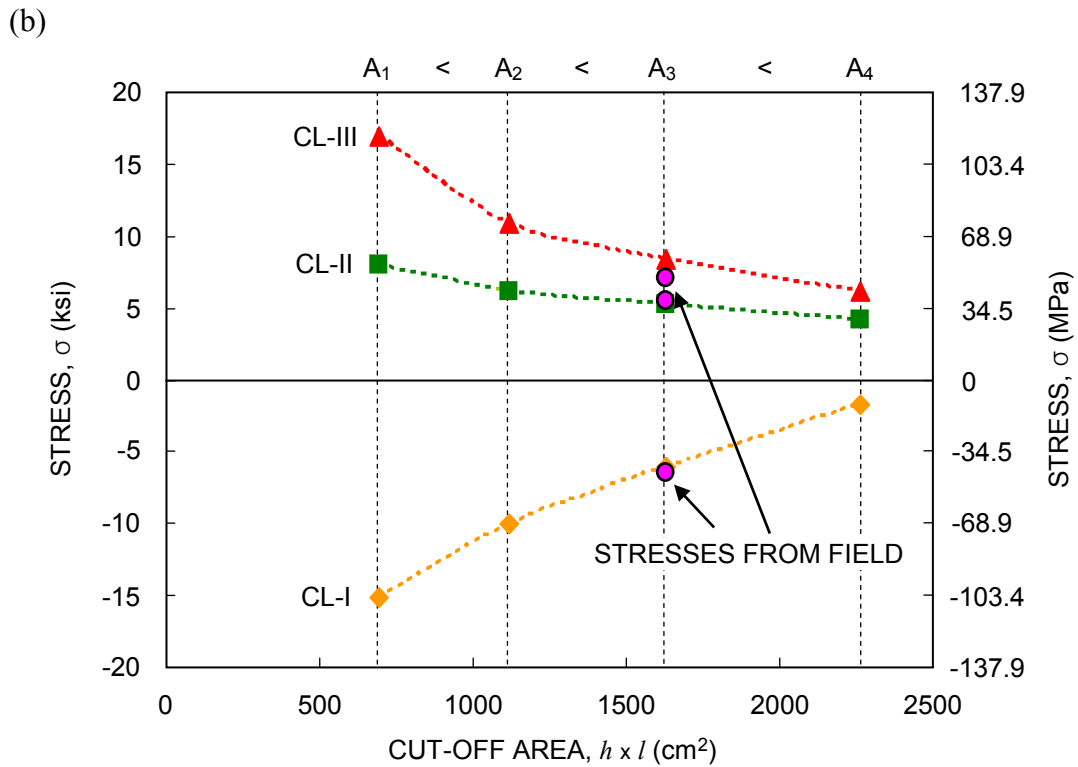
(b) stress distributions at critical locations

Figure 5-18   Sensitivity study according to the cut-off area ($h \times l$).
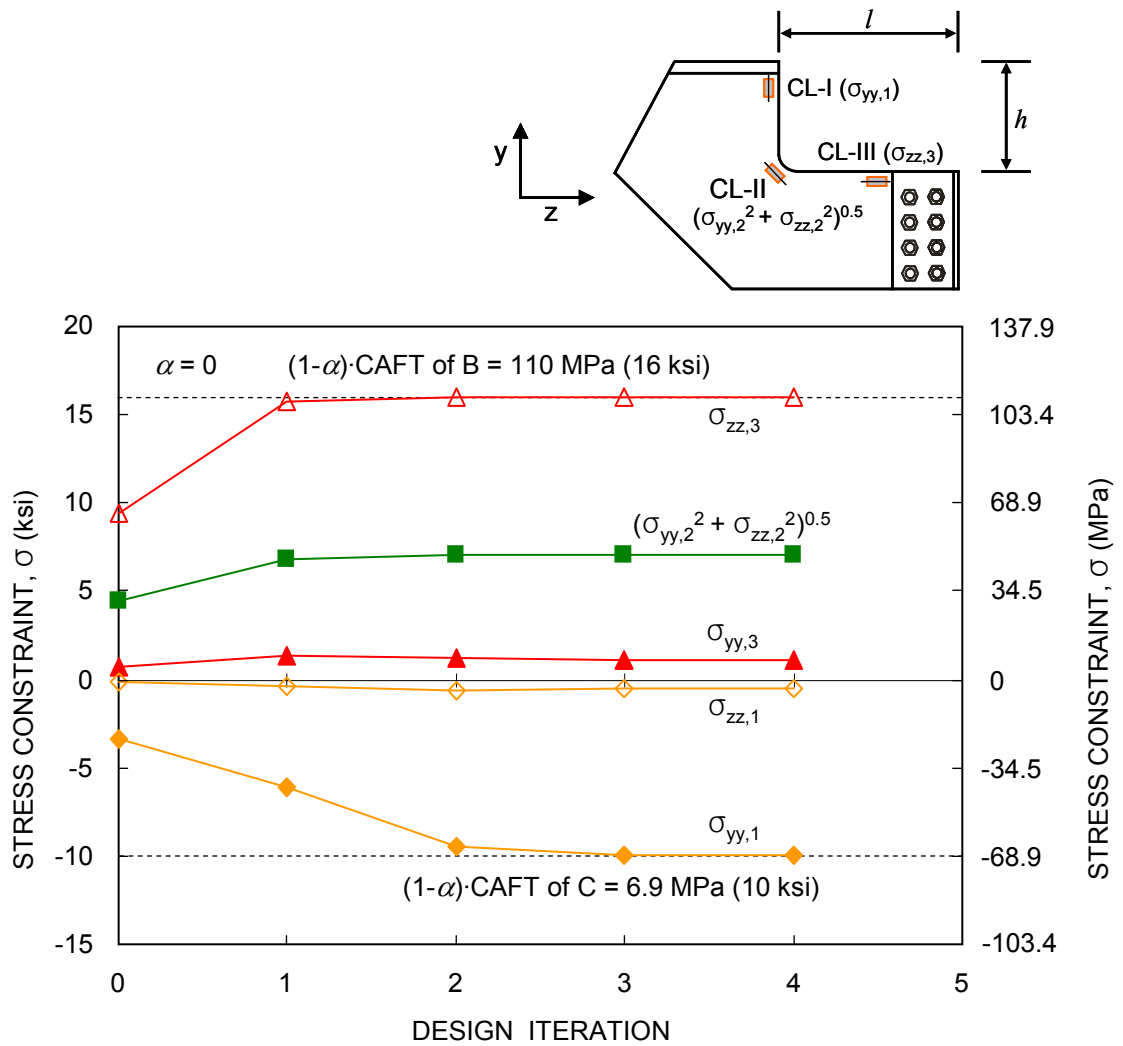
Figure 5-19   Design iteration for given inequality stress constraints.

(a)

(a) objective space

(b)
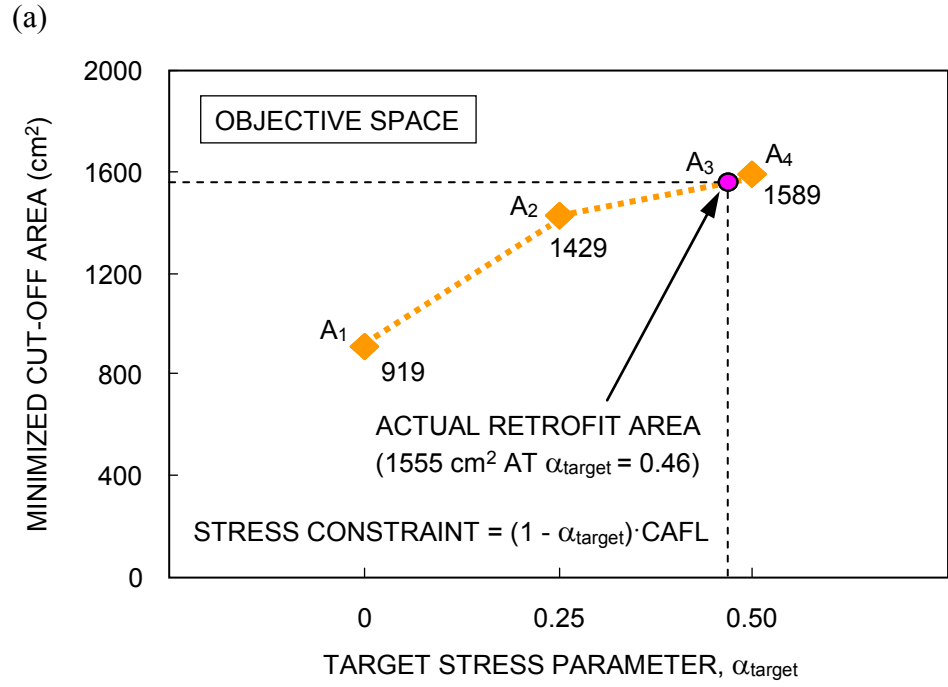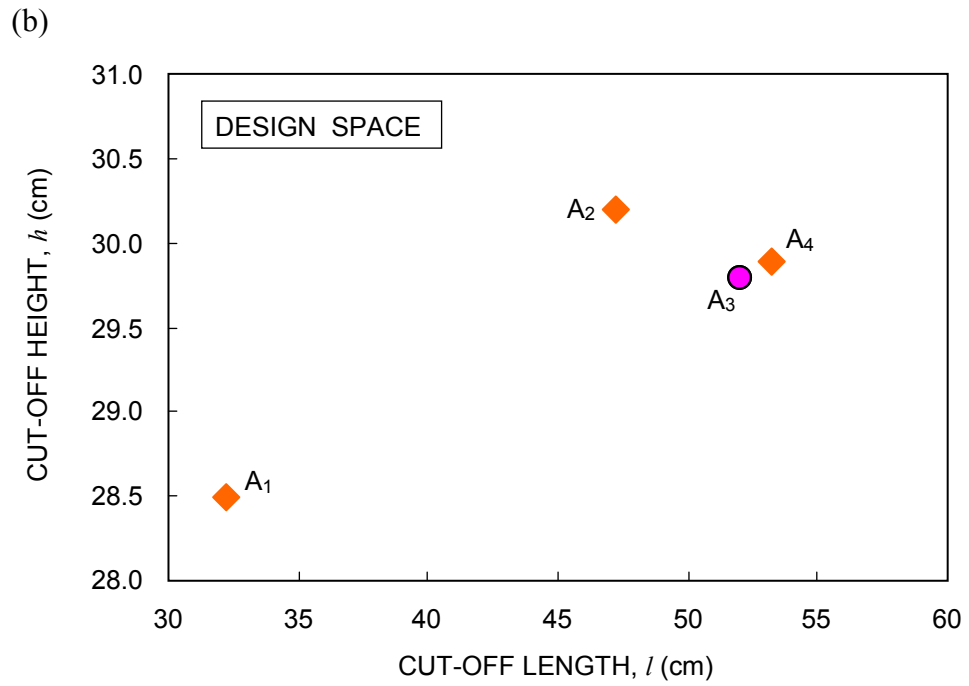
(b) design space

Figure 5-20 Retrofit design optimization.

273

(a)

(a) relationship between S_{re} and N_{total}

(b)
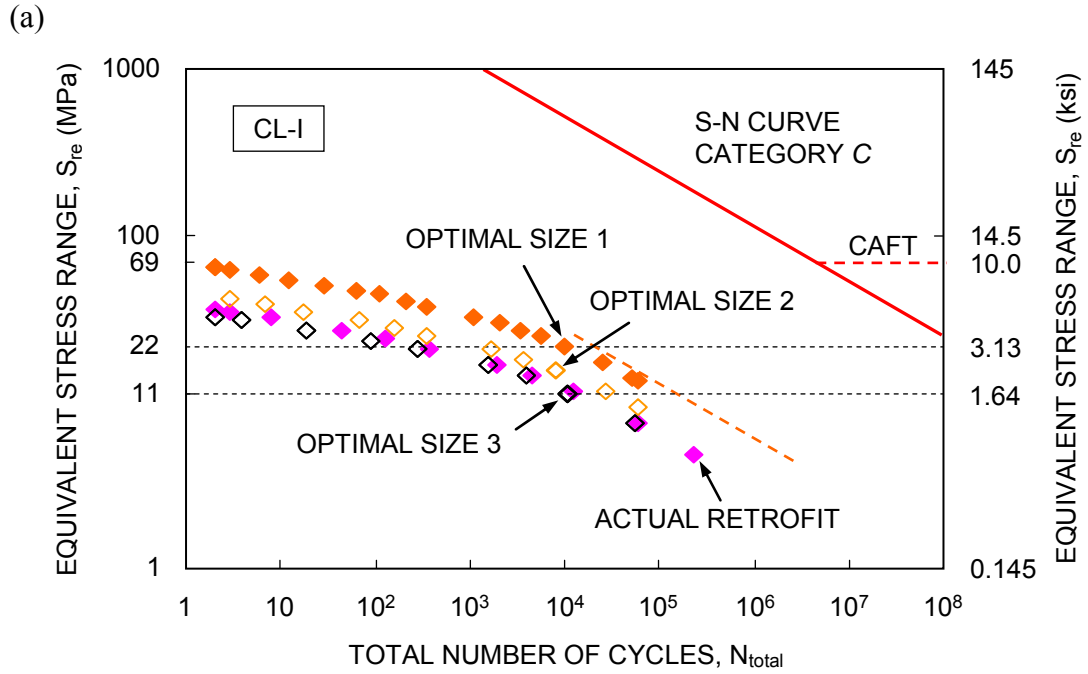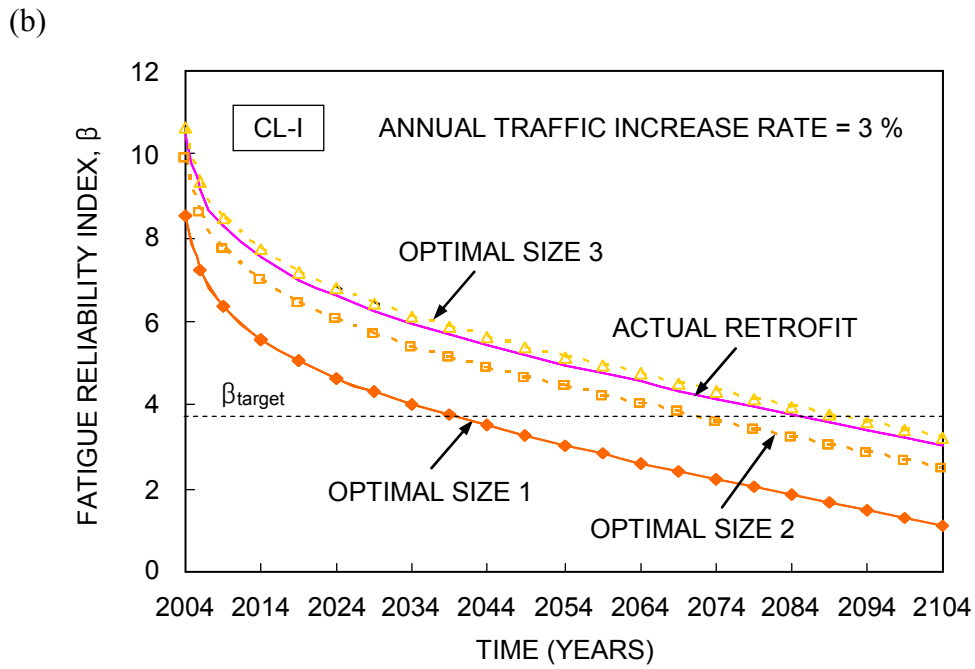
(b) fatigue reliability profiles

Figure 5-21   Fatigue reliability assessment of optimal cut-off areas at CL-I.

274

(a)

(a) relationship between S_{re} and N_{total}

(b)
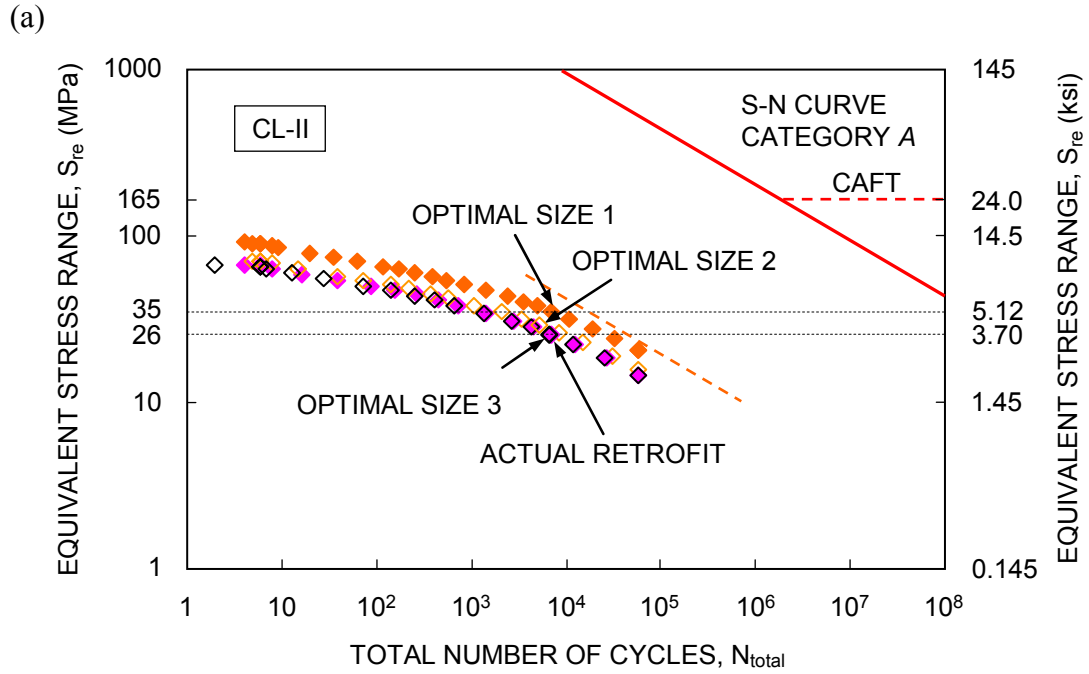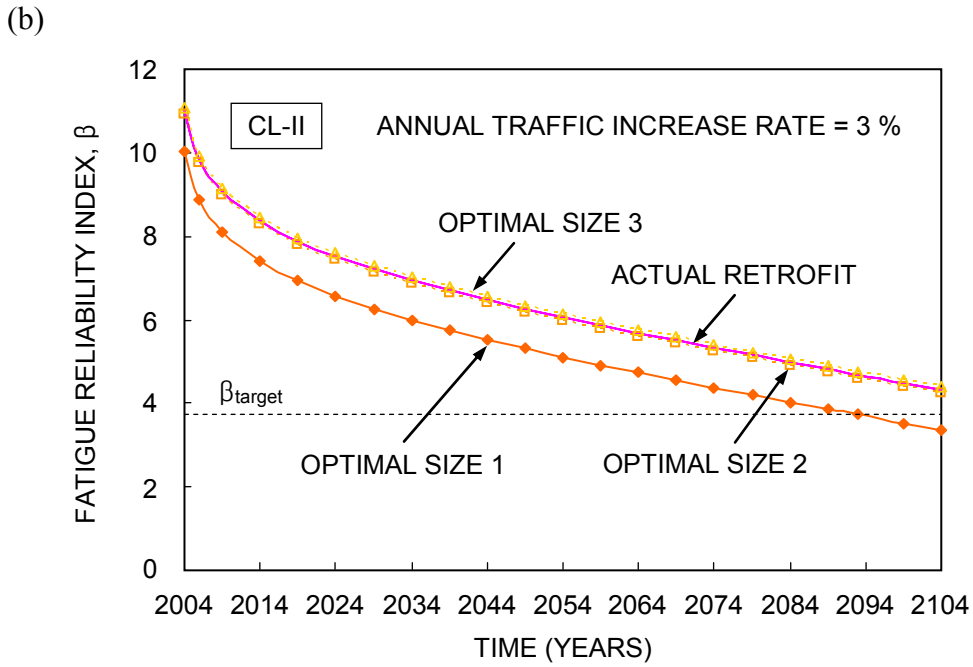
(b) fatigue reliability profiles

Figure 5-22   Fatigue reliability assessment of optimal cut-off areas at CL-II.

275

(a)

(a) relationship between S_{re} and N_{total}

(b)
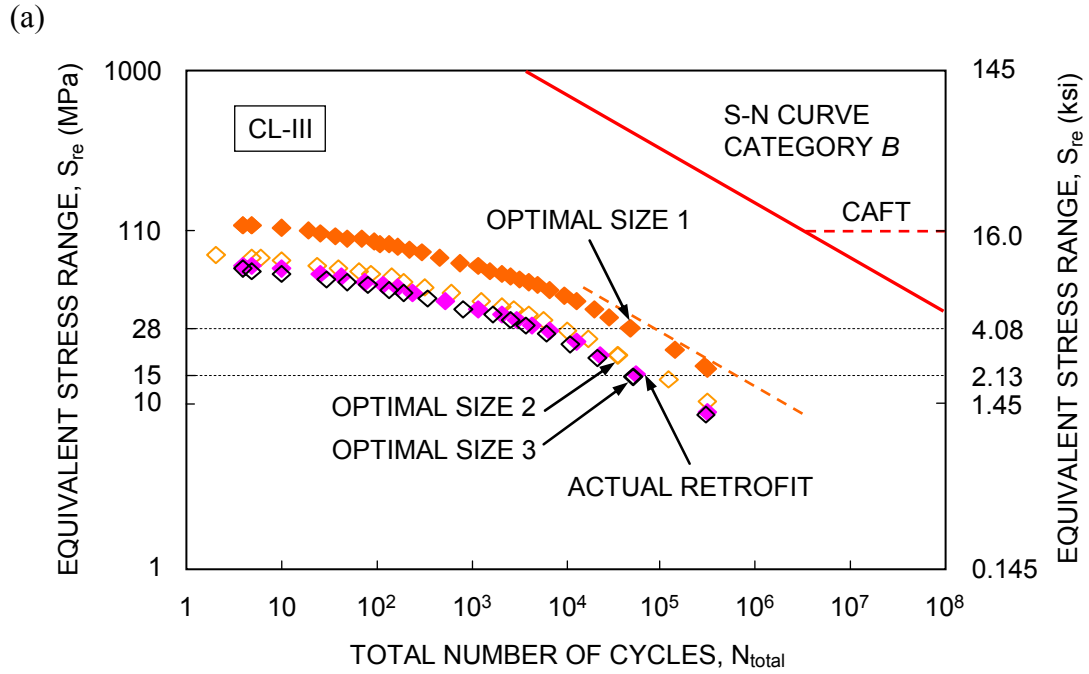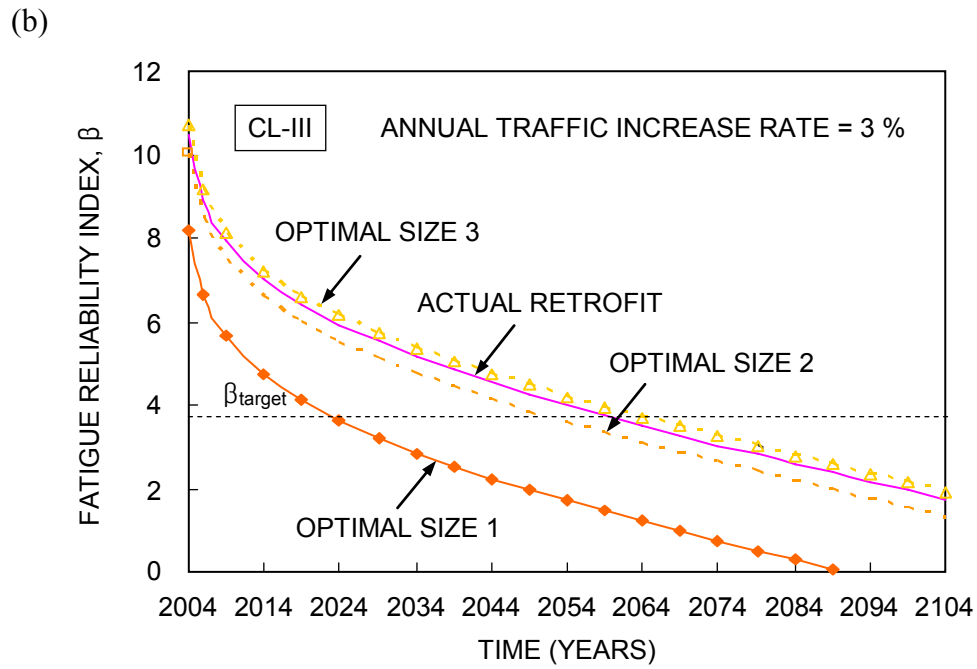
(b) fatigue reliability profiles

Figure 5-23   Fatigue reliability assessment of optimal cut-off areas at CL-III.
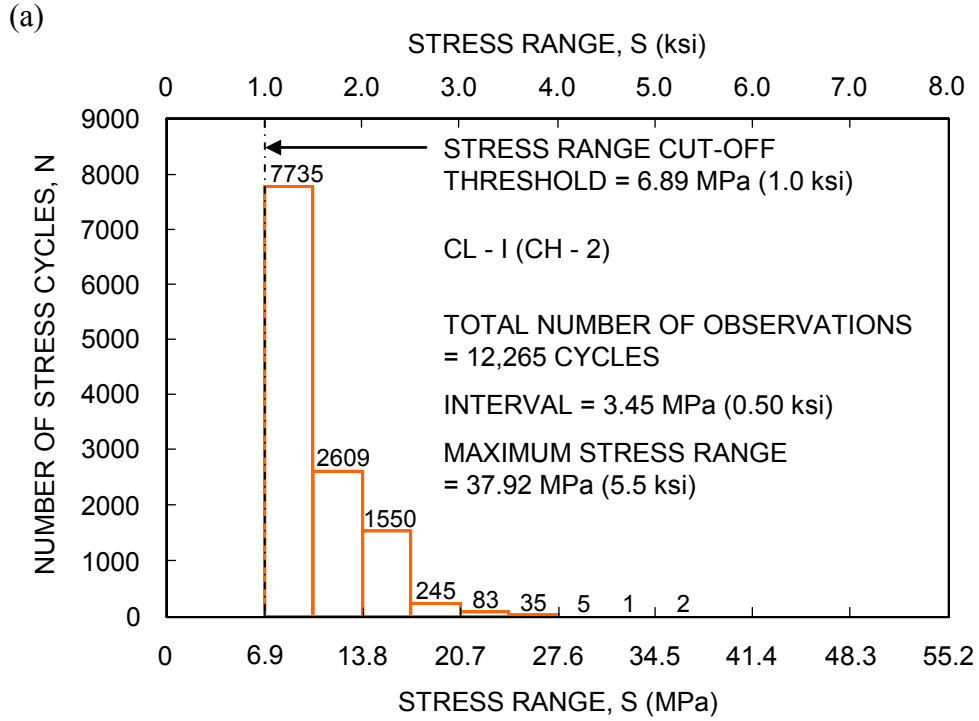
(a) at CL-I (CH-2)

(b) at CL-II (CH-7)

277

(c)
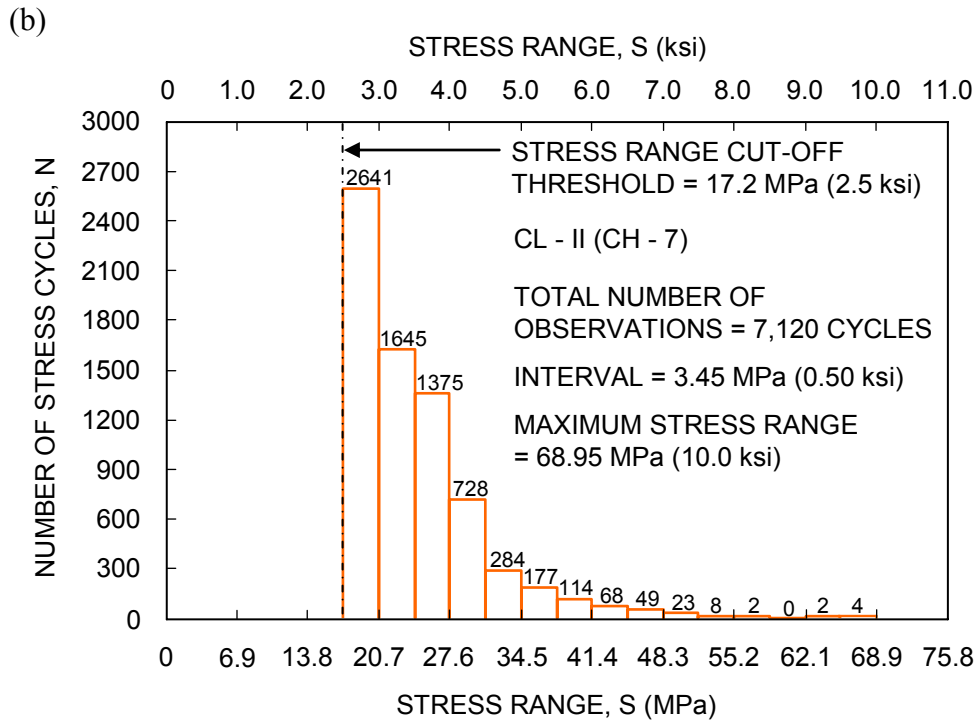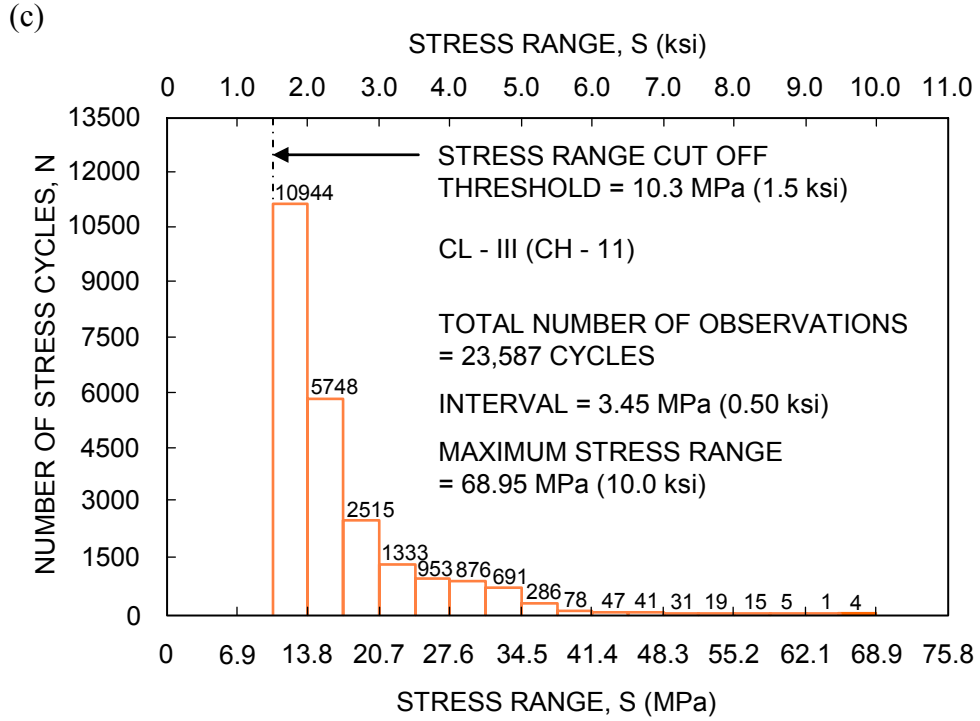
Figure 5-24   Stress-range bin histograms at the three critical locations.

(a)

(a) at CL-I

(b)

(b) at CL-II

279
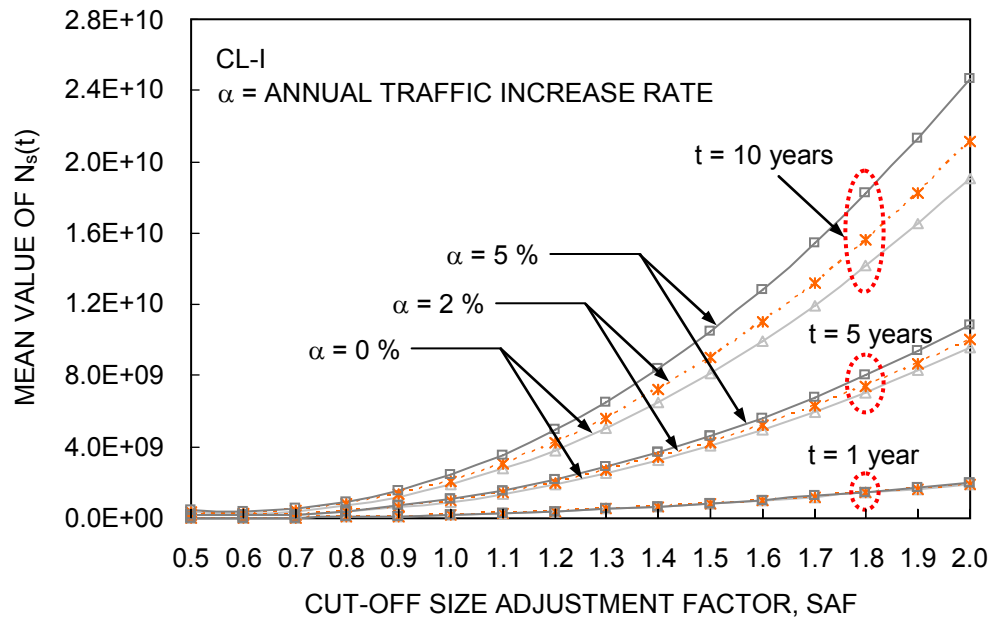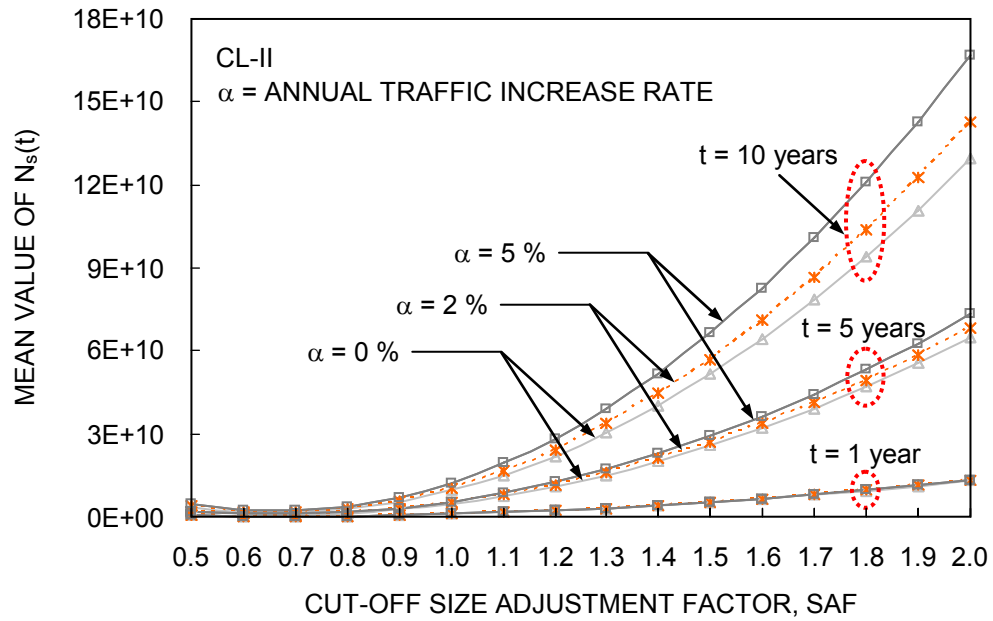
(c)
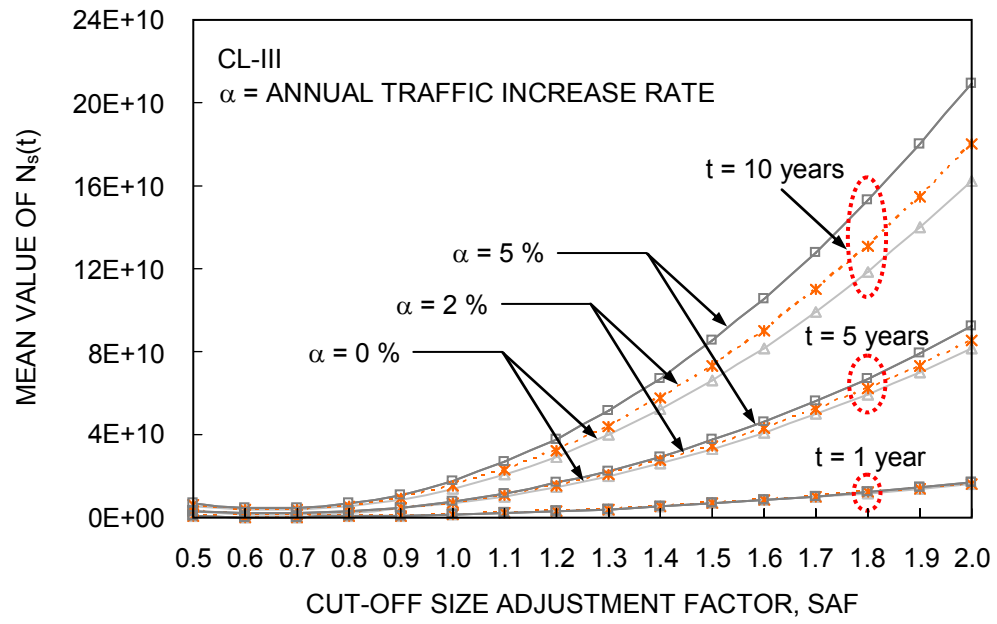
(c) at CL-III

Figure 5-25   Relationship between $\overline{N}_s(t)$ and SAF at the three critical locations.
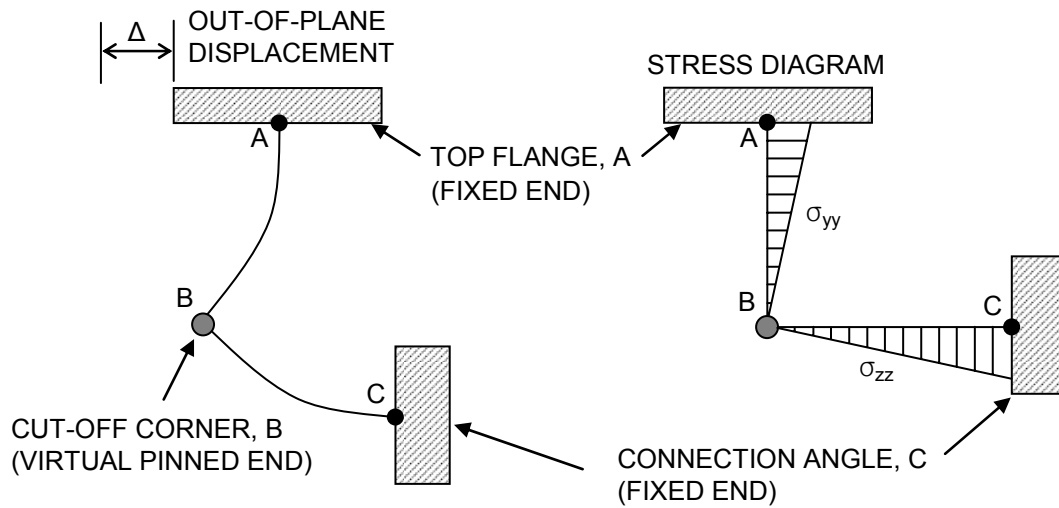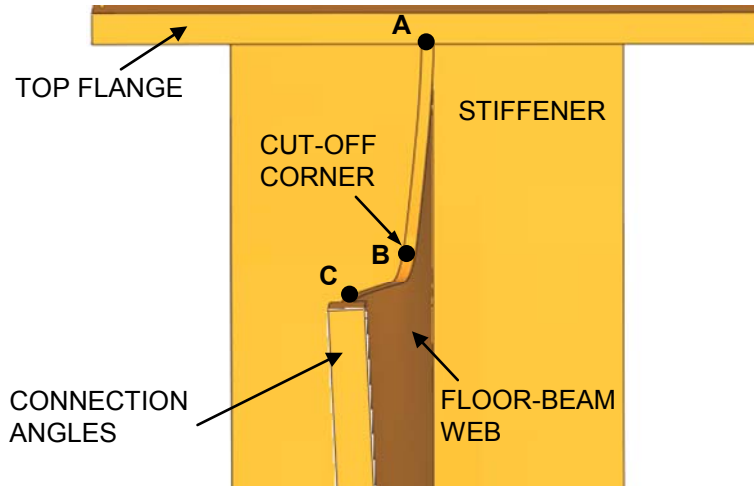
Figure 5-26   Modeling the structural behavior of the floor-beam system after retrofit.
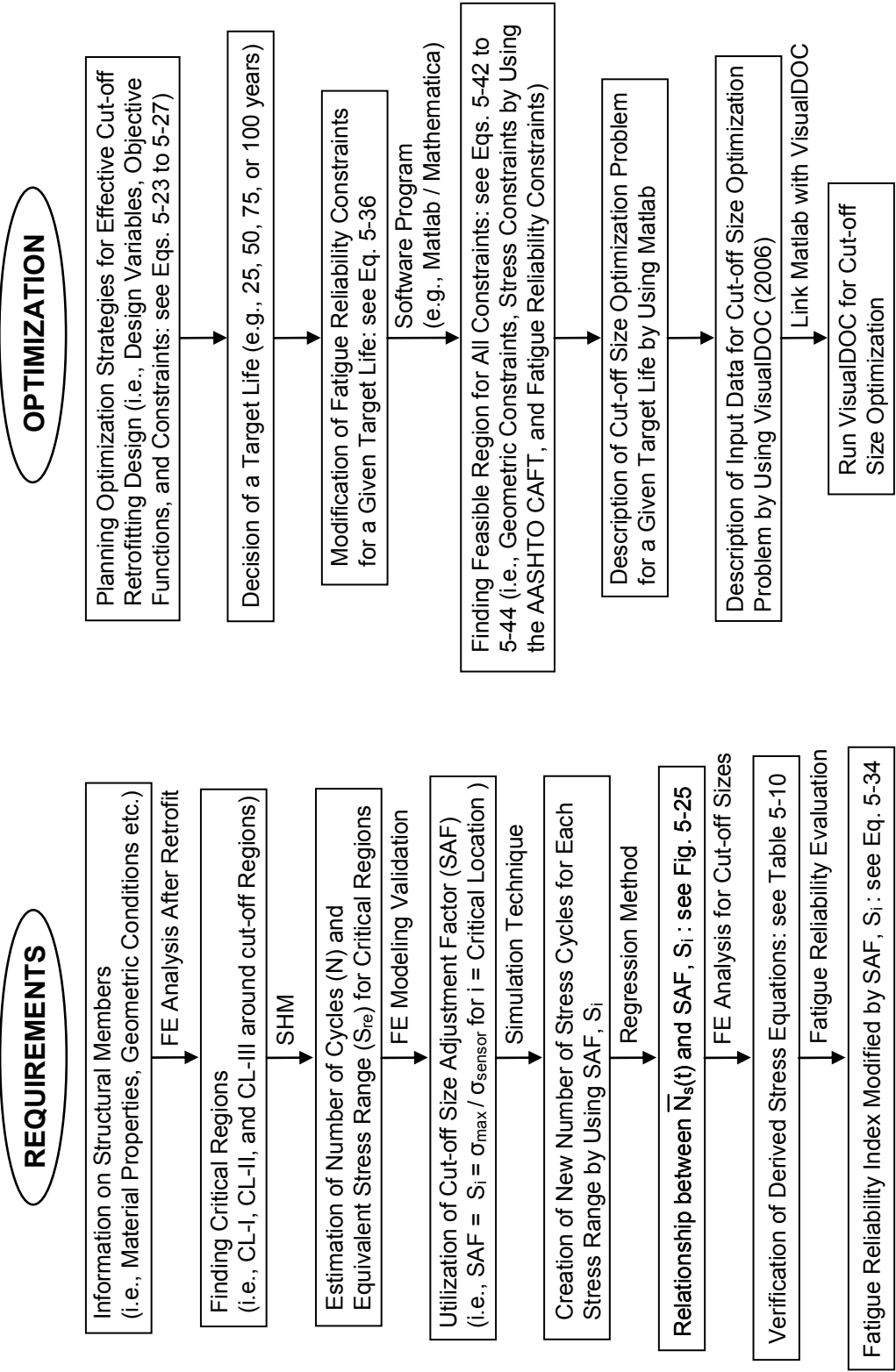
Figure 5-27 Flowchart for solving the proposed bi-objective optimization problem.

REQUIREMENTS

Information on Structural Members
(i.e., Material Properties, Geometric Conditions etc.)

FE Analysis After Retrofit

Finding Critical Regions
(i.e., CL-I, CL-II, and CL-III around cut-off Regions)

SHM

Estimation of Number of Cycles (N) and
Equivalent Stress Range (S_{re}) for Critical Regions

FE Modeling Validation

Utilization of Cut-off Size Adjustment Factor (SAF)
(i.e., SAF = $S_i = \sigma_{max} / \sigma_{sensor}$ for i = Critical Location)

Simulation Technique

Creation of New Number of Stress Cycles for Each
Stress Range by Using SAF, S_i

Regression Method

Relationship between $\overline{N}_s(t)$ and SAF, S_i : see Fig. 5-25

FE Analysis for Cut-off Sizes

Verification of Derived Stress Equations: see Table 5-10

Fatigue Reliability Evaluation

Fatigue Reliability Index Modified by SAF, S_i : see Eq. 5-34

OPTIMIZATION

Planning Optimization Strategies for Effective Cut-off
Retrofitting Design (i.e., Design Variables, Objective
Functions, and Constraints: see Eqs. 5-23 to 5-27)

Decision of a Target Life (e.g., 25, 50, 75, or 100 years)

Modification of Fatigue Reliability Constraints
for a Given Target Life: see Eq. 5-36

Software Program
(e.g., Matlab / Mathematica)

Finding Feasible Region for All Constraints: see Eqs. 5-42 to
5-44 (i.e., Geometric Constraints, Stress Constraints by Using
the AASHTO CAFT, and Fatigue Reliability Constraints)

Description of Cut-off Size Optimization Problem
for a Given Target Life by Using Matlab

Description of Input Data for Cut-off Size Optimization
Problem by Using VisualDOC (2006)

Link Matlab with VisualDOC

Run VisualDOC for Cut-off
Size Optimization

(a) a target life of 25 years with Δ_h = 2.54 mm (0.1 in) and α = 5%

(b) a target life of 50 years with Δ_h = 2.54 mm (0.1 in) and α = 5%

283
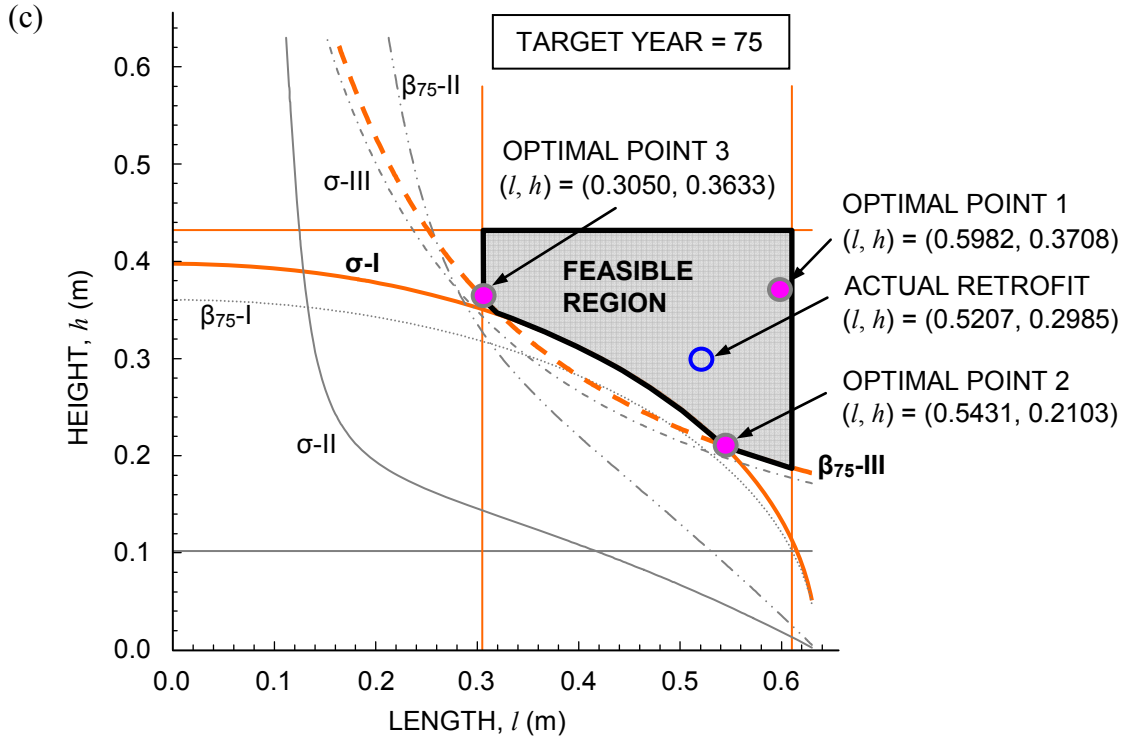
(c) a target life of 75 years with $\Delta_h = 2.54$ mm (0.1 in) and $\alpha = 5\%$
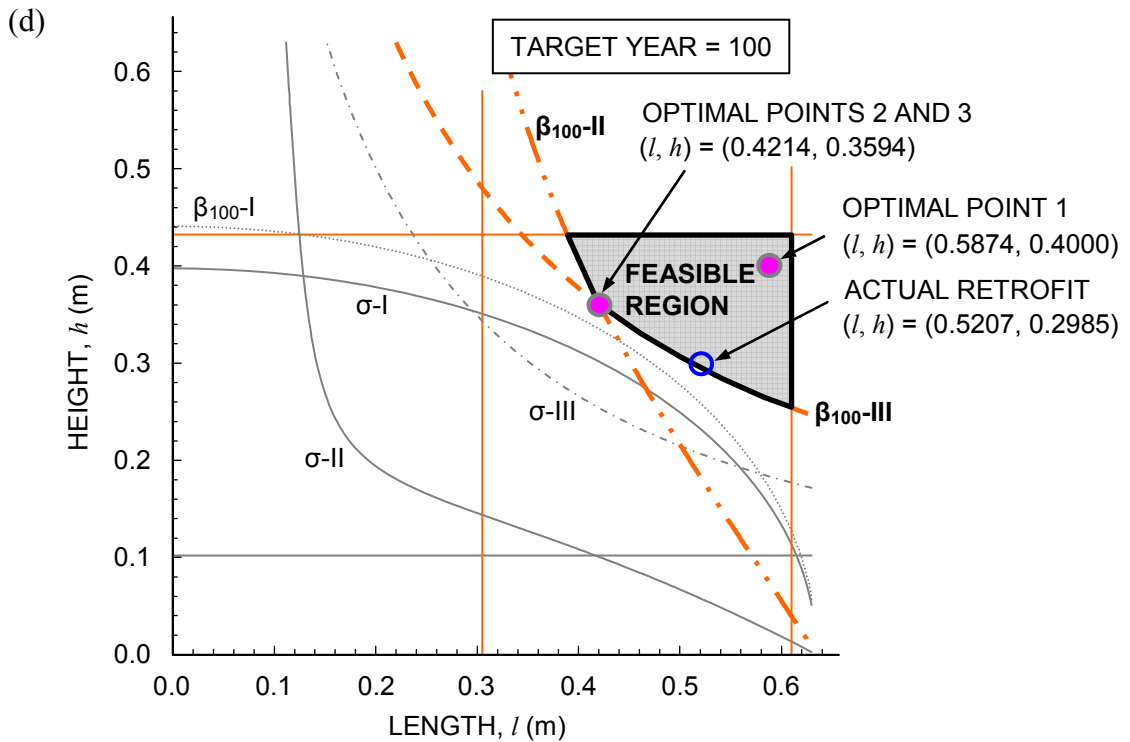
(d) a target life of 100 years with $\Delta_h = 2.54$ mm (0.1 in) and $\alpha = 5\%$

Figure 5-28   Feasible region and optimal cut-off sizes for different target lives.
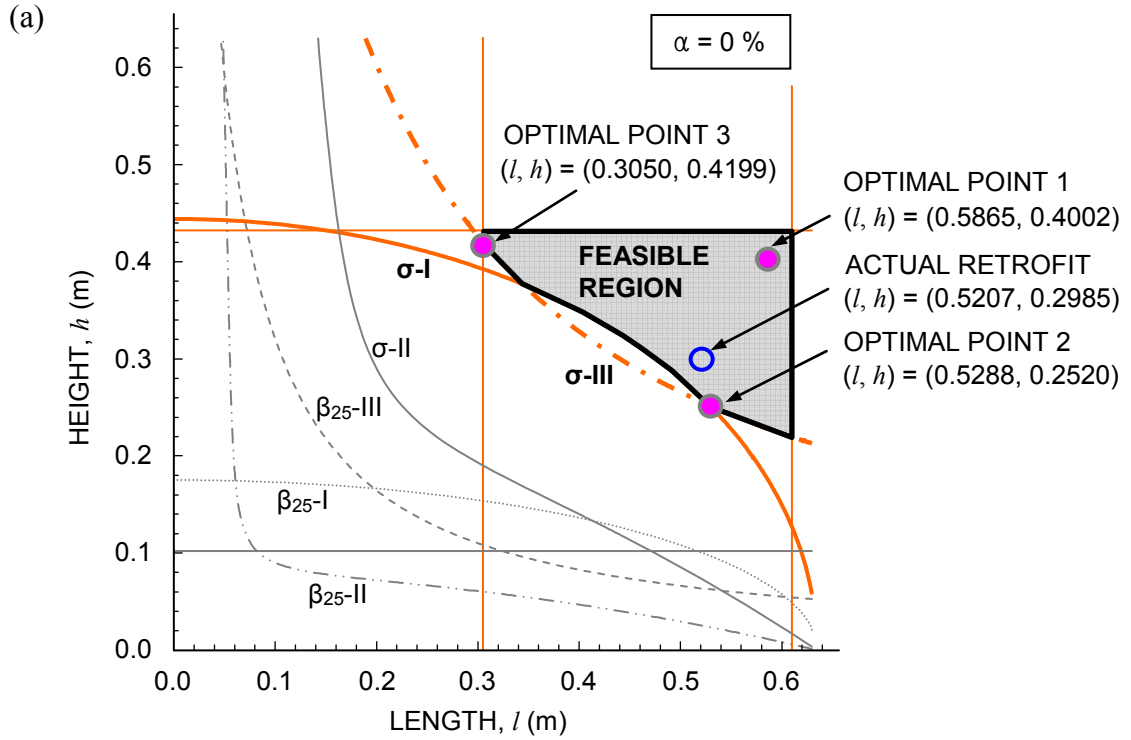
(a) $\alpha = 0\%$ and $\Delta_h = 3.175$ mm (0.125 in) for a target life of 25 years
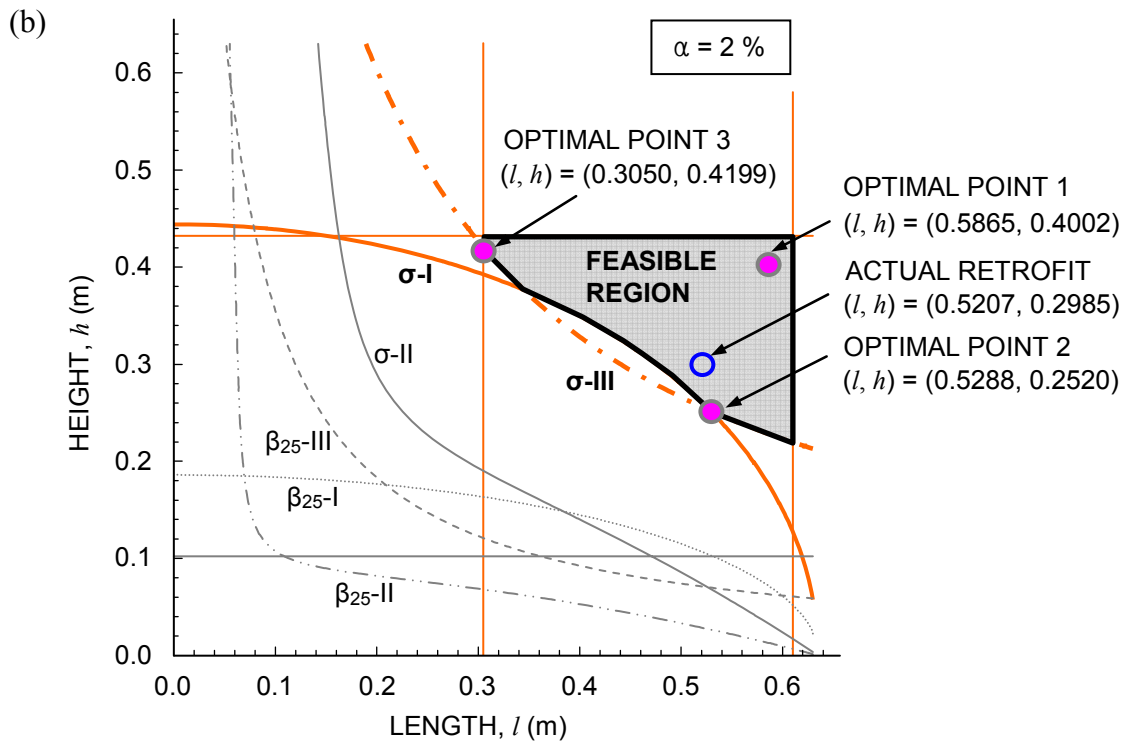
(b) $\alpha = 2\%$ and $\Delta_h = 3.175$ mm (0.125 in) for a target life of 25 years

(c)
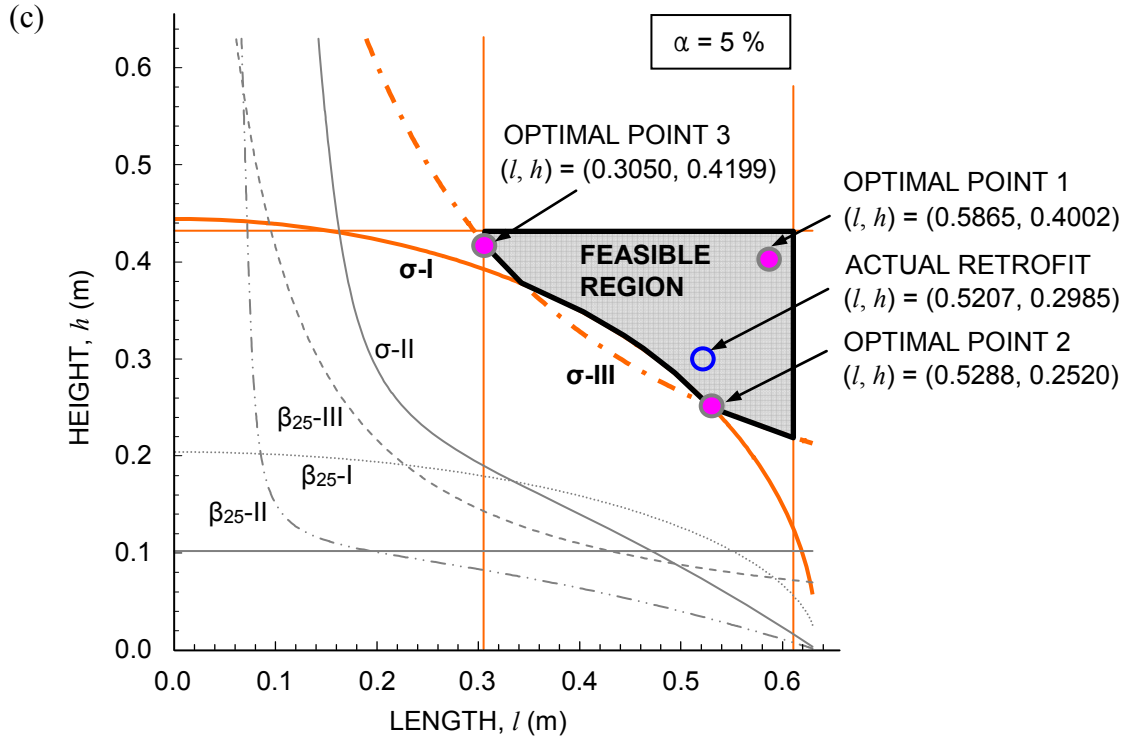
(c) $\alpha = 5\%$ and $\Delta_h = 3.175$ mm (0.125 in) for a target life of 25 years

Figure 5-29   Feasible region and optimal cut-off sizes for different α.
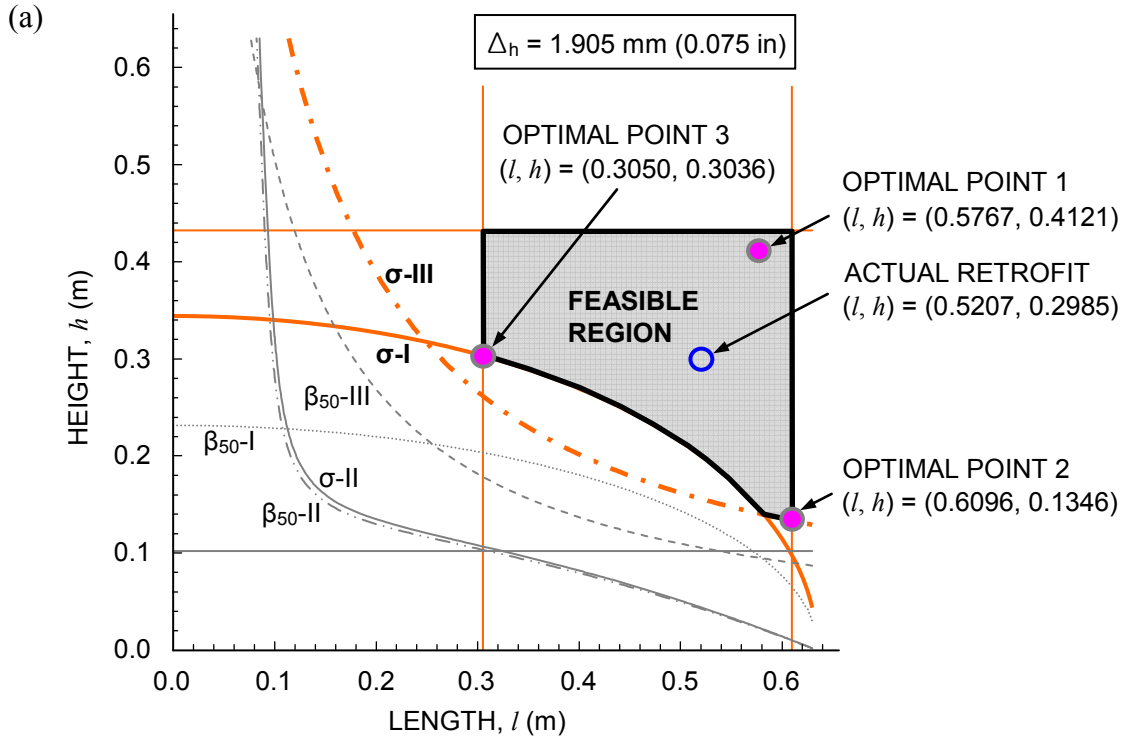
(a) Δ_h = 1.905 mm (0.075 in) and α = 2% for a target life of 50 years
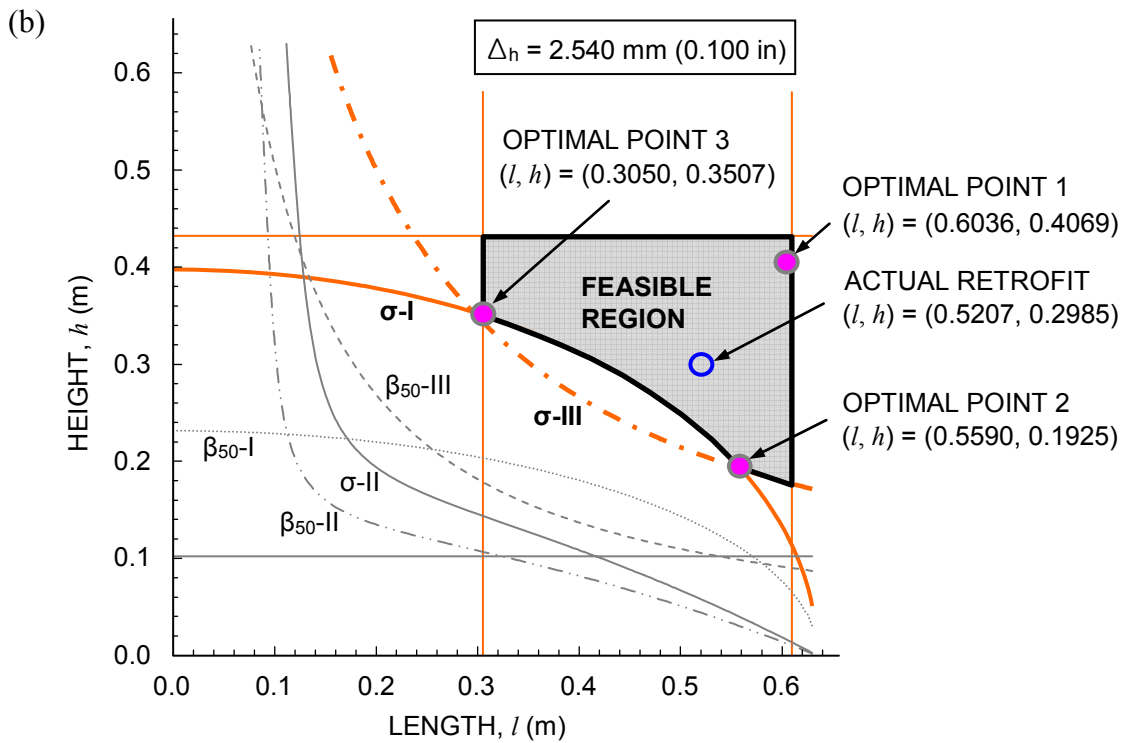
(b) Δ_h = 2.540 mm (0.100 in) and α = 2% for a target life of 50 years
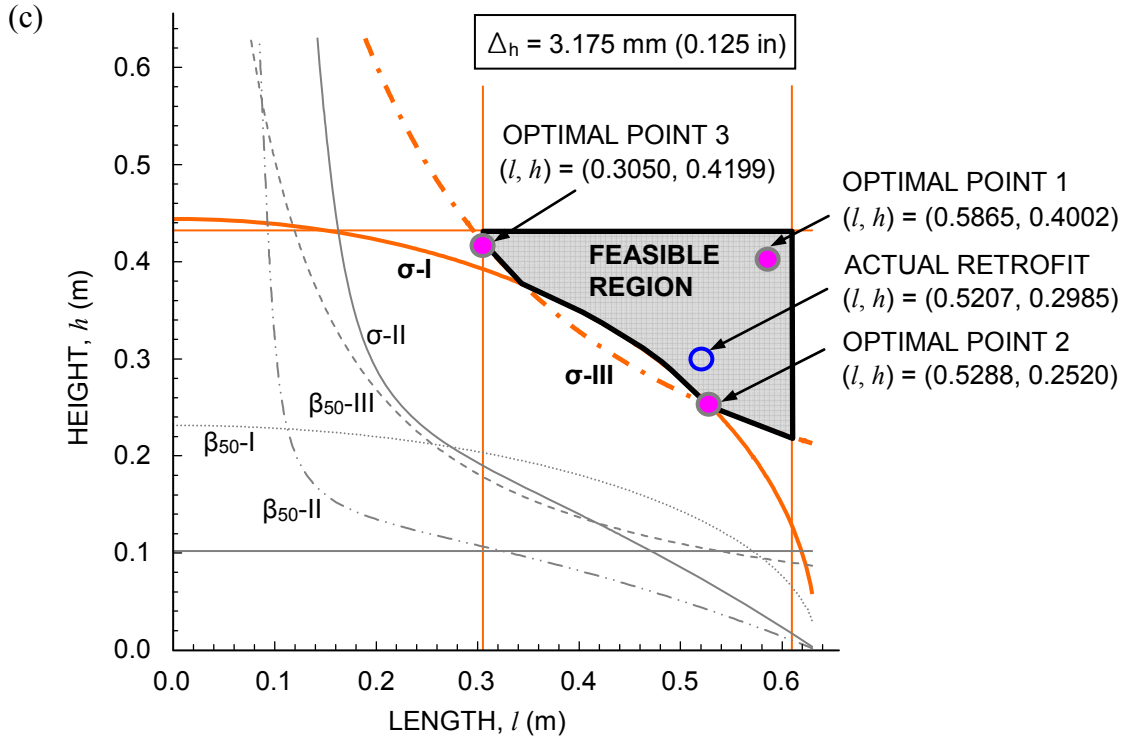
(c) Δ_h = 3.175 mm (0.125 in) and α = 2% for a target life of 50 years
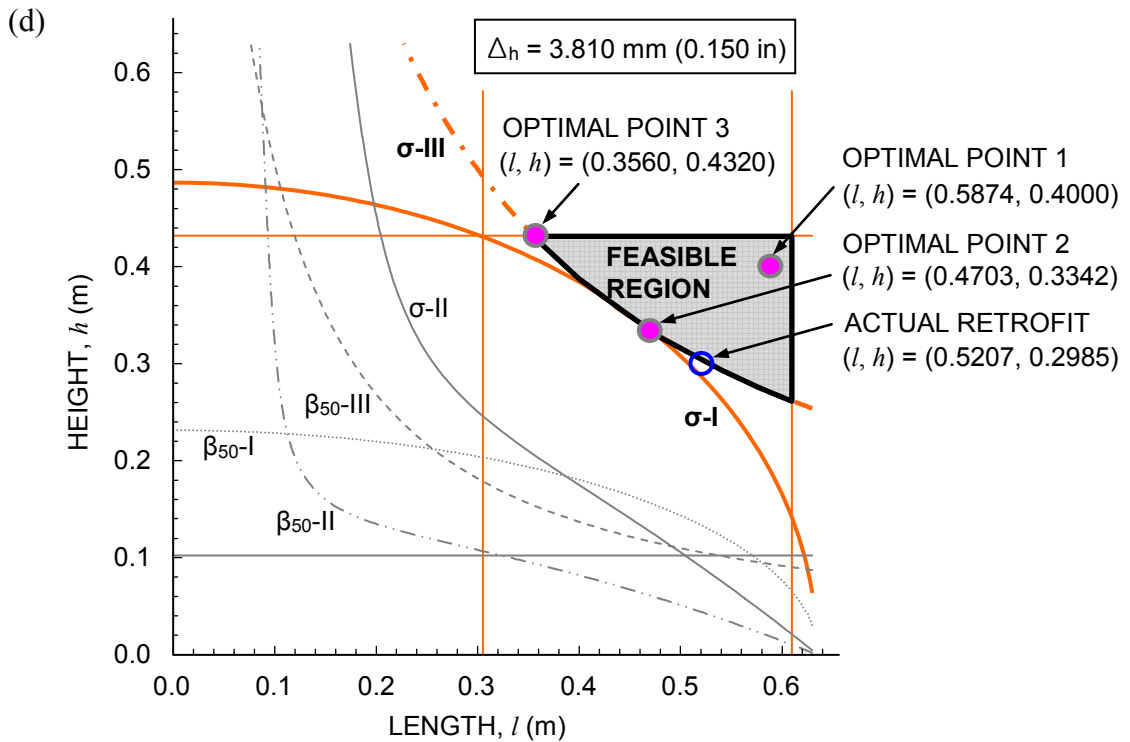
(d) Δ_h = 3.810 mm (0.150 in) and α = 2% for a target life of 50 years

Figure 5-30   Feasible region and optimal cut-off sizes for different Δ_h.

(a)

(a) objective space

(b)
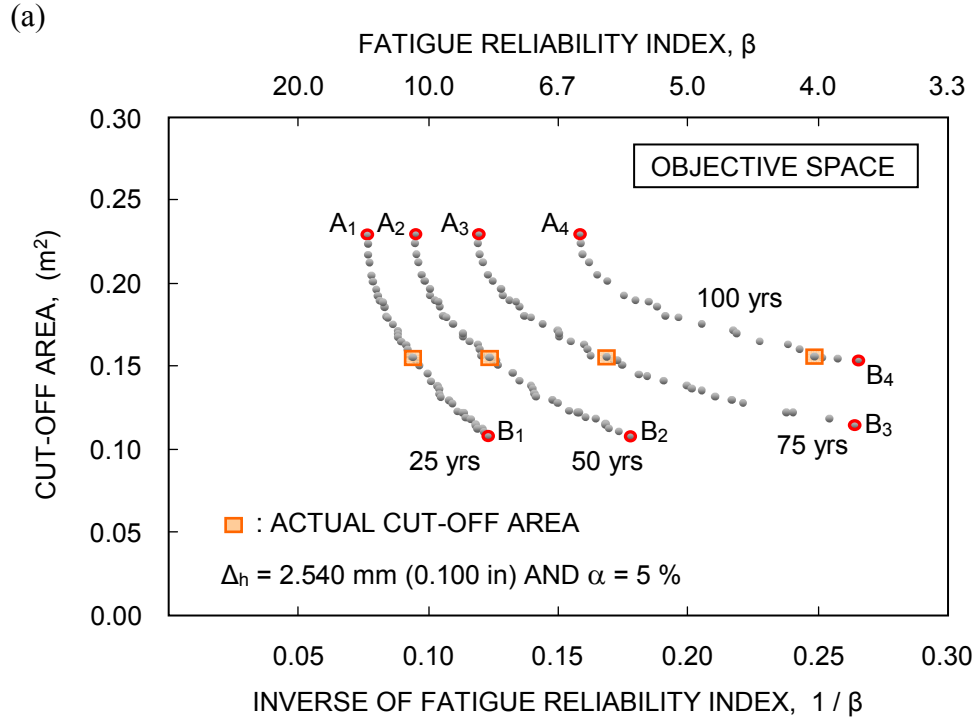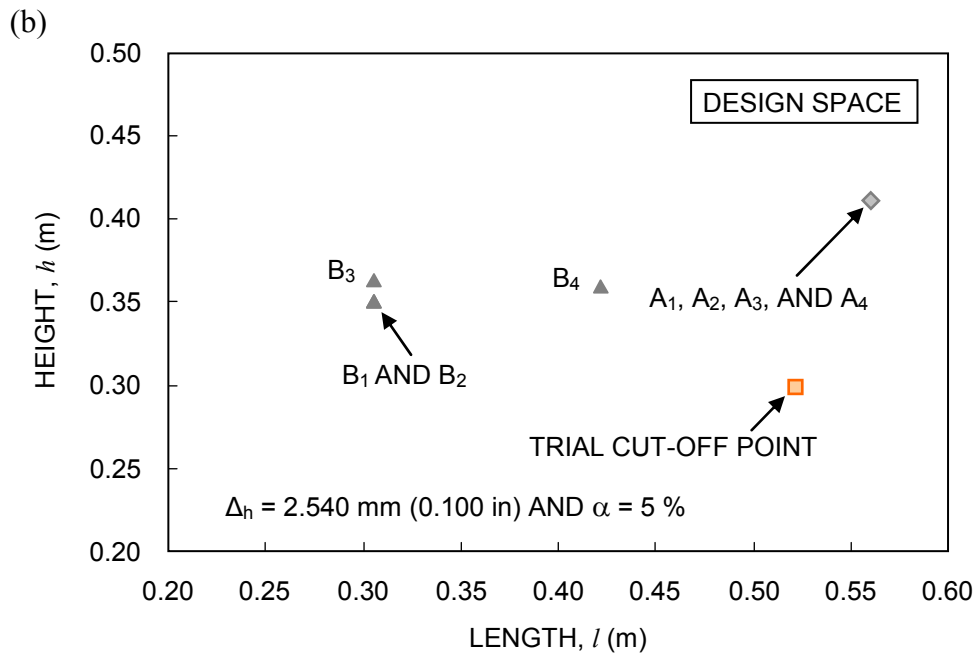
(b) design space

Figure 5-31   Pareto optimal solutions with $\Delta_h = 2.540$ mm (0.100 in) and $\alpha = 5\%$.

(a)

(a) objective space

(b)
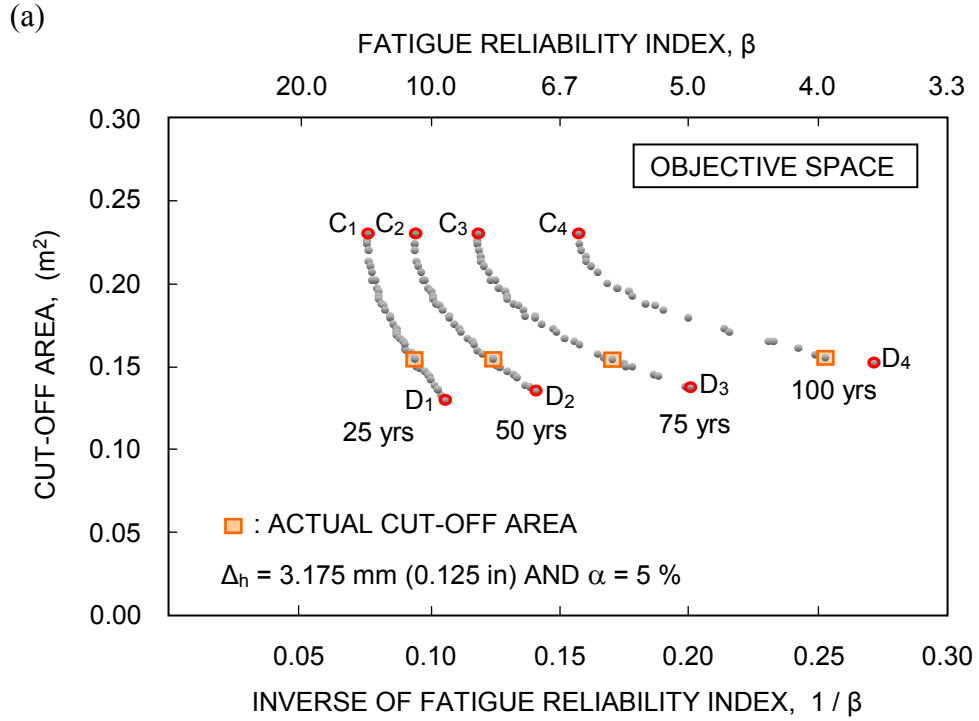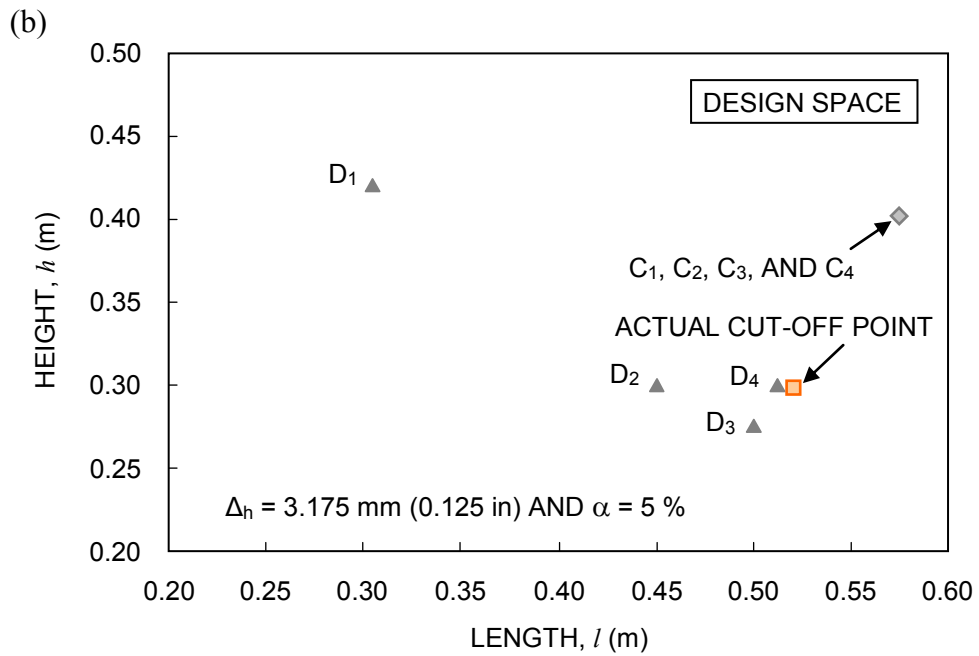
(b) design space

Figure 5-32   Pareto optimal solutions with $\Delta_h = 3.175$ mm (0.125 in) and $\alpha = 5\%$.
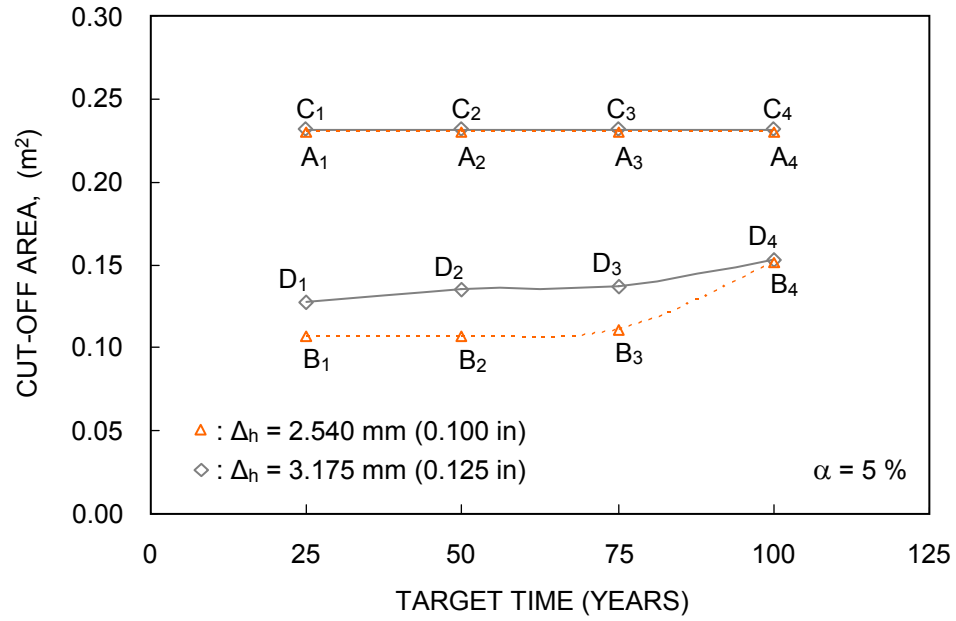
Figure 5-33   Time-dependent minimum cut-off areas for all Pareto optimal solutions indicated in Figure 5-31 and Figure 5-32.
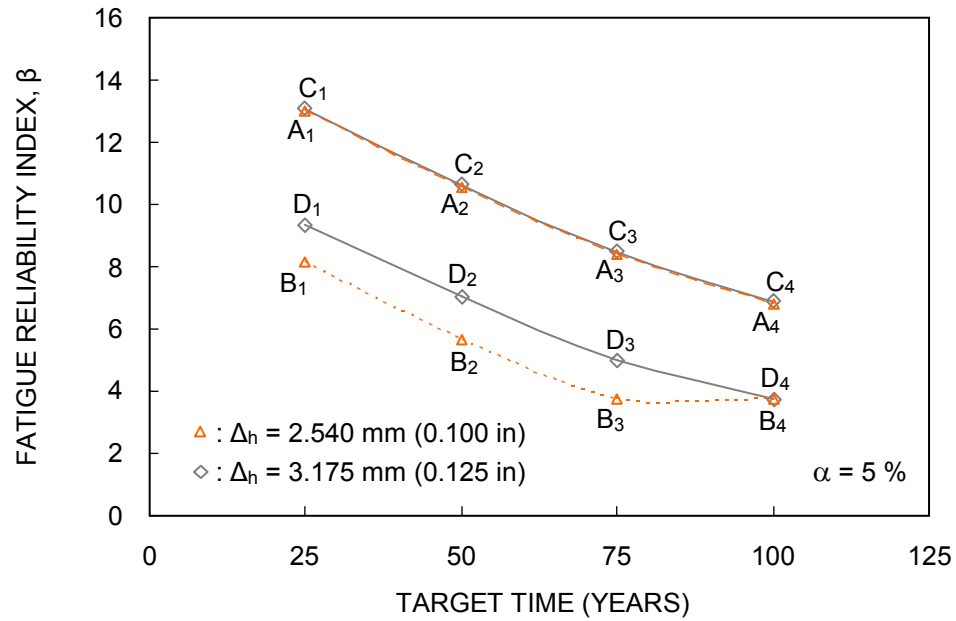
Figure 5-34   Time-dependent maximum reliability indices for all Pareto optimal solutions indicated in Figure 5-31 and Figure 5-32.

CHAPTER 6

SHIP RELIABILITY-BASED LIFE-CYCLE MANAGEMENT

6.1 INTRODUCTION

This chapter describes the reliability-based life-cycle management of ship structures for fatigue failure mode under uncertainties associated with fatigue resistance and sea load effects. In order to allocate limited financial resources to balance lifetime reliability of ship structural details and life-cycle cost using single-objective or multi-objective optimization are taken into account. The estimated fatigue reliability profile of the aluminum ship treated in Chapter 4 is incorporated into life-cycle cost optimization problem in order to find the optimal inspection and repair interventions.

The development of high-speed and high performance aluminum ships has recently become an important issue in aiming to improve ship operation capabilities. In design, many requirements for improving ship safety and serviceability are imposed based on current specifications. These requirements have to be satisfied to avoid sudden fatigue failure during voyages. However, in absence of reliable information on safety and durability of light-weight materials like aluminum (Hess III 2007), accurate assessment and/or prediction of structural performance for fatigue is not possible. Optimal planning for lifetime structural maintenance interventions has to include uncertainty. For this reason, a probabilistic methodology for lifetime structural performance assessment and management has to be developed in a rational way. A practical approach is herein proposed for planning the lifetime optimum maintenance

interventions on aluminum ships considering the time-dependent fatigue reliability, fatigue damage, and life-cycle cost.

Various optimal maintenance approaches under uncertainty have been proposed (Madsen et al. 1991, Frangopol & Liu 2007, Okasha & Frangopol 2009 and 2010, Frangopol 2010, and Kim & Frangopol 2010). Minimizing the life-cycle cost under given constraints on structural performance has been formulated. The computed single optimal solution may be severely limited when considering multiple objectives (Liu & Frangopol 2005). Alternatively, if a multi-criteria optimization approach is employed, multiple optimal solutions for decision makers will be provided. In this context, Kim & Frangopol (2010) presented a methodology for bi-objective optimization by minimizing the total monitoring cost and maximizing the availability of monitoring data. A multi-objective optimization approach is herein addressed. Three competing objectives are taken into account in this optimization: (a) minimization of the life-cycle maintenance cost, (b) maximization of the time-dependent fatigue reliability, and (c) minimization of the time-dependent fatigue damage.

Section 6.2 addresses briefly fatigue life assessment of aluminum ship structures based on the reliability method proposed in Chapter 4. In Section 6.3, applicable lifetime maintenance strategies are described for planning inspection and repair interventions of aluminum ships. Section 6.4 deals with life-cycle cost analysis as well as optimization problems considering the single- and multi-objective. In Section 6.5, the proposed approaches are illustrated on an aluminum ship detail consisting of welded attachments. The associated summaries and conclusions are

293

described in Section 6.6.

6.2 FATIGUE LIFE ASSESSMENT OF ALUMINUM SHIP STRUCTURES

As presented in Chapter 4, lifetime fatigue performance of aluminum ship structures can be possibly quantified using the reliability method based on the bi-linear *S-N* approach and available sea loading information which can be obtained from simulation programs, sea trial tests, model tests, and/or monitoring (Kwon et al. 2010). Clearly, the established bi-linear *S-N* curve for the aluminum fatigue detail (i.e., category 22 – 3.2) based on Eurocode 9 (1999) was used in terms of fatigue resistance (see Figure 4-10), while the established stress-range bin histogram data was used in terms of fatigue loading (see Figure 4-12).

If stress-range bin histogram data from a long-term monitoring program are available and reliable, fatigue damage, *D*, for a given service time can be obtained by using $D = \Sigma\, n_i / N_i$. In the following, fatigue damage rate from the calculated *D* in every service year is estimated by using linear regression for the entire service life. The corresponding equation for the fatigue damage index is approximated by:

$$D(t) = a \cdot t \tag{6-1}$$

where *a* = fatigue damage rate at service time *t* which can be estimated from stress-range bin histogram data. Theoretically, the fatigue damage ratio, *D*, is equal to 1.0 at failure. In the optimization problem, *D(t)* can be considered as an objective to be minimized, indicating the time-dependent fatigue damage index.

For fatigue life assessment of aluminum ships, the time-dependent reliability

analysis is performed with a well-defined fatigue limit-state function. Based on the *S-N* approach and Miner's rule (1945), the defined limit-state equations in Chapter 4 (see Eqs. 4-10(a) and (b)) are used in this study. Complete descriptions for all deterministic parameters and random variables were presented in Table 4-4 and Table 4-5. Based on the functions $g_1(t)$ or $g_2(t)$, the fatigue reliability analysis is obtained by using the reliability software RELSYS (Estes & Frangopol 1998). S_{re} can be treated as a Weibull random variable with COV(S_{re}) = 0.1, while other random variables (i.e., Δ, A, and e) can be considered as lognormal (see Table 4-4). The flowchart for the fatigue reliability assessment is also found in Figure 6-1. In this chapter, the estimated fatigue reliability profile will be used to provide possibilities for scheduling proper maintenance-management interventions including inspection, monitoring and repair during the entire ship service life.

6.3   LIFETIME MAINTENANCE STRATEGIES

During the fatigue deterioration processes of aluminum ship structures, proper repair interventions have to be made if fatigue cracks are detected by inspection. Otherwise, the associated fatigue details will eventually experience structural failure. In general, the detectability of fatigue damage depends on the quality of the non-destructive evaluation (NDE) method associated with probability of detection (PoD) of cracks. In this study, if $D(t)$ is greater than or equal to 0.3 (see Eq. 6-1), the detection is assumed to be perfect (i.e., PoD[$D(t) \geq 0.3$] = 1.0). It is noted that the predefined value $D(t) = 0.3$ is arbitrary. It practically depends on the type of inspection method employed. When detecting a fatigue crack, it is assumed that a repair follows

the inspection. Regular or irregular time intervals for inspections and repairs are considered in life-cycle cost analysis (LCA).

For planning lifetime structural maintenance strategies, establishing a fatigue reliability/damage profile is useful for estimating the time-dependent structural performance and damage levels during the anticipated service life. For a particular case, the profile is presented in Figure 6-2(a). After 17.23 years, the fatigue damage, D, reaches 1.0. This corresponds to the lower target reliability index, $\beta_{target,1}$ = 3.12. Conservatively, the upper target reliability index, $\beta_{target,2}$ = 4.41 can be selected to keep the structural performance in a safer level, implying that the cumulative number of cycles does not exceed N_D. In this case, the corresponding fatigue damage index is 0.473. As indicated in Figure 6-2(a), the fatigue reliability profile can have a transition gap at a certain time (as $N_t(t) = N_D = 5 \times 10^6$ cycles). This gap is due to the fact that, at this time, the S-N curve changes its slope (i.e., from m_1 to m_2), and also the value of fatigue detail coefficient changes from A_1 to A_2. Such a gap is highly sensitive to two statistical values, $COV(S_{re})$ and $COV(e)$. When fatigue damage is detected by an inspection, a proper repair is undertaken with the assumption that it will influence fatigue strength after repair. In this study, as shown in Figure 6-2(b), two strategies are considered by using the strength factor, R_I, as follows:

$$R_{I,1}(t) = R_{initial} - 0.8 \cdot D(t) \quad \text{for Strategy 1} \tag{6-2a}$$

$$R_{I,2}(t) = 0.3 \qquad\qquad \text{for Strategy 2} \tag{6-2b}$$

where $R_{initial}$ = fatigue strength in intact state = 1.0.

After repair, the original number of stress cycles, N, is updated by using Eq. 6-3(a) or (b). R_I is used to estimate the new number of cycles as

$$N_{new} = \frac{A}{[(1+R_I) \cdot R]^m} = 365 \cdot \alpha \cdot N_{avg} \cdot t_{new} \tag{6-3}$$

6.4 LIFE-CYCLE COST ANALYSIS AND OPTIMIZATION

In design or in-service, lifetime structural maintenance planning for future inspections and repairs of ship structures is made to prevent fatigue failure during voyages. The time-dependent structural performance quantified from the fatigue reliability analysis offers possibilities to plan lifetime maintenance-management interventions. A methodology is proposed herein to find optimum maintenance solutions (i.e., optimal inspection and repair times, optimal fatigue damage threshold) associated with inspections and repairs. For this purpose, life-cycle cost analysis as well as single- and multi-objective optimizations are performed considering the time-dependent fatigue reliability, fatigue damage, and/or life-cycle cost. As indicated previously, three competing objectives are taken into consideration in the multi-objective optimization: (a) minimization of the life-cycle maintenance cost (min C_{MT}), (b) maximization of the minimum fatigue reliability (max β_{min}), and (c) minimization of the maximum fatigue damage (min D_{max}). The procedure is summarized in the flowchart of Figure 6-1.

6.4.1 Life-Cycle Cost Analysis (LCA)

In a cost-effective manner, LCA can be carried out to find optimal

maintenance interventions. Different inspection and repair strategies are associated with different expected total life-cycle costs. A successful lifetime management planning is achieved by the minimization of the expected life-cycle cost. In particular, fatigue damage threshold, D_{th}, which directly affects the life-cycle cost, is used as an important variable in the LCA. For prescribed fatigue damage thresholds (i.e., $0.3 \leq D_{th} < 1.0$), repair actions are taken to improve structural performance. Regular and irregular time intervals for inspections and repairs can be used in the LCA approach.

In the design or assessment processes, LCA is implemented for the decision making process. In this study, LCA is formulated considering inspection, repair and expected failure cost using the discount rate of money r. For given D_{th}, the expected total remaining life-cycle cost, C_{ET}, is calculated as (Estes & Frangopol 2005 and Frangopol et al. 1997b):

$$C_{ET} = C_{INS} + C_{REP} + C_F \tag{6-4a}$$

$$C_{INS} = \sum_{i=1}^{k} \frac{C_{ins}}{(1+r)^{t_i}} \tag{6-4b}$$

$$C_{REP} = \sum_{j=1}^{n} \frac{C_{rep}}{(1+r)^{t_j}} \tag{6-4c}$$

$$C_F = C_f \cdot \max[P_f(t)] \tag{6-4d}$$

where C_{INS} and C_{REP} = discounted inspection and repair costs, respectively; C_f and C_F = failure and expected failure costs, respectively; k and n = number of inspections and repairs, respectively; C_{ins} and C_{rep} = undiscounted inspection and repair costs, respectively; t_i and t_j = application time of inspection and repair interventions i and j,

respectively; max $[P_f(t)]$ = maximum probability of failure during anticipated service life; and r = discount rate of money which is assumed 2%.

6.4.2 Single- or Multi-Objective Optimization

The life-cycle cost optimization is herein addressed by using single- and multi-objective approaches. The objective function C_{ET} is minimized in the single-objective optimization (see Eq. 6-5), while the expected maintenance cost, C_{MT}, fatigue reliability index, β, and fatigue damage index, D, are used as criteria for the multi-objective optimization (see Eq. 6-6). In both optimization problems, design variables are inspection and repair times. The number of lifetime inspections (e.g., k = 2, 3, 4, and 5) and both time and fatigue reliability constraints are specified.

The single- and multi-objective optimization problems are formulated as:

Find the design variables: inspection and repair times, t_i and t_j

(i) for the single-objective optimization

$$\min C_{ET}(t) = \sum_{i=1}^{k} \frac{C_{ins}}{(1+r)^{t_i}} + \sum_{j=1}^{n} \frac{C_{rep}}{(1+r)^{t_j}} + C_f \cdot \max[P_f(t)] \tag{6-5}$$

(ii) for the multi-objective optimization

$$\min C_{MT}(t) = \sum_{i=1}^{k} \frac{C_{ins}}{(1+r)^{t_i}} + \sum_{j=1}^{n} \frac{C_{rep}}{(1+r)^{t_j}} \tag{6-6a}$$

$$\max \ \{\min \ \beta(t)\} \tag{6-6b}$$

$$\min \ \{\max \ D(t)\} \tag{6-6c}$$

(iii) satisfying the inspection and repair time constraints

$$t_o \leq t_1 \tag{6-7a}$$

$$t_1 < t_2 < t_3 \tag{6-7b}$$

$$\vdots$$

$$t_{i-1} < t_i < t_{life} \text{ and } t_{j-1} < t_j < t_{life} \tag{6-7c}$$

and the fatigue reliability constraint

$$\min \; \beta(t) > \beta_{target,1} \tag{6-7d}$$

where C_{MT} = expected maintenance cost; t_o = first time (year) when fatigue damage, D, becomes at least 0.3 (i.e., $D \geq 0.3$), t_i = i-th inspection time (i = 1, 2, ….., k), and t_j = j-th repair time (j = 1, 2, ….., n); and $\beta_{target,1}$ = target reliability index corresponding to the critical fatigue damage (i.e., D = 1.0). The procedure for the multi-objective optimization is summarized in the flowchart of Figure 6-1.

In this study, the solution of the single-objective optimization is found by *fmincon* optimization function of Matlab (MathWorks 2009) using the sequential quadratic programming method. When implementing each iteration, an approximation is made of the Hessian of the Lagrangian function by using a quasi-Newton updating method. A quadratic programming subproblem is generated to find the solution (MathWorks 2009). The associated objective function and constraints are defined in Eqs 6-5 and 6-7, respectively. For the decision maker, a unique solution is provided by the single-objective optimization. Due to the budgetary restriction for the single choice, when the decision maker has to choose another (non-optimal) solution, a multi-

objective optimization approach will be alternatively useful. This is because multiple optimal solutions can be provided to the decision maker. In many practical optimization applications, the multi-objective optimization approach has been utilized in order to provide multiple choices (Arora 2004). As described previously, three objectives are herein achieved simultaneously under the predefined constraints (see Eq. 6-7). The genetic algorithm (GA) non-dominated sorting method, NSGA-II (Deb et al. 2002) is used in order to solve the multi-objective optimal maintenance planning formulation associated with Eqs. 6-6 to 6-7. The optimization consists of four steps (see also Figure 6-1):

Step 1: *Fatigue reliability/damage profile*

Based on relevant information on aluminum ship details (S-N curve, SHM data), a fatigue reliability/damage profile is obtained for predicting the lifetime structural performance and time-dependent fatigue damage without maintenance during the anticipated service life. Target reliability and critical damage levels on structural performance are imposed.

Step 2: *Objective*(*s*)

Single- or multi-objectives are used (see Eqs. 6-5 and 6-6, respectively).

Step 3: *Constraints*

Time constraints are imposed for inspection and repair (i.e., Eqs. 6-7(a) to (c)) and the fatigue reliability constraint (see Eq. 6-7(d)) is formulated.

Step 4: *Solving the optimization problem*

The single-objective optimization is solved by direct search method, while the multi-objective optimization is solved by using GA.

301

6.5 APPLICATION EXAMPLE

The same ship detail applied in Chapter 4, which consists of a 42.67 meter 32 knot aluminum crew boat (see Figure 4-11), is used. The 22-3.2 *S-N* curve is used for fatigue resistance (see Figure 4-10), while the stress-range bin histogram data (Sielski 2007a) for sea loading information are used with the assumption that the loading data was obtained from one-year measurement with the annual ship operation rate $\alpha = 0.8$ for a service life of 30 years.

6.5.1 Fatigue Reliability Evaluation and Maintenance Interventions

All necessary information on both the fatigue resistance and the loading data collected in Chapter 4 are used to not only estimate lifetime fatigue reliability and time-dependent fatigue damage but also plan lifetime structural maintenance interventions.

A fatigue reliability/damage profile is developed to predict the time-dependent structural performance and damage levels (see Figure 6-2(a)). For the lifetime maintenance planning interventions, applicable inspection and repair strategies are planned based on the established profile, as indicated in Figure 6-2(a) and (b). As noted previously, a transition gap of fatigue reliability exists at 8.15 years when N reaches N_D = five-million cycles. Two target reliability levels (i.e., $\beta_{target,1}$ = 3.12 and $\beta_{target,2}$ = 4.41) from the fatigue reliability/damage profile are determined for planning lifetime inspection and repair interventions.

Fatigue damage rate, a (see Eq. 6-1), is estimated from the stress-range bin histogram and the *S-N* values. The approximated a is 0.058045/year. For this

302

particular case, it is considered that the fatigue damage index, $D(t)$, reaches the critical damage index of 1.0 at 17.23 years, as shown in Figure 6-2(a). The first detection of fatigue damage $D(t) \geq 0.3$ will be possible after ship operation of 5.2 years. Two strategies are used to improve fatigue strength, by using the strength factor, R_I, of Eq. 6-2 (see also Figure 6-2(b)). When a repair intervention is taken, the original number of stress cycles, N, is updated by using Eq. 6-3, and the new service time, t_{new}, is estimated.

Several maintenance interventions associated with the two strategies considered are investigated based on the predefined fatigue damage thresholds $D_{th} =$ 0.473, 0.65, and 0.90. Figure 6-3 and Figure 6-4 show the results associated with the applications of Strategies 1 and 2, respectively. As shown in Figure 6-3(c) and Figure 6-4(c), the fatigue life satisfying $\beta_{target,1} = 3.12$ is preserved with two repair interventions only. If $\beta_{target,2} = 4.41$ (i.e., $D_{th} = 0.473$), transition gaps of the fatigue reliability do not exist because repair actions are already undertaken before N exceeds N_D, as shown in Figure 6-3(a) and Figure 6-4(a).

6.5.2   LCA with Regular or Irregular Time Intervals

In a cost effective manner, the LCA associated with the fatigue damage threshold D_{th} is formulated considering Strategies 1 and 2, with regular or irregular time intervals. For given D_{th}, the expected total life-cycle cost C_{ET} is computed by using Eq. 6-4. An optimum value is identified by minimizing C_{ET}. In this study, the ratios C_{ins} / C_f and C_{rep} / C_f are assumed 1/20,000 and 1/2,000, respectively, with $C_f =$ 100,000. Therefore, $C_{ins}: C_{rep}: C_f = 1: 10: 20,000$.

Using irregular inspection time intervals, Figure 6-5(a) and Figure 6-6(a) show the results of the cost analysis for all fatigue damage thresholds $D_{th} \geq 0.3$ using Strategies 1 and 2, respectively. It is noted that an increase in D_{th} is associated with a decrease in C_{REP} and an increase in C_F. Accordingly, there is a trade-off point where C_{ET} is a minimum. For Strategies 1 and 2, the optimal fatigue damage threshold, $D_{th,OPT}$, associated with the minimum C_{ET} is 0.72 and 0.78, respectively, and the maximum failure probability, $P_{f,max}$, is 0.000210 and 0.000302, respectively. The associated optimum number of inspections, k, and repairs, n, are $k = n = 2$. Figure 6-5(b) indicates the times of the first and second repair interventions for Strategy 1 (i.e., at 12.5 and 21.5 years) from the updated fatigue reliability profile, while the optimal repair times using Strategy 2 are 13.5 and 22.2 years (see Figure 6-6(b)).

In addition, it is assumed that the structural detail is regularly inspected during the service life of 30 years. If any inspection result is $D(t) \geq 0.3$, a repair is performed. Figure 6-7(a) and Figure 6-8(a) show the results of the cost analysis for different inspection time intervals. A life-cycle cost set minimized using different inspection time intervals is plotted. As shown in Figure 6-7(a) and Figure 6-8(a), C_{ET} is minimum when the regular inspection interventions are applied every 4.5 years (i.e., $k = 6$) for both cases. Figure 6-7(b) shows the updated fatigue reliability associated with $k = 6$ and $n = 2$ (repairs at 13.5 and 22.5 years) with $D_{th,OPT} = 0.78$ and $\beta_{min} = 3.43$. The updated fatigue reliability associated with Strategy 2 is shown in Figure 6-8(b). The optimum values are provided in Table 6-1.

6.5.3 Optimization

The life-cycle cost optimizations considering single- and multi-objective are performed. In the case of the single-objective optimization, C_{ET} is defined as the objective to be minimized, while the multi-optimization problem is solved by considering three objectives (i.e., min C_{MT}, max β_{min}, and min D_{max}). For given target number of lifetime inspections (i.e., k = 2, 3, 4, and 5), the design variables assigned are inspection and repair times which may be identical (i.e., t_i = t_j). In both optimizations, time constraints are imposed together with fatigue reliability constraints. Due to the given time constraints, all inspection times can be determined when $D(t_i)$ is at least 0.3, implying that a fatigue crack is detected perfectly (i.e, PoD$[D(t) \geq 0.3]$ = 1.0). Therefore, it is necessary that a repair intervention follows the inspection (i.e., $k = n$).

6.5.3.1 Single-Objective Optimization

The analysis for the single-objective optimization finding the optimal inspection and repair times is performed by *fmincon* optimization function of Matlab (MathWorks 2009) using Eqs. 6-5 and 6-7, for the predetermined number of inspections. Figure 6-9(a) shows the optimal inspection and repair times associated with the computed optimal total cost, $C_{ET,OPT}$. The fatigue reliability profiles associated with the optimal solutions are shown in Figure 6-9(b). It is observed that the lifetime structural performance under the five repair interventions can satisfy the upper target reliability, $\beta_{target,2}$ of 4.41, implying that the fatigue life does not exceed N_D = five-million cycles during the service life of 30 years. For other strategies, the

minimum fatigue reliabilities are between $\beta_{target,2} = 4.41$ and $\beta_{target,1} = 3.12$. The optimal solutions for Strategy 2 are shown in Figure 6-10(a). The results are similar to those for Strategy 1. For these optimal solutions, the updated fatigue reliability profiles are shown in Figure 6-10(b), satisfying $\beta_{target,1} = 3.12$.

6.5.3.2 Multi-Objective Optimization

As noted previously, if the cost associated with an optimum solution obtained from the single-objective optimization is not affordable, the decision maker has to select another (non-optimal) solution. The multi-objective optimization offers multiple optimal solutions for the decision maker. For this purpose, the multi-objective optimization is formulated by using Eqs. 6-6 and 6-7, and solved by using GAs (Deb et al. 2002).

For the two strategies considered, a total of 200 Pareto solutions using GAs are obtained at the 1000-th generation. These solutions satisfying Pareto optimality exhibit tradeoffs as shown in Figure 6-11 and Figure 6-12 for Strategies 1 and 2, respectively. The expected maintenance cost, C_{MT}, conflicts with the fatigue damage objective, D. Similarly, C_{MT} and the probability of fatigue failure are in conflict. The competing relationship between two objectives (i.e., D vs. β, β vs. C_{MT}, and D vs. C_{MT}) is observed by the 2-D projections in Figure 6-11 and Figure 6-12. As expected, a transition gap in reliability index is observed in $D = 0.473$ where the cumulative number of cycles, $N = N_D$. Figure 6-11(c) and (d) show the maintenance costs vs. β and D, respectively, for Strategy 1, with 12 representative optimized maintenance solutions (see Table 6-2). These solutions exhibit different balances of cost and β or D,

that is, an increase in β (or a decrease in D) leads to additional cost in maintenance. Figure 6-12(c) and (d) show the results associated with Strategy 2, with 10 representative maintenance solutions (see Table 6-2). Although the cost C_{MT} identified by the solutions associated with two or three repair interventions is relatively lower, more interventions may be required to improve the lifetime fatigue reliability and simultaneously reduce the maximum fatigue damage.

The Pareto sets identified in Figure 6-11 and Figure 6-12 can be used to find acceptable optimum solutions for two possible cases: (i) lifetime maximum damage threshold, $D_{max} = 0.50$, and (ii) lifetime minimum reliability, $\beta_{min} = 4.41$. Optimal solutions satisfying each case are selected from Pareto sets. Using Strategy 1 (see Figure 6-11(a)), the solutions S_{11}, S_{21} and S_{12}, S_{22} are associated with four and five repairs, respectively. Using Strategy 2 (see Figure 6-12(a)), the solutions S_{13} and S_{23} are associated with five repairs. The time-dependent fatigue damage, reliability, and cumulative maintenance cost profiles of solutions S_{11}, S_{12}, S_{13} and S_{21}, S_{22}, S_{23} are plotted in Figure 6-13 and Figure 6-14, respectively. The lifetime minimum reliability index $\beta_{min} = 3.98$ was satisfied for the first case (see Figure 6-13(b)). However, it is clear that the lifetime minimum cost depends on the repair interventions, as shown in Figure 6-13(c). In the second case, the results associated with the minimum cost (see Figure 6-14(c)) are similar to those of the first case. In both cases, the lowest minimum cost was obtained by using Strategy 1 with four repairs, while the highest reliability at the end of service life was obtained by using Strategy 1 with five repairs. As expected, there were no transition gaps of the fatigue reliability in the second case (i.e., $\beta_{min} = \beta_{target,2} = 4.41$).

6.6 SUMMARY AND CONCLUDING REMARKS

This study presented probabilistic approaches for estimating the time-dependent fatigue reliability of aluminum ship structures and for finding their lifetime optimum inspection/repair interventions considering fatigue reliability, fatigue damage, and life-cycle cost. The fatigue reliability analysis based on the bi-linear *S-N* approach and sea loading data, as addressed in Chapter 4, was performed for the lifetime performance assessment and prediction, while the life-cycle cost analysis as well as the single-objective and multi-objective optimizations were performed for implementing a cost- and performance-effective lifetime structural maintenance strategy. Fatigue reliability, fatigue damage, and life-cycle cost were considered as competing objectives for multi-criteria optimization, subject to time and reliability constraints. This approach was illustrated by using an aluminum ship detail.

The following conclusions are drawn:

1. Life-cycle cost analysis considering regular or irregular time intervals between inspections of aluminum ships under uncertainty can be carried out to find an optimal lifetime inspection and repair planning as well as an optimal lifetime fatigue damage threshold.

2. Single-objective optimal lifetime planning of inspection/repair of aluminum fatigue sensitive ship structures can be formulated and solved to minimize expected total cost.

3. Multi-objective optimization can be formulated and solved to provide the decision maker with alternative strategies for optimal inspection/repair planning of these structures selected from a Pareto set containing several competing

objectives such as lifetime fatigue reliability, fatigue damage, and maintenance cost.

4. Lifetime fatigue performance of aluminum ship structures can be quantified by using the proposed reliability method considering uncertainty. This approach is based on the *S-N* curve for fatigue resistance and stress-range bin histogram data from SHM for load effect.

5. The quantified lifetime structural performance can be used to provide alternatives for planning lifetime inspection/repair interventions.

6. Stress-range bin histogram data can be used not only to compute equivalent stress range but also to estimate time-dependent fatigue damage which may be affected by the annual ship operation rate.

Table 6-1   Optimal solutions.

Strategy		Optimal solution		Optimal fatigue damage threshold, $D_{th,OPT}$	Minimum fatigue reliability, β_{min}	Costs			
		Time of first repair, t_1 (years)	Time of second repair, t_2 (years)			C_{INS}	C_{REP}	C_F	min C_{ET}
Strategy 1	*Regular time intervals	13.5	22.5	0.78	3.43	22.2	70.4	30.1	122.7
	Irregular time intervals	12.5	21.5	0.72	3.53	7.2	71.8	21.0	100.0
Strategy 2	*Regular time intervals	13.5	22.5	0.78	3.43	22.2	70.4	30.1	122.7
	Irregular time intervals	13.5	22.2	0.78	3.43	7.1	70.6	30.1	107.8

* Inspection time intervals are every 4.5 years for both strategies (i.e., $k = 6$).

Table 6-2   Representative optimum solutions associated with multi-objective optimization.

Strategy	*Solution ID	Minimum fatigue reliability, β_{min}, during 30 years	Maximum fatigue damage, D_{max}, during 30 years	Lifetime maintenance cost, C_{MT}, during 30 years	Time of inspection/repair intervention (years) t_1	t_2	t_3	t_4	t_5
Strategy 1	A	3.55	0.708	79.4	12.20	21.10	-	-	-
	B	3.93	0.522	121.0	8.99	16.00	23.00	-	-
	C_1	4.41	0.473	156.3	8.14	14.56	20.97	27.38	-
	C_2	4.62	0.412	162.5	7.10	12.83	18.55	24.28	-
	D_1	4.41	0.472	189.1	8.13	14.50	20.91	24.76	28.98
	D_2	4.71	0.390	196.3	6.71	12.17	17.62	23.07	28.53
Strategy 2	E	3.45	0.763	78.3	13.15	21.57	-	-	-
	F	3.72	0.616	118.3	10.60	17.07	23.53	-	-
	G	3.93	0.522	158.6	8.99	14.24	19.49	24.75	-
	H_1	4.41	0.473	196.7	8.14	12.76	17.36	21.94	26.56
	H_2	4.47	0.453	199.1	7.81	12.25	16.69	21.13	25.56

* Solutions A, B, C_1, C_2, D_1 and D_2 are indicated in Figure 6-11(c) and (d), and solutions E, F, G, H_1 and H_2 are also indicated in Figure 6-12(c) and (d).
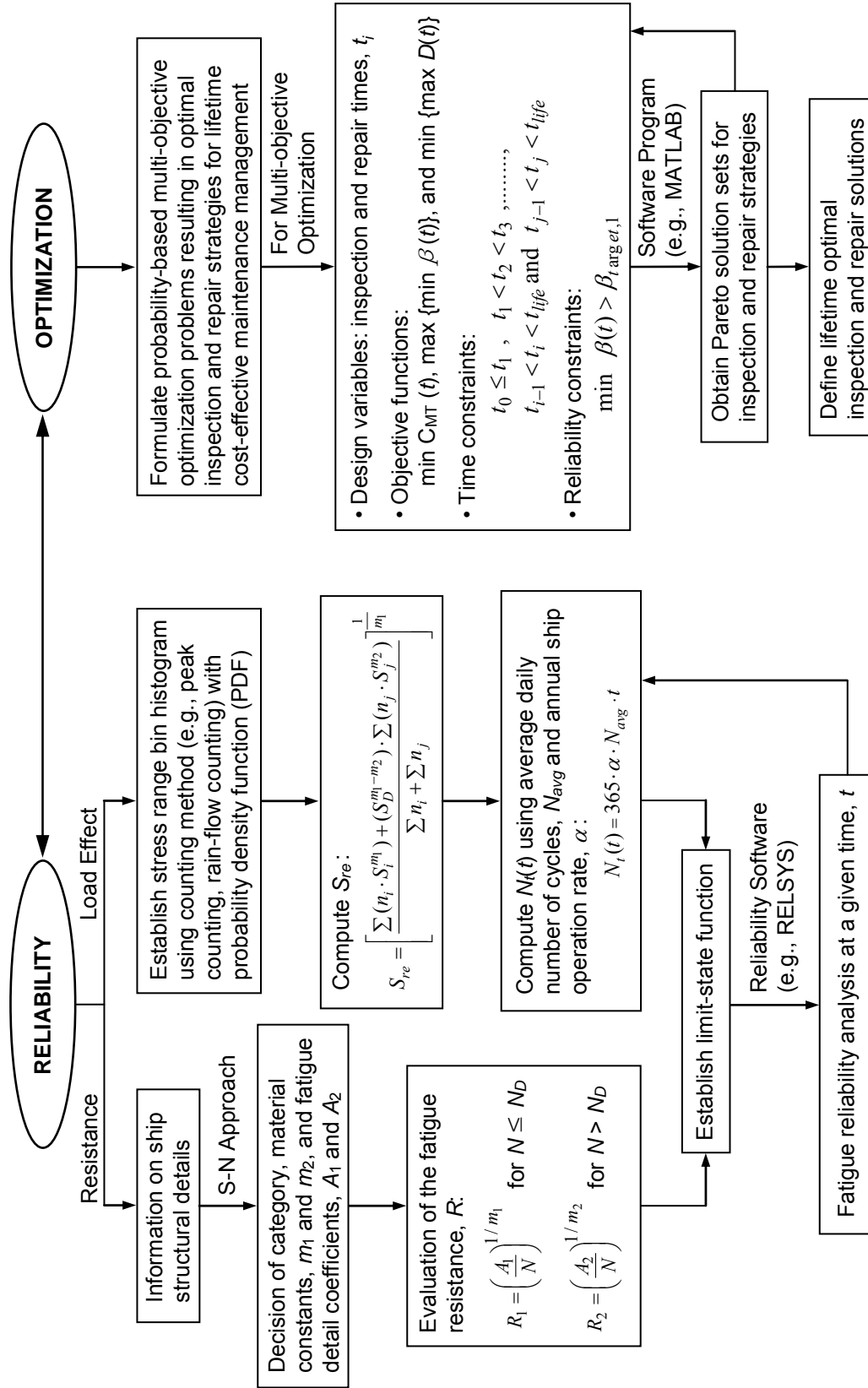
Figure 6-1 Flowchart for the fatigue reliability assessment and life-cycle cost optimization.
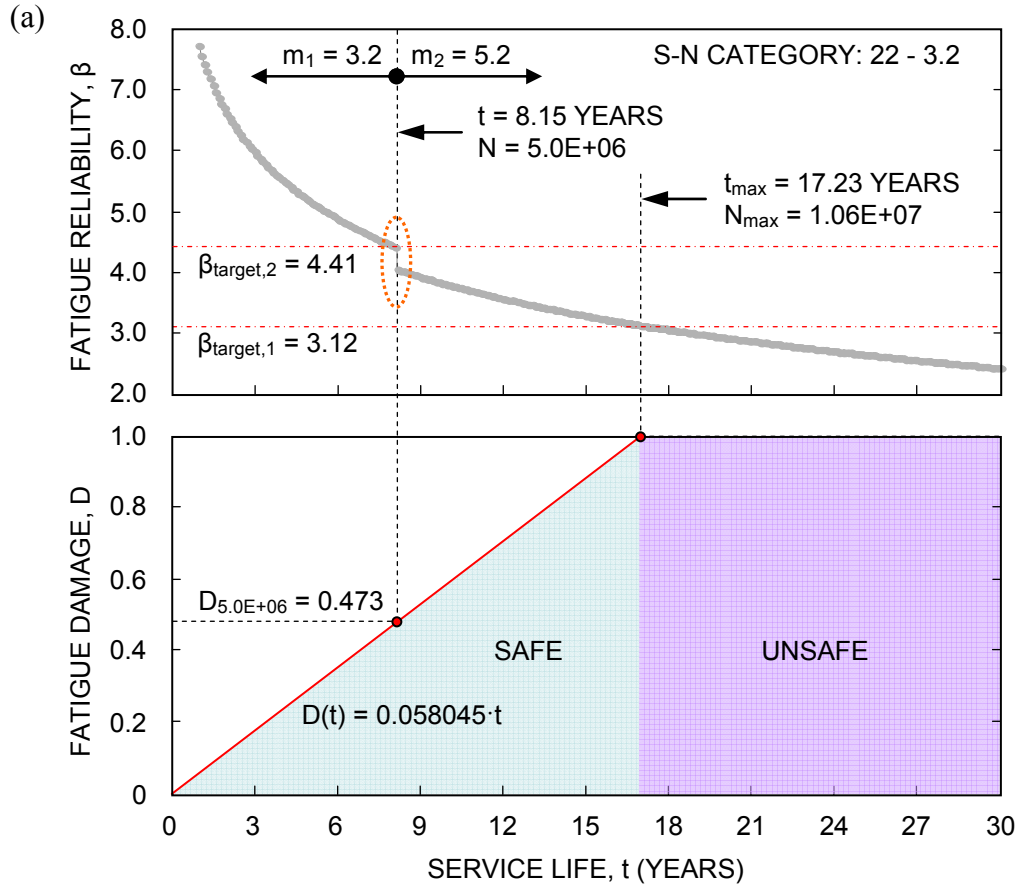
(a) fatigue reliability/damage profile
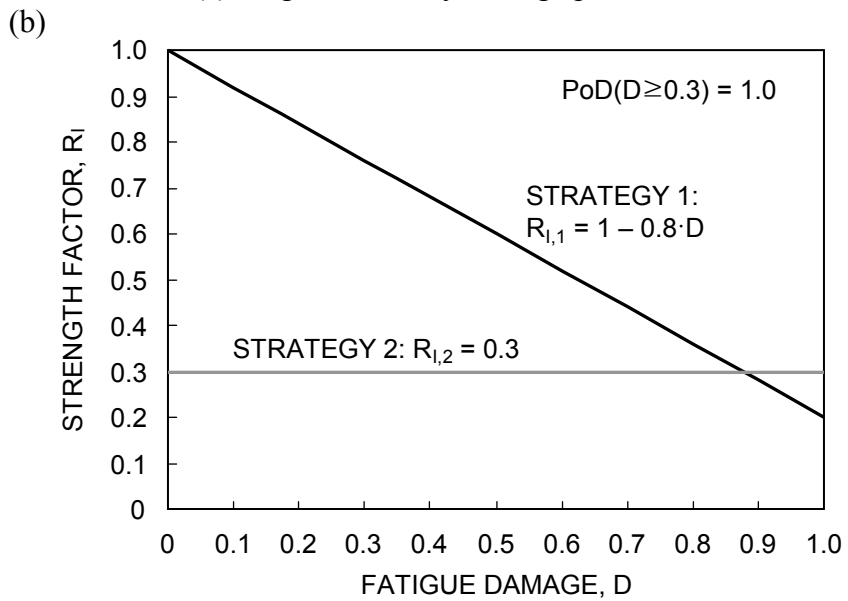
(b) two strategies using the fatigue strength factor, R_I

Figure 6-2   Lifetime maintenance strategies.
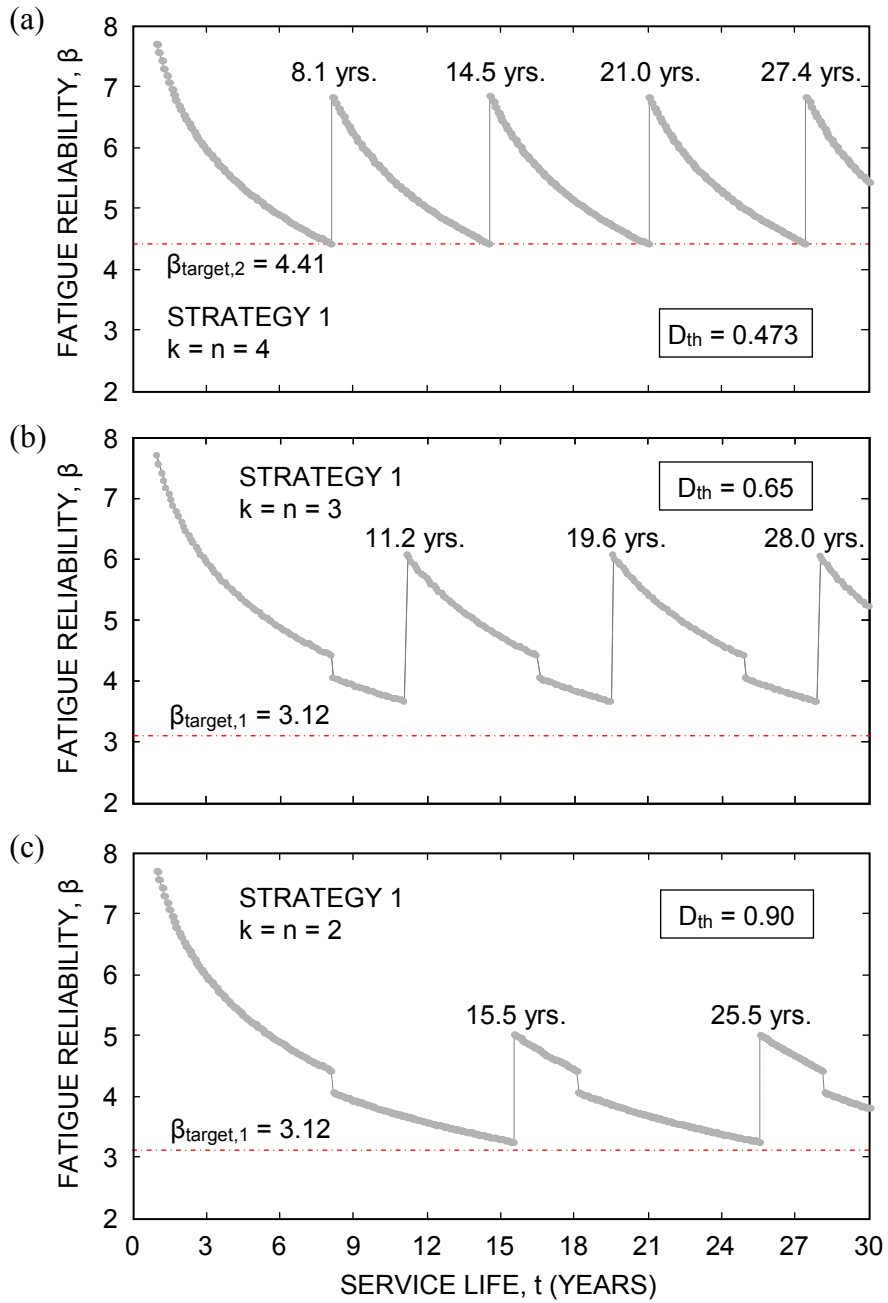
Figure 6-3 Fatigue reliability assessment by using Strategy 1 with three different damage thresholds: (a) $D_{th} = 0.473$, (b) $D_{th} = 0.65$, and (c) $D_{th} = 0.90$.

314
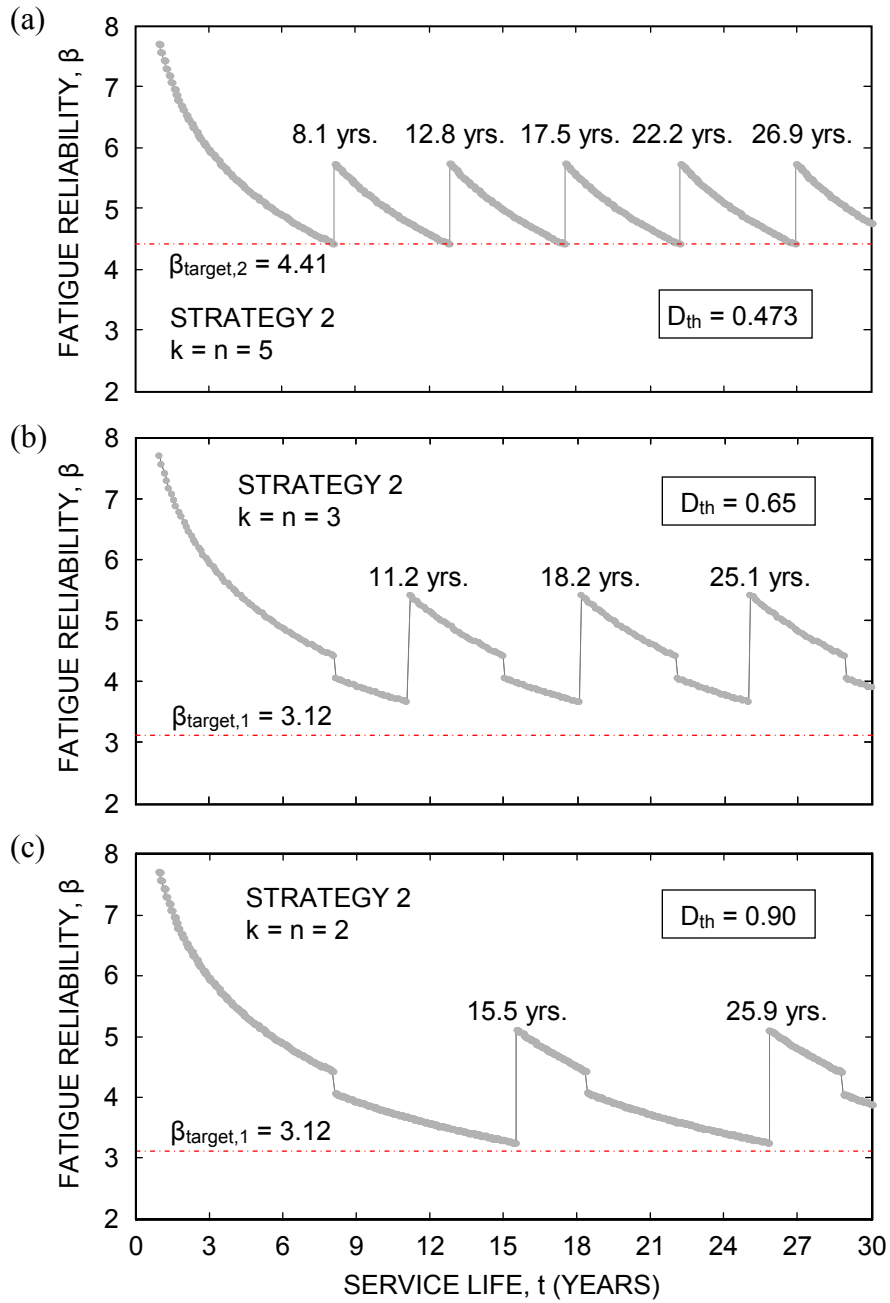
Figure 6-4   Fatigue reliability assessment by using Strategy 2 with three different damage thresholds: (a) $D_{th} = 0.473$, (b) $D_{th} = 0.65$, and (c) $D_{th} = 0.90$.

(a)

(a) costs versus damage threshold, D_{th}

(b)
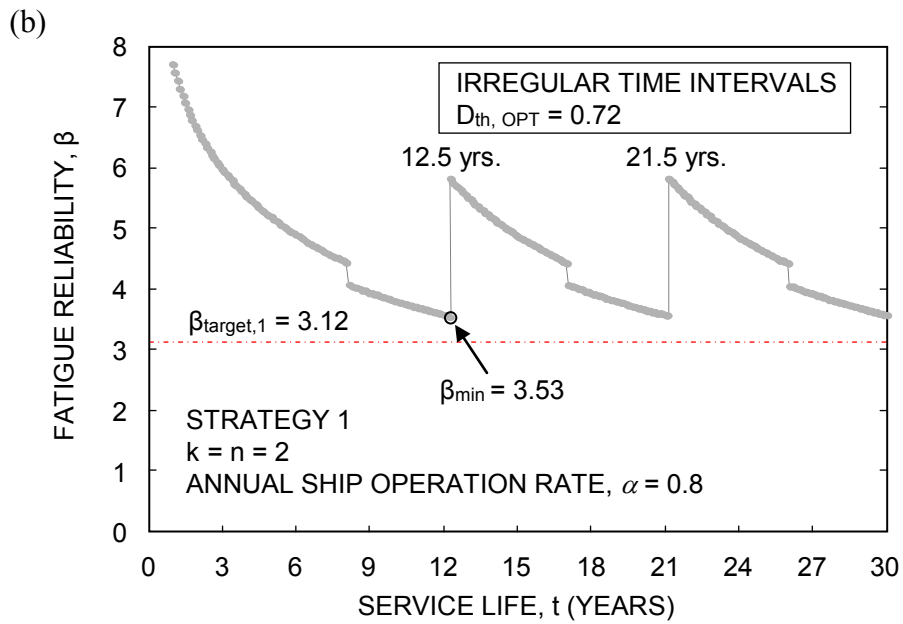
(b) fatigue reliability profile for optimal damage threshold, $D_{th,OPT} = 0.72$

Figure 6-5   LCA by using Strategy 1 and irregular inspection and repair time intervals.
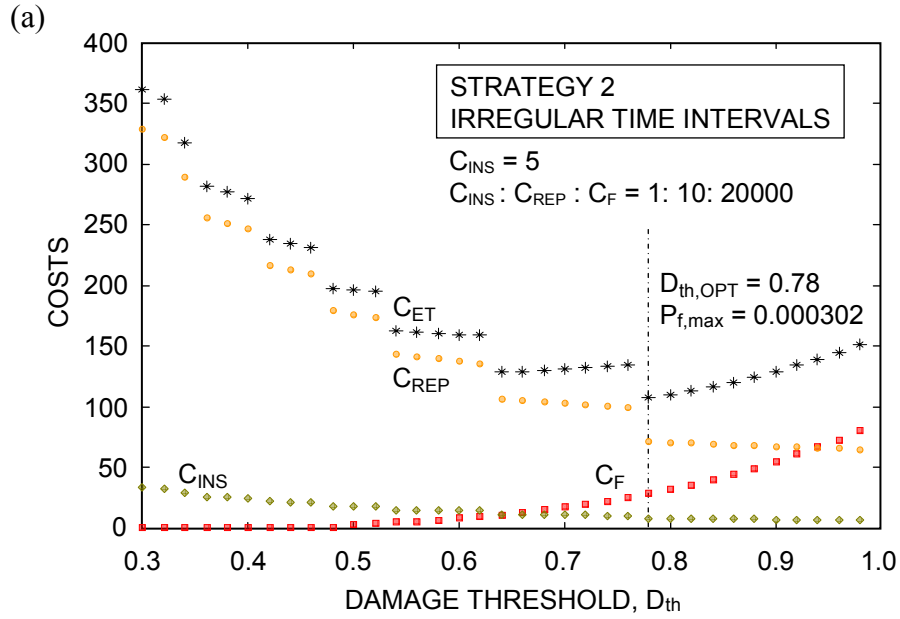
(a) costs versus damage threshold, D_{th}
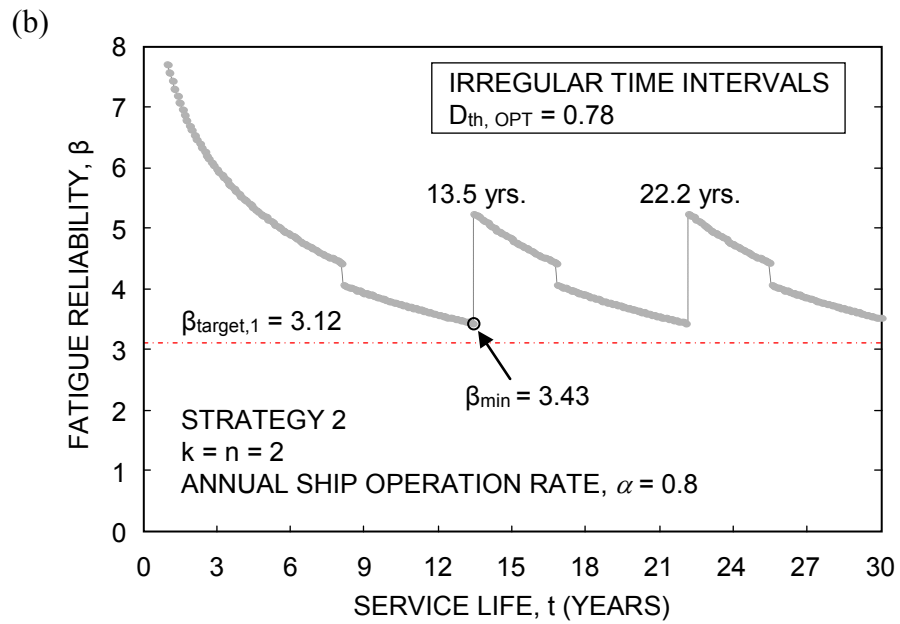
(b) fatigue reliability profile for optimal damage threshold, $D_{th,OPT} = 0.78$

Figure 6-6   LCA by using Strategy 2 and irregular inspection and repair time intervals.
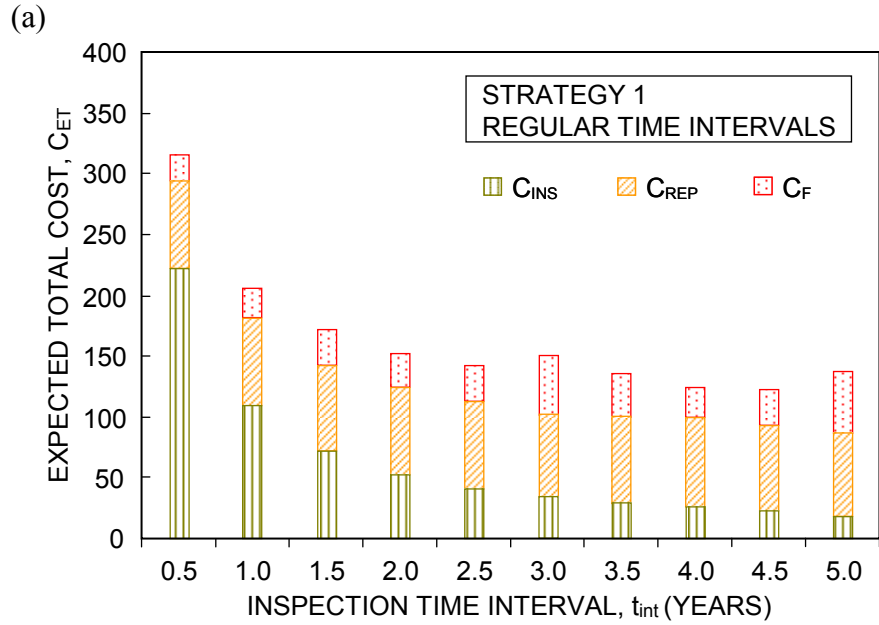
(a) costs profile for regular inspection and repair time intervals, t_{int}
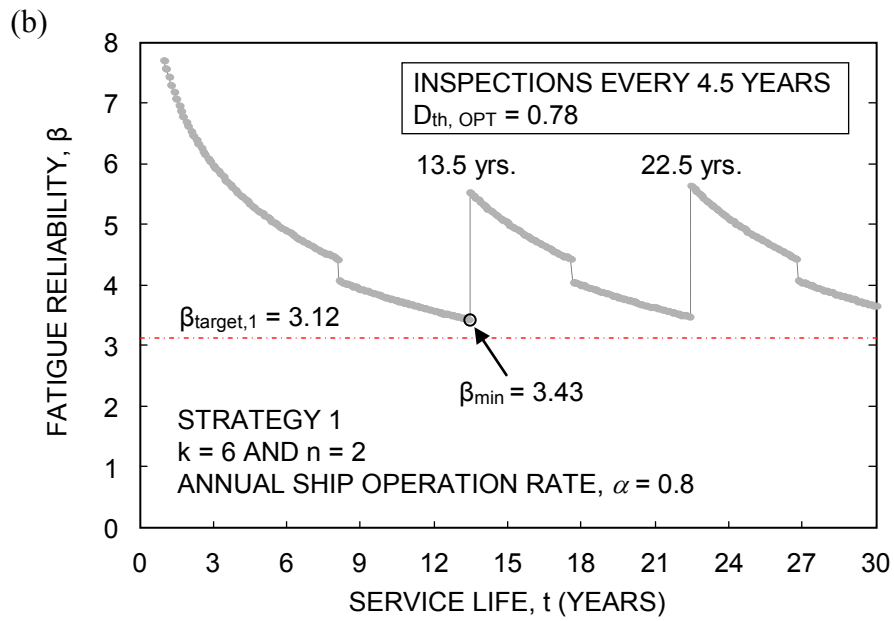
(b) fatigue reliability profile for optimal damage threshold, $D_{th,OPT} = 0.78$

Figure 6-7   LCA by using Strategy 1 and regular inspection and repair time intervals.

(a)

(a) costs profile for regular inspection and repair time intervals, t_{int}

(b)
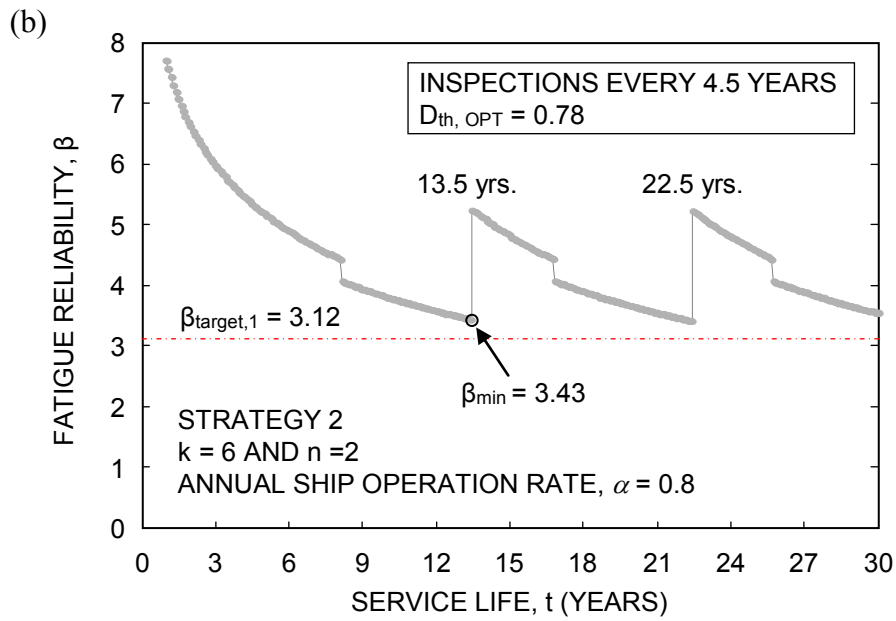
(b) fatigue reliability profile for optimal damage threshold, $D_{th,OPT} = 0.78$

Figure 6-8   LCA by using Strategy 2 and regular inspection and repair time intervals.

319
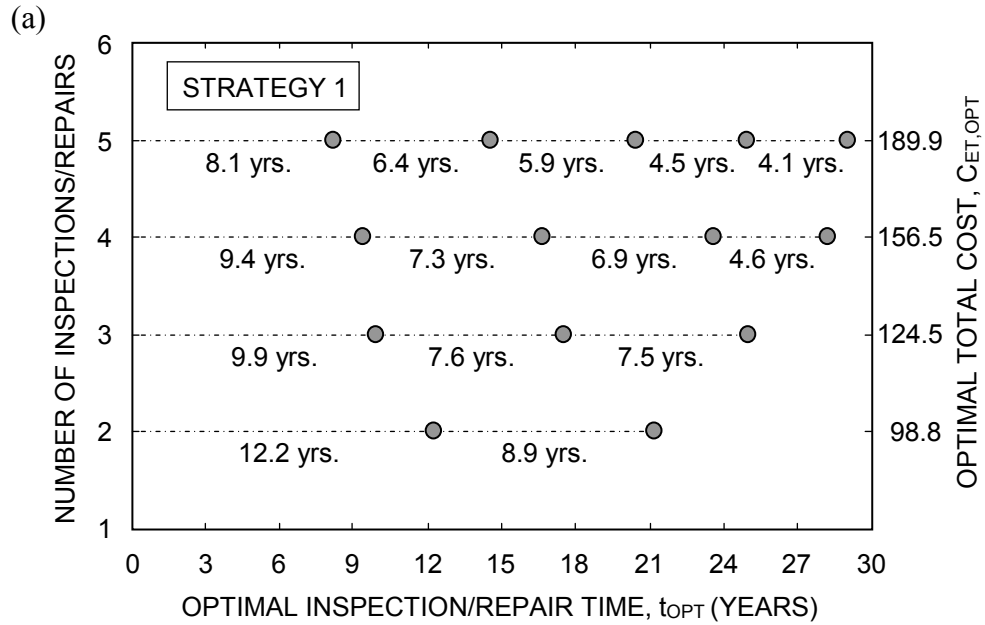
(a) optimal inspection/repair time, t_{OPT}
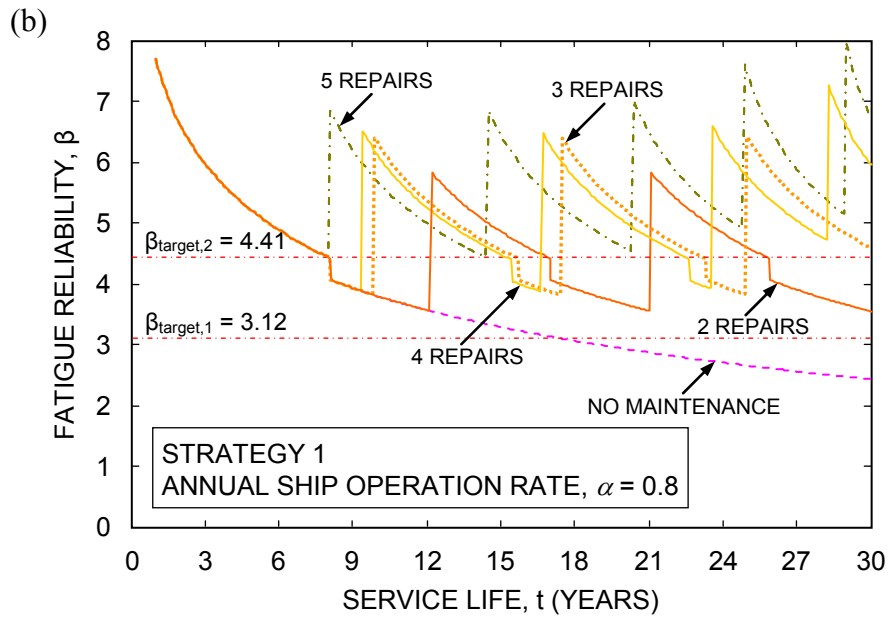
(b) fatigue reliability profile for t_{OPT}

Figure 6-9   Single-objective optimization by using Strategy 1.

(a)

STRATEGY 2

9.5 yrs.   5.6 yrs.   5.6 yrs.   4.2 yrs. 3.9 yrs.

10.5 yrs.   6.3 yrs.   6.1 yrs.   6.0 yrs.

10.9 yrs.   6.7 yrs.   6.7 yrs.

13.2 yrs.   8.4 yrs.

(a) optimal inspection/repair time, t_{OPT}

(b)

$\beta_{target,2} = 4.41$

$\beta_{target,1} = 3.12$

5 REPAIRS   3 REPAIRS   4 REPAIRS

2 REPAIRS

NO MAINTENANCE

STRATEGY 2
ANNUAL SHIP OPERATION RATE, $\alpha = 0.8$
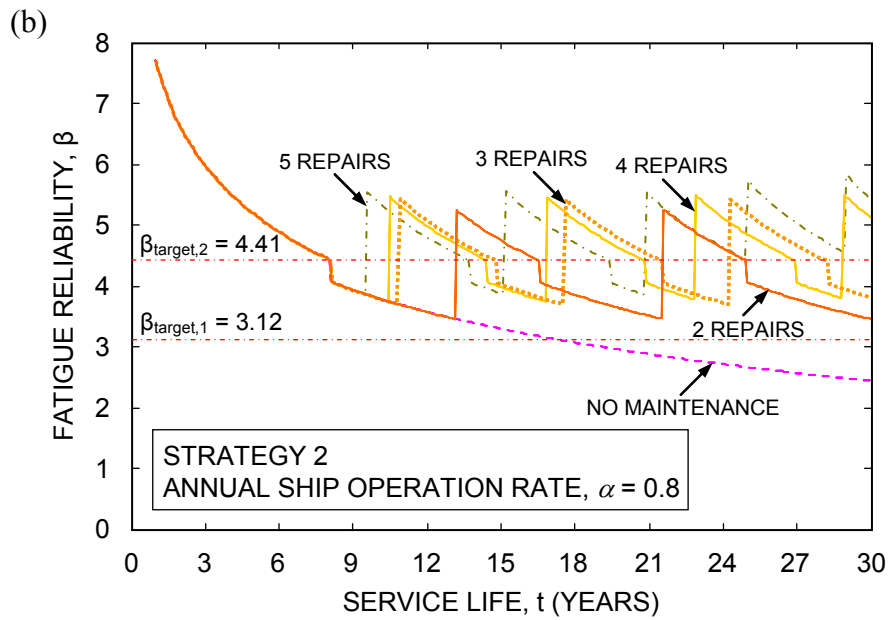
(b) fatigue reliability profile for t_{OPT}

Figure 6-10   Single-objective optimization by using Strategy 2.
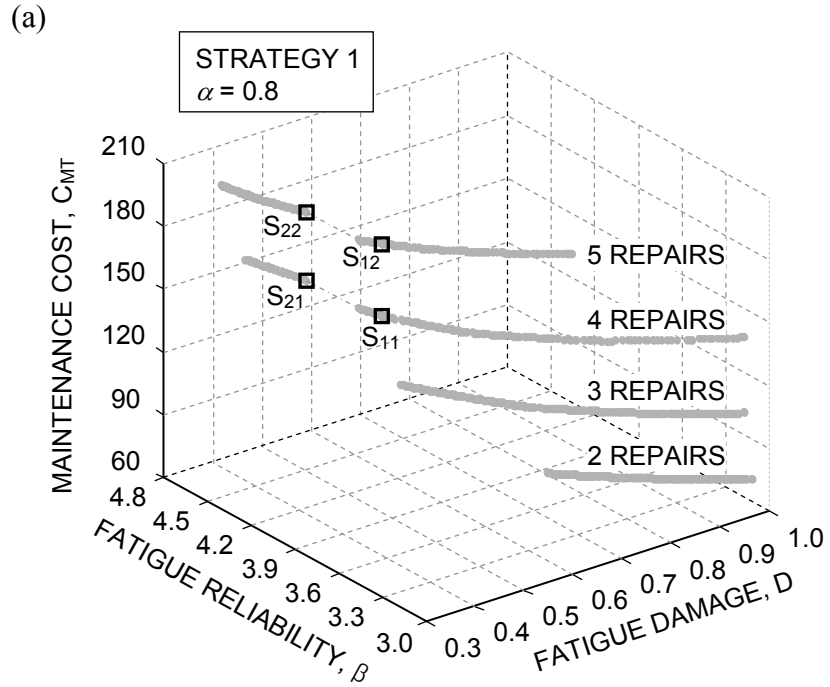
321

(a) Pareto sets associated with different numbers ($k = n$) of inspections/repairs

(b) Pareto solutions of D and β

(c)

(c) Pareto solutions of β and C_{MT}

(d)
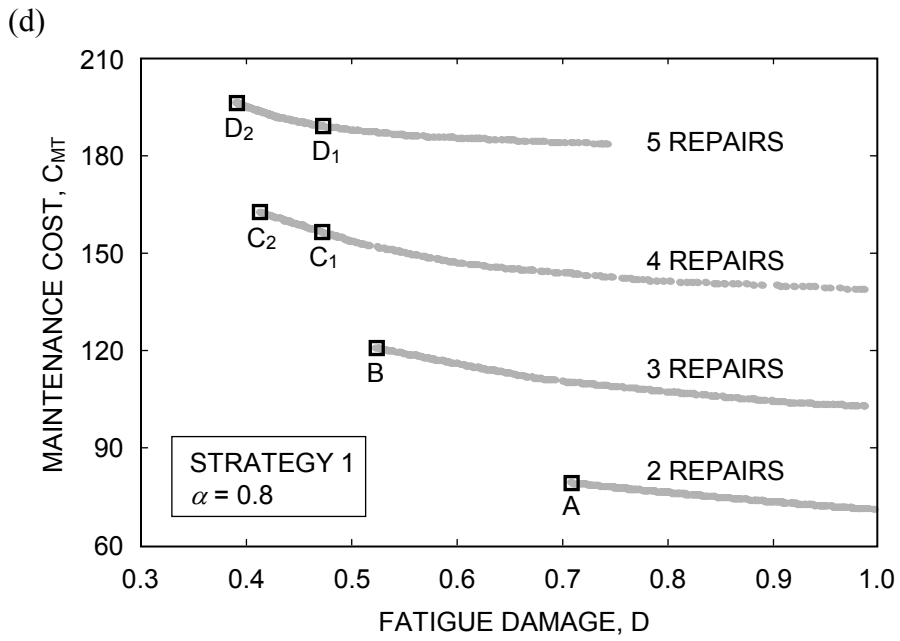
(d) Pareto solutions of D and C_{MT}

Figure 6-11   Multi-objective optimization by using Strategy 1.
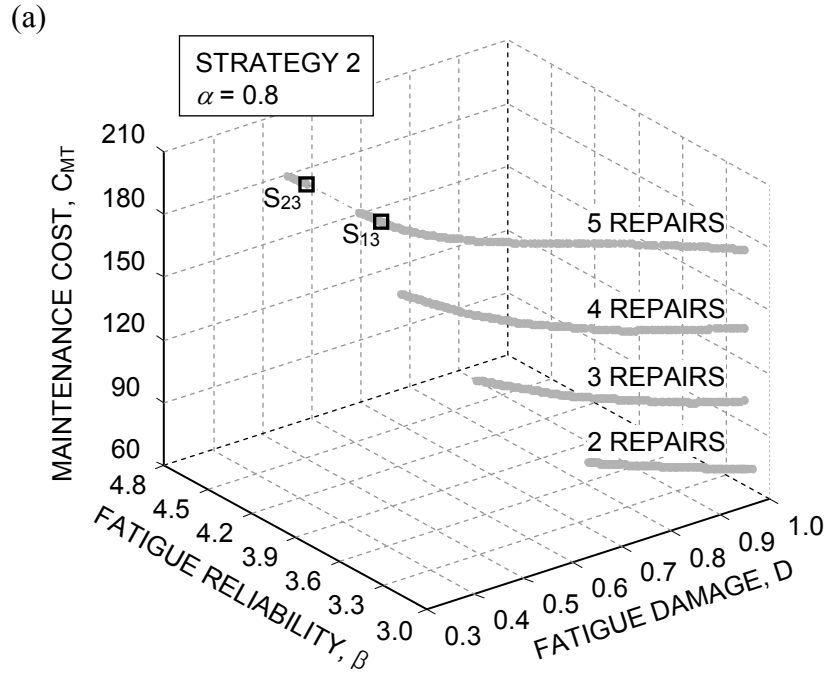
(a) Pareto sets associated with different numbers ($k = n$) of inspections/repairs
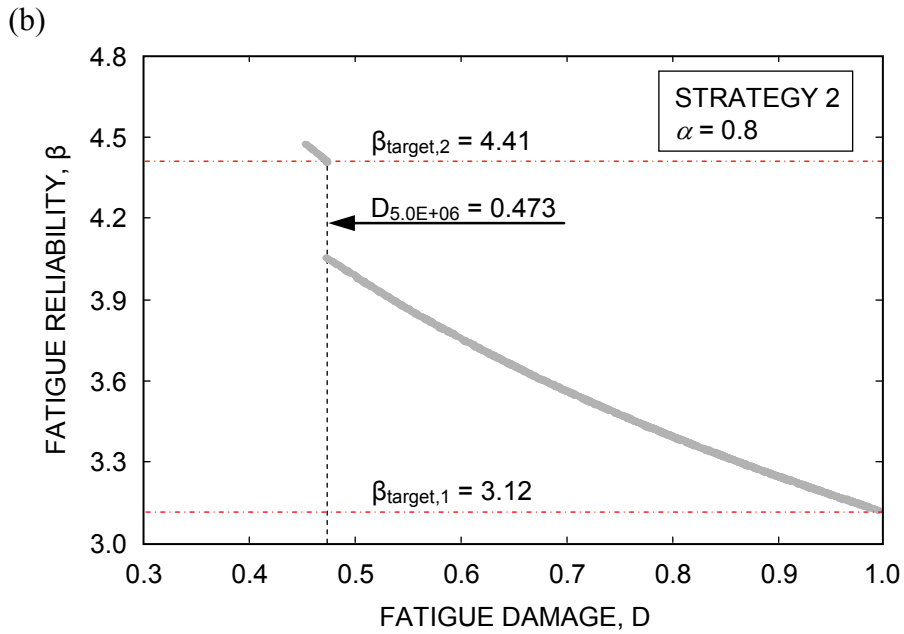
(b) Pareto solutions of D and β
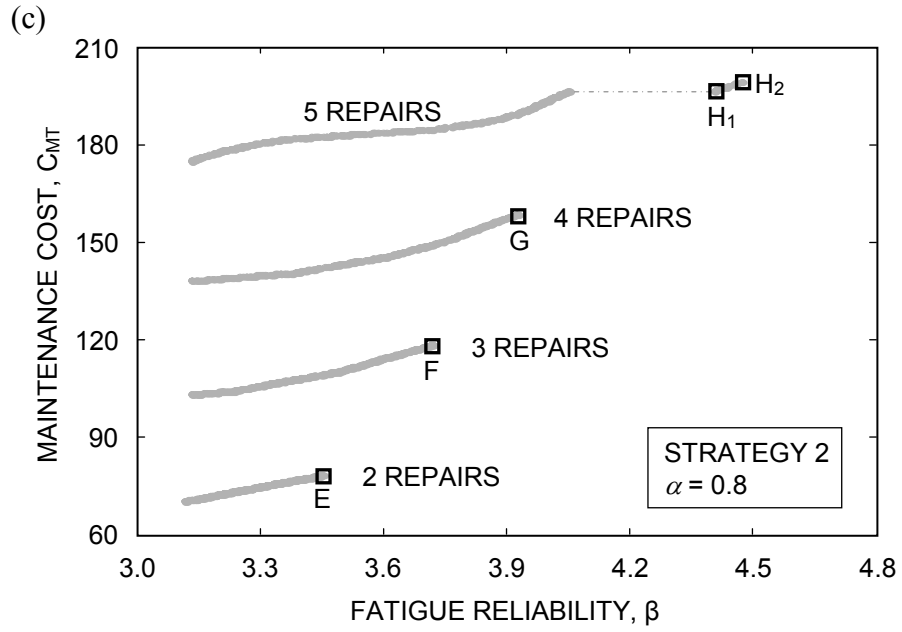
(c) Pareto solutions of β and C_{MT}
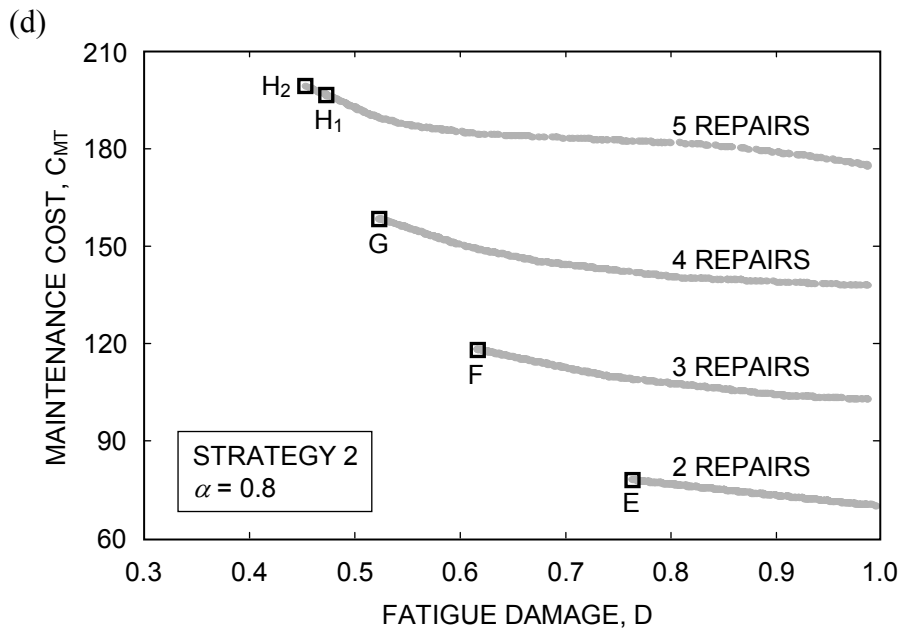
(d) Pareto solutions of D and C_{MT}

Figure 6-12   Multi-objective optimization by using Strategy 2.
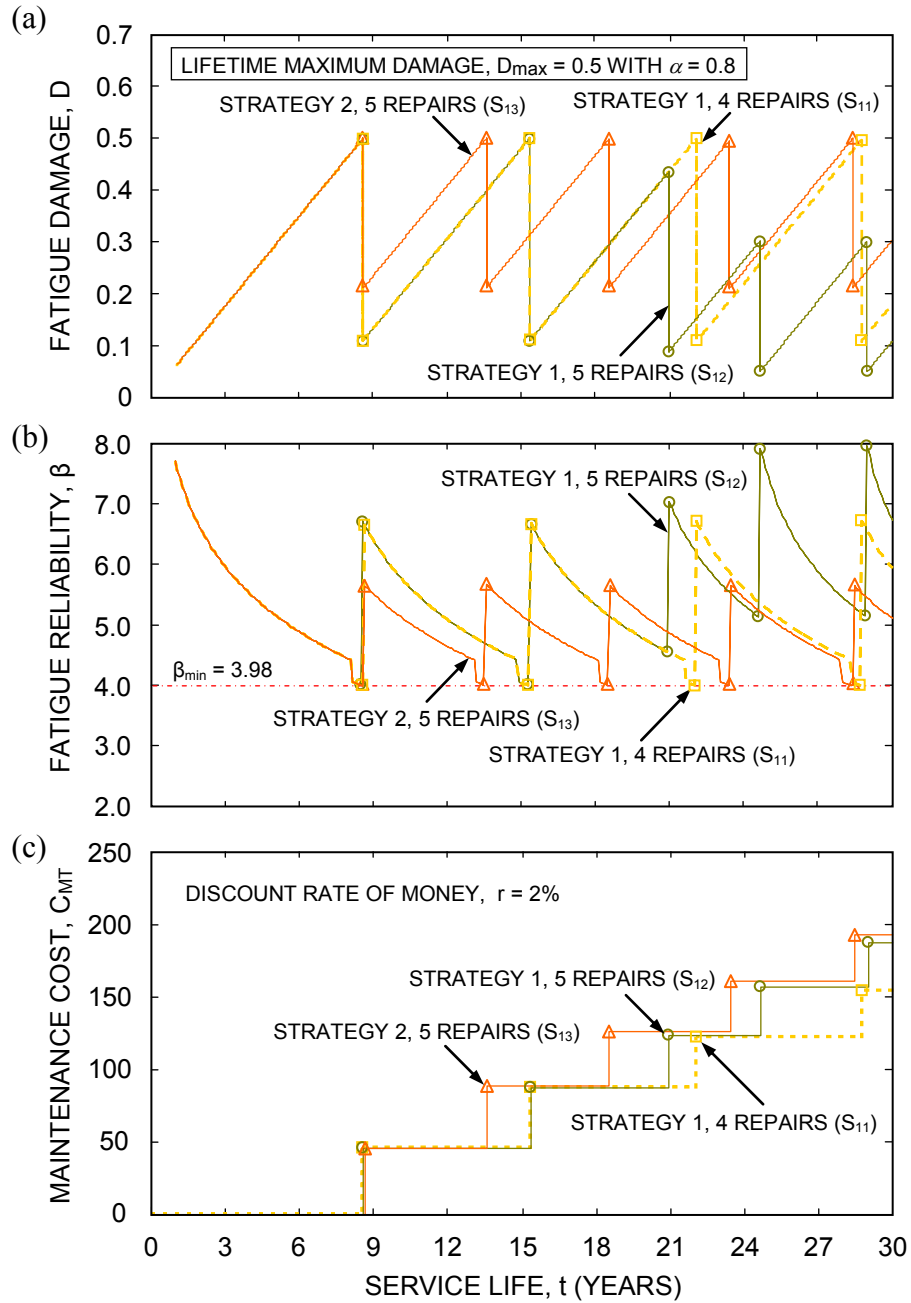
Figure 6-13 Profiles for lifetime maximum damage index, $D_{max} = 0.5$: (a) fatigue damage D, (b) fatigue reliability β, and (c) maintenance cost C_{MT}.
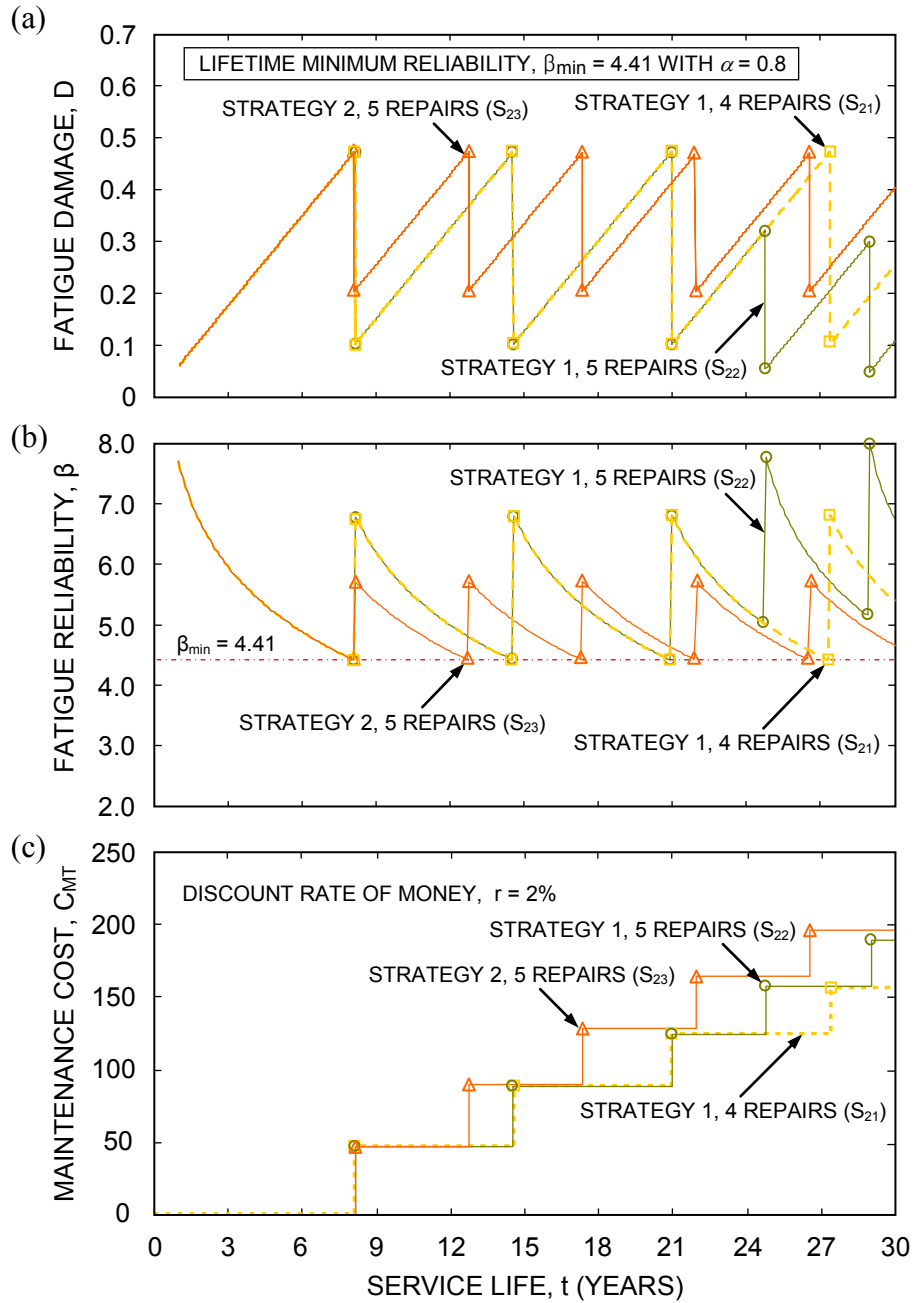
Figure 6-14 Profiles for lifetime minimum reliability index, $\beta_{min} = 4.41$: (a) fatigue damage D, (b) fatigue reliability β, and (c) maintenance cost C_{MT}.

CHAPTER 7

SYSTEM-BASED RELIABILITY APPROACH OF SHIP STRUCTURES

7.1 INTRODUCTION

This chapter describes the system-based reliability approach for the potential failure modes in order to estimate and predict lifetime system performance of the steel ship structures treated in this study. System reliability is evaluated considering uncertainties in their structural capacity and loads. Lifetime structural deterioration models are developed at system level by formulating time-dependent random functions associated with corrosion and fatigue cracking.

Steel hull girder structures are inevitably under an aggressive environment. For these structures, corrosion and/or fatigue are the most common types of structural deterioration processes (Ayyub et al. 2002a, Akpan et al. 2002, and Paik et al. 2005). In absence of accurate prediction for the occurrence and evolution of these processes, avoiding failure may be difficult. For this reason, individual failure modes under corrosion and fatigue have to be well identified in order to achieve successful performance assessment and lifetime prediction during the entire service life of ship hull structures. However, since hull girder structures can fail due to the occurrence of any failure mode, a system-based structural assessment method has to be implemented. A probabilistic approach considering resistance and loading uncertainties is herein proposed for assessing lifetime structural reliability of ship hull structures.

Estimation of the ultimate strength of hull girders subjected to vertical bending

has been a topic of continuous interest (Kuo & Chang 2003). In this context, many researchers proposed empirical formulae (Caldwell 1965, Faulker et al. 1973, Carlsen 1980, Paik & Mansour 1995, and Paik et al. 1996). In this study, the empirical formula proposed by Paik et al. (1996) is used to estimate the ultimate compressive (buckling) strength of a hull girder structure.

Both still water and wave-induced bending moments are taken into account. These bending moments are estimated by using the International Association of Classification Societies rule (IACS 2006) for ship hull girders. Under extreme sea wave loading, a simplified direct method developed by Loukakis & Chryssostomidis (1975) can be used for estimating the mean values of extreme wave-induced bending moments in consideration. In this study, the effects of ship operational and sea environmental conditions on structural reliability of hull girders in the intact condition are investigated as well.

Under corrosion and/or fatigue cracking, lifetime structural performance of ships can be assessed by using a system-based reliability method. Such a method uses all necessary information on both the deteriorating ultimate bending moment for structural resistance and still water and wave-induced bending moments for load effects. These loading conditions are associated with the action of sea waves and sea environment (Ayyub et al. 2002c). Several approaches have been proposed to assess lifetime structural performance for deteriorating structures under uncertainty (Soares & Garbatov 1999, Paik & Frieze 2001, Akpan et al. 2002, Khan & Parmentier 2006, Liu et al. 2010a, and Kwon & Frangopol 2010a). However, these approaches have been generally applied to reliability assessment for a single failure mode or simply

329

combined modes. In this study, a system reliability approach is proposed. For the identified failure modes, a series system model as well as a series-parallel system model are developed. The system models are used to assess and predict the time-dependent structural performance of hull girders for both sagging and hogging conditions. The proposed approach is illustrated on a ship hull girder structure.

Section 7.2 addresses estimation of ultimate bending strength and bending moment of ship structures for the application of the system reliability approach. In Section 7.3, system-based reliability assessment for the failure modes identified at a critical location of ship hull structures considered in this study is described. The application and suitability of using the system reliability method are summarized in Section 7.4 and the associated conclusions are drawn in Section 7.5.

7.2 ULTIMATE BENDING STRENGTH AND BENDING MOMENT

The bending strength of a hull girder, M_u, can be estimated by using an empirical formula considering buckling failure mode caused by the excessive compressive stresses for sagging and hogging moments (Kuo & Chang 2003). This is because the buckling stress of components is lower than their yielding stress. Therefore, the overall collapse of a hull girder is governed by the buckling failure under vertical bending moments (Paik & Mansour 1995). On the other hand, total wave bending moment, M_t, associated with ship operational and sea environmental conditions can be computed using design-oriented formulae and a simplified direct method.

330

7.2.1 Ultimate Bending Strength

The ultimate strength of a ship hull under vertical bending can be estimated by using various formulations (Akpan et al. 2002) obtained by different methods such as using: (i) buckling knockdown factor to the hull girder fully plastic bending moment; (ii) reduced elastic section modulus accounting for plate buckling; (iii) longitudinal stiffened single cell rectangular construction; (iv) load and end-shortening curves for beam column; (v) hard spots subjectively treated; and (vi) dynamic non-linear elasto-plastic finite element analysis of a large portion of the hull.

An empirical formula proposed by Paik et al. (1996) is herein used to predict the initial ultimate compressive (buckling) strength of undamaged plates and stiffened plates in ship deck and bottom for sagging and hogging conditions, respectively. Based on previously collected and newly developed numerical data, the bending strength of a hull girder is (Paik et al. 1996)

$$M_u = \sigma_u \cdot Z = \frac{\sigma_y \cdot Z}{\sqrt{0.995 + 0.936\lambda^2 + 0.170\beta^2 + 0.188\lambda^2 \cdot \beta^2 - 0.067\lambda^4}} \qquad (7\text{-}1)$$

where σ_y and σ_u = yield strength and ultimate buckling strength of the stiffened panel, respectively; λ and β = column (stiffener) and plate slenderness ratio, respectively, expressed as

$$\lambda = \frac{a}{\pi \cdot r} \cdot \sqrt{\frac{\sigma_y}{E}} = \frac{a}{\pi \cdot \sqrt{I/A}} \cdot \sqrt{\frac{\sigma_y}{E}} \qquad (7\text{-}2)$$

$$\beta = \frac{b}{t_p} \cdot \sqrt{\frac{\sigma_y}{E}} \qquad (7\text{-}3)$$

in which, E = Young's modulus of the material which can be treated as a random variable (Paik & Frieze 2001), a = length of the stiffener between transverse beams, b = breadth of plate between longitudinal stiffeners, t_p = plate thickness, r = radius of gyration of a stiffener where A = area of the stiffener with full plating and I = moment of inertia of the stiffener with full plating; and Z = elastic section modulus of the hull. A and I are given by

$$A = b \cdot t_p + h_w \cdot t_w + w_f \cdot t_f \tag{7-4}$$

$$I = \frac{b \cdot t_p^3}{12} + b \cdot t_p \cdot (z_o - \frac{t_p}{2})^2 + \frac{h_w^3 \cdot t_w}{12} + h_w \cdot t_w \cdot (z_o - t_p - \frac{h_w}{2})^2 + \frac{w_f \cdot t_f^3}{12}$$

$$+ \ w_f \cdot t_f \cdot (z_o - t_p - h_w - \frac{t_f}{2})^2 \tag{7-5}$$

where h_w and t_w = height and thickness of the stiffener web, respectively, w_f and t_f = width and thickness of the stiffener flange, respectively, and z_o = distance of the neutral axis from the base line of plate which is calculated by

$$z_o = \frac{1}{A} \cdot [\frac{b \cdot t_p^2}{2} + h_w \cdot t_w \cdot (t_p + \frac{h_w}{2}) + w_f \cdot t_f \cdot (t_p + h_w + \frac{t_f}{2})] \tag{7-6}$$

The section moduli in ship deck and bottom are calculated by using Eqs. 7-7 and 7-8, respectively (Paik et al. 1998)

$$Z_D = \frac{1}{D-g} \cdot [A_D \cdot (D-g)^2 + A_B \cdot g^2 + A_B' \cdot (g - D_B)^2 + \frac{A_S \cdot D \cdot (2D - 3g)}{3}]$$

$$\tag{7-7}$$

$$Z_B = \frac{1}{g} \cdot [A_D \cdot (D-g)^2 + A_B \cdot g^2 + A_B' \cdot (g - D_B)^2 + \frac{A_S \cdot D \cdot (2D - 3g)}{3}]$$

where D = ship depth, D_B = height of double-bottom; A_D, A_B and $A_B{}'$ = area of deck, outer and inner bottom, respectively, A_S = a half of the area of side shell and longitudinal bulkheads; and g = distance of the neutral axis expressed as

$$g = \frac{D \cdot (A_D + A_S) + A_B' \cdot D_B}{A_D + A_B + A_B' + 2A_S}$$

(7-9)

By substituting Eqs. 7-7 and 7-8 into Eq. 7-1, the ultimate buckling strength M_{us} and M_{uh} can be calculated for sagging and hogging conditions, respectively.

7.2.2 Bending Moment

In evaluating the safety of ship structures, reliable estimation of potential sea loadings is crucial for the assessment and prediction of lifetime structural performance during their entire service life. Structural loads on a ship result from its own weight, cargo, buoyancy, and operation (Ayyub et al. 2002c).

In general, ship hull girder loads can be classified into three types which are still water loads, low and high frequency wave-induced loads, and thermal loads (Munse et al. 1983 and Paik & Frieze 2001). Still water loads can be estimated considering the difference between the weight and buoyancy distributions along the ship's length. The low frequency wave-induced loads consist of vertical, horizontal, and torsional wave loads, while the high frequency dynamic loads are due to slamming or whipping and springing (Munse et al. 1983). Both wave loads and dynamic loads are related to and affected by many factors such as ship characteristics, ship speed, relative wave heading, and sea states associated with significant wave

heights (Ayyub et al. 2002c). When requiring statistical or extreme analyses of ship response data collected from simulation, experiment, or monitoring, significant wave height can be treated as a random variable with maximum wave-induced and dynamic bending moments.

In this study, still water and wave-induced bending moments are considered as load effects which can be frequently encountered under ship operational conditions at sea. By using the IACS recommendation (2006), the still water bending moment, M_{sw}, is estimated for sagging and hogging conditions as follows:

(a) for sagging condition

$$M_{sw} = -0.05185 \cdot C_{wv} \cdot L^2 \cdot B \cdot (C_b + 0.7) \cdot 10^{-3} \quad \text{MNm} \qquad (7\text{-}10a)$$

(b) for hogging condition

$$M_{sw} = +0.01 \cdot C_{wv} \cdot L^2 \cdot B \cdot (11.97 - 1.9 \cdot C_b) \cdot 10^{-3} \quad \text{MNm} \qquad (7\text{-}10b)$$

where L, B, and C_b = ship length, molded breadth, and block coefficient, respectively, and C_{wv} = wave coefficient; given by

$$C_{wv} = \begin{cases} 10.75 - [(300-L)/100]^{1.5} & \text{for } 90 \le L \le 300 \ m \\ 10.75 & \text{for } 300 < L < 350 \ m \\ 10.75 - [(L-350)/150]^{1.5} & \text{for } 350 \le L \le 500 \ m \end{cases} \qquad (7\text{-}10c)$$

To estimate the wave-induced bending moments, M_w, two approaches can be used: (i) IACS rule, and (ii) a simplified direct method (Loukakis & Chryssostomidis 1975). The IACS recommendation (2006) for estimating M_w is

(a) for sagging condition

$$M_w = -0.11 \cdot C_{wv} \cdot L^2 \cdot B \cdot (C_b + 0.7) \cdot 10^{-3} \quad \text{MNm} \tag{7-11a}$$

(b) for hogging condition

$$M_w = +0.19 \cdot C_{wv} \cdot L^2 \cdot B \cdot C_b \cdot 10^{-3} \quad \text{MNm} \tag{7-11b}$$

When considering ship operation during a certain period (i.e., under short-term extreme wave conditions), a simplified direct method can be alternatively used to estimate the maximum M_w. This method was developed by Loukakis & Chryssostomidis (1975). It is based on the parametric seakeeping tables established from direct ship motion results which are affected by ship size, ship speed, and significant wave height, among others (Paik et al. 1998). The root mean square value (i.e., $\sqrt{\lambda_o}$) from the seakeeping tables is first determined by using five parameters including Froude number ($F \cong 0.1623\ V/\sqrt{L}$), non-dimensional sea state (H_s/L), beam-to-draft ratio (B/T), length-to-beam ratio (L/B), and block coefficient (C_b) where significant wave height $H_s = 1.1\sqrt{L}$, V = ship operating speed and T = draft. In the following, the most probable extreme value M_w, which can be treated as mean value, is calculated as (Mansour 1987)

$$M_w = \sqrt{2 \cdot \lambda_o \cdot \ln N} + \frac{0.5772}{\sqrt{2 \cdot \lambda_o \cdot \ln N}} \tag{7-12}$$

where N = expected number of wave bending peaks (e.g., for an average wave moment period of 10 seconds and a three-hour storm, N = 3 x 60 x 60 / 10 = 1080).

As described previously, the total bending moment M_t is estimated by

combination of M_{sw} and M_w. Therefore, structural reliability evaluation of ship hull girders for bending is based on two load combinations as

$$M_t = x_{sw} \cdot M_{sw} + x_w \cdot x_s \cdot M_w \qquad (7\text{-}13)$$

where x_{sw} and x_w = random variables representing model uncertainty in still water bending moment and wave-induced bending moment, respectively, and x_s = random variable representing model uncertainty associated with non-linearity in wave-induced bending moment. For reliability-based ship assessment, the wave-induced bending moment, M_w, can be treated as a random variable since it depends on ship's principal characteristics, environmental influences, and operational conditions (Ayyub et al. 2002c). In this study, M_{sw} and M_w are assumed as Normal and Gumbel (Type I largest) distributions, respectively (Akpan et al. 2002 and Hussein & Soares 2009).

7.3   SYSTEM-BASED RELIABILITY ASSESSMENT

Based on the information on the ultimate hull bending strength, M_u, and extreme bending moment, M_t, the time-dependent structural performance assessment of hull girder structures can be carried out at the elementary and system levels for potential failure modes (e.g., corrosion, fatigue crack).

7.3.1   Limit-State Function

A general performance function can be established to define ship safety margin $g_i(X)$ for the identified i-th failure mode as

$$g_i(X) = M_{u,i} - M_t \quad \text{for } i = 1, 2, \ldots, k \qquad (7\text{-}14)$$

where $M_{u,i}$ = hull girder bending moment capacity and M_t = primary total bending moment on the hull. Based on the performance function $g_i(X)$, the failure or complementary (safe) probability of a structural member are defined, respectively, as

$$P_f = P[g(X) < 0] = \int_\Omega f_X (\mathbf{x}) \cdot d\mathbf{x} \qquad (7\text{-}15a)$$

$$P_s = P[g(X) > 0] = 1 - P_f \qquad (7\text{-}15b)$$

where X = a vector of random variables with joint probability density function (PDF), $f_\mathbf{X}(\mathbf{x})$, and Ω is the failure domain defined by

$$\Omega \equiv (g(X) < 0) \qquad \text{for an elementary reliability problem} \qquad (7\text{-}16a)$$

or,

$$\Omega \equiv \left\{ \bigcup_{k=1}^{n} \bigcap_{i \in C_k} (g_i(X) < 0) \right\} \qquad \text{for a system reliability problem} \qquad (7\text{-}16b)$$

where C_k and n refer to the k-th cut set and the number of cut sets, respectively, in which each cut set is defined as an intersection of elementary failure events.

When considering safety margin for the time-dependent ultimate bending capacity of ship hull girders deteriorated due to corrosion or fatigue cracking (Paik et al. 2005), the limit-state function can be expressed as

$$g_i(t) = x_u \cdot [\frac{A_i(t)}{A_o} \cdot \sigma_{uo}] \cdot Z - [x_{sw} \cdot M_{sw}(t) + x_w \cdot x_s \cdot M_w(t)] = 0 \qquad (7\text{-}17)$$

where $A_i(t)$ = time-dependent damaged cross-sectional area associated with reduction in thickness for corrosion or in length for fatigue crack, A_o = total (i.e., undamaged) cross-sectional area calculated by using Eq. 7-4, x_u = random variable representing

model uncertainty in ultimate strength, and σ_{uo} = ultimate buckling strength of intact stiffened panel (see Eq. 7-1).

For corrosion failure mode, the damaged cross-sectional area $A_1(t)$ is estimated by (Paik & Thayamballi 2002 and Ayyub et al. 2002a)

$$A_1(t) = b \cdot [t_p - r(t)] + h_w \cdot [t_w - r(t)] + w_f \cdot [t_f - r(t)] \tag{7-18}$$

where $r(t) = C_1 \cdot (t - t_o)^{C_2}$ = thickness reduction factor, in which t_o = coating life (in years), t = aging ship service life (in years), and C_1, C_2 = random variables representing corrosion growth coefficients. In this study, C_2 representing the slope of corrosion growth is taken as 1.0. It is noted that $r(t)$ included in each term of Eq. 7-18 is eliminated if there is no corrosion damage of the plate (i.e., $t_p(t) = t_p$), web (i.e., $t_w(t) = t_w$) or flange (i.e., $t_f(t) = t_f$).

For fatigue cracking damage, the fracture mechanics approach can be used to establish crack growth equations associated with the stress intensity factor, stress range, material and environmental properties. Typically, the Paris equation is used (Paris & Erdogan 1963):

$$\frac{da}{dN} = C \cdot (\Delta K)^m \tag{7-19a}$$

$$\Delta K = Y(a) \cdot S_{re} \cdot \sqrt{\pi \cdot a} \tag{7-19b}$$

where a = crack size, N = number of cycles and ΔK = stress intensity factor range while C and m are the fatigue coefficient and the fatigue exponent (i.e., material constant), respectively; and $Y(a)$ = a geometric factor, S_{re} = equivalent stress range. Assuming that $Y(a)$ is a constant and $m \neq 2.0$, the crack size, $a(N)$ or $a(t)$, by using

338

Eqs. 7-19(a) and 7-19(b) is

$$a(N) = [a_o^{1-m/2} + (1 - \frac{m}{2}) \cdot C \cdot S_{re}^m \cdot Y^m \cdot \pi^{m/2} \cdot N]^{2/(2-m)} \tag{7-20a}$$

$$a(t) = [a_o^{1-m/2} + (1 - \frac{m}{2}) \cdot C \cdot S_{re}^m \cdot Y^m \cdot \pi^{m/2} \cdot (365 \cdot \alpha \cdot N_{avg} \cdot t)]^{2/(2-m)} \tag{7-20b}$$

where a_o = initial crack size, α = annual ship operation rate, and N_{avg} = average daily number of cycles. Accordingly, $A_2(t)$ for crack growth of a stiffened steel panel is

$$A_2(t) = [b - a(t)] \cdot t_p + [h_w - a(t)] \cdot t_w + w_f \cdot t_f \tag{7-21}$$

In addition, corrosion-enhanced fatigue cracking damage can be considered. The corrosion–enhanced crack growth parameter C_{corr}, which is greater than 1.0, is included in $a(t)$ of Eq. 7-20(b) as (Ayyub et al. 2002a)

$$a_c(t) = [a_o^{1-m/2} + (1 - \frac{m}{2}) \cdot C_{corr} \cdot C \cdot S_{re}^m \cdot Y^m \cdot \pi^{m/2} \cdot (365 \cdot \alpha \cdot N_{avg} \cdot t)]^{2/(2-m)}$$

$$\tag{7-22}$$

where a_c = corrosion-enhanced fatigue crack size. $A_3(t)$ for corrosion-enhanced fatigue cracking damage is

$$A_3(t) = [b - a_c(t)] \cdot [t_p - r(t)] + [h_w - a_c(t)] \cdot [t_w - r(t)] + w_f \cdot t_f \tag{7-23}$$

7.3.2 System Reliability Analysis

Typically, structural details of a ship hull girder can fail due to a dominant critical failure mode (e.g., fatigue cracking, corrosion). Structural failure can be the result of different failure modes (Dissanayake & Karunananda 2008). Accordingly, a

system model can be developed considering potential failure modes. Assuming that all n failure modes ($g_i \leq 0$) are in a series system, its structural failure will occur in any one of its modes. The system failure probability of the structure is

$$P_{fsys} = P_f(g_1 \leq 0 \text{ or } g_2 \leq 0 \text{ or } \cdots \text{or } g_n \leq 0) \qquad (7\text{-}24)$$

Depending on the correlation between the failure modes, the first order bounds of a series system (Cornell 1967) range from fully dependent (lower bound) to completely independent (upper bound)

$$\max_{i=1}^{n}[P_{fi}] \leq P_{fsys} \leq 1 - \prod_{i=1}^{n}(1 - P_{fi}) \qquad (7\text{-}25a)$$

The bounds of a parallel system are associated with independent and fully dependent failure modes, respectively.

$$\prod_{i=1}^{n}(P_{fi}) \leq P_{fsys} \leq \min_{i=1}^{n}[P_{fi}] \qquad (7\text{-}25b)$$

where n = number of failure modes and P_{fi} = probability of occurrence of a failure mode; given by

$$P_{f_i} = \Phi(-\beta_i) \qquad (7\text{-}26)$$

in which, $\Phi(\cdot)$ = standard normal cumulative distribution function (CDF) and β_i = reliability index that is

$$\beta_i = \Phi^{-1}(1 - P_{f_i}) = -\Phi^{-1}(P_{f_i}) \qquad (7\text{-}27)$$

As a quantitative way to express ship condition, its overall safety is estimated by using the computed system failure probability. Based on the lower and upper

bounds of the system failure probability (see Eq. 7-25), a system reliability index, β_{sys}, can be calculated from both bounds

$$\beta_{sys} = -\Phi^{-1}(P_{fsys}) \qquad (7\text{-}28)$$

where P_{fsys} = probability of system failure.

The lower bound of P_{fsys} corresponds to the upper bound of β_{sys}, whereas its upper bound is related to the lower bound of β_{sys}.

In this study, the system-based reliability analysis is performed based on the established limit-state functions (see Eq. 7-17), by using the reliability software RELSYS (Estes & Frangopol 1998) in which the average of the Ditlevsen's upper and lower bounds (i.e., second-order bounds; Ditlevsen 1979) is considered as P_{fsys}.

7.4   APPLICATION EXAMPLE

For an illustrative purpose, a Very Large Crude Carrier (VLCC) Energy Concentration is herein investigated. This VLCC was built in Japan in March 1970 on the basis of the design practice provided by Det Norske Veritas (Gordo et al. 1996 and Khan & Parmentier 2006). However, after only 10 years of operation (i.e., in July 1980), the ship failed during a discharge of oil at Rotterdam due to severe corrosion growth near midship. Therefore, corrosion damage mode has to be considered as a primary criterion for lifetime structural performance assessment. Structural details and principal dimensions of the VLCC are found in Khan & Parmentier (2006; see also Figure 7-1). Overall ship length and her dead weight are 326.75 m and 216,269 tons, respectively, with L = 313.00 m, B = 48.19 m, D = 25.20 m, and T = 19.60 m. The

computed coefficients, C_b and C_{wv} are 0.73 and 10.75, respectively. It is also considered that design ship speed, $V_d = 15.5$ knots and $H_s = 10.7442$ m. The deck and bottom are made of high strength steel (HTS) with yield strength $\sigma_y = 315$ MPa, while the main parts of side shell, longitudinals and bulkheads are made of mild steel (MS) with $\sigma_y = 235$ MPa, as shown in Figure 7-1(a). In this study, it is assumed that the ship has experienced both corrosion and fatigue cracking. In addition, there are two assumptions that general corrosion (i.e., uniform) of hull girder is prevalent and that fatigue cracking is dominant in midship.

By using Eqs. 7-1 through 7-9, the ultimate bending strength, M_u, of the intact VLCC is computed for sagging and hogging conditions in deck and bottom, respectively. All properties associated with the midship section are presented in Table 7-1. For sagging and hogging moments, the computed M_{us} and M_{uh} are 16,028 MNm and 17,264 MNm, respectively. As load effects, still water and wave-induced moments are estimated based on IACS formulae (2006; see Eqs. 7-10 and 7-11) with the ship particulars (i.e., L, B, C_b, and C_{wv}). For sagging and hogging conditions, the computed mean values of M_{sw} are 3,763 MNm and 5,371 MNm, respectively, while the mean values of M_w are 7,986 MNm and 7,038 MNm, respectively.

As mentioned previously, short-term extreme wave conditions are considered to estimate the maximum wave-induced bending moments according to various sea states, by using the simplified direct method (see Eq. 7-12). Five parameters (i.e., F, H_s/L, B/T, L/B and C_b) are calculated by imposing different ship speeds to the design speed, V_d, (i.e., $V = 0.25\ V_d$, $V = 0.5 V_d$, $V = 0.75 V_d$, and $V = 1.0 V_d$) for a three-hour storm period (i.e., $N \approx 1000$). They are used to find the non dimensional root mean

square values from the seakeeping tables provided in Loukakis & Chryssostomidis (1975). Detail computation procedures are also found in Paik et al. (1998). By applying the simplified direct method, wave-induced bending moments varying in effective wave heights or different ship operating speeds are estimated. For given ship speed, Figure 7-2(a) shows the variation of the wave-induced bending moment, M_w, with increase in the significant wave height. When specified sea states are considered, variation of M_w according to different ship speeds is also plotted in Figure 7-2(b). If V and H_s are 11.625 knots and 10.7442 m, respectively, the dimensional root mean square value $\sqrt{\lambda_o} = 1{,}990$ MNm and the extreme wave-induced bending moment is 7,396 MNm. This extreme wave-induced bending moment is 92.6% for sagging and 105.1% for hogging, as compared to the values in the intact VLCC obtained from IACS formulae. As shown in Figure 7-2(b), the wave-induced bending moments for given significant wave heights increase almost linearly with increase in ship speed. For the lifetime structural reliability assessment, these results are used to estimate the mean value of wave-induced bending moment, $E(M_w)$, considering ship operational profile among sea state, ship speed, and relative wave heading, as addressed in Kwon et al. (2010). The equation for $E(M_w)$ is

$$E(M_w) = \sum_{i=1}^{ss} \sum_{j=1}^{sp} \sum_{k=1}^{wh} P_{SS,i} \cdot P_{SP,j} \cdot P_{WH,k} \cdot M_{w,ijk} \qquad (7\text{-}29)$$

where $P_{SS,i}$ = probability of occurrence of the i–th sea state ($i = 1, 2, \ldots, ss$), $P_{SP,j}$ = probability of occurrence of the j–th ship speed ($j = 1, 2, \ldots, sp$) and $P_{WH,k}$ = probability of occurrence of the k–th relative wave heading ($k = 1, 2, \ldots, wh$) for the applicable sea events. Ignoring the effect of the relative wave heading (i.e., $P_{WH,k}$ =

343

1.0), $E(M_w)$ is estimated by using Eq. 7-29 with applicable ship operational profile between sea state and ship speed. Based on the probabilistic data (i.e., probability of joint occurrence) developed by Glen et al. (1999; see Table 7-2), $E(M_w)$ is computed to be 1161 MNm for both sagging and hogging conditions.

The effects of ship operating speed, V (i.e, SP), and sea state, S (i.e., SS), on structural reliability of intact hull girders are now investigated. The corresponding limit-state function (see Eq. 7-17) is

$$g(V,S) = x_u \cdot \sigma_{u_O} \cdot Z - [x_{sw} \cdot M_{sw} + x_w \cdot x_s \cdot M_w(V,S)] = 0 \qquad (7\text{-}30)$$

By using Eqs. 7-10(a) and 7-10(b), the computed M_{sw} is used for sagging and hogging conditions, respectively. Figure 7-3(a) and (b) show reliability indices in ship deck and ship bottom, respectively, that decrease with increases in sea states for given ship speeds. The reliabilities estimated in sea states 4, 5, and 6 are not significantly affected by the ship speed, whereas those in sea states 7 and 8 decrease with increases in ship speed. When exceeding sea state 7, the estimated reliabilities for both loading conditions do not satisfy the target reliability levels estimated using IACS formulae. Figure 7-4(a) and (b) show variation of reliabilities according to different ship speeds in a same sea state. With exception of the result in a given sea state 8, the reliabilities are not very sensitive to ship operating speed.

Due to the attack of corrosion and/or fatigue, each and every member of the VLCC can experience its thickness and/or length reduction. Assuming that repair actions are not taken, the ultimate bending strength of the ship will be reduced through lifetime. As indicated in Figure 7-1(b), the time-dependent ultimate bending moment,

$M_u(t)$, is estimated for four identified damage scenarios: (i) failure mode I - web corrosion only, (ii) failure mode II – plate corrosion only, (iii) failure mode III – fatigue crack; and (iv) failure mode IV – corrosion-enhanced fatigue crack. All probabilistic characteristics associated with the annual corrosion rates and crack growth parameters are given in Table 7-3. It is assumed that the failure modes III and IV are associated with fatigue crack growth in plates between longitudinal stiffeners. For sagging and hogging conditions, the time-dependent mean ultimate bending strength $E(M_u)$ is shown in Figure 7-5(a) and (b) for corrosion (cases I and II) and fatigue (cases III and IV), respectively. For the same loading conditions, $E(M_u)$ decreases more in plate corrosion than in web corrosion, while it decreases less in fatigue cracking only than in corrosion-enhanced fatigue cracking.

Based on all necessary information on both structural resistance and loads, the time-dependent reliability analysis associated with individual failure modes I, II, III, and IV is performed using the reliability software RELSYS (Estes & Frangopol 1998) using the limit-state function in Eq. 7-17. Complete descriptions for the deterministic parameters and random variables associated with Eq. 7-17 are indicated in Table 7-3 and Table 7-4. The reliability indices estimated are shown in Figure 7-6(a) and (b). For both corrosion and cracking attack, it is found that reliability indices associated with hogging (ship bottom) are lower than those associated with sagging (ship deck).

In this, two system models A and B are considered: series and series-parallel system models, as indicated in Figure 7-7(a) and (b), respectively. For these system models, system failure probability, P_{fsys}, and system reliability index, β_{sys}, are estimated considering the first- and second-order bounds. If the first-order bounds

(Cornell 1967) are considered, the system failure probabilities for upper and lower bounds can be computed by using Eq. 7-25 based on the elementary probability of failure. Their associated system reliability indices can be easily calculated by converting the system failure probabilities for both bounds (see Eq. 7-28). Figure 7-8(a) and (b) show the results of P_{fsys} and β_{sys}, respectively, when considering the first-order bounds for the series system model (i.e., model A). If all failure modes are perfectly correlated, the first-order lower bound of P_{fsys} can be used to estimate the time-dependent system probability of failure (see Figure 7-8(a)). On the other hand, its upper bound can be estimated when the failure modes are statistically independent, implying that they do not have any relationship. For a same bound, the system reliability indices for hogging moment are obtained in lower levels than those for sagging moment (see Figure 7-8(b)). However, since these bounds are often too wide for practical use, the Ditlevsen's bounds (i.e., second-order bounds) can be used in a more reasonable way. The associated results are shown in Figure 7-9 and Figure 7-10 for the system models A and B, respectively. The upper and lower bounds of Ditlevsen are formed in more narrow range as compared to the results obtained from the first-order bounds (see Figure 7-8). As shown in Figure 7-9 and Figure 7-10, the hogging moment is considered as a governing load effect. For both system models A and B, the average of Ditlevsen's bounds of P_{fsys} and its corresponding β_{sys} are plotted in Figure 7-11(a) and (b), respectively. As a result, β_{sys} obtained from the series system (i.e., model A) is more critical than that for the series-parallel system (i.e., model B) regardless of sagging and hogging conditions.

In addition, the elementary and system reliability indices estimated in a service

life of 10 years are presented in Table 7-5. For the system models A and B considering four identified potential damage modes (i.e., failure modes I, II, III, and IV), the estimated system reliability indices for sagging moment range from 2.632 (first-order upper bound of P_{fsys}) to 3.057 (first-order lower bound of P_{fsys}) in model A, while those for hogging moment range from 2.280 in model A (first-order upper bound of P_{fsys}) to 2.758 in model B (Ditlevsen's lower bound of P_{fsys}).

7.5 SUMMARY AND CONCLUDING REMARKS

This study presented a system-based approach for estimating the time-dependent reliability associated with an aging hull girder in the presence of potential failure modes under corrosion and fatigue. Estimation of the ultimate strength of a hull girder subjected to vertical bending was based on an empirical formula derived by Paik et al. (1996), whereas still water and wave-induced bending moments were estimated using IACS recommendation (2006) and a simplified direct method developed by Loukakis & Chryssostomidis (1975), respectively. Effects of ship operational and sea environmental conditions on structural reliability in the intact hull condition were investigated. This approach was illustrated on a hull girder structure which is the VLCC Energy Concentration.

The following conclusions are drawn:

1. Structural reliability analysis can be performed considering a single failure mode only. Under simultaneous presence of several failure modes, a series system model as well as a series-parallel system model can be used to estimate the system reliability.

347

2. The time-dependent deterioration models associated with the ultimate buckling strength of hull girder structures can be developed at system level considering all potential failure modes which may be encountered during the entire service life.

3. The time-dependent random functions associated with corrosion and fatigue cracking can be formulated by using reduction factors in thickness and in length.

4. The time-dependent structural performance of hull girders can be rationally assessed and predicted by using the proposed system-based reliability approach.

5. Structural performance in the intact hull condition can be assessed according to ship operational and sea environmental conditions. The structural performance is more affected by the sea states than by the ship operating speed.

Table 7-1   Properties of the VLCC and ultimate bending strength for sagging and hogging conditions.

Parameters		Notation	Values
Area at deck, inner/outer bottom, and side shell (Paik & Mansour 1995)		A_D	20,381.8 cm^2
		$A_B{}'$	0
		A_B	20,790.4 cm^2
		A_S	16,470.9 cm^2
Section modulus		Z_D	65,575,783 cm^3
		Z_B	66,302,820 cm^3
Yield strength at deck, bottom, and side shell (Paik & Frieze 2001)		σ_y	Normal, $E(\sigma_y) = 315$ MPa $COV(\sigma_y) = 0.1$
Young's modulus (Paik & Frieze 2001)		E	Lognormal, $E(E) = 205,800$ MPa $COV(E) = 0.03$
Ultimate bending strength	for sagging	M_{us}	16,028 MNm
	for hogging	M_{uh}	17,264 MNm

Table 7-2   Probability of joint occurrence (Glen et al. 1999).

NATO Sea State (significant wave height H_s in meters)	Speed (knots)					* M_w (MNm)
	0-6	6-10	10-14	14-18	Sum	
1 (0-0.1)	0.0014	0.0028	0.0065	0.0457	0.0564	
2 (0.1-0.5)	0.0000	0.0012	0.0082	0.0472	0.0566	490
3 (0.5-1.25)	0.0014	0.0053	0.0800	0.2103	0.2970	
4 (1.25-2.5)	0.0000	0.0148	0.0686	0.1826	0.2660	
5 (2.5-4.0)	0.0000	0.0075	0.0392	0.1167	0.1634	1212
6 (4.0-6.0)	0.0006	0.0154	0.0527	0.0570	0.1256	3275
7 (6.0-9.0)	0.0062	0.0082	0.0164	0.0041	0.0349	6305
Sum	0.0096	0.0552	0.2717	0.6636	1.0000	

* M_w estimated by using the simplified direct method (Loukakis & Chryssostomidis 1975; see Figure 7-2)

Table 7-3 Probabilistic characteristics of the annual corrosion rates and crack growth coefficients.

Deterministic parameters and random variables			Distribution
Corrosion damage (Akpan et al. 2002)	Coating life, t_o (years)		Deterministic 3.0
	Corrosion growth coefficient (slope), C_2		Deterministic 1.0
	Deck plating	Annual corrosion rates, C_1 (mm/yr)	Weibull $E(C_1) = 0.065$, $COV(C_1) = 0.5$
	Deck longitudinals (web)		Weibull $E(C_1) = 0.065$, $COV(C_1) = 0.5$
	Bottom shell plating		Weibull $E(C_1) = 0.170$, $COV(C_1) = 0.5$
	Bottom shell longitudinals (web)		Weibull $E(C_1) = 0.065$, $COV(C_1) = 0.5$
Cracking damage	*Initial crack length, a_o in mm (Yazdani 1984)		Lognormal $E(a_o) = 0.882$, $COV(a_o) = 0.36$
	**Crack growth parameter, C in MPa $\sqrt{m}$ (Yazdani & Albrecht 1989)		Lognormal $E(C) = 2.37E\text{-}13$, $COV(C) = 0.15$
	Equivalent stress range, S_{re} (MPa)		Lognormal $E(S_{re}) = 34.5$, $COV(S_{re}) = 0.1$
	Material constant (slope), m (Yazdani & Albrecht 1989)		Deterministic 3.279
	Average daily number of cycles, N_{avg}		Deterministic 5500
	Annual ship operation rate, α		Deterministic 0.75
	Geometric factor, Y		Deterministic 1.0

* Probabilistic characteristics of initial crack length for high strength steel welded beam
** The mean value of C considered for high strength steel

Table 7-4 Random variables used for reliability assessment.

Random variables		Notation	Distribution	Reference
Model uncertainty in ultimate strength		x_u	Normal $E(x_u) = 1.0$, $COV(x_u) = 0.15$	Mansour & Hoven 1994, and Akpan et al. 2002
Model uncertainty in still water bending moment		x_{sw}	Normal $E(x_{sw}) = 1.0$, $COV(x_{sw}) = 0.05$	
Model uncertainty in wave-induced bending moment		x_w	Normal $E(x_w) = 0.9$, $COV(x_w) = 0.15$	
Model uncertainty in non-linearity of wave-induced bending moment		x_s	Normal $E(x_s) = 1.15$, $COV(x_s) = 0.03$	
Section modulus	Ship deck	Z_D	Lognormal $COV(Z_D) = 0.1$	see Table 7-1
	Ship bottom	Z_B	Lognormal $COV(Z_B) = 0.1$	
Still water bending moment	for sagging	M_{Sw} (MNm)	Normal $E(M_{Sw}) = 3,763$, $COV(M_{Sw}) = 0.4$	IACS 2006, Akpan et al. 2002, and Hussein & Soares 2009
	for hogging		Normal $E(M_{Sw}) = 5,371$, $COV(M_{Sw}) = 0.4$	
Wave induced bending moment		M_w (MNm)	Gumbel $E(M_{Sw}) = 1,161$, $COV(M_{Sw}) = 0.1$	Glen et al. 1999 (see Table 7-2), and Akpan et al. 2002

Table 7-5　System-based reliabilities of the VLCC associated with a service life of 10 years.

Approach	Damage mode		Reliability index at time horizon	
			Sagging moment (Ship deck)	Hogging moment (Ship bottom)
Single failure mode (Basic level)	Mode I - web corrosion only		3.082	2.797
	Mode II - plate corrosion only		3.063	2.735
	Mode III - fatigue crack		3.093	2.816
	Mode IV - corrosion-enhanced fatigue crack		3.057	2.729
Multiple failure mode (System level)	Model A (series system)	First-order lower bound	3.057	2.729
		First-order upper bound	2.632	2.280
		*Ditlevsen's lower bound	3.056	2.727
		*Ditlevsen's upper bound	3.002	2.688
		Average of Ditlevsen's bounds	3.028	2.707
	Model B (series-parallel system)	*Ditlevsen's lower bound	3.090	2.758
		*Ditlevsen's upper bound	2.999	2.712
		Average of Ditlevsen's bounds	3.041	2.734

* Ditlevsen's bounds refer to system failure probabilities

$t_f = 33$ mm

$w_f = 200$ mm

$t_w = 15$ mm

$h_w = 797$ mm

$t_p = 25$ mm

$b = 1000$ mm

CRACK

CORROSION

FAILURE MODE I: WEB CORROSION ONLY
FAILUER MODE II: PLATE CORROSION ONLY
FAILURE MODE III: FATIGUE CRACK
FAILURE MODE IV: CORROSION-ENHANCED FATIGUE CRACK

25200

23000

24100

3715

6475

MS

HTS

HTS

FRAME SPACING
= 5100

Note: all dimensions are in mm

(a) midship section detail (adapted from Khan & Parmentier 2006)   (b) critical element detail for potential failure modes

Figure 7-1   Detail of VLCC Energy Concentration.

354

(a) for different significant wave heights

(b) for different ship operating speeds
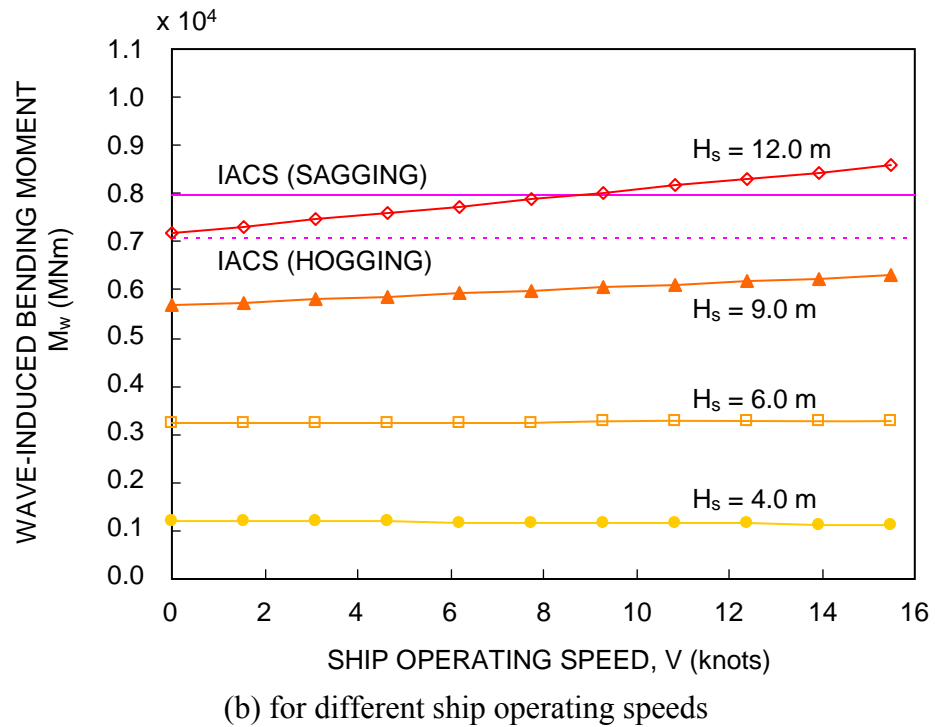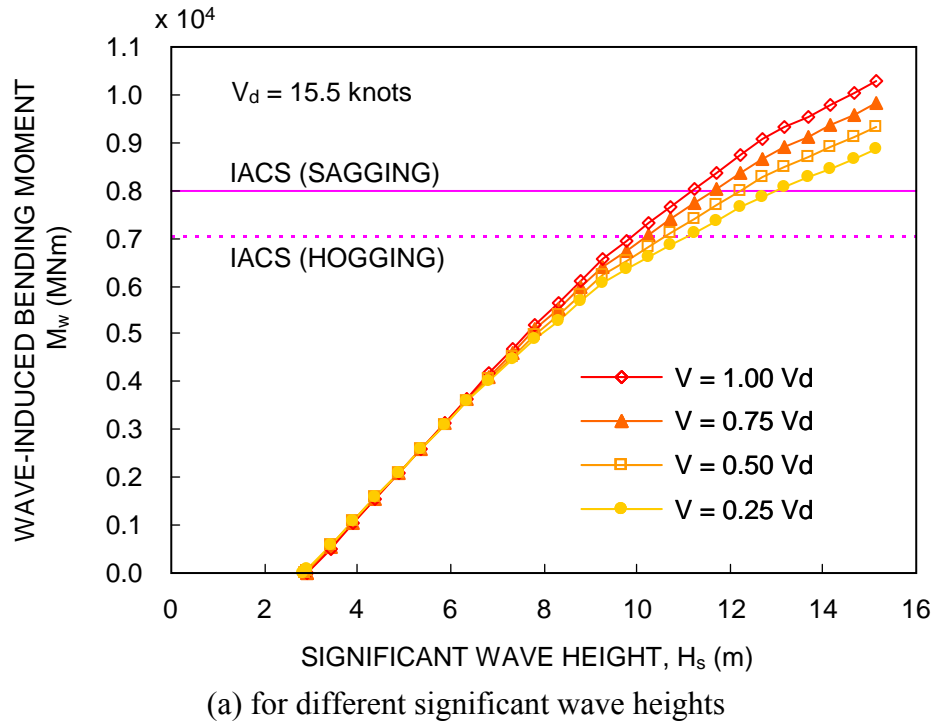
Figure 7-2   Variation of the wave-induced bending moment.

355
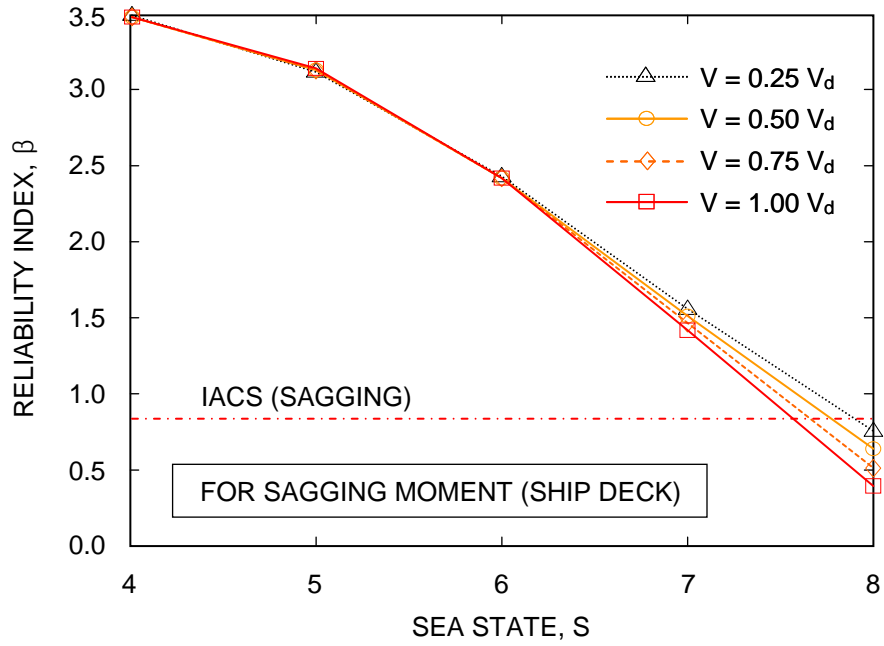
(a) for sagging moment (ship deck)
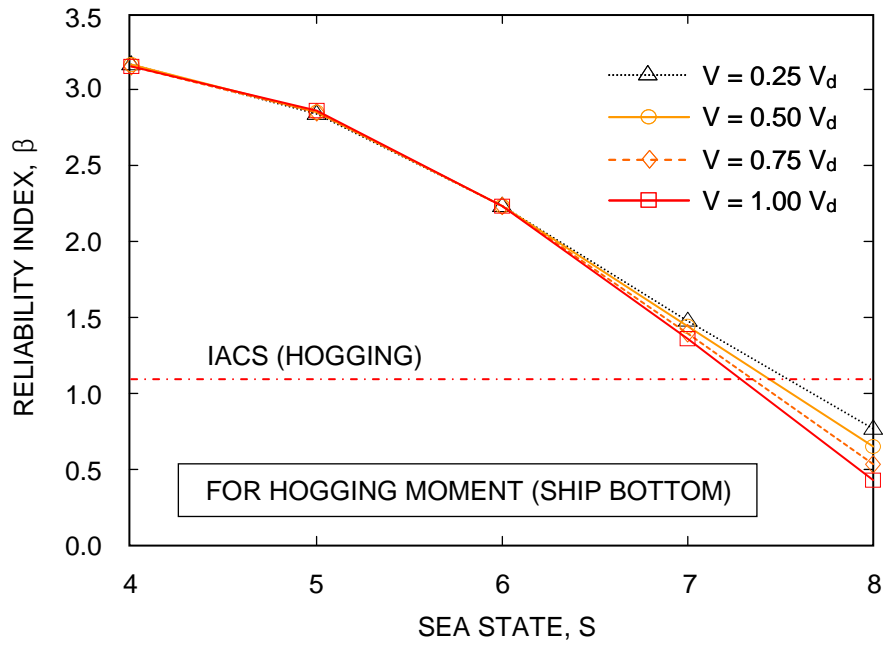
(b) for hogging moment (ship bottom)

Figure 7-3   Reliability index for different ship speeds of the intact VLCC.
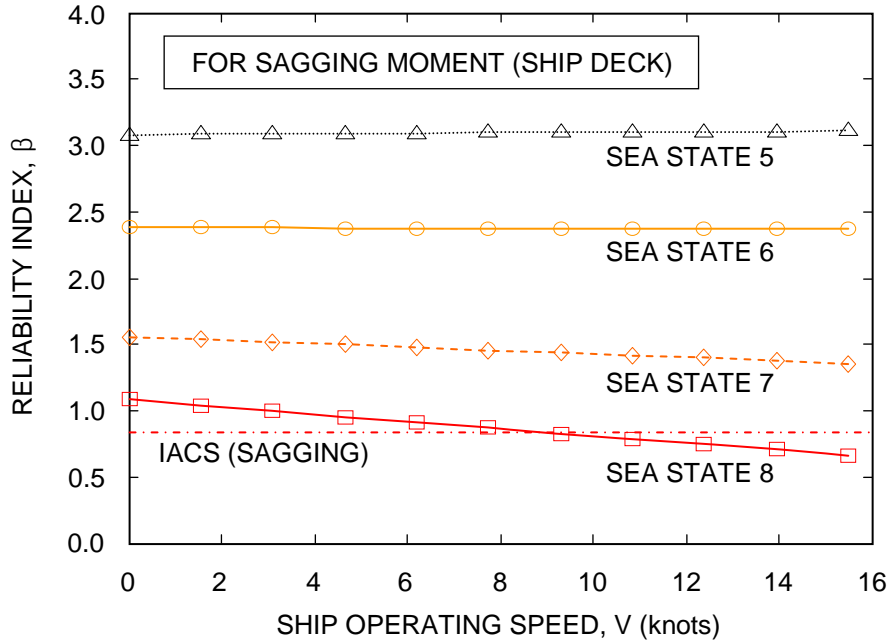
(a) for sagging moment (ship deck)
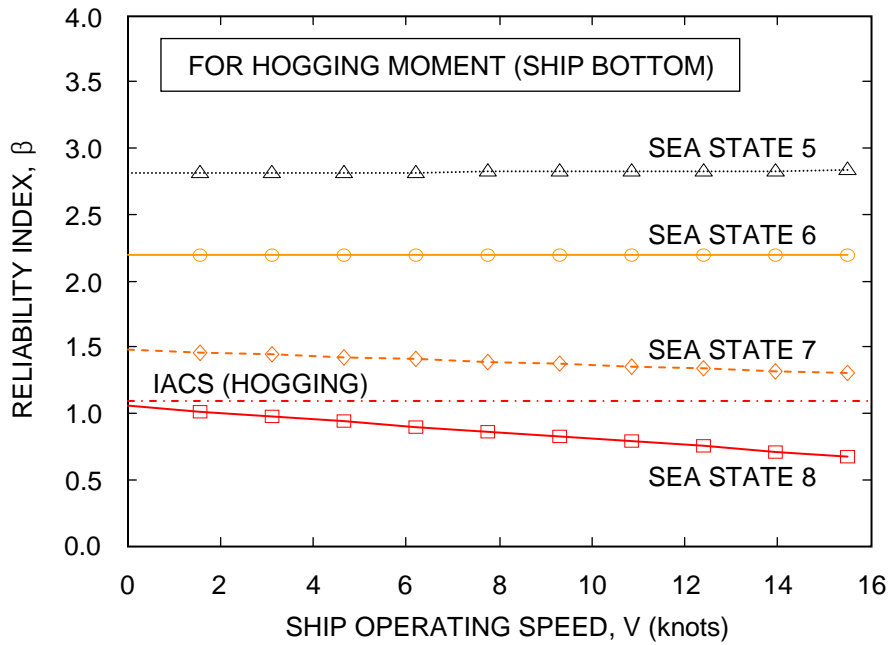
(b) for hogging moment (ship bottom)

Figure 7-4   Reliability index for different sea states of the intact VLCC.
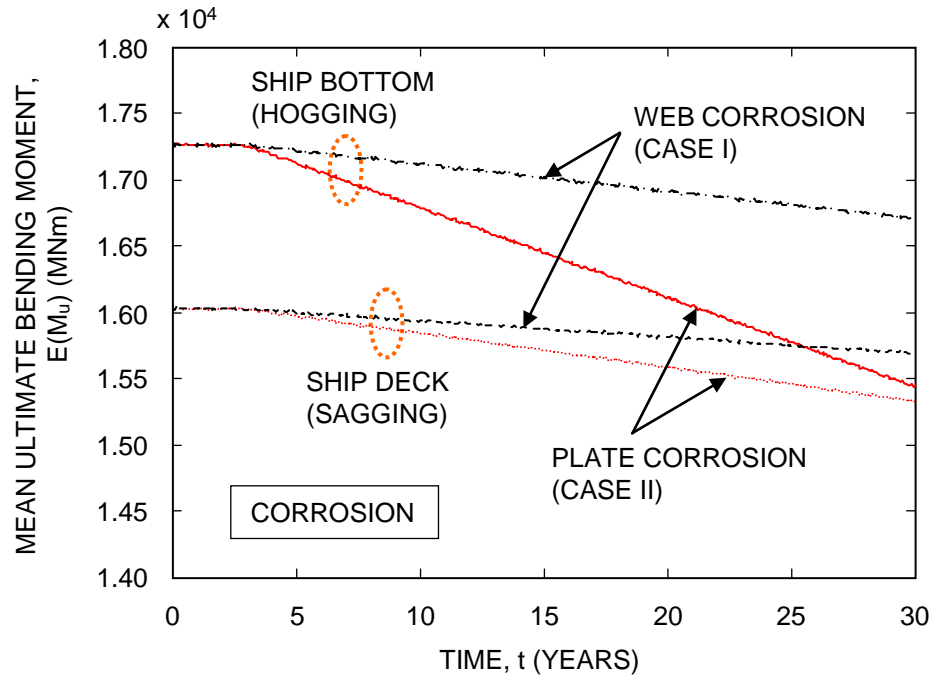
(a) for failure modes I and II under corrosion
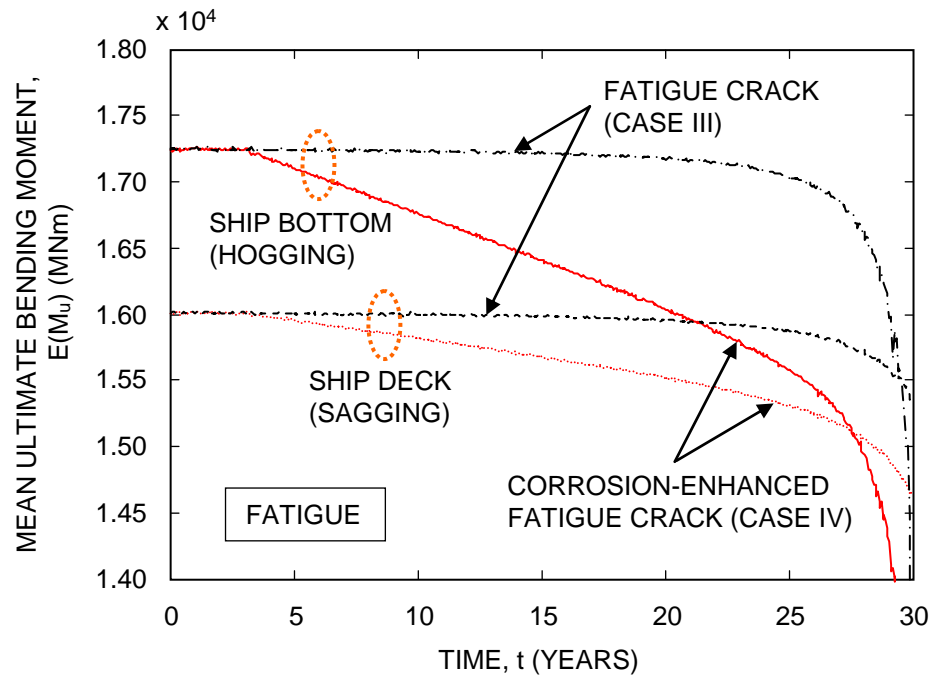
(b) for failure modes III and IV under fatigue

Figure 7-5   Mean ultimate bending moment.
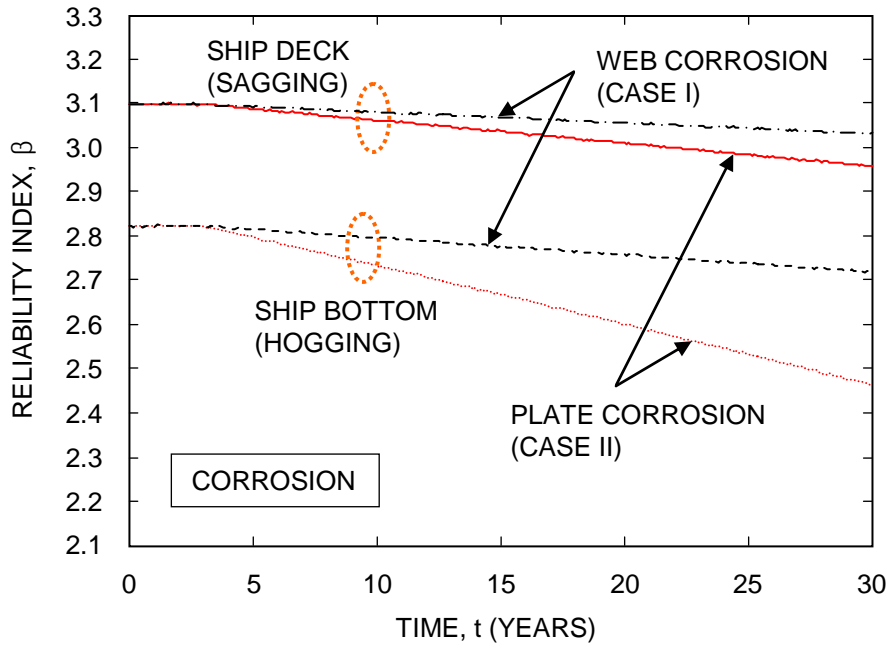
(a) failure modes I and II under corrosion
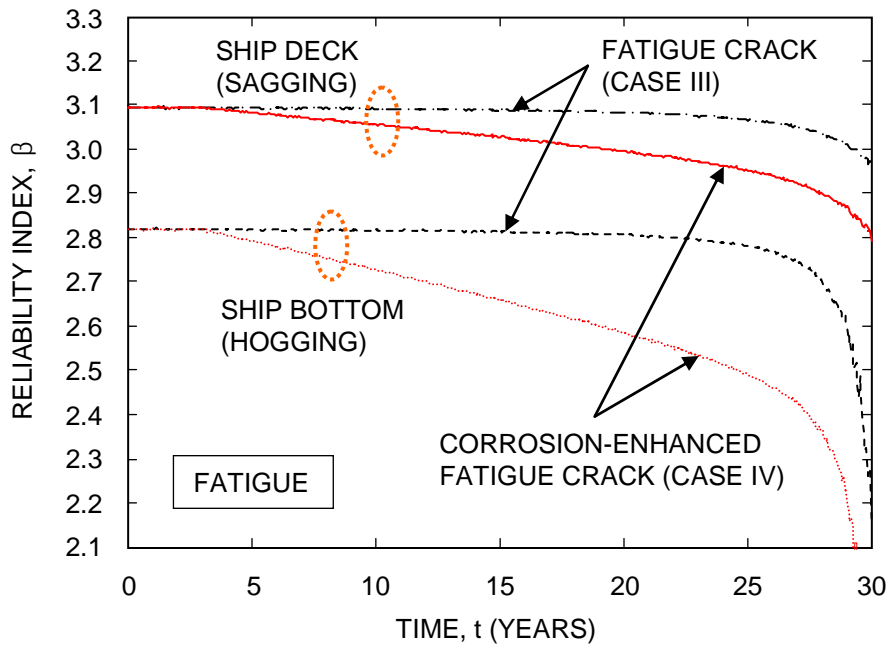
(b) failure modes III and IV under fatigue

Figure 7-6   Reliability index for a single failure mode.

359
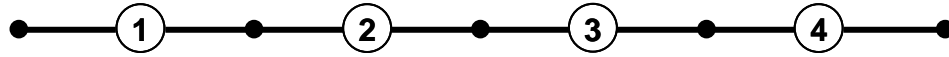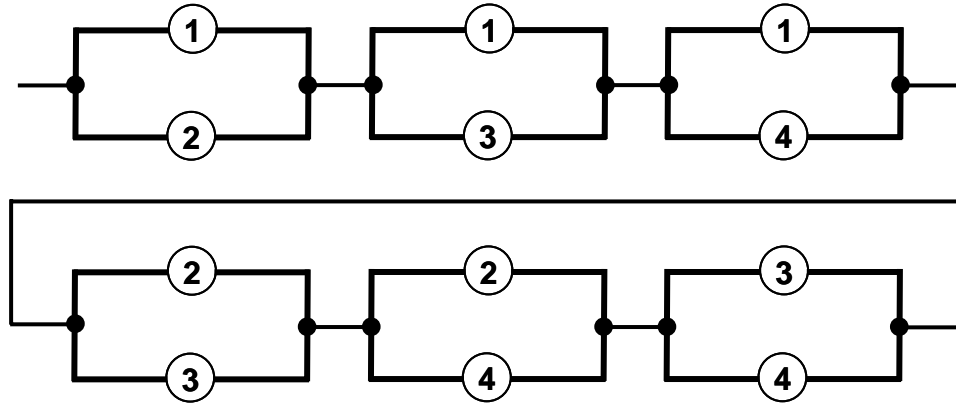
(a) system model A

① FAILUE MODE I   ② FAILURE MODE II

③ FAILURE MODE III   ④ FAILURE MODE IV

(b) system model B

Figure 7-7   System models considering multiple failure modes.
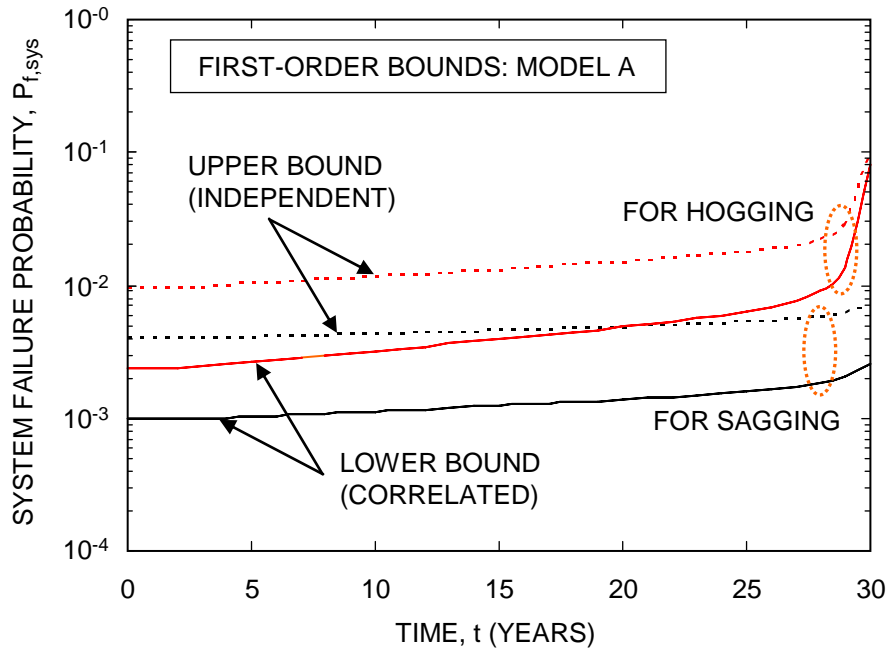
(a) system failure probability
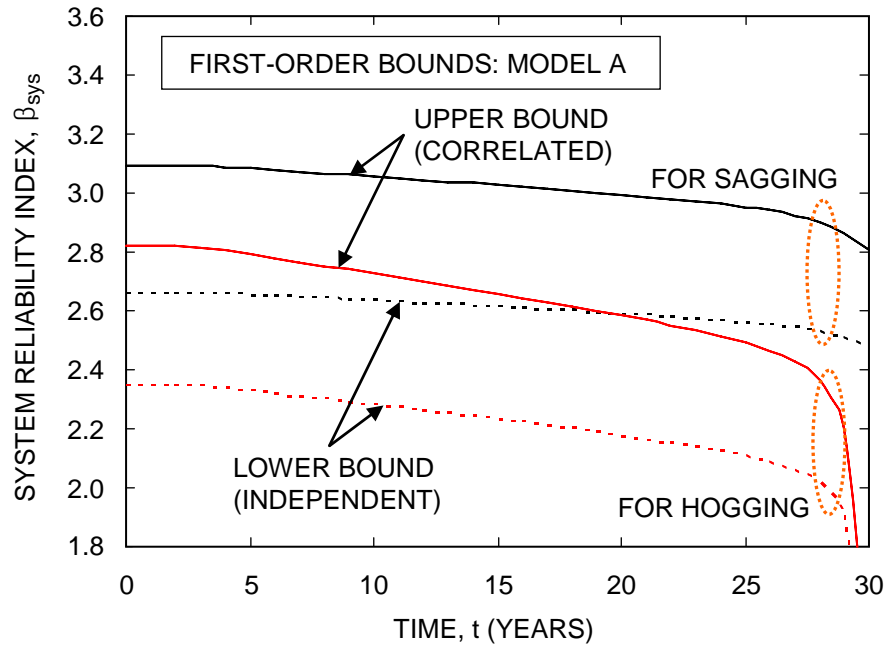
(b) system reliability

Figure 7-8   Lifetime performance assessment using first-order bounds for system model A.
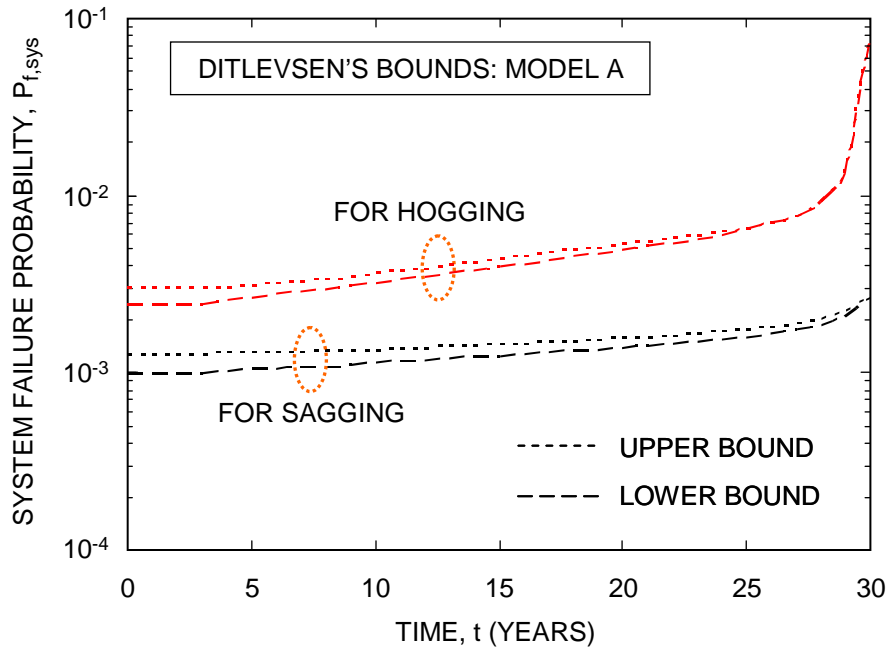
(a) system failure probability
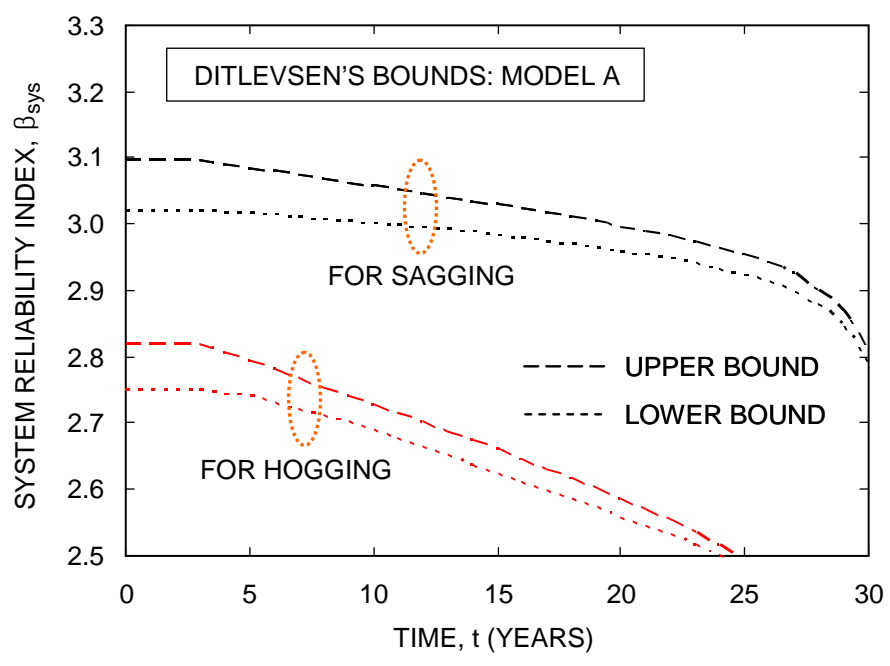
(b) system reliability

Figure 7-9   Lifetime performance assessment using Ditlevsen's bounds for system model A.

(a) system failure probability

(b) system reliability
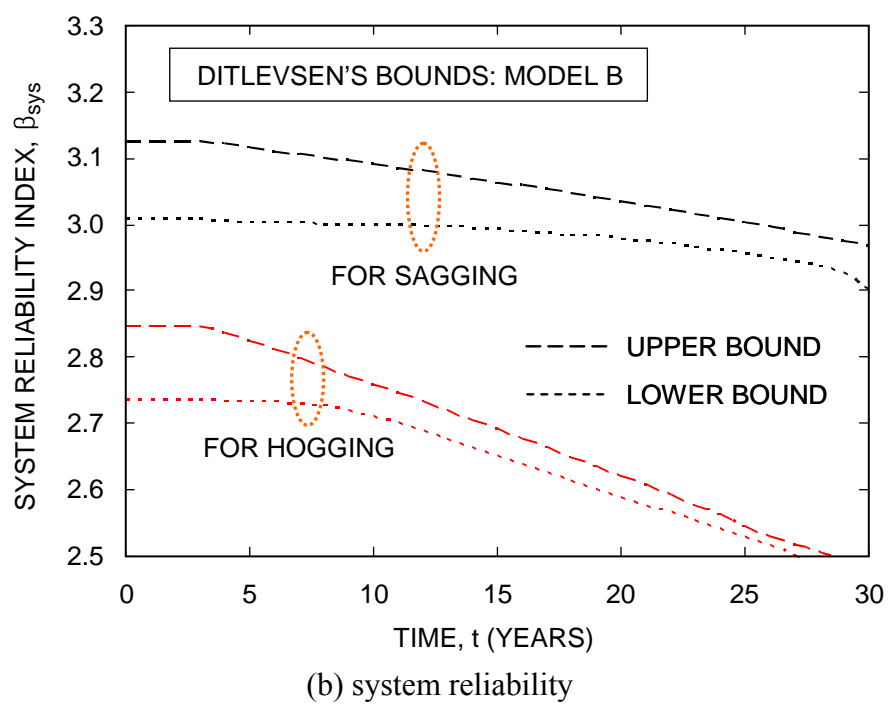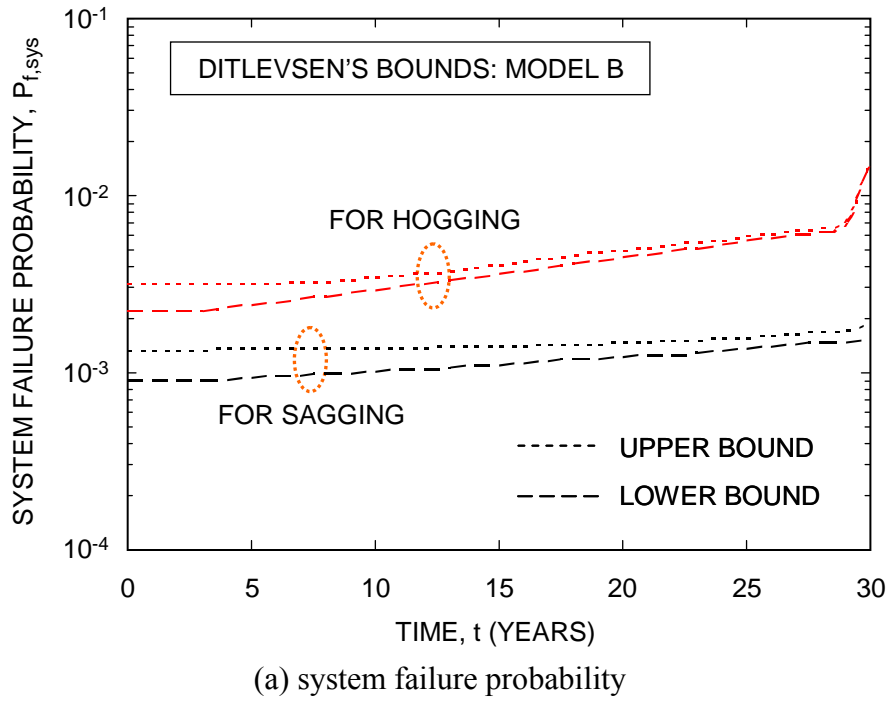
Figure 7-10   Lifetime performance assessment using Ditlevsen's bounds for system model B.
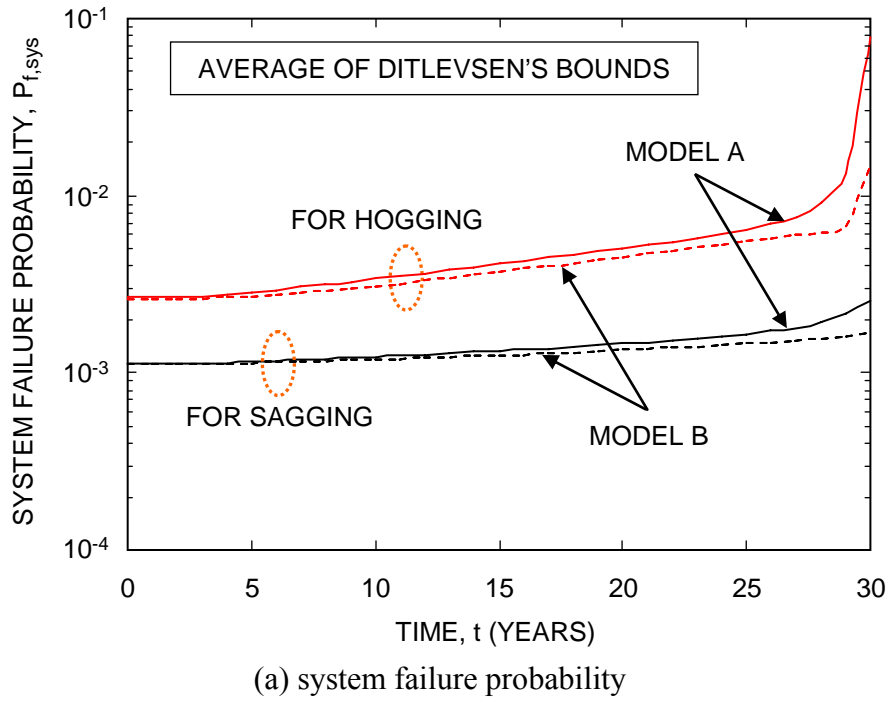
(a) system failure probability
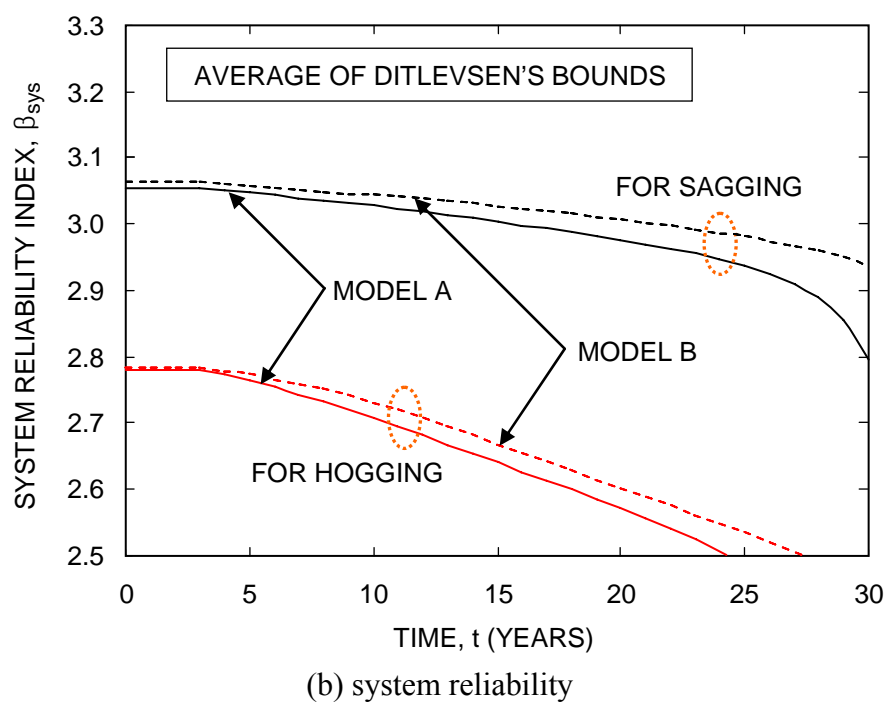
(b) system reliability

Figure 7-11   Lifetime performance assessment using average of Ditlevsen's bounds for system models A and B.

364

CHAPTER 8

CONCLUSIONS

8.1 INTRODUCTION

The objective of this study was to develop rational and efficient probabilistic approaches and methods for the reliability assessment, performance prediction and life-cycle management of fatigue sensitive structures by incorporating field test data under uncertainty. For illustrative purposes, corresponding applications in each chapter were presented and the findings were investigated.

Section 8.2 presents a summary and the conclusions drawn from the study on the fatigue reliability assessment and lifetime performance prediction of fatigue sensitive bridge and ship structures. Included in Section 8.3 are a summary and the conclusions drawn from the study on the reliability-based life-cycle management of bridge and ship structures susceptible to fatigue. A summary and the conclusions on the system-based reliability assessment and performance prediction of ship structures are presented in Section 8.4. Suggestions for future work are made in Section 8.5.

8.2 CONCLUSIONS ON FATIGUE RELIABILITY ASSESSMENT AND PERFORMANCE PREDICTION

The conclusions on fatigue reliability assessment and lifetime performance prediction of bridge and ship structures, which have been emphasized in Chapters 3 and 4, respectively, are presented here.

365

8.2.1 Bridge Structures

In Chapter 3, reliability approaches for fatigue performance assessment and lifetime prediction of steel highway bridges by incorporating SHM data were presented based on (i) the linear *S-N* approach and (ii) the bi-linear *S-N* approach. The stress-range bin histogram data collected on two existing bridges, the Neville Island Bridge and the Birmingham Bridge, were used to illustrate the proposed reliability approaches.

For assessing fatigue resistance in-service, current AASHTO linear *S-N* curve considering a single slope (i.e., $m = 3.0$) in all *S-N* categories was used in the fatigue reliability assessment, while a probabilistic method using the bi-linear *S-N* approach representing two different slopes (i.e., $m_1 = 3.0$, $m_2 = 4.0$) was developed for useful estimation of fatigue life below the CAFT. In terms of load demand, SHM data were used to estimate corresponding linear and bi-linear equivalent stress ranges for fatigue. Under uncertainties associated with loading history, appropriate PDFs (i.e., Lognormal, Weibull, Gamma, or Rayleigh) were used as lifetime prediction models of stress ranges.

From the analyses of the time-dependent fatigue reliability assessment and performance prediction of steel highway bridges subjected to fatigue, the following conclusions were drawn:

- The field monitoring data can be reliably used to estimate load effect for the time-dependent fatigue performance assessment and lifetime prediction of existing steel bridges. Based on the stress-range bin histogram established from SHM data, appropriate PDFs can be predicted and used to estimate the linear

and bi-linear equivalent stress ranges under loading uncertainty.

- The upper and lower bounds of stress range cut-off thresholds from the established stress-range bin histogram can be reasonably predefined considering the AASHTO fatigue criteria associated with the CAFT and the frequency limit.

- According to the predefined stress range cut-off thresholds and the assumed PDFs, the mean value and standard deviation of equivalent stress ranges can be computed. By using the estimated statistical information, uncertainty associated with fatigue loading is reduced.

- Probabilistic treatments of two important parameters, fatigue detail coefficient and equivalent stress range, can improve the fatigue reliability assessment. Consequently, the remaining fatigue life of a structure can be reliably predicted by using the proposed probabilistic approach.

- The application of the bi-linear *S-N* approach with two different slopes leads to additional fatigue life than that estimated by using the direct extension provided in the AASHTO linear *S-N* approach.

- The bi-linear equivalent stress range can be effectively used to estimate probabilistic fatigue life associated with the propagation of fatigue cracks derived from a fracture mechanics model.

- In assessment phase, the bi-linear *S-N* approach, which is developed by the analytical derivations using the concept of decreasing the CAFT (Crudele & Yen 2006), can be applied for the useful fatigue life estimation of structural details.

367

8.2.2   Ship Structures

In Chapter 4, probabilistic-based approaches and methods for fatigue reliability assessment and service life prediction of steel and aluminum ship structures susceptible to fatigue were presented.

For the fatigue reliability evaluation of high-speed naval ships, the linear *S-N* approach in the identified steel-based details was used to assess structural capacity for fatigue, whereas model test data were used to estimate probabilistic lifetime sea loads. Under uncertainties associated with fatigue resistance and load effect, two PDFs (i.e., Lognormal, Weibull) were used. The unfiltered (raw) data collected on a scaled JHSS monohull was used to establish the stress-range bin histogram using peak counting method. For aluminum ship structures, fatigue reliability was investigated based on the bi-linear *S-N* approach within 100-million cycles (Eurocode 9, 1999) and the stress-range bin histogram data from SHM. Lognormal and Weibull PDFs were also used for fatigue resistance and sea load effect, respectively.

From the analyses of the time-dependent fatigue reliability assessment and performance prediction of ship structures, the following conclusions were drawn:

- The model test data can be effectively used for estimating probabilistic lifetime sea loads representative of the equivalent stress range and the average daily number of cycles.

- Using a filtering process, low frequency wave-induced and high frequency slam-induced whipping moments can be extracted from unfiltered test data in order to identify structural responses separately.

- Based on the established stress-range bin histograms, individual equivalent

stress ranges for given ship operational and wave conditions (which are related to ship characteristics, ship speeds, relative wave headings, and sea states) can be computed and used to estimate the predicted equivalent stress range considering all possible occurrences.

- Based on the estimated probabilistic lifetime sea loads and the *S-N* approach, fatigue reliability and service life prediction of ship structures can be investigated throughout the anticipated service life.

- The time-dependent fatigue life of aluminum ship structures can be reliably assessed and predicted by using the probabilistic approach based on the bi-linear *S-N* approach and the histogram data from SHM. The quantified lifetime structural performance can be effectively used to plan life-cycle maintenance interventions in an optimal way.

8.3 CONCLUSIONS ON RELIABILITY-BASED LIFE-CYCLE STRUCTURAL MANAGEMENT

The conclusions on reliability-based life-cycle management of bridge and ship structures susceptible to fatigue, which have been emphasized in Chapters 5 and 6, respectively, are presented in this section.

8.3.1 Bridge Structures

In Chapter 5, probability-based approaches and methods were developed to perform the reliability-based life-cycle management of steel highway bridges.

An approach was presented to conduct bridge fatigue assessment and life-cycle

management by integrating three prediction models: FRM, CGM, and PDM. The FRM was used to quantify bridge performance levels during the entire service life, while the CGM and the PDM were used to predict crack growth rate and to schedule inspection time associated with probability of cracking detection, respectively. The application of the combined approach was illustrated on an existing highway bridge.

Based on the analyses of the reliability-based life-cycle bridge management, the following conclusions were drawn:

- For bridge fatigue assessment and maintenance, the PDM representing NDE capabilities can be combined with CGM and FRM in order to schedule inspection interventions according to the probability of detection with respect to the propagated flaw sizes.

- For the welding defects of steel bridges, the combined approach offers the possibility for establishing reliability-based inspection and repair scenarios.

- All necessary information including cracking data from NDE and S_{re} from field monitoring can be used to develop the prediction models FRM, CGM and PDM.

- Based on the AASHTO *S-N* approach, the FRM can provide the lifetime fatigue performance in terms of reliability and number of cycles.

- Fatigue life evaluation associated with crack propagation can be evaluated by the CGM. This prediction model is useful for estimating the remaining fatigue life.

An approach to finding the optimal cut-off size of the connection details for retrofitting distortion-induced fatigue cracking in steel highway bridges using SHM

data under uncertainty was presented. The associated single- and bi-objective optimization problems were formulated. Two competing objectives indicating minimization of the cut-off area (as used in single-objective optimization) and maximization of the fatigue reliability of the connection details were formulated. The concept of the cut-off size adjustment factor (SAF) was introduced. This factor was used to develop the nonlinear relationship with respect to the cut-off size. The optimal cut-off size was found by using the stress range histogram data of an existing bridge monitored by the ATLSS Engineering Research Center.

From the analyses of the retrofit design optimization for bridge management, the following conclusions were drawn:

- For retrofit design optimization of bridge connection details, SHM data and FE stress outputs can be used to perform the single- or bi-objective optimization as well as fatigue reliability assessment.

- The developed optimization approach can be applied for finding the optimal cut-off size of connection details for retrofitting distortion-induced fatigue cracking of steel highway bridges under uncertainty.

- Based on the predefined stress constraints associated with the *S-N* CAFT, various optimal cut-off retrofit solutions can be obtained from the single-objective optimization. The remaining fatigue lifetime of candidate optimal retrofit solutions can be possibly predicted by incorporating fatigue reliability evaluation.

- The SHM data can be used to represent the fatigue stress ranges at the identified critical locations after retrofit based on the developed SAF and also

to find the mean values of $N_S(t)$.

- The geometrical constraints on connection details, stress constraints associated with the AASHTO CAFT, and fatigue reliability constraints defining structural service life after retrofit can be used to provide practical solutions for decision-makers.

8.3.2 Ship Structures

In Chapter 6, probabilistic approaches were developed for estimating the time-dependent fatigue reliability of aluminum ship structures and for finding their lifetime optimum inspection/repair interventions considering fatigue reliability, fatigue damage, and life-cycle cost. The fatigue reliability analysis based on the bi-linear *S-N* approach and sea loading data was performed for the lifetime performance assessment and prediction, while the life-cycle cost analysis as well as the single- and multi-objective optimizations were performed for implementing a cost- and performance-effective lifetime structural maintenance strategy. Fatigue reliability, fatigue damage, and life-cycle cost were considered as competing objectives for multi-criteria optimization, subject to time and reliability constraints. This approach was illustrated by using an aluminum ship detail.

From the analyses of the reliability-based life-cycle optimal management of ship structures, the following conclusions were drawn:

- Life-cycle cost analysis considering regular or irregular time intervals between inspections of aluminum ships under uncertainty can be carried out to find the optimal lifetime inspection and repair planning as well as the optimal lifetime

fatigue damage threshold.

- Single-objective optimal lifetime planning of inspection/repair of aluminum fatigue sensitive ship structures can be formulated and solved to minimize expected total cost.

- Multi-objective optimization can be formulated and solved to provide the decision maker with alternative strategies for optimal inspection/repair planning of these structures selected from a Pareto set containing several competing objectives such as lifetime fatigue reliability, fatigue damage, and maintenance cost.

- Lifetime fatigue performance of aluminum ship structures can be quantified by using the proposed reliability method considering uncertainty. This approach is based on the *S-N* curve for fatigue resistance and stress-range bin histogram data from SHM for load effect.

- The quantified lifetime structural performance can be used to provide alternatives for planning lifetime inspection/repair interventions.

- Stress-range bin histogram data can be used not only to compute the equivalent stress range but also to estimate the time-dependent fatigue damage which may be affected by the annual ship operation rate.

8.4   CONCLUSIONS ON SYSTEM-BASED RELIABILITY ASSESSMENT AND PERFORMANCE PREDICTION

In Chapter 7, a system-based approach for estimating the time-dependent reliability associated with an aging hull girder in the presence of potential failure

modes under corrosion and fatigue was presented. The estimation of the ultimate strength of a hull girder subjected to vertical bending was based on an empirical formula derived from numerous test results, whereas still water and wave-induced bending moments were estimated using IACS recommendation and a simplified direct method, respectively. Effects of ship operational and sea environmental conditions on structural reliability in the intact hull condition were investigated. This approach was illustrated on a hull girder structure.

From the analyses of the system-based reliability assessment and performance prediction of ship structures, the following conclusions were drawn:

- Structural reliability analysis can be performed considering a single failure mode only. Under simultaneous presence of several failure modes, a series system model as well as a series-parallel system model can be used to estimate the system reliability.

- The time-dependent deterioration models associated with the ultimate buckling strength of hull girder structures can be developed at the system level considering all potential failure modes which may be encountered during the entire service life.

- The time-dependent random functions associated with corrosion and fatigue cracking can be formulated by using reduction factors in thickness and in length.

- The time-dependent structural performance of hull girders can be rationally assessed and predicted by using the proposed system-based reliability approach.

- Structural performance in the intact hull condition can be assessed based on ship operational and sea environmental conditions. The structural performance is more affected by the sea states than by the ship operating speed.

8.5 FUTURE WORK

Future research should be performed in the following directions:

- The developed prediction models in this study are based on current available information from SHM. To improve fatigue life estimation, the updating process can be further explored to update current information by using likelihood functions.

- To integrate loading information into fatigue life estimation, SHM has been utilized. The planning of reliable long-term SHM that considers fatigue performance as well as deterioration processes should be optimized.

- Experimental validation of the bi-linear *S-N* approach based on the analytical derivations is needed to support the concept that in fatigue life estimation the bi-linear *S-N* approach is more accurate than the traditional linear *S-N* approach.

- Life-cycle cost analyses can be performed in order to formulate an optimal cost-based bridge maintenance-management strategy under uncertainty. The developed combined method can be applied to schedule inspection, repair, and maintenance, in a cost-effective manner, for keeping bridge fatigue reliability above the target level during the anticipated service life.

- Further research is needed to expand the developed size optimization approach for cost-oriented reliability-based shape optimization of retrofitting distortion-induced fatigue cracking in steel bridges.

- The integration of the system reliability assessment into the life-cycle structural management can be developed at the system level based on the system reliability profiles in order to reflect global impact by load effect on a structure which may be unequal to local damage, consider uncertainties occurred inevitably at the system level, and balance lifetime reliability of structural systems and life-cycle management interventions in life-cycle cost analysis.

- The presented work focused primarily on the analyses of fatigue sensitive structures for helping to ensure their lifetime safety and serviceability. The developed work can be extended to cover other failure modes of new and existing structures under natural or man-made hazards such as plastic failure and progressive collapse.

REFERENCES

Aalberts, P.J. and Nieuwenhuijs, M. (2006). Full scale wave and whipping induced hull girder loads. *Proceedings of the Fourth International Conference on Hydroelasticity in Marine Technology*, 10-14 September, Wuxi, China, National Defence Industry Press: Beijing, China, 65-78.

AASHTO (1990). Guide Specifications for fatigue evaluation of existing steel bridges. *American Association of State Highway and Transportation Officials*, Washington, DC.

AASHTO Guidelines (1992). AASHTO Standard Specification for highway bridges. 15th Ed., *American Association of State Highway and Transportation Officials*, Washington, DC.

AASHTO Guidelines (2002). AASHTO Standard Specification for highway bridges. 17th Ed., *American Association of State Highway and Transportation Officials*, Washington, DC.

AASHTO (2008). AASHTO LRFD Bridge Design Specifications. 4th Ed., with Interims, *American Association of State Highway and Transportation Officials*, Washington, DC.

ABAQUS (2007). ABAQUS Version 6.7-1: Users manual. *Hibbitt, Karlsson, & Sorensen, Inc.,* Pawtucket, RI.

Akpan, U.O., Koko, T.S., Ayyub, B.M. and Dunbar, T.E. (2002). Risk assessment of aging ship hull structures in the presence of corrosion and fatigue. *Marine Structures*, 15(3): 211-231.

Aktan, A.E., Catbas, F.N., Grimmelsman, K.A. and Pervizpour, M. (2003). Development of a model health monitoring guide for major bridges. *Federal Highway Administration Reseach and Development*, July 2003.

Alampalli, S. and Lund, R. (2006). Estimating fatigue life of bridge components using measured strains. *Journal of Bridge Engineering*, ASCE, 11(6): 725-736.

Anderson T.W. and Darling D. A. (1952). Asymptotic theory of certain, goodness-of-fit criteria, based on stochastic processes. *Annals of Mathematical Statistics*, 23(2): 193–212.

Ang, A.H.-S. and Tang, W.H. (1984). Probability concepts in engineering planning and design volume II. *John Wiley & Sons*.

ASCE Committee on Fatigue and Fracture Reliability (1982). Fatigue reliability. *Journal of Structural Division*, Proceedings of the ASCE 108(ST1).

ASTM Standard E 1049-85 (1997). Standard practices for cycle counting in fatigue analysis. *In: Annual Book of ASTM Standards*, Vol. 03.01, 710-718, Philadelphia 1999, 1997 (reapproved).

Ayyub, B.M., Akpan, U.O, Rushton, P.A., Koko, T.S., Ross, J. and Lua, J. (2002a). Risk-informed inspection of marine vessels. *Ship Structure Committee*, Report No. (SSC-421), Washington, DC.

Ayyub, B.M., Assakkaf, I.A., Kihl, D.P. and Siev, M. W. (2002b). Reliability-based design guidelines for fatigue of ship structures. *Naval Engineers Journal*, ASNE, 114(2): 113-138.

Ayyub, B.M., Assakkaf, I.A., Sikora, J.P., Adamchak, J.C., Atua, K., Melton, W. and Hess III, P.E. (2002c). Reliability-based load and resistance factor design (LRFD) guidelines for hull girder bending. *Naval Engineers Journal*, ASNE, 1142(2): 43-68.

Bannantine, J.A., Comer, J.J. and Handrock, J.L. (1990). Fundamentals of metal fatigue analysis. *Prentice Hall*.

Barsom, J.M. and Rolfe, S.T. (1999). Fracture and fatigue control in structures: Application of fracture mechanics. *Technology & Engineering*, 3rd Ed.

Berens, A.P. (1996). Applications of statistical methods to nondestructive evaluation: Discussion. *Technometrics*, 38(2): 113-116.

Berens, A.P. (1997). NDE reliability data analysis, non-destructive evaluation and quality control: Qualitative non-destructive evaluation. *ASM Metals Data book*, Vol. 17, 5th Ed.

Berens, A.P. and Hovey, P.W. (1981). Evaluation of NDE reliability characterization. *Air Force Wright-Aeronautical Laboratory*, Wright-Patterson Air Force Base, Dayton.

Brady, T.F. (2004). Global structural response measurement of Swift (HSV-2) from JLOTS and Blue Game rough water trials. *Naval Surface Warfare Center, Carderock Division (NSWCCD)*, Report No. NSWCCD-65-TR-2004/33, West Bethesda, MD.

Brady, T.F., Bachman, R.J., Donnelly, M.J. and Griggs, D. B. (2004). HSV-2 swift instrumentation and technical trials plan. *Naval Surface Warfare Center, Carderock Division (NSWCCD)*, Report No.NSWCCD-65-TR-2004/18, West Bethesda, MD.

BS 5400, Part 10 (1980). Steel, concrete, and composite bridges: Code of practice for fatigue. *British Standards Institute*, London, England.

Caldwell, J. B. (1965). Ultimate longitudinal strength. *Transactions of RINA*, Vol. 107, 411-430.

Carlsen, C.A. (1980). A parametric study of collapse of stiffened plates in compression. *The Structural Engineer*, 58(2): 33-40.

Chiou, J.W. and Chen, Y.K. (1990). Fatigue prediction analysis validation from Sl-7 hatch corner strain data. *Ship Structure Committee*, Report No. SSC-338, Washington, DC.

Chong, K.P., Carino, N.J. and Washer, G. (2003). Health monitoring of civil infrastructures. *Smart Materials and Structures*, 12(3): 483-493.

Chung, H.Y. (2004). Fatigue reliability and optimal inspection strategies for steel bridges. *Dissertation*, Department of Civil and Environmental Engineering, University of Texas at Austin.

Chung, H.Y., Manuel, L. and Frank, K.H. (2006). Optimal inspection scheduling of steel bridges using nondestructive testing techniques. *Journal of Bridge Engineering*, ASCE, 11(3): 305-319.

Clarke, S.N., Goodpasture, D.W., Bennett, R.M., Deatherage, J.H. and Burdette, E.G. (2000). Effect of cycle-counting methods on effective stress range and number of stress cycles for fatigue-prone details. *Transportation Research Record*, 1740, Transportation Research Board, Washington, DC.

Connor, R.J. and Fisher, J.W. (2002). Report on field inspection, assessment, and analysis of floor-beam connection cracking on the Birmingham Bridge Pittsburgh PA, final report. *Advanced Technology for Large Structural Systems (ATLSS) Engineering Research Center*, Report No. 02-10, Lehigh University, Bethlehem, PA.

Connor, R.J. and Fisher, J.W. (2006). Identifying effective and ineffective retrofits for distortion fatigue cracking in steel bridges using field instrumentation. *Journal of Bridge Engineering*, ASCE, 11(6): 745-752.

Connor, R.J., Fisher, J.W., Hodgson, I.C. and Bowman, C.A. (2004), Results of field monitoring prototype floor-beam connection retrofit details on the Birmingham Bridge, final report. *Advanced Technology for Large Structural Systems (ATLSS) Engineering Research Center*, Report No. 04-04, Lehigh University, Bethlehem, PA.

Connor, R.J., Hodgson, I.C., Mahmoud, H.N. and Bowman, C.A. (2005). Field testing and fatigue evaluation of the I-79 Neville Island Bridge over the Ohio River. *Advanced Technology for Large Structural Systems (ATLSS) Engineering Research Center*, Report No. 05-02, Lehigh University, Bethlehem, PA.

Cornell, C.A. (1967). Bounds on the reliability of structural systems. *Journal of Structural Division*, ASCE, 93(ST1): 171-200.

Crawshaw, J. and Chambers, J. (1984). A concise course in a-level statistics: With worked examples. *Stanley Thornes*.

Crudele, B.B. and Yen, B.T. (2006). Analytical examination of S-N curves below Constant Amplitude Fatigue Limit. *Proceedings of the 1st International Conference on Fatigue and Fracture in the Infrastructure*, Philadelphia, PA.

Deb, K., Pratap, A., Agarwal, S. and Meyarivan, T. (2002). A fast elitist multiobjective genetic algorithm: NSGA-II. *IEEE Transactions on Evolutionary Computation*, 6(2):182–97.

Demers, C.E. and Fisher, J.W. (1989). A survey of localized cracking in steel bridges: 1981 to 1988. *Advanced Technology for Large Structural Systems (ATLSS) Engineering Research Center,* Report No. 89-01, Lehigh University, Bethlehem, PA.

Devine, E.A. (2009). An overview of the recently-completed JHSS Monohull and Trimaran structural seaways loads test program. *Naval Surface Warfare Center, Carderock Division (NSWCCD)*, PowerPoint Briefing, 30 October, 2009.

Dexter, R.J., Connor, R.J. and Kaczinski, M.R. (1997). Fatigue design of modular bridge expansion joints. *National Cooperative Highway Research Program (NCHRP)*, Report No. 402, Transportation Research Board, National Research Council, Washington, DC.

Dexter, R.J., Wright, W.J. and Fisher, J.W. (2004). Fatigue and fracture of steel girders. *Journal of Bridge Engineering*, ASCE, 9(3): 278-286.

Dissanayake, P.B.R. and Karunananda, P.A.K. (2008). Reliability index for structural health monitoring of aging bridges. *Structural Health Monitoring*, 7(2): 175-183.

Ditlevsen, O. (1979). Narrow reliability bounds for structural systems. *Journal of Structural Mechanics*, 7(4): 453-472.

Downing, S.D. and Socie, D.E. (1982). Simple rainflow counting algorithms. *International Journal of Fatigue*, 4(1): 31-40.

Estes, A.C. and Frangopol, D.M. (1998). RELSYS: A computer program for structural system reliability analysis. *Structural Engineering and Mechanics*, Techno-Press 6(8): 901-919.

Estes, A.C. and Frangopol, D.M. (1999). Repair optimization of highway bridges using system reliability approach. *Journal of Structural Engineering*, ASCE, 125(7): 766–775.

Estes, A.C. and Frangopol, D.M. (2005). Life cycle evaluation and condition assessment of structures. *Handbook of Structural Engineering*, 2nd Ed., CRC Press, Chapter 36, 1-51.

Eurocode 3 (2005). Design of steel structures. Part 1-9: Fatigue strength of steel structures. BS EN 1993-1-9, Brussels.

Eurocode 9 (1999). Design of aluminium structures - Part 3: Structures susceptible to fatigue. Brussels: CEN.

Faber, M.H. (2000). Reliability based assessment of existing structures. *Progress in Structural Engineering and Materials*, 2(2): 247-253.

Faulker, D., Adamchak, J.C., Snyder, G.J. and Vetter, M.F. (1973). Synthesis of wedged grillages to withstand compression and normal loads. *Computers Structures*, Vol. 3, 221-246.

Fisher, J.W. (1977). Bridge fatigue guide: design and detail. *American Institute of Steel Construction*, New York.

Fisher, J.W. (1984). Fatigue and fracture in steel bridges: Case studies. *John Willey & Sons*, New York.

Fisher, J.W. (1989). Executive summary: Fatigue cracking in steel bridge structures. *Advanced Technology for Large Structural Systems (ATLSS) Engineering Research Center*, Report No. 89-03, Lehigh University, Bethlehem, PA.

Fisher, J.W., Frank, K.H., Hirt, M.A. and McNamee, B.M. (1970). Effect of weldments on the fatigue strength of steel beams. *National Cooperative Highway Research Program (NCHRP)*, Report No. 102, Transportation Research Board, National Research Council, Washington, DC.

Fisher, J.W., Hausammann, H., Sullivan, M.D. and Pense, A.W. (1979). Detection and repair of fatigue damage in welded highway bridges. *National Cooperative Highway Research Program (NCHRP)*, Report No. 206, Transportation Research Board, National Research Council, Washington, DC.

Fisher, J.W., Jin, J., Wagner, D.C. and Yen, B.T. (1990). Distortion induced cracking in steel bridge members. *Advanced Technology for Large Structural Systems (ATLSS) Engineering Research Center*, Report No. 90-07, Lehigh University, Bethlehem, PA.

Fisher, J.W., Kulak, G.L. and Smith, I.F. (1998). A fatigue primer for structural engineers. *National Steel Bridge Alliance*, Chicago, IL.

Fisher, J.W., Nussbaumer, A., Keating, P.B. and Yen, B.T. (1993). Resistance of welded details under variable amplitude long-life fatigue loading. *National Cooperative Highway Research Program (NCHRP)*, Report No. 354, Transportation Research Board, National Research Council, Washington, DC.

Fisher, J.W., Slockbower, R.E., Hausammann, H. and Pense, A.W. (1981). Long time observation of a fatigue damaged bridge. *Journal of the Technical Councils*, ASCE, 107(1): 55-71.

Frangopol, D.M. (2010). Life-cycle performance, management, and optimization of structural systems under uncertainty: Accomplishments and challenges. *Structure and Infrastructure Engineering*, 2010 (in press).

Frangopol, D.M. and Estes, A.C. (1997). Lifetime bridge maintenance strategies based on system reliability. *Structural Engineering International Journal of IABSE*, 7(3): 193-198.

Frangopol, D.M., Kong, J.S. and Gharaibeh, E.S. (2001). Reliability-based life-cycle management of highway bridges. *Journal of computing in civil engineering*, ASCE, 15(1): 27–34.

Frangopol, D.M., Lin, K.Y. and Estes, A.C. (1997a). Reliability of reinforced concrete girders under corrosion attack. *Journal of Structural Engineering*, 123(3): 286-297.

Frangopol, D.M., Lin. K.Y. and Estes, A.C. (1997b). Life-cycle cost design of deteriorating structures. *Journal of Structural Engineering*, ASCE, 123(10): 1390-1401.

Frangopol, D.M. and Liu, M. (2007). Maintenance and management of civil infrastructure based on condition, safety, optimization and life-cycle cost. *Structure and Infrastructure Engineering*, 3(1): 29-41.

Frangopol, D.M. and Maute, K. (2003). Life-cycle reliability-based optimization of civil and aerospace structures. *Computers and Structures*, 81(7): 397-410.

Frangopol, D.M. and Messervey, T.B. (2007). Integrated life-cycle health monitoring maintenance, management and cost of civil infrastructure. *International Symposium on Integrated Life-cycle Design and Management of Infrastructure*, Lichu, F. Limin, S. and Zhi, S., eds., Tongji University Press, Shanghai, 216-218: full 12 page paper on CD-ROM (keynote paper).

Frangopol, D.M. and Neves, L.C. (2003). Probabilistic performance prediction of deteriorating structures under different maintenance strategies: Condition, safety and cost. *Proceedings of the 3rd International Workshop on Life-Cycle Cost Analysis and Design of Civil Infrastructure Systems and fib - JCSS Workshop on Probabilistic Modeling of Deterioration Processes in Concrete Structures*.

Frangopol, D.M., Strauss, A. and Kim, S. (2008). Bridge reliability assessment based on monitoring. *Journal of Bridge Engineering*, ASCE, 13(3): 258-270.

Ghorbanpoor, A. and Benish, N. (2003). Non-destructive testing of Wisconsin highway bridges. *The Wisconsin Department of Transportation*.

Glen, I.F., Paterson, R.B. and Luznik, L. (1999). Sea operational profiles for structural reliability assessment. *Ship Structure Committee*, Report No. (SSC-406), Washington, DC.

Gordo, J.M., Soares, C.G. and Faulkner, D. (1996). Approximate assessment of the ultimate longitudinal strength of the hull girder. *Journal of Ship Research*, SNAME, 40(1): 60-69.

Harlow, D.G. and Wei, R.P. (1999). Probabilities of occurrence and detection of damage in airframe materials. *Fatigue & Fracture of Engineering Materials & Structures*, 22(5): 427-436.

Hendawi. S. and Frangopol, D.M. (1994). System reliability and redundancy in structural design and evaluation. *Structural Safety*, Elsevier, 16(1-2): 47-71.

Hess III, P.E. (2007). Structural health monitoring for high-speed naval ships. *Proceedings of the 6th International Workshop on Structural Health Monitoring*, DEStech Publications, Inc., Lancaster, PA (keynote paper).

Hildstrom, G.A. (2007). JHSV analysis engine. *Naval Surface Warfare Center, Carderock Division (NSWCCD)*, Report No. NSWCCD-65-TR-2006/15, West Bethesda, MD, 2007.

Hodgson, I.C., Connor, R.J., Mahmoud, H.N. and Bowman, C.A. (2006). Approaches to the Fort Duquesne Bridge retrofit of fatigue and fracture details: Field testing and fatigue evaluation. *Advanced Technology for Large Structural Systems (ATLSS) Engineering Research Center*, Report No. 06-06, Lehigh University,

Bethlehem, PA.

Hussein, A.W. and Soares, C.G. (2009). Reliability and residual strength of double hull tankers designed according to the new IACS common structural rules. *Ocean Engineering*, 36(17-18): 1446-1459.

IACS (2006). Common structural rules for double hull oil tankers. *International Association of Classification Societies*, London, <http://www.iacs.org>.

Kaplan, P., Sargent, T.P. and Cilmi, J. (1974). Theoretical estimates of wave loads on the SL-7 container ship in regular and irregular seas. *Ship Structure Committee*, Report No. SSC-246, Washington, DC.

Keating, P.B. and Fisher, J.W. (1986). Evaluation of fatigue tests and design criteria on welded details." *National Cooperative Highway Research Program (NCHRP)*, Report No. 286, Transportation Research Board, National Research Council, Washington, DC.

Khan, I.A. and Parmentier, G. (2006). Ultimate strength and reliability analysis of a VLCC. *Proceedings of the 3rd Internaltional ASRANet Colloquium*, Glasgow, UK, 1-14.

Kim, S. and Frangopol, D.M. (2010). Optimal planning of structural performance monitoring based on reliability importance assessment. Probabilistic Engineering Mechanics, 25(1): 86-98.

Kirsch, U. (1993). Structural optimization: Fundamentals and applications. Springer-Verlag, Berlin and New York.

Kong, J.S. and Frangopol, D.M. (2004). Cost-reliability interaction in life-cycle cost optimization of deteriorating structures. *Journal of Structural Engineering*, ASCE, 130(11): 1704–1712.

Kong, J.S. and Frangopol, D.M. (2005). Probabilistic optimization of aging structures considering maintenance and failure cost. *Journal of Structural Engineering*, ASCE, 131(4): 600–616.

Kong, J.S., Frangopol, D.M. and Gharaibeh, E.S. (2000). Life prediction of highway bridges with or without preventive maintenance. *8th ASCE Specialty Conference on Probabilistic Mechanics and Structural Reliability*, PMC2000-300.

Kosteas, D. (1999). Design example in fatigue based on European Standard ENV 1999-2 (Eurocode 9). *Training in Aluminium Application Technologies (TALAT)*, 2712: 1-14.

Kulicki, J.M., Mertz, D.R. and Murphy, R.E. (1989). Dynamic response and proposed retrofit of two tied-arch bridges. *Proceeding of 6th International Bridge Conference*, The Engineers Society of Western Pennsylvania, Pittsburgh, PA, 12-22.

Kuo, H.C. and Chang, J.R. (2003). A simplified approach to estimate the ultimate longitudinal strength of ship hull. *Journal of Marine Science and Technology*, 11(3): 130-148.

Kwon, K. and Frangopol, D.M. (2008). Bridge fatigue reliability assessment and prediction. In Bridge Maintenance, Safety, Management, Health Monitoring and Informatics, edited by Koh, H-M. and Frangopol, D.M., Taylor & Francis Group, London, CD-ROM, 3022-3029.

Kwon, K. and Frangopol, D.M. (2009). Fatigue reliability assessment of steel bridges based on monitoring and FE modeling. Safety, Reliability and Risk of Structures, Infrastructures and Engineering Systems, edited by Furuta, Frangopol and Shinozuka, Taylor & Francis Group, London, CD-ROM, 1056-1061.

Kwon, K. and Frangopol, D.M. (2010a). Bridge fatigue reliability assessment using probability density functions of equivalent stress range based on field monitoring data. *International Journal of Fatigue*, 32(8): 1221-1232.

Kwon, K. and Frangopol, D.M. (2010b). Bridge retrofit design optimization for fatigue based on monitoring and FE analysis. In Bridge Maintenance, Safety, Management and Life-Cycle Optimization, edited by Frangopol, D.M., Sause, R. and Kusko, C.S., Taylor & Francis Group, London, CD-ROM, 775-782.

Kwon, K. and Frangopol, D.M. (2010c). Fatigue life assessment and lifetime management of aluminum ships using life-cycle optimization. *Journal of Ship Research*, (submitted).

Kwon, K., Frangopol, D.M. and Kim, S. (2010). Fatigue performance assessment and lifetime prediction of high-speed ship structures based on probabilistic lifetime sea loads. *Structure and Infrastructure Engineering*, doi: 10.1080/15732479.2010.524984.

Lin, W.M. and Yue, D.K.P. (1990). Numerical solutions for large-amplitude ship motions in the time-domain. *Proceedings of the 18th Symposium Naval Hydrodynamics*, 20-22 August, University of Michigan, Ann Arbor, MI, National Academy Press, Washington, DC.

Liu, M. and Frangopol, D.M. (2005a). Bridge annual maintenance prioritization under uncertainty by multiobjective combinatorial optimization. *Computer-Aided Civil and Infrastructure Engineering*, 20(5): 343-353.

385

Liu, M. and Frangopol, D.M. (2005b). Multiobjective maintenance planning optimization for deteriorating bridges considering condition, safety, and life-cycle cost. *Journal of Structural Engineering*, ASCE, 131(5): 833–842.

Liu, M. and Frangopol, D.M. (2006). Multiobjective optimization for risk-based maintenance and life-cycle cost of civil infrastructure systems. *Plenary Lecture in System Modeling and Optimization*, Vol. 199, 123-137.

Liu, M., Frangopol, D.M. and Kim, S. (2009). Bridge safety evaluation based on monitored live load effects. *Journal of Bridge Engineering*, ASCE, 14(4): 257-269.

Liu, M., Frangopol, D.M. and Kwon, K. (2010a). Fatigue reliability assessment of retrofitted steel bridges integrating monitored data. *Structural Safety*, Elsevier, 32(1): 77-89.

Liu, M., Frangopol, D.M. and Kwon, K. (2010b). Optimization of retrofitting distortion-induced fatigue cracking of steel bridges using monitored data under uncertainty. Engineering Structures, Elsevier, 32(11): 3467-3477.

Liu P.L., Lin H.Z. and Der Kiureghian A. (1989). CalREL user manual. *Report No. UCB/SEMM-89/18*, Structural Engineering, Mechanics and Materials, Department of Civil Engineering, University of California, Berkeley, CA, April, 1989.

Loukakis, T.A. and Chryssostomidls, C. (1975). Seakeeping standard series for cruiser-stern ships. *Transactions of the Society of Naval Architects and Marine Engineers*, Vol. 83, 67-127.

Maddox, S.J. (2003). Review of fatigue assessment procedures for welded aluminium structures. *International Journal of Fatigue*, Elsevier, 25(12): 1359-1378.

Madsen, H.O., Torhaug, R. and Cramer, E.H. (1991). Probability-based cost benefit analysis of fatigue design, inspection and maintenance. *Proceedings in Marine Structural Inspection, Maintenance and Monitoring Symposium, the Ship Structure Committee and the Society of Naval Architects*, eds., New York, NY.

Mahmoud, H.N., Connor, R.J. and Bowman, C.A. (2005). Results of the fatigue evaluation and field monitoring of the I-39 northbound bridge over the Wisconsin rive. *Advanced Technology for Large Structural Systems (ATLSS) Engineering Research Center*, Report No. 05-04, Lehigh University, Bethlehem, PA.

Mansour, A.E. (1987). Extreme value distributions of wave loads and their application to marine structures. *Proceedings of Marine Structural Reliability Symposium*, Arlington, VA, 159-167.

Mansour, A.E., Wirsching, P.H., White, G.J. and Ayyub, B.M. (1996). Probability-based ship design: Implementation of design guidelines. *Ship Structure Committee*, Report No. SSC-392, Washington, DC.

Marsh, P.S. and Frangopol, D.M. (2007). Lifetime multiobjective optimization of cost and spacing of corrosion rate sensors embedded in a deteriorating reinforced concrete bridge deck. *Journal of Structural Engineering*, 133(6): 777-787.

MathWorks (2009). Optimization Toolbox^{TM} 4: User's guidelines. *The MathWorks, Inc.*

Mertz, D.R. (1984). Displacement-induced fatigue cracking in welded steel bridges. *Dissertation*. Department of Civil and Environmental Engineering, Lehigh University, Bethlehem, PA.

Michaelson, R.W. (2000). User's guide for SPECTRA: Version 8.3. *Naval Surface Warfare Center, Carderock Division (NSWCCD)*, Report No. NSWCCD-65-TR-2000/07, West Bethesda, MD, 2000.

Miki, C. (2007). Retrofitting engineering for steel bridge structures. *International Institute of Welding*.

Miner, M.A. (1945). Cumulative damage in fatigue. *Journal of Applied Mechanics*, 12(3): 159-164.

Moan, T., Hovde, G.O. and Blanker, A.M. (1993). Reliability-based fatigue design criteria for offshore structures considering the effect of inspection and repair. *Proceedings of Offshore Technology Conference*, 591-600.

Munse, W.H., Wilbur, T.W., Tellalian, M.L., Nicoll, K. and Wilson, K. (1983). Fatigue characterization of fabricated ship details for design. *Ship Structure Committee*, Report No. (SSC-318), Washington, DC.

Nowak, A.S. (2004). System reliability models for bridge structures. *Bulletin of the Polish Academy of Sciences Technical Sciences*, 52(4): 321-328.

Okasha, N.M. and Frangopol, D.M. (2009). Lifetime-oriented multi-objective optimization of structural maintenance considering system reliability, redundancy and life-cycle cost using GA. *Structural Safety*, Elsevier, 31(6): 460-474.

Okasha, N.M., Frangopol, D.M. and Decò, A. (2010a). Integration of structural health monitoring in life-cycle performance assessment of ship structures under uncertainty. *Marine Structures*, Elsevier, 23(3): 303-321.

Okasha, N.M., Frangopol, D.M., Saydam, D. and Salvino, L.W. (2010b). Reliability analysis and damage detection in high-speed naval craft based on structural health monitoring data. *Structural Health Monitoring*, doi: 10.1177/1475921710379516.

Okasha, N.M. and Frangopol, D.M. (2010). Novel approach for multicriteria optimization of life-cycle preventive and essential maintenance of deteriorating structures. *Journal of Structural Engineering*, ASCE, 136(8): 1009-1022.

Pachurin, G.V. (2008). Ruggedness of structural materials and working life of metal components. *Steel in Translation*, 38(3): 217-220.

Paik, J.K. and Frieze, P.A. (2001). Ship structural safety and reliability. *Progress in Structural Engineering and Materials*, 3(2): 198-210.

Paik, J.K. and Mansour, A.E. (1995). A simple formulation for predicting the ultimate strength of ships. *Journal of Marine Science and Technology*, Society of Naval Architects of Japan, 1(1):52-62.

Paik, J.K., Satish Kumar, Y.V. and Lee, J.M. (2005). Ultimate strength of cracked plate elements under axial compression or tension. *Thin-Walled Structures*, Vol. 43, 237-272.

Paik, J.K. and Thayamballi, A.K. (2002). Ultimate strength of ageing ships. *Journal of Engineering for the Maritime Environment*, 216(M1): 57-77.

Paik, J.K., Thayamballi, A.K., Che, J.S. (1996). Ultimate strength of ship hulls under combined vertical bending, horizontal bending and shearing forces. *Transactions of the Society of Naval Architects and Marine Engineers*, Vol. 104, 31-59.

Paik, J.K., Thayamballi, A.K. and Yang, S.H. (1998). Residual strength assessment of ships after collision and grounding. *Marine Technology*, 35(1): 38-54.

Palmgren, A. (1924). The service life of ball bearings. *Zeitschrift des Vereines Deutscher Ingenieure*, 68(14): 339-341.

Pareto, V. (1971). Manual of political economy. Schwier, A. S., Page, A. N., and Kelley, A. M., Eds., Trans., New York, (Original work published 1906).

Paris, P.C. and Erdogan, F. (1963). A critical analysis of crack propagation laws. *Journal of Basic Engineering*, ASME, 85(4): 528-534.

Pedersen, P.T. and Jensen, J.J. (2009). Estimation of hull girder vertical bending moments including non-linear and flexibility effects using closed form expressions. *Proc. IMechE*, 223(3): 377-390.

Pourzeynali, S. and Datta, T.K. (2005). Reliability analysis of suspension bridges against fatigue failure from the gusting of wind. *Journal of Bridge Engineering*, ASCE, 10(3): 262-271.

Raju, S.K., Moses, F. and Schilling, C.G. (1990). Reliability calibration of fatigue evaluation and design procedures. *Journal of Structural Engineering*, ASCE, 116(5): 1356-1369.

Righiniotis, T.D. (2004). Influence of management actions on fatigue reliability of a welded joint. *International Journal of Fatigue*, Elsevier, 26(3): 231-239.

Righiniotis, T.D. and Chryssanthopoulos, M.K. (2003). Probabilistic fatigue analysis under constant amplitude loading. *Journal of Constructional Steel Research*, Elsevier, 59(7): 867-886.

Roddis, W.M. and Zhao, Y. (2001). Out-of-plane fatigue cracking in welded steel bridges. *Welding Innovation*, 18(2).

Roeder, C.W., MacRae, G., Crocker, P., Arima, K. and Wong, S. (2000). Dynamic response and fatigue of steel tied-arch bridge. *Journal of Bridge Engineering*, ASCE, 5(1): 14-21.

Rummel, W.D. (1982). Recommended practice for a demonstration of non-destructive evaluation (NDE) reliability on aircraft production parts. *Materials Evaluation*.

Rummel, W.D. and Matzkanin, G.A. (1997). Nondestructive evaluation (NDE) capabilities data book. 3rd Ed., NTIAC Texas Research Institute Austin, Inc.

Salvino, L.W. and Brady, T.F. (2008). Hull monitoring system development using a hierarchical framework for data and information management. *Proceedings of the 7th International Conference on Computer and IT Applications in the Maritime Industries*, (COMPIT'08), 21-23 April, Liège, Belgium, 589-602.

Sielski, R.A. (2007a). Aluminum structure design and fabrication guide. *Ship Structure Committee*, Report No. SSC-452, Washington, DC.

Sielski, R.A. (2007b). Research needs in aluminum structure. Proceedings of the 10th International Symposium on Practical Design of Ships and Other Floating Structures, Houston, Texas.

Sikora, J.P., Dinsenbacher, A. and Beach, J.E. (1983). A method for estimating lifetime loads and fatigue lives for swath and conventional monohull ships. *Naval Engineers Journal*, 95(3): 63-85.

Soares, C.G. and Garbatov, Y. (1999). Reliability of maintained ship hulls subjected to corrosion and fatigue under combined loading. *Journal of Constructional Steel Research*, 52(1): 93-115.

Sumitro, S., Kurokawa, S., Shimano, K. and Wang, M.L. (2005). Monitoring based maintenance utilizing actual stress sensory technology. *Smart Materials and Structures*, 14(3): S68-S78.

Tada, H., Paris, P.C. and Irwin, G.R. (1973). The stress analysis of cracks handbook. 2nd Ed., St. Louis: Paris Productions.

Thoft-Christensen, P. and Baker, M.J. (1982). Structural reliability theory and its applications. *Springer-Verlag*, Berlin.

Thoft-Christensen, P. and Murotsu, Y. (1986). Application of structural system reliability theory. *Springer-Verlag*, Berlin.

Tiryakioğlu, M. (2008). Statistical distributions for the size of fatigue-initiating defects in Al-7%Si-0.3%Mg alloy castings: A comparative study. *Materials Science and Engineering A*, 497(1-2): 119-125.

Wirsching, P.H. (1984). Fatigue reliability for offshore structures. *Journal of Structural Engineering*, ASCE, 110(10): 2340-2356.

Wirsching, P.H., Ortiz, K. and Chen, Y.N. (1987). Fracture mechanics fatigue model in a reliability format. *Proceedings of the 6th Int. Syrup. on OMAE*, Houston, TX.

Wu, M.K. and Moan, T. (2006). Numerical prediction of wave-induced long-term extreme load effects in a flexible high-speed pentamaran. *Journal of Marine Science and Technology*, 11(1): 39-51.

Yazdani, N. (1984). Risk analysis of extending bridge service life. *PhD Dissertation*, University of Maryland, MD.

Yazdani, N. and Albrecht, P. (1989). Crack growth rates of structural steel in air and aqueous environments. *Engineering Fracture Mechanics*, 32(6): 997-1007.

Yen, B.T., Hodgson, I.C., Zhou, E. and Crudele, B.B. (2009). Estimation of fatigue life below CAFL. *Proceedings of the second International Conference on Fatigue and Fracture in the Infrastructure*, Philadelphia, PA.

Yen, B.T., Huang, T., Lai, L.Y. and Fisher, J.W. (1990). Manual for inspecting bridges for fatigue damage conditions. *PennDOT/FHWA*, Report No. FHWA-PA-89-022-85-02.

Zhang, R. and Mahadevan, S. (2001). Fatigue reliability analysis using nondestructive inspection. *Journal of Structural Engineering*, ASCE, 127(8): 957-965.

Zhao, Y. and Roddis, K.W.M. (2007). Fatigue behavior and retrofit investigation of distortion-induced web gap cracking. *Journal of Bridge Engineering*, ASCE, 12(6): 737-745.

Zhou, E.Y. (2006). Assessment of bridge remaining fatigue life through field strain measurement. *Journal of Bridge Engineering*, ASCE, 11(6): 737-744.

APPENDIX A: LIST OF NOTATIONS

Notation used in this study is as follows:

A : fatigue detail coefficient

A_1 : fatigue detail coefficient above the CAFT

A_2 : fatigue detail coefficient below the CAFT

a : crack size

a_f : final (critical) crack size

a_i : initial crack size

B : fatigue exponent

C : fatigue coefficient

C_{ET} : expected total remaining life-cycle cost

C_f, C_F : failure and expected failure costs

C_{INS} : discounted inspection cost

C_{ins} : undiscounted inspection cost

C_{MT} : expected maintenance cost

C_{REP} : discounted repair cost

C_{rep} : undiscounted repair cost

D : Miner's damage accumulation index

D_{th} : fatigue damage threshold

e : typical measurement error factor

$f_{\mathbf{X}}(\boldsymbol{x})$: joint probability density function (PDF)

G : non-dimensional function of the geometry

$g(\boldsymbol{X})$: a response model and $\boldsymbol{X}$ is a random variable vector

h : cut-off height of floor-beam

k : number of inspections

l : cut-off length of floor-beam

M_{sw} : still water bending moment

M_u : ultimate bending strength of a hull girder

M_w : wave-induced bending moment

m : material constant (*S-N* slope)

m_1 : material constant above the CAFT

m_2 : material constant below the CAFT

N : number of stress cycles of stress range

N_{avg} : average daily number of stress cycles which is the mean value of the collected daily number of stress cycles from SHM within T_{shm}

N_{avg}^* : predicted average daily number of cycles

N_c : total number of stress cycles to fatigue failure under variable stress range

N_D : number of cycles corresponding to the constant amplitude fatigue limit in aluminum ships

N_s : specified number of cycles associated with the CAFT

$N_S(t)$: product of $N(t)$ and S_{re}^m

$\overline{N}_{shm}$: mean value of $N_S(t)$ with the SAF during the monitoring period

N_t : accumulated number of stress cycles applied to the fatigue details during the period from the start of fatigue damages to the time t

393

N_{total} : total number of observations during the monitoring period T_{shm}

n : number of repairs

n_i : number of observations in the predefined stress-range bin, S_{ri}

P_f : probability of failure

P_{fsys} : system failure probability

$P_{SP,j}$: probability of occurrence of the j-th ship speed

$P_{SS,i}$: probability of occurrence of the i-th sea state

$P_{WH,k}$: probability of occurrence of the k-th relative wave heading

R : nominal fatigue resistance

R_1 : nominal fatigue resistance above the CAFT

R_2 : nominal fatigue resistance below the CAFT

R_I : strength factor

$R_{initial}$: fatigue strength in intact state

r : discount rate of money

S : stress range

S_D : constant amplitude fatigue limit in aluminum ships

S_L : cut-off limit corresponding to $N_L = 100$ million cycles

S_{re} : equivalent stress range

S_{re}^{*} : bi-linear/predicted equivalent stress range

T_i : remaining fatigue life at the i-th identified critical location

T_{min} : predefined minimum remaining fatigue life after retrofit

α : annual traffic increase rate in bridges/ annual ship operation rate in ships

α_{target} : target stress parameter considering remaining fatigue life of a bridge

β : fatigue reliability index

β_i : fatigue reliability index at the i-th identified critical location

β_{target} : target reliability index

β_{sys} : system reliability index

λ_y, ζ_y : mean value and standard deviation of ln y

$\sigma_{yy,i}, \sigma_{zz,i}$: maximum vertical stress and maximum longitudinal stress in the cut-off

        region of the floor-beam for the identified critical locations, i

$\sigma_{max,i}$: predefined maximum tensile stress at the i-th identified critical location

σ_y, σ_u : yield strength and ultimate buckling strength of the stiffened panel

Δ : Miner's critical damage accumulation index

Δ_h : out-of-plane displacement

ΔK : stress intensity factor range

$\Delta K(a)$: generalized stress intensity factor range

ΔK_{th} : stress intensity threshold range

Ω : failure domain

$\Phi^{-1}(\cdot)$: inverse standard normal cumulative distribution function (CDF)

APPENDIX B: DERIVATIONS OF DISTORTION-INDUCED STRESSES

According to Figure 5-26, the structural behavior of the web of the floor-beam after retrofit, under constant out-of-plane displacement, Δ_{top}, applied at the top of the web only, the computed stress σ_1 at critical location CL-I can be expressed as

$$\sigma_1 = \sigma_{yy} = \frac{M_{yy}}{S_{yy}} = \frac{3(E \times I_{yy})}{S_{yy} \times h^2} \times (\Delta_{top} - \Delta_{h,1}) \tag{B-1}$$

where E, I_{yy} and S_{yy} = constants related to the material and cross section properties of the web of the floor-beam after retrofit; and $\Delta_{h,1}$ = out-of-plane displacement at height h and length l, for σ_1 (see Figure B.1), that is

$$\Delta_{h,1} = \Delta_h \times \left(\frac{l}{L_c}\right)^2 = \Delta_{top} \times \left[3\left(\frac{H-h}{H}\right)^2 - 2\left(\frac{H-h}{H}\right)^3\right] \times \left(\frac{l}{L_c}\right)^2 \tag{B-2}$$

where L_c = length of the floor-beam affected by the end constraints under Δ_{top} which may be obtained from the FE modeling as $L_c = 0.635$ m (25.0 in) in this study.

Let $C_1 = \dfrac{3(E \times I_{yy} \times \Delta_{top})}{S_{yy}}$, then

$$\sigma_1 = \frac{C_1}{h^2} \times \left\{1 - \left[3\left(\frac{H-h}{H}\right)^2 - 2\left(\frac{H-h}{H}\right)^3\right] \times \left(\frac{l}{L_c}\right)^2\right\}$$

$$= C_1 \frac{H^3 \times L_c^2 - (H+2h) \times (H-h)^2 \times l^2}{H^3 \times L_c^2 \times h^2} \tag{B-3}$$

396

Similarly, the computed stress σ_3 at critical location CL-III can be expressed as

$$\sigma_3 = \sigma_{zz} = \frac{M_{zz}}{S_{zz}} = \frac{3(E \times I_{zz})}{S_{zz} \times l^2} \times \Delta_{h,3} \qquad \text{(B-4)}$$

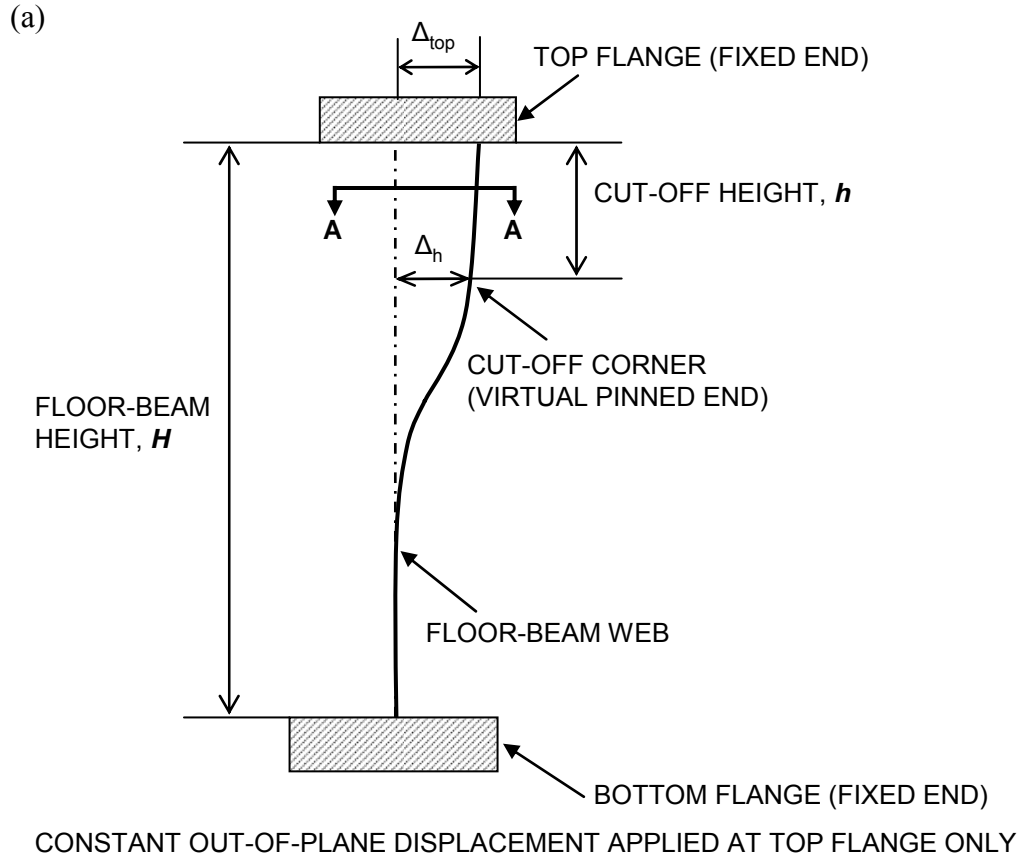where E, I_{zz} and S_{zz} = constants related to the material and cross section properties of the web of the floor-beam after retrofitting; and $\Delta_{h,3}$ = out-of-plane displacement at height h and length l, for σ_3 (see Figure B.1), that is

$$\Delta_{h,3} = \Delta_h \times \left(\frac{l}{h}\right) = \Delta_{top} \times \left[3\left(\frac{H-h}{H}\right)^2 - 2\left(\frac{H-h}{H}\right)^3\right] \times \left(\frac{l}{h}\right) \qquad \text{(B-5)}$$
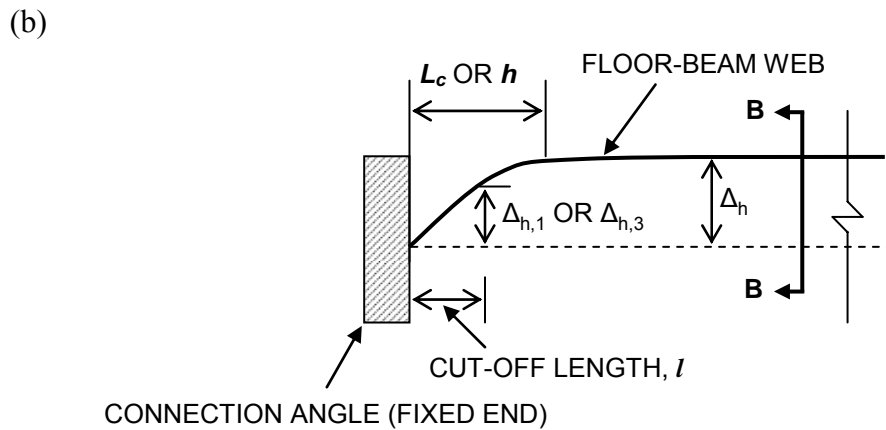
Let $C_3 = \dfrac{3(E \times I_{zz} \times \Delta_{top})}{S_{zz} \times H^3}$, then

$$\sigma_3 = \frac{C_3 \times H^3}{l^2} \times \left[3\left(\frac{H-h}{H}\right)^2 - 2\left(\frac{H-h}{H}\right)^3\right] \times \left(\frac{l}{h}\right)$$

$$= C_3 \frac{(H+2h) \times (H-h)^2}{l \times h} \qquad \text{(B-6)}$$

It should be noted that the effects of the cut-off length l on $\Delta_{h,1}$ and $\Delta_{h,3}$ are different, that is, $(l / L_c)^2$ for $\Delta_{h,1}$ and (l / h) for $\Delta_{h,3}$. In addition, σ_2 can be derived by using the regression model that is related to σ_1 and σ_3, which have been validated by the FE modeling as presented in Table 5-10.

Δ_{top}

TOP FLANGE (FIXED END)

CUT-OFF HEIGHT, **h**

A   **A**

Δ_h

CUT-OFF CORNER
(VIRTUAL PINNED END)

FLOOR-BEAM
HEIGHT, **H**

FLOOR-BEAM WEB

BOTTOM FLANGE (FIXED END)

CONSTANT OUT-OF-PLANE DISPLACEMENT APPLIED AT TOP FLANGE ONLY

(a) section view B-B

(b)

L_c OR **h**

FLOOR-BEAM WEB

B

$\Delta_{h,1}$ OR $\Delta_{h,3}$

Δ_h

B

CUT-OFF LENGTH, **l**

CONNECTION ANGLE (FIXED END)

(b) plan view A-A

Figure B.1   Derivations of σ_1, σ_2 and σ_3

398

VITA

The author was born on May 1, 1972 in Wonju, Korea. He is the third child of Jinseok Kwon and Wongi Jang. He was raised in Wonju, and attended Dai-Sung High School. After graduating in February of 1991, he entered Ajou University in March, 1991 and served in the Korean army for 2 years and 3 months from June, 1992 to September, 1994. In August of 1998, he earned his Bachelor of Science degree in Architectural Engineering. Since that time, he worked in Han-Sol Construction Company until January, 2001. In March of 2001, he continued his study at Ajou University, and earned the Master of Science degree majoring in structural engineering in February of 2003. After working in O-Seong Architectural/Structural Design Office for a year, he started his master program at Lehigh University in the fall of 2004. In the January of 2007, his study continued in Ph.D. program at Lehigh University, and worked with Dr. Dan M. Frangopol.